FLEXURAL STRENGTHENING OF PRESTRESSED HOLLOW-CORE SLABS USING NEAR-SURFACE MOUNTED (NSM) CFRP REINFORCEMENT

By

STEVEN FOUBERT

A Thesis submitted to the Faculty of Graduate Studies of

The University of Manitoba

in partial fulfillment of the requirements of the degree of

MASTER OF SCIENCE

Department of Civil Engineering

University of Manitoba

Winnipeg, Manitoba, Canada

ABSTRACT

Prestressed hollow core slabs are essential components in structures such as bridges, parking garages, marine structures, and commercial and industrial buildings. Material degradation and altered functional requirements may seriously threaten the structural integrity of these reinforced concrete structures. Using FRP composites, the NSM strengthening technique presents a viable solution to these challenges. However, further investigation is required to establish comprehensive empirical design guidelines. The intent of this research project is to investigate the NSM technique in conjunction with common design concepts such as prestressed concrete, precast hollow core slabs, the complex behaviour of disturbed regions, and fiber-reinforced composite materials. An experimental program was developed, which included eleven full-scale slab specimens, subject to a four-point load configuration. The main parameters included the prestressing reinforcement ratio, CFRP strengthening ratio, and in-service opening location. Experimental results showed that prestressed concrete strengthened in flexure with NSM-CFRP is a viable technique for lower reinforcement ratios.

ACKNOWLEDGEMENTS

First and foremost, the author would like to express the deepest appreciation to his supervisor, Dr. Ehab El-Salakawy, P.Eng., Professor of Civil Engineering and Canada Research Chair in Durability and Modernization of Civil Structures in the department of Civil Engineering at the University of Manitoba. Dr. El-Salakawy has provided mentorship and inspiration throughout this project. His continuous determination and unsurpassed knowledge was absolutely essential to the successful completion of this lifetime achievement. Special thanks go to Rick Haldane-Wilsone, P.Eng. for his powerful support and encouragement to pursue such a significant academic challenge. A warm thank you goes to Dr. Mostafa El-Mogy, P.Eng., who provided essential clarification and guidance, and most importantly for becoming a lifelong friend.

In addition, a sincere thank you goes to Chad Klowak, Brendan Paschal, and Grant Whiteside at the University of Manitoba's W.R. McQuade Structures Laboratory for their comradery and valued assistance during the modification and testing of the specimens. Acknowledgment is extended to the Canada Research Chair Program (CRC), Tetra Tech, Lafarge Canada Inc. and Vector Construction Ltd. for their financial support and industry perspectives.

Finally, to the love, enduring support, and continuous excitement of family and friends; to them this thesis is dedicated.

STEVEN FOUBERT
University of Manitoba
December 2013

TABLE OF CONTENTS

LIST OF TABLES

LIST OF FIGURES

LIST OF NOTATIONS

a_b	Smallest FRP strip cross section dimension
A_g	Gross cross sectional area of test specimen, not considering steel or FRP reinforcement
A_p	Area of prestressing tendons
b_b	Largest FRP strip cross section dimension
c	Distance from a point to the neutral axis
c_a	Adhesive cover from laminate to extreme outer fiber in tension
c_c	Concrete cover from longitudinal void to extreme outer fiber in tension
c_r	Concrete cover between NSM groove and internal reinforcement
CR	Loss of prestress due to creep of concrete
d	Distance from extreme compression fiber to centroid of longitudinal tension reinforcement
d_b	Strand diameter
$d_{b\text{-}FRP}$	Diameter of FRP round bar
d_p	Distance from extreme compression fiber to centroid of prestressing steel
d_v	Effective shear depth
e	Eccentricity of prestressing tendon
e_g	Edge distance from groove to edge of concrete
e_l	Edge distance from center of laminate to edge of concrete
E_c	Modulus of elasticity of concrete
E_{ci}	Modulus of elasticity of concrete at transfer

E_f	Tensile modulus of elasticity of FRP
E_F	Modulus of elasticity of FRP laminate
E_p	Modulus of elasticity of prestressing tendons
ES	Loss of prestress due to elastic shortening of concrete
f_c	Compressive stress in concrete
f_c'	Specified compressive strength of concrete
f_{ci}	Initial compressive strength of concrete
f_c	Compressive strength of concrete
f_{cir}	Concrete stress at the center of gravity of tendons due to the prestressing effect at transfer and the self-weight of the member at sections of maximum moment
f_{ps}	Stress in prestressed reinforcement
$f_{ps,s}$	Stress in prestressed reinforcement under service loads
f_{pu}	Specified tensile strength of prestressing tendons
f_{py}	Specified yield strength of prestressing tendons (0.90 f_{pu} for low-relaxation strands)
f_{sj}	Stress in prestressing steel at jacking
h	Overall thickness or height of member
h_g	Height of NSM groove
h_s	Height of FRP strip
I_g	Moment of inertia of section about centroidal axis, second moment of area of cross-section
K_{cr}	Factor used to calculate prestress loss due to creep of concrete
l_{df}	Development length of an FRP laminate
l_a	Anchorage length of an FRP laminate
L_e	Effective embedment length

L_s	Length of slab element
M_{cr}	Experimental cracking moment
$M_{cr\text{-}p}$	Theoretical cracking moment
M_s	Service moment
M_{sw}	Moment generated by the self-weight of an element
M_u	Experimental ultimate flexural capacity
$M_{u\text{-}p}$	Theoretical ultimate flexural capacity
n	Number of plies of FRP reinforcement
P	Effective force in prestressing reinforcement (after allowance for all prestress losses)
P_e	Effective force in prestressing reinforcement (after allowance for all prestress losses)
r	Radius of gyration
REL_1	Loss of prestress due to relaxation of prestressing steel before transfer
REL_2	Loss of prestress due to relaxation of prestressing steel after transfer
R_n	Nominal strength of a member
s_g	Spacing between grooves
S_{DL}	Dead load effects
S_{LL}	Live load effects
SH	Loss of prestress due to shrinkage of concrete
t	Age of concrete after casting
t_f	Nominal thickness of one ply of FRP reinforcement
t_F	Nominal thickness of one ply of FRP reinforcement
w_g	Width of groove
w_s	Width of FRP strip

y_b	Distance from centoidal axis of gross section to extreme bottom fiber
α	Multiplier on $f_c^{'}$ to determine the intensity of an equivalent rectangular stress distribution for concrete
β	Ratio of depth of equivalent rectangular stress block to depth of the neutral axis
ε_{bi}	Strain level in concrete substrate at time of NSM-FRP installation
$\varepsilon_{cr\text{-}FRP}$	Experimental mid-span strain in CFRP strip at estimated cracking stage
$\varepsilon_{cr\text{-}s}$	Experimental mid-span strain in prestressed tendon at estimate cracking stage
ε_{fd}	Debonding strain of externally bonded FRP reinforcement
ε_{fu}	Design rupture strain of FRP reinforcement
ε_{pf}	Strain in prestressed reinforcement
ε_{pnet}	Net tensile strain in the prestressing steel beyond decompression, at the nominal strength
ε_{ps}	Strain in prestressed reinforcement at nominal strength
$\varepsilon_{y\text{-}FRP}$	Experimental mid-span strain in CFRP strip at yielding
$\varepsilon_{y\text{-}s}$	Experimental mid-span strain in prestressed tendon at yielding
$\varepsilon_{u\text{-}FRP}$	Experimental mid-span strain in CFRP strip at ultimate
$\varepsilon_{u\text{-}s}$	Experimental mid-span strain in prestressed tendon at ultimate
λ	Factor accounting for low-density concrete
ρ_{frp}	CFRP strengthening reinforcement ratio
ρ_p	Prestressed steel reinforcement ratio
ϕ	Strength reduction factor
ϕ_c	Resistance factor for concrete
ϕ_p	Resistance factor for prestressing tendons
ϕ_s	Resistance factor for non-prestressed reinforcement

Δ_{cr} Change in cracking load between theoretical prediction and experimental result for the same specimen ($M_{cr}/M_{cr\text{-}p}$*100)

Δ_{u} Change in ultimate capacity between theoretical prediction and experimental result for the same specimen ($M_{u}/M_{u\text{-}p}$*100)

Δ_{Mu} Change in ultimate capacity between the experimental result of the control specimen and another test specimen ($M_{u(i)}/M_{u(Control)}$*100)

ψ_f FRP strength reduction factor (0.85 for flexure)

CHAPTER 1 – INTRODUCTION

1.1 General

Material degradation and altered functional requirements may seriously threaten the structural integrity of reinforced concrete (RC) structures. Concrete decay and reinforcement corrosion are common problems associated with structures exposed to harmful elements such as de-icing salts, saline water, and adverse chemicals. In addition, changes to the original use of a structure may require it to sustain increased service or ultimate loads. These structural deficiencies must be addressed to ensure the short- and long-term behaviour of building elements meet all minimum performance standards. Strengthening techniques can be an effective solution to restore and/or enhance the original strength and serviceability of a reinforced concrete member. To date, strengthening systems have successfully been applied to a considerable range of common civil infrastructure such as bridges, parking garages, marines structures, and industrial or commercial buildings.

The challenges associated with ageing infrastructure are an ongoing reality that plague building components all throughout their lifecycle. There is an obvious mandate to develop practical solutions to rehabilitate structures burdened with distressed materials or obsolete design parameters. In recent years, considerable attention has been given to rehabilitation techniques to restore and enhance the capacity of RC structures using non-corrodible fiber-reinforced polymer (FRP) composite materials. One such method with a proven history as a viable solution is the near-surface mounting (NSM) technique. The Canadian Standards Association (CSA S806-12) and American Concrete Institute (ACI 440.2R-08) are some of the noteworthy institutions to publish design guidelines on this strengthening technique. NSM strengthened RC elements are typically in-service steel-reinforced concrete members with FRP laminates bonded within pre-cut grooves along the tensile region. Experimental research has shown that NSM reinforcement is subject to premature and sudden debonding, which prevents the strengthened member from achieving the ultimate flexural capacity. Research focuses on maximizing the bond strength between NSM laminates and the RC structure.

A comprehensive understanding of the flexural behaviour of strengthened RC elements is essential to maximize the potential applications for the NSM technique. Published design guidelines and experimental studies predominantly focus on unaltered conventionally reinforced concrete beams. Several important areas are still devoid of critical understanding. Further experimental study should refine the recommended practices, and should explore new applications for the NSM-FRP technique. Prestressed concrete is a ubiquitous building material that exhibits a distinct flexural response, but has not garnered substantial research attention. Likewise, precast hollow core (HC) slabs possess a unique cross section and internal reinforcement arrangement, which effectively restricts the layout of NSM reinforcement. Also,

the addition of in-service openings to RC elements is a common practice, with outdated or inadequate design guidelines. Openings added to existing construction create an immediate strength deficiency, and may require restoration of the original members strength and serviceability characteristics. The intent of this research is to investigate the NSM technique in conjunction with several important design concepts such as prestressed concrete, precast hollow core slabs, the complex behaviour of disturbed regions in reinforced concrete, and fiber-reinforced composite materials.

1.2 Background

Several types of RC structures operate under extreme weather conditions or aggressive chemical environments. It is also common for structures to undergo changes while still in service, which may require them to resist an increased applied load. Prolonged use under these detrimental conditions can deteriorate the constituent materials and threaten the structures strength and serviceability performance. Strengthening techniques are commonly employed to restore or enhance the performance of the original structure, which may also be exposed to harsh environments. In such a case, the NSM technique, using FRP composites, has emerged as a viable solution to strengthen RC structures. The non-corrodible and durable nature of FRP composites can successfully mitigate the effects of inclement conditions, and effectively improve the structures performance. Unfortunately, structural elements strengthened with surface-bonded reinforcement are plagued by a premature debonding failure mechanism. NSM research focuses on maximizing the strength of the bond between the FRP laminates and the concrete substrate. Several physical and mechanical properties affect the bond performance, such as concrete strength, type and arrangement of internal steel reinforcement, type of FRP reinforcement,

groove size, groove spacing, edge distance, bonded length, adhesive material, etc. It is clear that extensive research is required to develop a comprehensive understanding of the behaviour of NSM-FRP strengthened RC members.

Generally, concrete elements reinforced with mild steel exhibit sufficient ductility to allow the concrete to crack under service loads. According to Hassan (2002), non-prestressed reinforcement plays a minor role on the stiffness of a concrete section before cracking. After cracking however, the tensile stresses are essentially distributed to the internal reinforcement. A strengthened member, outfitted with NSM reinforcement, experiences an improved stiffness compared to its unstrengthened counterpart. The linear-elastic nature of FRP materials allow this stiffening effect to continue even after the internal steel has reached the yielding point. However, the effectiveness and practicality of the NSM technique is questionable for concrete with considerably different deformability characteristics. Concrete prestressed with high-strength steel is one such element developed with the intention to remain uncracked under service loads. Strengthening guidelines published to date (S806-12, 2012; 440.2R-08, 2008; ISIS 2008) provide very few recommendations to strengthen concrete prestressed with high-strength steel. Furthermore, prestressed concrete (PC) is a structural element commonly used in infrastructure subject to adverse environmental conditions. Bridges, parking garages, and industrial buildings are a few examples that employ PC, where de-icing salts and chemicals threaten the structures integrity. The investigation of the NSM-FRP technique on PC is important to restore the performance of a structure subject to detrimental conditions.

Moreover, the purpose and use of civil infrastructure can change to meet the needs of evolving communities, growing businesses, or to accommodate new tenants. Alterations to existing

construction can include stairs, access hatches, elevators, escalators, windows, utility ducts, and much more. Canadian and American building codes provide limited recommendations for the provision of in-service openings. The codes suggest that an opening should be reinforced to restore the original strength and serviceability performance. Conventional strengthening options have included steel plates, beams, or frames, supported by columns. The NSM technique may provide a less obtrusive alternative solution. Openings are common to flat-plate elements, and can be added to long-spanning roof and floor members, such as hollow-core slabs.

1.3 Research Significance

Strengthening RC with NSM-FRP is becoming a well-established technique, with proven and diverse applications. This technique has garnered significant attention for over a decade, and has allowed the empirical models suggested by design guidelines to become increasingly refined. Canadian and American guidelines recommend a maximum allowable strain in the NSM reinforcement, to account for the premature debonding mechanism that is common to NSM-strengthened members. American guidelines further suggest general limits for tensile and compressive stresses under service and ultimate loads. However, there is currently a lack of research in the area of PC strengthened with NSM reinforcement. Yost et al. (2007) suggest that both internal and external reinforcement ratios influence the flexural behaviour of a strengthened specimen under service and ultimate loads. This study investigates the effect of the prestressing ratio and the FRP strengthening ratio on the serviceability and ultimate limit states. Further investigation is required to verify that these limits are applicable to common building elements found in everyday construction, such as HC slabs. Attention should be given to HC slabs as they have a unique cross section that restricts the layout of externally bonded laminates. Furthermore,

very limited research has been dedicated to the combined effect of NSM-FRP reinforcement and in-service openings on the flexural behaviour of PC. Building codes provide little recommendations to accommodate an opening in RC that is still in service. It is possible there exists a better alternative than the built-up steel sections currently used today.

1.4 Project Scope

Strengthening HC slab elements is studied through the experimental testing of common flexural members widely used in industry today. The scope of this research program is limited to the flexural strengthening of simply-supported precast prestressed HC slabs with and without openings using near-surface mounted carbon fibre reinforced polymer (NSM-CFRP) strip reinforcement. The depth, length and level of prestressing are selected so that the slab's shear capacity is sufficiently high to ensure a flexural failure mode is the governing mode of failure. CFRP composites are chosen for their high-strength characteristics and lower deformability, which better compliment the characteristics exhibited by PC under service and ultimate load conditions. FRP strip reinforcement is considered as it has emerged as the leading alternative for reinforcement suitable with the NSM strengthening technique. The longitudinal voids unique to HC slabs confine the layout of the NSM reinforcement to web locations only. Openings are restricted to the two most general locations along a structural element, namely at mid-span, and along the shear span between the support and loading points. Test specimens represent different combinations of the aforementioned characteristics, ultimately intended to understand the flexural behaviour and to expand on existing design guidelines. The analysis will be based on crack pattern, deflection, reinforcement strain, ultimate strength, and failure mode.

1.5 Objectives

The objectives of this research are derived from the need to strengthen prestressed HC slabs under service conditions, which for a multitude of possible reasons are structurally deficient in strength. An opening cut into an existing slab already in service naturally decreases the strength of the slab, particularly if the opening interrupts the internal pretensioned steel tendons. This creates a strength-deficiency. It is therefore essential that any strengthening technique under consideration must completely restore the slab's original design capacity, and must also enhance the capacity to accommodate any superimposed load associated with the equipment for which the opening is intended to service.

The core objectives of this research program are as follows:

1) Determine the influence of NSM-FRP reinforcement on the flexural behaviour of prestressed concrete members.
2) Investigate the strength and serviceability effects of adding in-situ openings to prestressed hollow-core slabs.
3) Employ the NSM-FRP technique to restore the strength-deficiency of prestressed slabs containing an opening, and provide a net increase in ultimate flexural capacity as compared to the original design.
4) Provide design recommendations to predict the structural behaviour of strengthened and unstrengthened prestressed HC slabs with and without openings.

1.6 Methodology

An experimental program was developed to achieve the aforementioned research objectives. The experimental program includes the design, construction, and testing of 11 full-scale precast prestressed HC slab specimens. These test prototypes are categorized into three series, each of which studies a unique parameter intended to address this research's core objectives. The specimens are simply supported and subject to four-point bending in order to analyze the flexural response and predict the behaviour at the serviceability and ultimate limit states.

Series I Addresses Objective 1 by studying the effects of NSM-FRP on prestressed concrete. Series I compares specimens specifically to investigate the strengthening reinforcement ratio parameter. This parameter is tested against two internal reinforcement ratios. This series considers three different strengthening reinforcement ratios. The desired outcome is a correlation between the amount of strengthening reinforcement and the net improvement in strength and serviceability behaviour for a given internal reinforcement ratio.

Series II Addresses Objective 2 by studying the strength and serviceability effects of openings in prestressed HC slabs. Series II specimens are used to investigate the cut-out or service-opening parameter. This series considers openings with constant dimensions in two significant locations along the longitudinal axis of the slab specimens: centered at mid-span, within the flexural zone; and between the loading point and the end support, along the shear span. The desired outcome is an understanding of the strength and serviceability effects that adding an opening will have on prestressed concrete elements.

Series III Addresses Objective 3 by employing the NSM-FRP technique to restore a strength-deficiency, as well as provide a net increase in flexural capacity caused by the provision of an opening. Series III compares specimens to investigate the strengthened opening parameter. This series will use a constant strengthening reinforcement ratio to strengthen openings at two different locations along the slab's longitudinal axis. FRP laminates will be used to strengthen constant-sized openings along the flexural span, as well as the shear span. The desired outcome is to determine the viability of the NSM-FRP technique for reinforcing openings in prestressed plate members.

Objective 4 will be addressed based on the experimental results of Series I, II and III specimens. Design guidelines will be suggested based on the conclusions of this thesis.

1.7 Structure of Thesis

The following is a brief description of the contents of each chapter in this thesis:

Chapter 1 – The first chapter introduces the methodology that went into creating this research project, including the process implemented to identify and define a relevant problem, the stages of gathering information, executing the experimental program, and outlining the results and conclusions. It also presents a supporting argument for the significant of this research program, as well as the objects this study accomplishes.

Chapter 2 – This chapter reviews the literature published to date on the flexural theories of conventional, prestressed, and FRP reinforced concrete. It also provides essential background

information on openings in reinforced concrete and the near surface mounted technique and the various design parameters associated with developing an effective strengthening solution.

Chapter 3 – This chapter outlines the experimental program conducted at the University of Manitoba including the material properties, specimen strength capacities, test configuration, and instrumentation layout.

Chapter 4 – This section presents the results of the experimental program, including the effects that the various parameters have on: load-deflection behaviour; strains in the concrete, steel, and FRP; crack patterns; and the ultimate capacity and mode of failure. These results are compared to available codes and standards.

Chapter 5 – The final chapter showcases the key findings from the analysis of the experimental work. Recommendations for future research are also presented as a follow-up to this study.

CHAPTER 2 – LITERATURE REVIEW

2.1 General

A state-of-the-art literature review was undertaken to collect information regarding the most recent advancements on the various design concepts required to conduct this study, namely: precast HC slab design, prestressed concrete, openings in RC slabs, FRP composite reinforcement, and strengthening techniques. A brief summary of the flexural theory pertinent to understand this thesis are presented for conventionally RC, PC, and FRP-RC; and also the disturbances caused by openings. According to GangaRao et al. (2007), there are five key design parameters which influence the flexural response of NSM-FRP RC sections: i) mechanical properties of the concrete, ii) size and shape of the section, iii) mechanical properties of the internal/external reinforcement, iv) the reinforcement ratio and its distribution along the cross section, v) the efficiency of the concrete/reinforcement bond. The aim of the literature review presented in this section is to explain the aforementioned design parameters chosen for this experimental program that addresses the research objectives stated in Chapter 1. The specified design parameters are explained in detail in the experimental program section, Chapter 3. It is

important to note that only the essential background literature is included in this section, while a more in-depth summary is presented in the Appendices.

The following sections highlight key flexural theories related to concrete reinforced with conventional steel, high-strength steel, and FRP composites. As there are significant differences in the structural behaviour between regular reinforcing steel, high-strength steel tendons, and FRP composite materials, the key mechanical properties of each material is discussed in ***Appendix A***. The NSM technique is a method of rehabilitation and has a large number of design variables which are presented to help the reader understand the reasoning for selecting the parameters for the experimental program. The NSM technique is further explained in ***Appendix B***. The following summaries are intended to familiarize the reader with the effects that different types of reinforcement pose on the flexural behaviour of RC elements, with respect to: ultimate capacity and mode of failure, stress-strain relationship, load-deflection response, and cracking behaviour. Obviously, significant attention is given to the flexural behaviour of RC strengthened with NSM-FRP.

2.2 Flexural Theory and Behaviour of Steel-Reinforced Concrete

An RC section, subjected to a bending moment and shear force, experiences a flexural behaviour that can be divided into three prominent stages: pre-cracking, post-cracking, and the constant moment stage. As the loading increases from zero a deformation is experienced by the member and is directly proportional to the applied load. This linear relationship is defined mainly by the stiffness of the uncracked concrete in the tensile region. This stage is termed the pre-cracking stage, or the elastic region, where the strains in the tensile and compression zones are fully

recoverable upon unloading. This stage is identified as Stage I on the following diagram. Figure 2.1 illustrates the typical load-deflection behaviour for a simply-supported RC section. GangaRao et al. (2007) suggests that the internal reinforcement ratio has a negligible effect on the behaviour of the member before cracking.

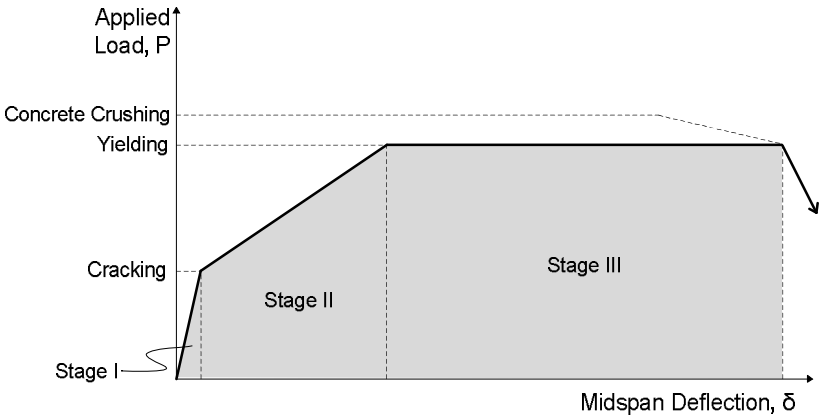

Figure 2.1: Load-Deflection Curve for Reinforced Concrete

The transition from stage I to Stage II is reached when the internal normal stresses exceed the tensile capacity of the concrete. Upon cracking, the stiffness of a section transitions from the gross moment of inertia to cracked moment of inertia. This moment of inertia is reduced to an effective stiffness (I_e) as a function of the ratio between applied moment and cracking moment. After cracking, the post-cracking stiffness is noticeably reduced, as illustrated by a decrease the slope of the load-deflection relationship (Stage II in Figure 2.1). Energy is released with each crack, causing a reduction in stiffness and a corresponding increase in flexibility and deflection. During this phase a concrete section experiences unstable crack formation and expansion. Tensile stresses are transferred from the concrete substrate to a stiffer element, typically the internal steel reinforcement. The superior tensile strength of steel provides reserve stiffness for the transformed section, allowing a member to sustain an increase in load-carrying capacity.

Wand and Salmon (1985) confirmed the assumption that the bond between internal reinforcement and a concrete substrate is ideal, and is strong enough to prevent any significant slip of the bars relative to the concrete during loading. This however is not the case for many externally-applied reinforcement schemes. In the latter case, the bond strength becomes a significant design parameter, essentially limiting the allowable capacity of the structural member. For a simply-supported member subject to flexural loading, cracking typically originates along the mid-span region where the bending moment is greatest. Flexural cracks develop at the tension face, and propagate vertically towards the neutral axis. If the flexural capacity is sufficiently large, inclined flexural-shear cracks develop along the shear span, near the loading points and the supports. At this stage deformations are recoverable until the steel reinforcement begins to yield.

As the tensile stresses reach the proportional limit the internal steel reinforcement exhibits a non-linear stress-strain relationship. The change in slope between Stage II and Stage III is the result of plastic deformations in the steel. The section is now in a plastic state, and the deformations are no longer recoverable. Once the full cross section of the steel reinforcement has yielded there is no additional strength to resist an increase in applied load; the section will continue to deflect with no further increase in load-carrying capacity. Loading the member beyond the moment-curvature yield limit will lead to secondary failure, manifested by the crushing of concrete in the compression zone. Reinforced concrete members can be designed for a tension, balanced, or a concrete compression failure mode. To take advantage of steels elastic-plastic behaviour, steel reinforced sections are typically designed to be under-reinforced to first achieve a tension failure, which ensures steel yielding before concrete crushing. This is a safety control as it allows large deflections and wide crack widths to warn of impending failure.

2.3 Flexural Theory and Behaviour of Prestressed Concrete

Prestressed concrete (PC) is the preloading of a structural element prior to the application of the design loads, for the purpose of enhancing its overall structural performance. According to Abeles and Bardhan-Roy (1981) the primary intention of PC is to apply a force to the concrete, effectively preloading the member so that cracking and deflection are recoverable to a higher degree. Figure 2.2 illustrates three prominent stages of the load-deflection relationship for PC subject to flexural loading. The three stages are similar to those experienced by conventionally reinforced concrete, albeit achieved at higher load levels. When compared to conventional RC, PC enhances the pre-cracking stiffness of the member, effectively delaying cracking and reducing the deformation. According to Nilson (1978), varying the level of compressive prestress can affect the number and width of cracks, and can also control the amount of deflection under service loads. Unlike RC, the serviceability state for PC is within Stage I, prior to any concrete cracking.

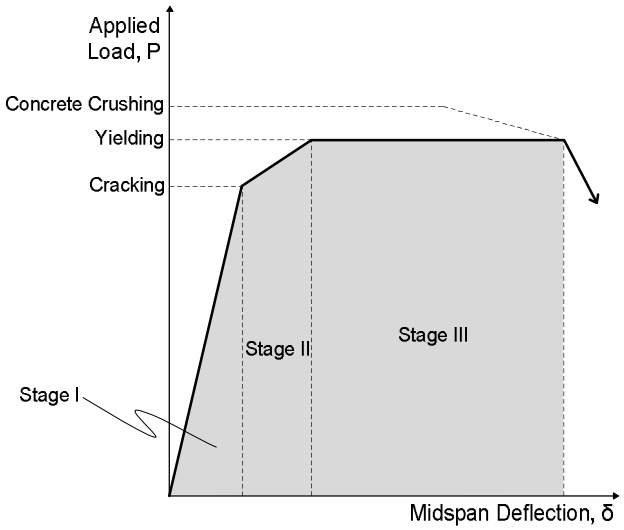

Figure 2.2: Load-Deflection Curve for Prestressed Concrete

For a typical RC section subject to bending, the tensile strength of the material is reached at a relatively low load. At this load, a crack will form along the tension face of the member since there is no restraint provided against the upward extension of the crack. Prestressed concrete however exerts an axial force that adds a compressive stress normal to the cross section, which is superimposed with the tensile stress created during flexural bending to reduce the amount of tensile stress experienced by the section, effectively increasing the cracking load and reducing deflection. To maximize the preloaded compressive stress pretensioned strands are positioned eccentrically from the centroid of the section, typically within the tensile zone of a flexural member. Once the tensile strength of the concrete has been exceeded and the section experiences cracking, PC behaves in a similar manner to RC.

The improved durability associated with PC is a major advantage. The possibility of avoiding cracks is particularly important for structures subject to aggressive chemical environments. In addition, the use of high-strength steel allows for significantly less internal reinforcement to achieve the same ultimate capacity, thus allowing a reduction in cross section. High-strength steel produces an enhancement to the flexural strength while allowing the use of shallower sections, which makes prestressed elements ideal for longer spans. PC slabs are widely used as floor and roof members. Since PC slabs are so common it is very likely that these building elements will undergo in-service modifications during their life-cycle. For example, openings are commonly added to accommodate intake/exhaust ducts along industrial building roofs, or utility conduits along parking garage floors.

2.4 Flexural Theory and Behaviour of FRP-Reinforced Concrete

The behaviour of FRP-reinforced concrete (FRP-RC) sections differs from those reinforced with conventional steel reinforcement. FRP composites subjected to pure axial tension stresses exhibit linear stress-strain behaviour up to failure without any yielding characteristics. As a result, a tension failure of FRP-RC sections is sudden and brittle, and should therefore be avoided. Compression failure offers a more favourable response, as the ductility of concrete crushing is employed to provide greater warning of impending failure. ACI 440.1R (2006) requires FRP-RC sections be designed for a primary compression failure, and should provide high reserve strength to carry loads beyond the design loads. Bakis et al. (2002) declare that serviceability considerations such as deflection and crack width usually govern when designing with internal FRP reinforcement. Code limitations are satisfied by over-reinforcing the section, typically resulting in redundant reserve strength. According to GangaRao et al. (2007), an FRP-RC member loaded to its ultimate capacity should exhibit signs of failure apparent by concrete crushing around the loading points and spalling near the maximum moment region.

2.5 Flexural Theory and Behaviour of EB/NSM-FRP Strengthened Concrete

This section presents only the general theory and behaviour of strengthened members, and as such applies to both externally bonded (EB) and near-surface mounted (NSM) structural elements. Upon initial loading of an EB/NSM-FRP strengthened member, the behaviour in the service range is very similar to that of an unstrengthened member. Al-Mahmoud et al. (2009) and Hassan and Rizkalla (2004) determined that FRP strengthening has an insignificant effect on the pre-cracking stiffness and cracking load, and is predominantly dependent on the concrete section

dimensions and the moment of inertia. Similar to previous load-deflection graphs, the flexural response for FRP strengthened concrete is divided into three or four prominent stages, depending on the mode of ultimate failure.

Stage I is similar to that of a conventionally reinforced section. Again, Stage II begins after cracking where the tensile stresses are effectively transferred from the concrete to the surrounding reinforcement. In this case the reinforcement includes the internal steel as well as the externally bonded laminates via the epoxy matrix. Compared with an unstrengthened member, the addition of external reinforcement provides greater stiffness, as shown by the increase in slope of the curve after cracking. The stresses and strains increase linearly until the internal steel reinforcement begins to yield. The strain distribution for a beam strengthened with NSM-FRP is illustrated in Figure 2.3.

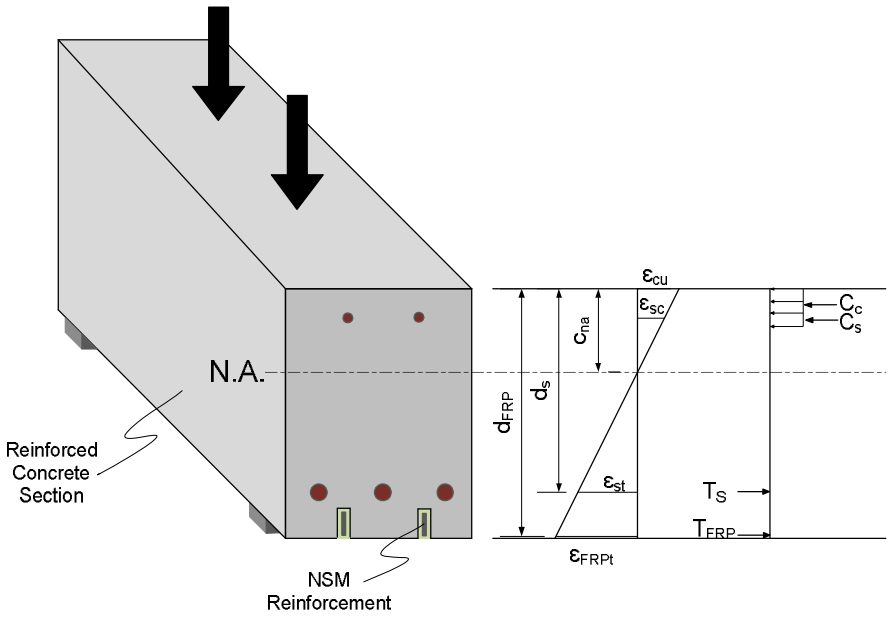

Figure 2.3: Cross-Sectional Strain Distribution

Stages III and IV significantly diverge from conventionally reinforced concrete behaviour. The flexural behaviour of a strengthened specimen near the ultimate state is governed by the type and sequence of failure. GangaRao and Vijay (1998) performed an experimental investigation which outlined two additional and distinct modes of failure common for RC strengthened with bonded laminates: FRP rupture and premature debonding. Most subsequent studies experienced variations of these two modes of failure (El-Hacha and Rizkalla, 2004; Hassan and Rizkalla, 2004; De Lorenzis and Teng, 2006; Yost et al., 2007). The flexural behaviour of an RC member strengthened with FRP composites whose mode of failure is by FRP rupture is illustrated by the load-deflection curve in Figure 2.4. As a reference, the behaviour of a conventionally reinforced element (hatched line) is placed on the graph to distinguish the effects of the FRP reinforcement.

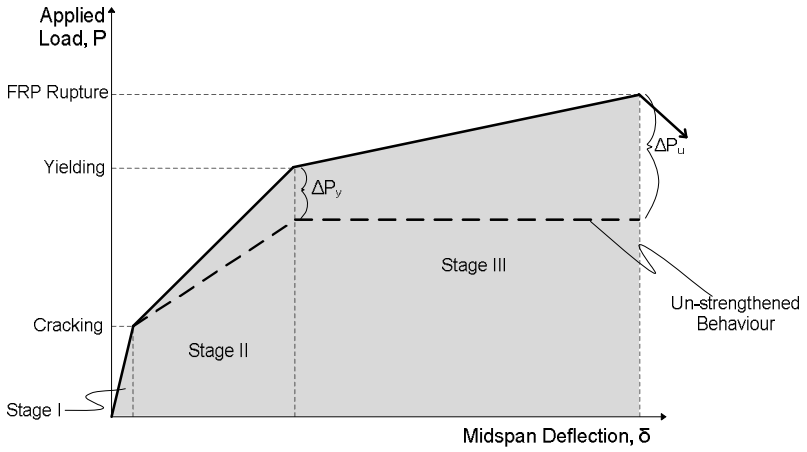

Figure 2.4: Load-Deflection Curve – FRP Rupture Mode of Failure

If the bond strength is sufficiently high the structural member may fail by rupture of the FRP laminates after steel yielding; as shown in the figure above. However, if high tensile stresses develop within the epoxy and surrounding concrete at an early stage in the loading process it is likely the laminates will detach from the concrete substrate. Early debonding is the most

common mode of failure with FRP-strengthened RC elements. The flexural behaviour of an RC member strengthened with FRP composites whose mode of failure is by FRP debonding is illustrated by the load-deflection curve in Figure 2.5.

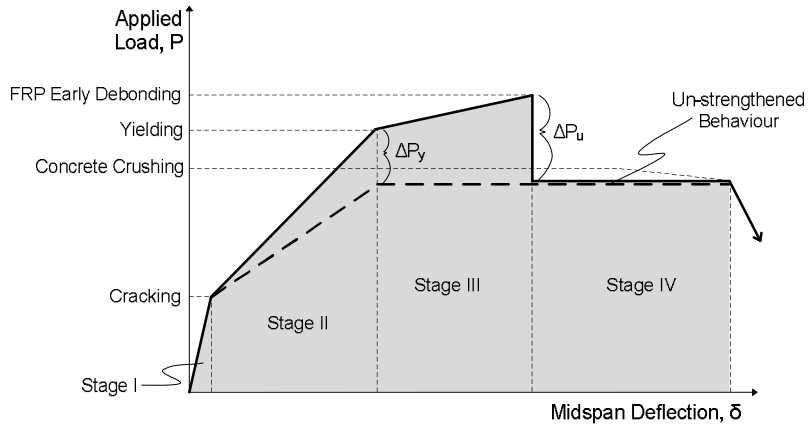

Figure 2.5: Load-Deflection Curve – Premature Debonding Mode of Failure

After debonding, Hassan and Rizkalla (2004) suggest a member will continue to behave as if no strengthening system were present. According to the recommendations outlined by ACI 440.2R-08, rupture of the external FRP laminates, secondary concrete crushing, and primary concrete crushing failure modes are generally acceptable when designing strengthened elements. The guideline requires that adequate ductility be achieved by allowing the internal steel reinforcement to yield, followed by rupture or concrete crushing.

Tensile and shear stress concentrations are important to consider as excessive stresses lead to sudden debonding failure of the NSM laminates. Hassan and Rizkalla (2004) suggest that since adhesive materials have different elastic moduli compared with concrete, there is an abrupt change in the tensile stress at each material interface, causing a disturbed region with a high stress concentration. As loading is applied to a structural element tensile stress develops along

the length of the reinforcement at two main interfaces: the concrete-adhesive interface, and the laminate-adhesive interface, as shown in Figure 2.6. This tensile stress is referred to as bond stress throughout the thesis. Design parameters which influence bond stress include: the tensile strength of the concrete and epoxy, groove dimensions, laminate surface characteristics, embedment length, and proximity to internal reinforcement (De Lorenzis and Teng, 2006).

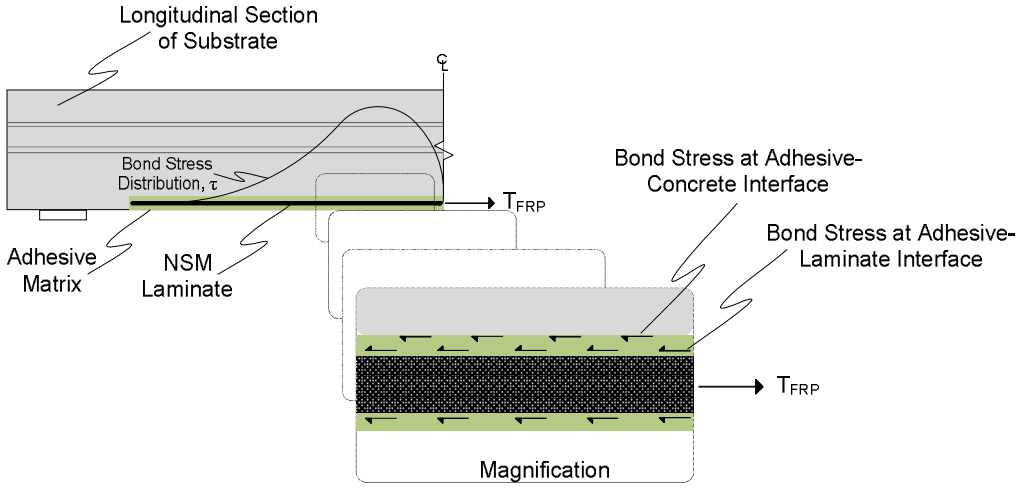

Figure 2.6: Distribution of Bond Stress

To date, few studies (El-Hacha and Rizkalla, 2004; Yost et al., 2007) have experienced full development strength of the FRP laminates. FRP rupture is not a common mode of failure due to inherent and limiting weakness of the bond strength between the FRP laminate, the epoxy binding matrix, and the concrete substrate. Hassan and Rizkalla (2004) and De Lorenzis and Teng (2007) identified four common modes of debonding failure: failure at the laminate-adhesive interface (pull-out), failure at the concrete-adhesive interface (within the concrete substrate), failure at the concrete-adhesive interface (within the adhesive matrix), and epoxy split failure. Figure 2.7 illustrates these common modes of debonding failure.

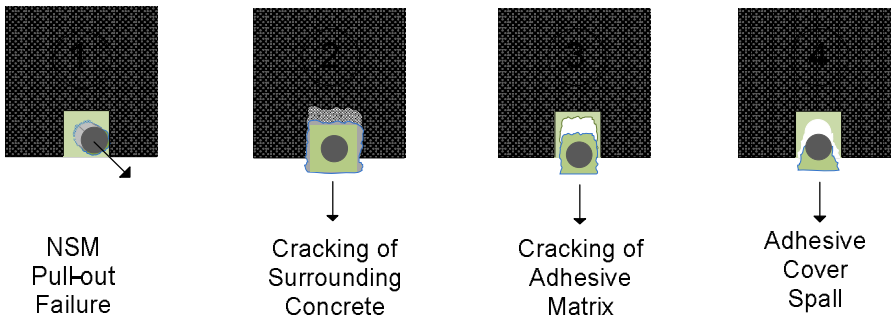

Figure 2.7: Sketch of Debonding Failure Modes

2.6 History of Strengthening Reinforced Concrete in Flexure

Traditional methods used to strengthen RC structures involve epoxy-bonding steel plates along the soffit of a member to enhance its tensile resistance. According to a synopsis of strengthening methods by Bakis et al. (2002), rigid steel plates require a significant amount of equipment and machinery to customize and manipulate on site. In addition, when subject to outdoor or aggressive chemical environments the steel is susceptible to corrosion, and is likely to deteriorate the bond strength of the composite system. Another common strengthening technique discussed by the authors is concrete or steel jacketing, whereby the strengthening material is mechanically placed or bonded around the structural element. A notable advantage of this technique is the reduced risk of the element failing due to early debonding of the strengthening reinforcement. The disadvantages of this technique include: the increase in cross section and dead load, the potentially undesired change in stiffness of the member, and the significant installation time and labour. In recent years, there has been extensive research on the subject of strengthening techniques to repair and enhance the capacity of reinforced concrete structures using non-corrodible fiber reinforced polymer (FRP) composite materials. One such method which is garnering much attention is the near-surface mounting (NSM) technique. NSM strengthening of RC structural elements is achieved by cutting longitudinal or transverse grooves along the

tension face of existing concrete, and inserting FRP bars or strips in an orientation that resists these tensile stresses. Since this reinforcement is not fully encased in concrete, studies have shown that premature and sudden debonding failure prevents the FRP laminates from reaching their full tensile strength, thus limiting the effectiveness of this strengthening technique. GangaRao et al. (2007) noted that strengthening reinforced concrete with FRP laminates is suitable for: repairing deteriorated beams and slabs to restore their strength and stiffness; limiting crack width under increase service loads; designing new structural elements with depth limitations; enhancing the flexural and shear strength of in-service members; and providing confinement for concrete columns.

2.7 Comparison Studies of EB-FRP versus NSM-FRP

El-Hacha and Rizkalla (2004) conducted an experimental comparison on simply supported T-beams internally reinforced with deformed steel bars as tensile and compression reinforcement, and strengthened with NSM-FRP and EB-FRP. The objective of the study was to investigate the affect that 'bond configuration' has on the flexural response of identical test specimens. The experimental parameter was the laminate material, namely CFRP and GFRP strips. Firstly, the load-deflection relationship when using CFRP laminates indicated that both EB- and NSM-CFRP strips exhibited similar pre-cracking behaviour, and contributed to an increase in stiffness up to the yielding point. After yielding however, the NSM-CFRP provided a much greater increase in stiffness than the EB-CFRP when compared to the control beam. After steel yielding the cracks continued to propagate and widen at an increased rate; and it was determined that EB-CFRP strips were much more susceptible to debonding at this stage than identical strips embedded into the flange soffit. The beam outfitted with EB- and NSM-CFRP strips experienced

an increase in strength of 25% and 99%, respectively, compared with the unstrengthened control beam.

An identical study was conducted with EB- and NSM-GFRP strips. The load-deflection relationship indicated that both EB- and NSM-GFRP strips exhibited similar pre-cracking behaviour. After cracking the laminates effectively contributed to an increase in the stiffness of the beam, as compared with the control specimen. The stiffening effect continued until the EB-GFRP separated from the concrete substrate due to adhesive shear failure at the concrete-adhesive interface. At failure, the EB-GFRP strips slipped instantaneously from the end anchorages. A more ductile behaviour was observed in the beam strengthened with NSM-GFRP. The increase in ultimate strength at failure of the EB-GFRP strips and the NSM-GFRP strips were approximately 28% and 85%, respectively. Thus, regardless of the type of laminate, the NSM strengthening technique is more effective than the EB strengthening technique.

2.8 Flexural Behaviour of Slabs Strengthened with EB-FRP

Al-Rousan et al. (2012) performed an experimental investigation on eight simply-supported one-way RC slabs (2440 × 600 × 125 mm) that were strengthened with CFRP composite sheets, and subject to four-point bending. The objective of the study was to determine the effects that the strengthening ratio and the layout of CFRP laminates have on the flexural behaviour of the concrete specimens. Increasing the strengthening ratio effectively increased the ultimate capacity of the strengthened specimens. Increasing the number of CFRP sheets resulted in a corresponding decrease in the strains experienced by the tensile reinforcement. The yield load increased dramatically for high levels of strengthening. The authors used the deflection ductility

index to comment on the ductility of the specimens. This ductility index is determined from the ratio of mid-span deflection at ultimate and the mid-span deflection at yielding of the tension steel. Results show that strengthened specimens experience lower ductility than the control specimen. The layout of the CFRP sheets was also varied to determine the effect of bond surface on the flexural response of the strengthened specimens. It was determined that as the contact area between the laminates and the concrete substrate increased, there was a corresponding improvement to the stiffness of the member, for any given strengthening ratio. Interestingly, increasing the bonded area provided little improvement over the same number of sheets with a smaller bonded area. The study concluded that CFRP laminates can inhibit the growth of large cracks by redistributing the stresses, and may lead to the development of several smaller cracks at smaller spacing.

2.9 Flexural Behaviour of Openings in Reinforced Concrete

It is well established that openings in RC members constitute as a discontinuity, generating a disturbed region with a non-linear stress distribution. Examples of D-regions are areas near concentrated loads and supports, corbels, deep beams, joints, openings, and other discontinuities. St. Venant's principle suggests that the localized effect of a disturbance is a maximum at the location of the disturbance, and gradually decreases to zero approximately one member depth from the point of the disturbance. In order to mitigate unnecessary effects caused by these high stress concentrations it is important that any opening is placed a minimum distance of two slab depths away from any support or loading point. Tan and Zhao (2004) performed an experimental investigation which concluded that cracking around openings (particularly at the corners of rectangular openings) decrease the localized stiffness, and the strength capacity of the member.

ACI 318M-11 Section 13.4 and CSA A23.3-04 Clause 13.10.10 provide very general guidance when considering how to design openings in reinforced concrete. The codes mention that any size of opening shall be permitted within a slab system as long as the member with the opening achieves the strength required to resist the effects of the governing factored load combination. Typically, the structural integrity at an opening can be maintained by providing a similar amount of reinforcement around the opening that would normally pass through the opening. Adding an opening to a reinforced concrete system that is already in service must be able to meet the strength and serviceability requirements of the original design.

Seliem et al. (2008) investigated the effects of using CFRP to strengthen openings on five in-service RC slabs (3353 × 3000 mm) located in a multi-storey concrete structure. The parameter under consideration included the type of strengthening system: EB-CFRP laminates, EB-CFRP laminates with CFRP anchors, and the NSM technique. The slabs were tested under 4-point bending along the short direction to create a constant moment region, and subject to cyclic loading. Testing concluded the addition of a 610 × 610 mm opening at the center of the slab reduced the ultimate strength by 18%, and resulted in a noticeable reduction in slab stiffness. At a service load of 65% of the ultimate load, the deflection was 60% greater when compared with the control specimen. Adding NSM-CFRP strips restored 10% of the slab's capacity, with no noticeable increase in stiffness. Strengthening the slab using externally bonded strips improved the capacity by 6%, and reduced the ultimate deformation due to early debonding of the laminates. At 65% of the ultimate load, the EB-CFRP laminates with end anchorages effectively improved the stiffness of the slab system, resulting in a reduced deflection of 28% for the un-strengthened slab with an opening. The EB laminates with CFRP anchors proved to be the most

effective, completely restoring the slabs capacity and preventing complete detachment of the laminates.

Smith and Kim (2008) conducted an experimental study consisting of six simply-supported one-way RC slabs with rectangular 900 × 1200 mm openings, strengthened with EB-FRP strips. The specimens were 3400 mm long, 160 mm deep, with a clear span of 3200 mm. The main variable under consideration is the location of the applied loading. The externally bonded FRP strips were positioned on either side of the opening in the direction of primary bending. The amount of FRP strengthening for two of the specimens was calculated based on the interrupted amount of steel reinforcement in the opening region. Initial cracking was preceded closely by diagonal cracks originating from each corner of the opening and propagating to the nearest corner of the slab. As the applied load increased, additional flexural cracks formed closer to the loading points, followed by cracking along the shear span. Testing revealed no significant difference between the crack patterns of the strengthened specimens and the corresponding control specimen. However, the location of the loading was determined to influence the cracking behaviour. When the loading is concentrated along the outer bands, the cracking is restricted from propagating to the ends/corners of the slab, and instead is directed towards the nearest edge. This crack pattern results in localized debonding of the laminates. Conversely, if the load is applied only along the cut-out band, the cracks are free to propagate to the corners of the slab, creating a more wide-spread area of debonding for the laminate, expediting the delamination mode of failure. All strengthened specimens experienced a flexural failure, initiated by FRP delamination. For each of the FRP-strengthened slabs, debonding occurred in the concrete, not at the epoxy or FRP interface, indicating a strong bond between the laminates and the concrete substrate.

Enochsson et al. (2007) performed an experimental and numerical evaluation of 11 RC two-way slabs strengthened with CFRP sheets. The simply-supported slabs had side lengths of 2600 mm and a thickness of 100 mm. A system of airbags was used to evenly distribute the applied loading along the slab surface. The two main variables considered are the size of the opening and the layout of the CFRP reinforcement. Two different sizes of openings located at the center of the slabs were considered to be 850 × 850 mm and 1200 × 1200 mm. The CFRP sheet configurations were as follows: parallel to each side of the cut-out only, diagonal at each corner only, and a combination of the first two configurations. The study followed a simplified approach to determine the amount of CFRP reinforcement required to replace the amount of steel reinforcement interrupted by the opening. The area of steel was converted to an effective area of CFRP. Experimental results suggest for the homogeneous control slab cracking initiated at mid-span in the form of flexural cracks.

For slabs with openings, cracking initiated at the corners of the openings and propagated diagonally. It was noted that crack widths were smaller for slabs strengthened with CFRP strips. Slabs with large and small openings exhibited a nearly identical load-deflection behaviour and failure mechanism as the homogeneous control slab. The only significant difference is that the slabs with openings failed at a lower level of deflection. This behaviour suggests that two-way slabs are able to effectively redistribute the internal stresses around a service opening. The ultimate deflection of the slabs with openings strengthened with FRP exhibit a similar ductile response as those with unstrengthened openings. On average, adding FRP does little to improve the ductility of the system. All slabs with openings strengthened with CFRP strips exhibit an increased load-carrying capacity. Regardless of the size of the opening, the CFRP strips oriented at 45 degrees at the opening corners provided the smallest capacity enhancement, followed by

strips placed parallel to each of the opening edges. The most effective strengthening layout was a combination of both layouts, where the strips are placed parallel to each opening edge, as well as diagonally at the opening corners. Strengthening openings with CFRP is most effective on slabs with larger openings. Regardless of the orientation of the FRP strips, the capacity enhancement was 20-50% greater for the larger opening compared to the smaller opening. A possible explanation for this is that slabs with a smaller opening have better capacity to redistribute the internal stresses before the steel yields.

Tan and Zhao (2004) conducted an experimental and analytical investigation of eight one-way RC slabs (2400 × 2700 mm) with openings, strengthened with EB-FRP systems. The parameters include the opening size, opening location, and the strengthening layout. The experimental results found that with the addition of an opening, the cracking load decreased by the ratio of opening width to slab width. The post-cracking stiffness for the homogeneous control slab exhibited a stiffer response, as it did not contain an opening. For the slab with an opening, cracking originated at the corner of the opening and propagated transversely in an inclined direction along the edges of the opening. The ultimate load capacity of the homogeneous slab was approximately 65% larger than a similar slab with an opening. Providing CFRP strengthening effectively restored the stiffness of the slabs, comparable to the homogeneous control specimen. The CFRP strengthened slabs achieved an ultimate load comparable to the homogenous control specimen, and exhibited a brittle failure in contrast to a more ductile behaviour for the unstrengthened slabs. Based on an analytical study the effect of the opening length is less sensitive than that of the opening width, since the load is carried by longitudinal bands bordering the opening. When the opening size is small, normal flexural failure will govern, but for slabs with larger openings, failure was initiated by CFRP debonding from a

significant crack location and may result in a flexural or shear mode of failure. The study also concluded that placing externally bonded laminates parallel to the transverse edge of the opening is not as effective as placing them diagonally at the opening corners.

2.10 NSM Design Parameters

2.10.1 Overview

Research papers published to date (De Lorenzis and Nanni, 2002; El-Hacha and Rizkalla, 2004; De Lorenzis and Teng, 2007; Yost et al., 2007; Al-Mahmoud et al., 2009) suggest that the effectiveness of an NSM-FRP strengthening system is dependent on several key parameters. This literature review section will not explain all the design variables, but instead will only focus on those pertinent to the experimental work included in this thesis. The reader is strongly encouraged to reference ***Appendix B*** for an extensive summary and explanation of the research done to date on each of the following NSM design parameters:

1. Substrate geometry, condition, and physical properties (Section B.1)
2. Type of NSM-FRP and its mechanical properties (Appendix A, Sections 2.10.2 & B.2)
3. Internal reinforcement type and ratio (Section 2.10.3)
4. Groove width (Section 2.10.4)
5. Groove depth (Section 2.10.4)
6. Groove surface topography
7. Embedment length (Section B.3)
8. Laminate spacing (Section B.4)

9. Edge distance (Section B.5)
10. Laminate orientation (Section B.6)
11. Resin type and mechanical properties (Section B.7)

Figure 2.8 and Figure 2.9 illustrate a typical plan and cross-section view, respectively, for a hollow core slab outfitted with NSM-FRP bars and strips. The nomenclature and symbols used throughout this thesis are illustrated in the following diagrams, and are explained in the List of Notations section found on *page xvi*, at the beginning of this thesis.

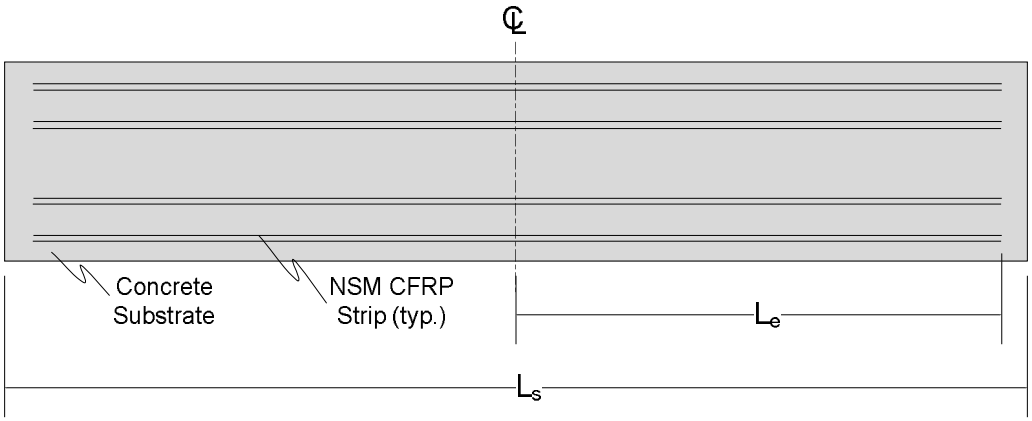

Figure 2.8: Hollow-Core Slab Outfitted With NSM-FRP

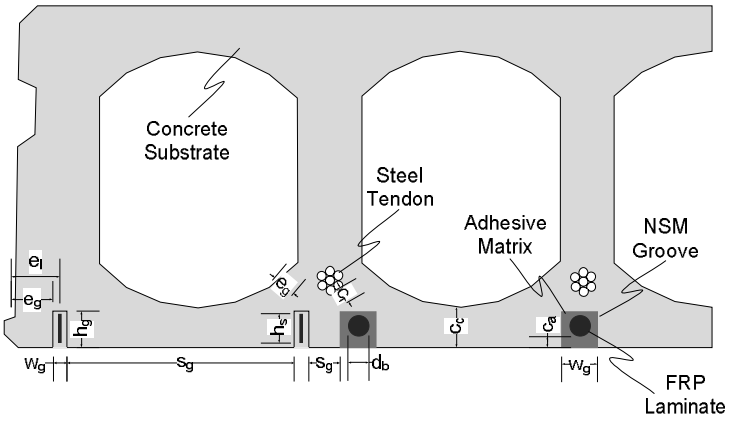

Figure 2.9: Illustration of NSM Nomenclature

2.10.2 Laminate type

El-Hacha and Rizkalla (2004) conducted an experimental comparison on simply supported T-beams strengthened with NSM-CFRP and GFRP strips. The objective of the study was to investigate the effect that laminate type has on the flexural response of strengthened beams with identical axial stiffness. To achieve a similar stiffness the authors chose five GFRP thermoplastic strips as equivalents to two CFRP strips. As expected, the load-tensile strain behavior of the NSM-CFRP strips was similar to the NSM-GFRP strips. The beams strengthened with two CFRP strips failed by rupture of the laminates at an ultimate tensile strain of 1.12 – 1.34%. Whereas the beams strengthened with five GFRP strips failed at a much higher ultimate tensile strain of 2.2%, by concrete crushing. Eventually the beam experienced laminate debonding at the concrete-epoxy interface. The large ultimate strain capacity of the GFRP material resulted in large shear stress concentrations at the concrete-epoxy interface. Beams strengthened with GFRP yield much larger deformations at failure as compared to identical beams strengthened with CFRP reinforcement. Experimental load-deflection behaviour indicated that RC beams strengthened with CFRP strips produced a greater increase in member strength and stiffness compared to beams strengthened with GFRP strips.

2.10.3 Internal reinforcement ratio

Yost et al. (2007) studied the behaviour of full-scale steel reinforced beams strengthened in flexure with NSM-CFRP strips subject to four-point bending. The experimental variables were three different ratios of internal steel reinforcement. The significance of the conducted study was to determine the effect of steel reinforcement on the strengthened flexural response, based on the resulting yield and ultimate strengths, flexural failure modes, and member ductility. When

compared with the control beam, the strengthened specimens with internal reinforcement ratios of $0.68\rho_b$, $0.47\rho_b$, and $0.34\rho_b$ exhibited 11%, 18%, and 29%, respectively. The investigation indicated that the beams with the largest reinforcement ratio compared to the balanced reinforcement ratio ($0.68\rho_b$) strengthened with a single CFRP strip exhibited no significant increase in stiffness after steel yielding. For beams with the same internal reinforcement ratio strengthened with two CFRP strips the increase in ultimate strength for the beams with ratios of $0.68\rho_b$, $0.47\rho_b$, and $0.34\rho_b$ exhibited 23%, 44%, and 61%, respectively. This concludes that the improvement in strength is inversely proportional to the ratio of internal steel reinforcement. The same relationship was found to be true for the increase in yield loads.

Hassan and Rizkalla (2004) conducted a finite element analysis of a simply supported steel reinforced T-beam, strengthened with a single NSM FRP bar, and subject to 3-point bending. The internal tensile steel reinforcement ratio varied from 0% to 2.0% within the maximum moment region. The objective of the analysis was to model the redistribution of tensile stresses between the internal steel and NSM-FRP reinforcement after reaching the yielding load. The analysis indicated that decreasing the internal reinforcement ratio correlates to an increase in bond stresses surrounding the NSM laminate, which leads to a decrease in the ultimate bond failure load. Intuitively, equilibrium requires the full transmission of additional tensile stresses to neighboring FRP reinforcement. The NSM system is particularly susceptible to high bond-stress concentrations after the internal steel has yielded, corresponding to the stage where any additional load is transferred to the reinforcement with a higher axial stiffness, namely the NSM-FRP reinforcement and its surrounding bond matrix. Analytical results from Hassan and Rizkalla (2003) suggests that increasing the internal steel reinforcement ratio shifts down the neutral axis depth and increases the debonding load. Increasing the amount of tensile reinforcement will

increase the stiffness of the section, thus for a given applied load the induced bond stresses were reduced. In the absence of internal reinforcement (ρ_s = 0%), doubling the NSM reinforcement ratio nearly doubles the ultimate failure load of the section. As the reinforcement ratio is increased, the ultimate failure load of the specimen will increase, however, the contribution of the NSM reinforcement is significantly reduced. Results conclude that for high internal reinforcement ratios the contribution of the NSM-CFRP strips is significantly reduced.

2.10.4 Groove size

El-Hacha and Rizkalla (2004) conducted an experimental investigation of simply supported T-beams strengthened with GFRP strips embedded into grooves of varying sizes. The research objective was to study the distribution of bond stresses along the groove at the concrete-epoxy interface. A single beam was strengthened with several GFRP strips embedded into grooves of varying width. Ultimate failure was a result of debonding of the concrete surrounding the grooves. The smaller grooves experienced significant cracking before the larger groove. It was found that for a given loading the bond stress was larger for the grooves with a smaller surface area. Thus, increasing the groove size will reduce the bond stress at the concrete-epoxy interface and may result in an increase in debonding load.

Galati and De Lorenzis (2009) carried out a series of experimental pull-out tests on single deformed FRP bars embedded into reinforced concrete blocks. At one end, a tensile force was applied to the FRP coupon, the mid-section of the bar was embedded into a rectangular groove over a length of 180 mm, and the other end was free to easily measure any slip during loading. The parameter under consideration is the groove size, specifically, width-to-depth ratios equal to

0.75, 1.00 and 1.25. The significance of the research is to measure the effect of varying the width for a given depth on the development of bond stresses along the FRP reinforcement. Results indicate that as the width-to-depth ratio increases, the number of visible cracks in the concrete surrounding the groove decreases significantly. Enlarging the groove caused a decrease in concrete tensile stresses, thus reducing the likelihood of cracking. Increasing the ratio from 0.75 to 1.00 or 1.25 resulted in no observable cracking in the surrounding concrete. Enlarging the groove size from 0.75 to 1.00, or from 1.00 to 1.25 resulted in a 39% and 8% increase in bond strength, respectively. The authors concluded that small ratios lead to early cracking of the surrounding concrete, which in turn leads to small lateral displacements of the concrete and epoxy, reducing the confining pressure around the NSM reinforcement. Theoretically this ratio can be increased until the tensile stresses in the concrete are not critical to decrease the confining pressure, and thus no further increase in bond strength will be realized by increasing the width-to-depth ratio. In general, increasing the groove size will yield an increase in the average bond strength until it no longer becomes the governing mode of failure.2.11 Hollow Core Slabs Strengthened with FRP Materials

El-Gabbas et al. (2009) performed an experimental and analytical investigation on the structural behaviour of precast prestressed hollow core concrete slabs, strengthened in flexure with CFRP laminates. The variables considered were the FRP strengthening ratio, external restraints, and a comparison study between near surface mounted reinforcement and externally bonded reinforcement. The significance of the study is to report on the flexural behavior of strengthened hollow core slabs. The researchers observed that crack propagation for all slabs exhibited traditional flexural patterns for specimens subjected to four point bending. The strengthened specimens however, experienced a higher number of cracks with smaller spacing. The cracks

widths were also smaller compared to those experienced by the control specimen. This indicates that the bond strength between the NSM system and prestressed concrete was sufficient to produce a significant stiffening effect, such that crack width and spacing decreased, and crack distribution became more uniform. The strengthening reinforcement had relatively no effect on the cracking load. The authors suggested that the laminates provided a negligible influence on the gross moment of inertia of the slab's cross section. The deformability of the strengthened slabs increased proportionally to the increase in capacity, when the mode of failure was a flexural failure. When the mode of failure was by flexural-shear, the deformability of the section was dramatically reduced, despite a significant increase in flexural capacity. The study concluded the NSM technique is favorable for strength improvements as well as seismic applications were deformability must be similar to or enhanced with respect to the original design. When restricting the mode of failure to pure flexure, the improved stiffness generated by strengthening prestressed slabs makes the NSM technique attractive for designs governed by serviceability requirements. The authors were able to predict the deflection of a strengthened slab with reasonable accuracy using numerical integration of the moment curvature relationship.

2.12 Code/Guideline Review – NSM Technique

2.12.1 CSA S806-12

According to the CSA/S806-12 standards (CSA 2012), Design and Construction of Building Structures with Fiber-Reinforced Polymers, any structural component to be strengthened with surface-bonded FRP is required to support the specified un-factored loads without any strengthening. When analysing a structural member, the design must consider three states of the

structure: the existing structure prior to strengthening, the structure after strengthening with the FRP fully effective, and the structure after strengthening with the FRP no longer effective. The CSA design requirements cover a limited number of specific structural concrete elements, including: beams, columns, walls, masonry beams, fully grouted masonry columns, masonry walls, and composite steel-concrete beams. The component most applicable to the scope of this study is the reinforced concrete beam. To apply the NSM technique a minimum clear concrete cover of 20 mm is required, otherwise the technique is not recommended. The code suggests using the strain compatibility approach to calculate the moment resistances, assuming that the strain in all reinforcement and concrete is directly proportional to the distance from the neutral axis; perfect bond exists between the concrete, steel, and FRP composites; and the maximum strain in the compression fiber is assumed to be 0.0035. For NSM FRP reinforcement, the maximum tensile strain is not to exceed 0.007. The Code requires the following flexural failure modes be considered for the ultimate limit state: crushing of the concrete in compression before rupture of the FRP or yielding of the reinforcing steel; and yielding of the steel and/or rupture of the FRP in tension followed by concrete crushing. The following modes of debonding failure are recommended to be considered: shear/tension failure of the concrete substrate in the vicinity of the FRP cut-off point (anchorage failure or concrete cover separation); and debonding of adhesive bond line due to vertical section translations caused by cracking (delamination). For surface-bonded FRP strengthening systems, the Code specifies that the anchorage length beyond the point where no strengthening is required is calculated with the following equation. Where l_a is the anchorage length, n_F is the number of plies, E_F is the modulus of FRP, t_F is the thickness of a single ply, and f'_c is the concrete design strength.

$$l_a = \sqrt{\frac{n_F E_F t_F}{\sqrt{f'_c}}} \qquad \textbf{Equation 2.1}$$

The minimum specified anchorage length is 300 mm, unless it is suitably anchored. The Code specifies that for one-way slabs, the flexural strength is to be determined as a beam of unit width, and the maximum spacing of the FRP laminates is three times the slab thickness, or 400 mm.

2.12.2 ACI 440.2R-08

The following presents a summary of relevant strengthening requirements as outlined by the ACI 440.2R-08 Guide for the Design and Construction of Externally Bonded FRP Systems for Strengthening Concrete Structures (ACI Committee 440, 2008). The ACI Committee establishes strengthening limits to avoid collapse of the structure as a result of debonding or other failure mode of the FRP system due to damage, vandalism, or other causes. The existing strength of the structural member should be sufficient to resist the following load. Where ϕ is the FRP strength reduction factor, S_{DL} is the effects due to dead loads, and S_{LL} are the effects due to live loads.

$$(\phi R_n)_{existing} \geq (1.1S_{DL} + 0.75S_{LL})_{new} \qquad \textbf{Equation 2.2}$$

The design flexural strength should always be equal to or greater than the factored moment. The code recommends that an additional strength reduction factor, ψ_f, be applied to the flexural contribution of the FRP reinforcement to account for the different failure modes associated with FRP strengthening, namely delamination. The flexural strength for FRP-strengthened concrete

members reinforced with mild steel or bonded prestressing tendons can be determined based on strain compatibility, internal force equilibrium, and the controlling mode of failure. According to the ACI code, to prevent a crack-induced debonding failure mode, the effective strain in the FRP laminates should be limited by the following equation. Where ε_{fd} is the debonding strain of an EB-FRP laminate, and ε_{fu} is the design rupture strain.

$$\varepsilon_{fd} = 0.41\sqrt{\frac{f'_c}{nE_f t_f}} \leq 0.9\varepsilon_{fu} \qquad \textbf{Equation 2.3}$$

The ACI code states that for NSM-FRP applications, the debonding strain (ε_{fd}) can vary from $0.6\varepsilon_{fd}$ to $0.9\varepsilon_{fd}$, depending of factors such as member dimensions, steel and FRP reinforcement ratios, and surface roughness of the FRP laminate. The committee recommends the use of $\varepsilon_{fd} = 0.7\varepsilon_{fu}$. To achieve this debonding strain, the bonded length should be greater that the development length.

There are several serviceability limits imposed on prestressed concrete strengthened with NSM-FRP. According to the ACI code, adequate ductility is achieved if the strain in the prestressing steel is a minimum of 0.013. In the case the strain cannot be achieved, a strength reduction factor is imposed to account for a less ductile mode of failure. The proper strength reduction factor is determined from the following equation. Where ε_{ps} is the strain in the prestressed reinforcement at nominal strength.

$$\phi = \begin{cases} 0.9 \; for \; \varepsilon_{ps} \geq 0.013 \\ 0.65 + \dfrac{0.25(\varepsilon_{ps} - 0.010)}{0.013 - 0.010} \; for \; 0.010 < \varepsilon_{ps} < 0.013 \\ 0.65 \; for \; \varepsilon_{ps} \leq 0.010 \end{cases}$$ **Equation 2.4**

Under service conditions, a prestressed member strengthened with externally bonded FRP laminates should avoid inelastic deformations. The compressive stress in the concrete should be limited to 45% of the compressive strength, and the stress in the steel under service load should be limited by the following equations. Where $f_{ps,s}$ is the stress in prestressed reinforcement under service loads, f_{py} is the specified yield strength of prestressing tendons, and f_{pu} is the specified tensile strength of prestressing tendons.

$$f_{ps,s} \leq 0.82 f_{py}$$ **Equation 2.5**

$$f_{ps,s} \leq 0.74 f_{pu}$$ **Equation 2.6**

The development length, over which the bond capacity of the FRP laminate is developed, is determined by the following equation:

$$l_{df} = \sqrt{\frac{nE_f t_f}{\sqrt{f_c'}}}$$ **Equation 2.7**

The ACI code specifies that for NSM round bars the minimum size of groove should be 1.5 times the bar diameter. For grooves with a rectangular bar or strip, the minimum groove size should be $3.0a_b \times 1.5b_b$, where a_b is the smallest bar dimension. In addition, the clear groove spacing should be a minimum of twice the depth of the NSM groove, for the purpose of avoiding any overlap of the tensile stresses generated around the NSM laminates.

CHAPTER 3 – EXPERIMENTAL PROGRAM

3.1 General Design Concept

The test specimens considered in this investigation include 11 prestressed concrete slabs, subject to four-point bending, and are experimentally tested to failure under monotonic loading conditions using a stroke-controlled hydraulic actuator. The test specimens have a constant thickness of 203 mm, total length of 5,000 mm, and are simply supported over a clear span of 4,850 mm. Each specimen is reinforced with high-strength low-relaxation steel tendons. Each specimen was designed to simulate a typical full-scale prestressed roof or floor member. The slab specimens are designed according to Canadian standard CSA/A23.4-04 (2004) and CSA S6-06 (2006) to satisfy both flexural and shear requirements. All test slabs have a shear span-to-depth ratio (a_v/d_s) of 11.4. This ratio, in conjunction with a relatively low level of prestressing reinforcement was selected so that the ultimate strength of the specimens would be controlled by a flexural mode of failure, and to avoid any predominant shear-failure behaviour. For those specimens strengthened with NSM-CFRP, the strengthened capacity was determined using strain compatibility in accordance with the CSA S806-12 (2012) and ACI 440.2R-08 (2008).

Strengthening ratios were selected to ensure the anticipated theoretical strengthened flexural capacity was well below the shear capacity, again, to avoid a premature shear mode of failure. Two, four and eight strips achieved modest but significant strengthened capacities, which also maintained NSM reinforcement symmetry along the specimen cross section. The voids are shaped with a combination of straight vertical sides, and a curved profile along the top and bottom of the void. Although different void profiles are available, they are unique to each precast supplier. Figures 3.1 and 3.2 illustrate the nominal cross-section for the HC slab test specimens.

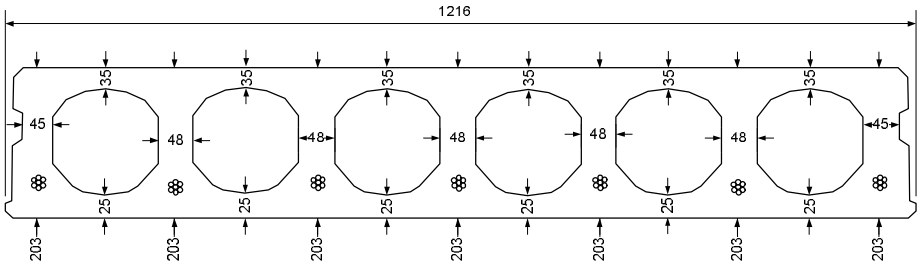

Figure 3.1: Nominal Hollow-Core Slab Dimensions

Figure 3.2: Typical Hollow-Core Slab Cross Section

The specimens were fabricated by a local precast concrete supplier. To replicate the quality of materials used in local construction projects no modifications were made to the concrete mixture, formwork, high-strength steel, or methods of prestressing. ***Appendix C*** contains detailed

AutoCAD drawings of the reinforcement configuration, loading points, support locations, opening layout, and strengthening details.

The nomenclature for the specimens follow the label format I-1-S0-NO, where the roman numeral 'I' denotes the test series (I, II, III), the '1' denotes the level of prestressing (1 or 2), the 'S0' denotes the number of strips used to strengthen the member (S2, S4, S8), and the lettering 'NO' indicates the presence and type of in-situ opening (NO: No Opening; FO: Flexural span Opening; SO: Shear span Opening).

3.2 Experimental Program Synopsis

3.2.1 Overview

The tested parameters in this experimental investigation are the internal prestressing reinforcement ratio, the NSM-CFRP reinforcement ratio, an opening along the flexural span, and an opening along the shear span. These design parameters are divided into three different test series, employed to address the project's four primary objectives. The following experimental program synopsis is organized to clearly present the results which address the main objectives, as outlined in Chapter 1.

3.2.2 Test series I

Series I prototypes are designed to provide a correlation between the amount of strengthening and the expected capacity increase. Three strengthening reinforcement ratios are considered: 0.000457, 0.000913, and 0.001830. Also, to expand the breath of the application of these results,

two levels of internal reinforcement ratios are considered: 0.00274 and 0.00336. The two parameters investigated in this series include the internal prestressing reinforcement ratio and the NSM-CFRP strengthening ratio. The internal reinforcement ratios were selected based on common codes used as roof and floor elements for typical industrial and commercial applications; as well as slab availability by the local HC slab supplier. Low prestressing ratios were selected so that tension failure was the governing mode of failure, which also provided a suitable gap between the theoretical flexural capacity and the theoretical shear capacity. Seven prestressed tendons were cast into each specimen, approximately 45 mm from the soffit of the member. This single tendon layout was selected to ensure that a CFRP strip would always be placed beneath an internal strand to determine the effect of stress concentrations due to the presence of additional tensile reinforcement; also to ensure that a single strand would be removed when adding an in-situ opening to the slabs in Series II and Series III. In accordance with the NSM layout specifications suggested by ACI 440.2R-08 (2008), the minimum dimensions of the grooves for rectangular laminates were three times the strip width, and approximately 1.5 times the strip height. However, the effective spacing between strips for specimen I-1-S8-NO was only 25 mm, instead of the recommended two times the groove depth (approx. 45 mm). Since the webs of HC slabs are maximum 45 mm wide, it is not possible to achieve the recommended spacing without compromising the concrete cover to the NSM groove. For this reason the clear edge distance of four times the depth of the NSM groove could not be achieved either. The groove dimensions and layout are similar for all test series. See ***Appendix C*** for complete details and dimensions.

Series I specimens are designed to address Objective 1, which is to determine the flexural influence of strengthening prestressed concrete with NSM CFRP strips. This series compares the

flexural response of seven of the total 11 specimens: I-1-S0-NO, I-1-S2-NO, I-1-S4-NO, I-1-S8-NO, I-2-S0-NO, I-2-S2-NO, and I-2-S4-NO. The tested parameters in Series I include:

1) NSM-CFRP strengthening reinforcement ratio (0.000457, 0.000913 and 0.001830)
2) Internal prestressing steel reinforcement ratio (0.00274 and 0.00336)

The schematic in Figure 3.3 provides a simplified illustration of the analytical comparisons between specimens necessary to achieve a correlation between the strengthening ratio and the ultimate flexural capacity for slabs with various original design strengths. The numbers in brackets below each prestressing strand indicate the nominal diameter of the respective tendon. The figure illustrates the top and bottom viewpoint for each test specimen, indicating the orientation of the distributed line loads, the support locations, and the extent and number of steel tendon and NSM-CFRP strip reinforcement.

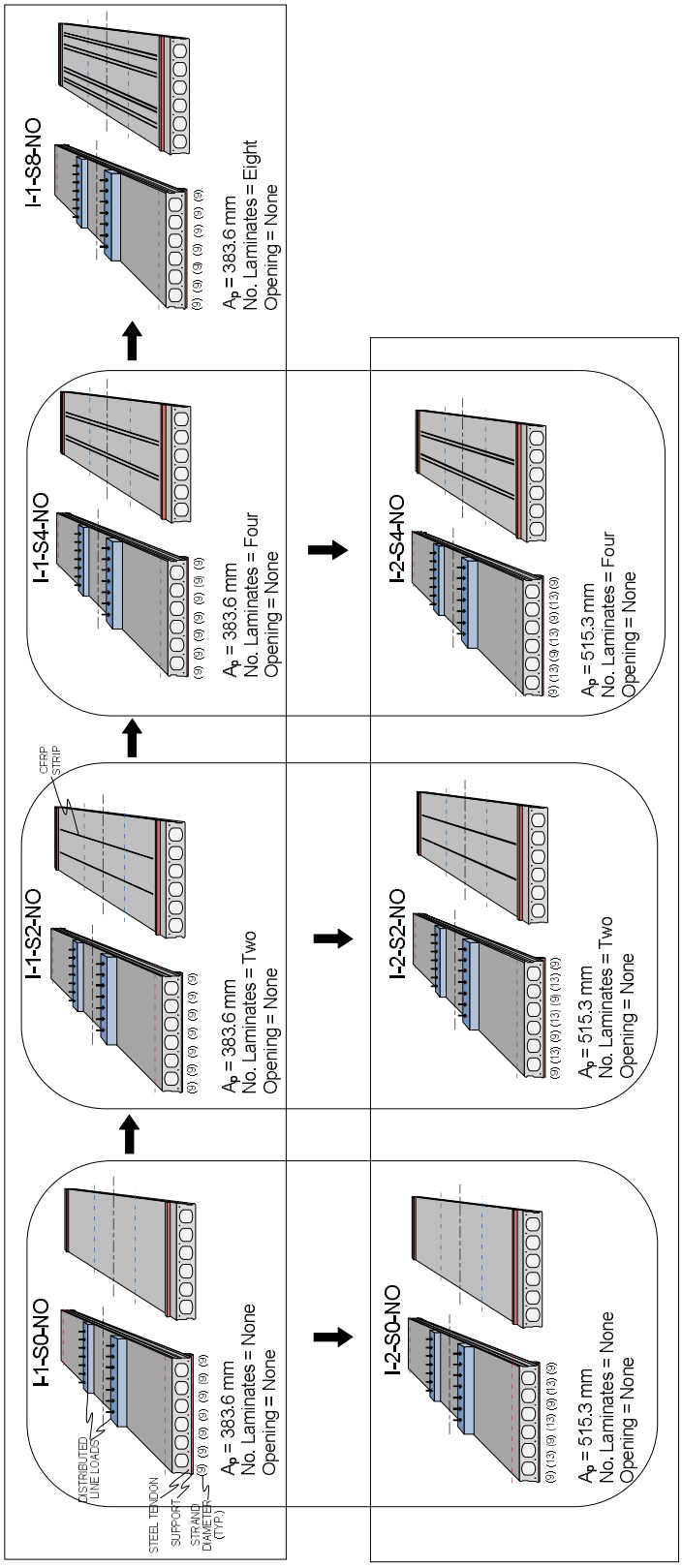

Figure 3.3: Illustrative Test Parameter Schematic - Series I

3.2.3 Test series II

Series II prototypes are designed to study the influence that in-service openings have on the flexural response of prestressed HC slabs. The test specimens are reinforced with the lower level of internal prestressing reinforcement. All design concepts are similar to Series I specimens except the openings. Two locations of openings were selected to obtain a general understanding of the effect that opening location has on the flexural response of the test specimens. An opening size was selected based on common fractions of the width of the simply supported slab element. The ratio of the opening was selected to be 0.25 b × 0.5 b, representing the transverse dimension and the longitudinal dimension, respectively, where b is the width of the HC slab element. The resulting opening dimensions are 308 × 600 mm. The opening locations along the slab profile are dictated by several design constraints, namely: mechanical unit specifications, functionality obstructions, and flexure or shear capacity constraints. For this reason two main opening locations were selected to generally represent design possibilities. An opening was placed in the flexural zone, at mid-span along the constant moment region. The second location was selected to be along the shear span. Research has shown that stress concentrations and disturbed regions develop approximately one slab depth from loading points, supports, and openings. Therefore the opening along the shear span was placed two slab depths away from the loading point to allow the stress disturbances caused by the loading point and the opening to dissipate and avoid superimposition and premature/undesired failure modes.

Series II test specimens are designed to address Objective 2, which is to investigate the strength and serviceability effects of adding in-situ openings to PC-HC slabs. This series compares the flexural response of three of the total 11 specimens; I-1-S0-NO, II-1-S0-FO, and II-1-S0-SO. In

this case two new series II specimens are being compared to the original control specimen, I-1-S0-NO, as described in the previous section. The tested parameters in Series II include:

1) An opening along the mid span (flexural critical) of the slab element
2) An opening along the shear span of the slab element

The schematic in Figure 3.4 provides a simplified illustration of the comparisons between specimens necessary to determine the effects of adding openings at various locations along the simply supported span as compared with an unaltered control specimen.

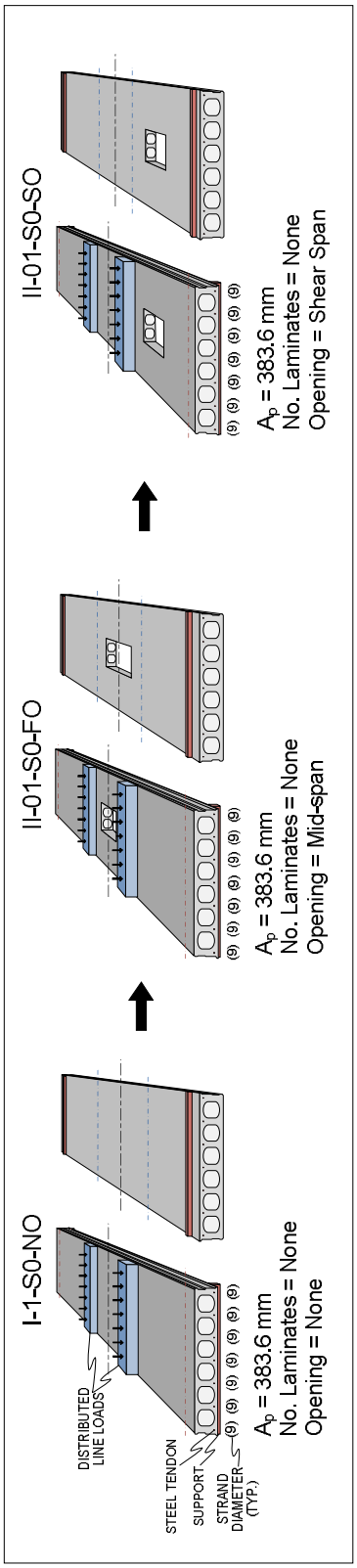

Figure 3.4: Illustrative Test Parameter Schematic - Series II

3.2.4 Test series III

Series III prototypes were designed to incorporate the test results generated from Series I and Series II specimens. This series investigates strengthened openings along the flexural and shear spans, with identical layouts to those chosen for Series II specimens. An opening placed within the flexural span reduces the compression area and interrupts a pretensioned tendon, effectively reducing the flexural capacity by a yet undetermined amount. Strengthening a specimen with an opening and comparing the flexural response to a specimen without an opening will indicate how the stress concentrations around the disturbed area impact the surrounding internal and external reinforcement and failure mechanism. Similar to the previous parameter, an opening along the shear span will produce a different impact on the flexural response. This parameter will reveal the loss of shear capacity, and the effectiveness of a flexural strengthening system on restoring the lost capacity. The lowest strengthening reinforcement ratio was selected to avoid an undesirable shear mode of failure. To ensure a flexural response, two CFRP strips were selected, yielding a strengthening reinforcement ratio of 0.000457.

Studies have shown that the presence of openings result in the formation of cracks longitudinal to the axis of the slab. Stress concentrations developed at the corners of slabs produce a component tensile strain which initiates cracks that propagate at approximately a 45 degree angle from the corners of the opening. To resist this tensile stress, two NSM-CFRP strips are added in the transverse direction. As explained in Chapter 2, the optimal orientation of the crack control reinforcement should be placed so that the long-axis of the reinforcement is perpendicular to the 45 degree crack emanating from the corners of the opening. The relatively short width of these specimens however does not provide sufficient development length when placed in a diagonal

orientation, but instead must be placed along the slab's transverse axis. In any orientation, these strips intersect the longitudinal strips, thus their orientation is limited to being bonded with their greater dimension along the soffit of the slab, as shown in Figures 3.5 and 3.6.

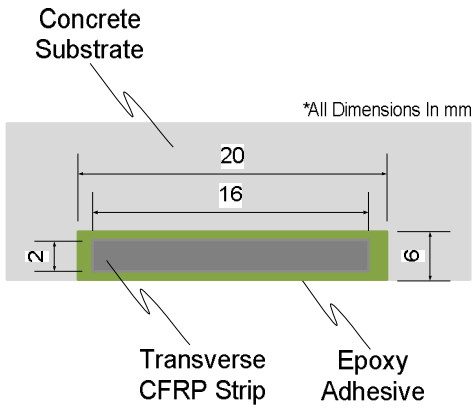

Figure 3.5: Transverse CFRP Strip Layout

Figure 3.6: Typical CFRP Groove Layout Around Opening

Series III test specimens are designed to address Objective 3, which is to employ the NSM-FRP technique to restore a strength deficiency, as well as provide a net increase in flexural capacity caused by the addition of an opening. The series compares five of the 11 specimens. Two new series III specimens are tested and compared to those unstrengthened specimens from Series I

and II; I-1-S0-NO, II-1-S0-FO, III-1-S2-FO, II-1-S0-SO, and III-1-S2-SO. The tested parameters in Series III include:

1) An opening along the flexural span of the slab element (Series II)
2) An opening along the shear span of the slab element (Series II)
3) Strengthening reinforcement (CFRP) ratio

The results of Series I and Series II are used to develop a correlation between the capacity enhancement generated by the provision of CFRP strips and the capacity reduction resulting from the addition of an in-situ opening, to determine the net increase/decrease of adding CFRP to an in-situ opening. The schematic in Figure 3.7 provides a simplified illustration of the comparisons required to generate the results necessary to address Objective 3.

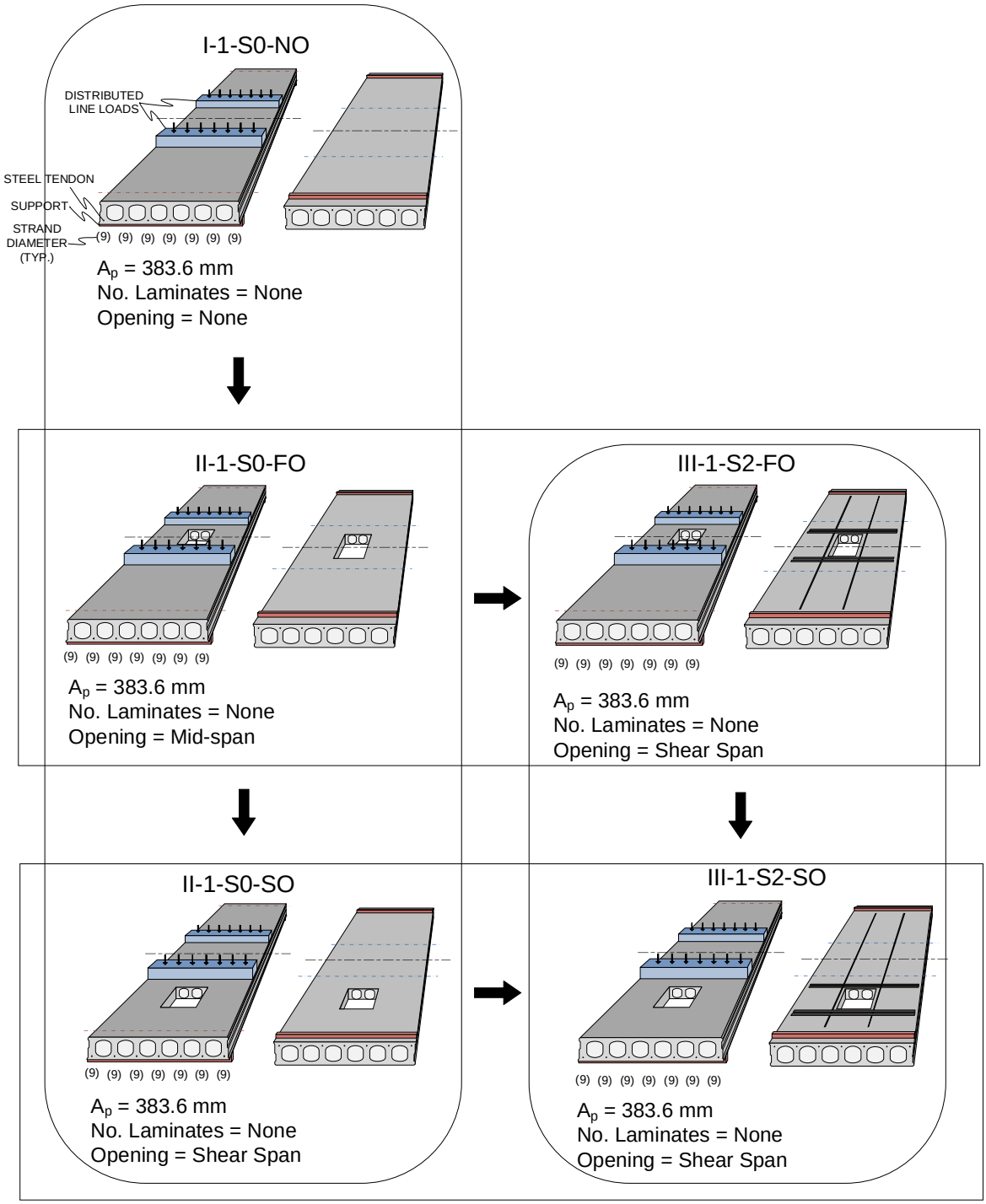

Figure 3.7: Illustrative Test Parameter Schematic - Series III

The experimental results acquired from Series I, II, and III will be analyzed and compiled to generate design recommendations to predict the structural performance of strengthened and unstrengthened HC slabs with and without openings.

3.3 Parameter Summary Matrix

Table 3.1 summarizes the experimental test parameters: internal reinforcement ratio, opening location, and number of CFRP laminates for each specimen.

Table 3.1: Test Series Matrix

	Specimen	Internal Reinforcement Ratio	Opening Location	Number of. CFRP Laminates
Series I	I-1-S0-NO	0.00274	None	None
	I-1-S2-NO			2
	I-1-S4-NO			4
	I-1-S8-NO			8
	I-2-S0-NO	0.00336		None
	I-2-S2-NO			2
	I-2-S4-NO			4
Series II	I-1-S0-NO*	0.00274	None	None
	II-1-S0-FO		Flexural span	
	II-1-S0-SO		Shear span	
Series III	I-1-S0-NO*	0.00274	None	None
	II-1-S0-FO*		Flexural span	None
	III-1-S2-FO			2
	II-1-S0-SO*		Shear span	None
	III-1-S2-SO			2

*Duplicate specimens used in more than one test series.

3.4 General Specimen Properties and Characteristics

Table 3.2 summarizes the nominal specimen properties such as the area of steel tendons, the prestressing ratio, the number of CFRP laminates, the area of the CFRP laminates, and the corresponding strengthening ratio. A complete list of all design details for each specimen can be found in Table D.1 in ***Appendix D***.

Table 3.2: Nominal Specimen Properties

	Specimen	Area Steel Tendons (mm^2)	Prestressing Ratio	Number of CFRP Laminates	Area of CFRP Laminates (mm^2)	Strengthening Ratio
Series I	I-1-S0-NO	383.6	0.00274	0	-	-
	I-1-S2-NO			2	64	0.000457
	I-1-S4-NO			4	128	0.000913
	I-1-S8-NO			8	256	0.001830
	I-2-S0-NO	515.3	0.00336	0	-	-
	I-2-S2-NO			2	64	0.000457
	I-2-S4-NO			4	128	0.000913
Series II	I-1-S0-NO	383.6	0.00274	0	-	-
	II-1-S0-FO		0.00299			
	II-1-S0-SO					
Series III	I-1-S0-NO		0.00274			
	II-1-S0-FO		0.00299			
	III-1-S2-FO			2	64	0.000457
	II-1-S0-SO			0	-	-
	III-1-S2-SO			2	64	0.000457

All strength calculations take into consideration the initial and long-term prestress losses. All prestress loss calculations can be found in ***Appendix E***. Table 3.3 specifies the strength characteristics for each specimen, including the flexural, cracking, and shear limits, as a result of

the addition of an opening or NSM-CFRP strips. Sample capacity calculations can be found in ***Appendix F***.

Table 3.3: Theoretical Specimen Strength Characteristics

	Specimen	No. CFRP Laminates	Opening Location	Flexural Capacity (kNm)	Cracking Moment (kNm)	Shear Capacity (kNm)
Series I	I-1-S0-NO	0	None	106.8	82.9	193.2
	I-1-S2-NO	2		123.4	81.5	191.5
	I-1-S4-NO	4		143.1	84.1	193.2
	I-1-S8-NO	8		179.5	84.7	
	I-2-S0-NO	0		139.2	104.8	214.1
	I-2-S2-NO	2		156.6	105.7	
	I-2-S4-NO	4		174.3	106.3	
Series II	I-1-S0-NO	0		106.8	82.9	193.2
	II-1-S0-FO		Flexural span	92.3	70.5	
	II-1-S0-SO		Shear span	106.8	68.8	152.5
Series III	I-1-S0-NO		None	106.8	82.9	193.2
	II-1-S0-FO		Flexural span	92.3	70.5	
	III-1-S2-FO	2	Flexural span	109.3	69.4	191.5
	II-1-S0-SO	0	Shear span	106.8	68.8	152.5
	III-1-S2-SO	2	Shear span	123.4	69.4	

3.4 Test Setup

The test setup selected for this research program followed the typical layout of a four-point bending test, chosen to maximize the constant moment region along the mid-span. Figure 3.8 illustrates the components used in the test procedure. A 5000-kN MTS hydraulic actuator was used to apply two monotonic concentrated loads centered over the mid-span of each specimen. The loads were transferred to the concrete specimens via a single longitudinal rigid steel spreader beam, stiffened with web stiffeners for superior rigidity; then through transverse rollers attached

to two transverse spreader beams, each subjected a distributed line load along the full width of the slab. Plaster was used between the transverse spreader beams and the slab to fill any surface irregularities, and to avoid a premature localized bearing failure.

Figure 3.8 - Test Setup

The end supports included full width steel bearing plates, 50 mm wide. The bearing plates were supported by rollers to allow movement during loading as the curvature of the specimen increased. One of the rollers was locked using a keeper plate. To ensure uniform contact between the supports and the concrete surface a thin layer of neoprene was affixed along the support surfaces. Figure 3.9 illustrates a simplified sketch of the test setup components as well as key dimensions.

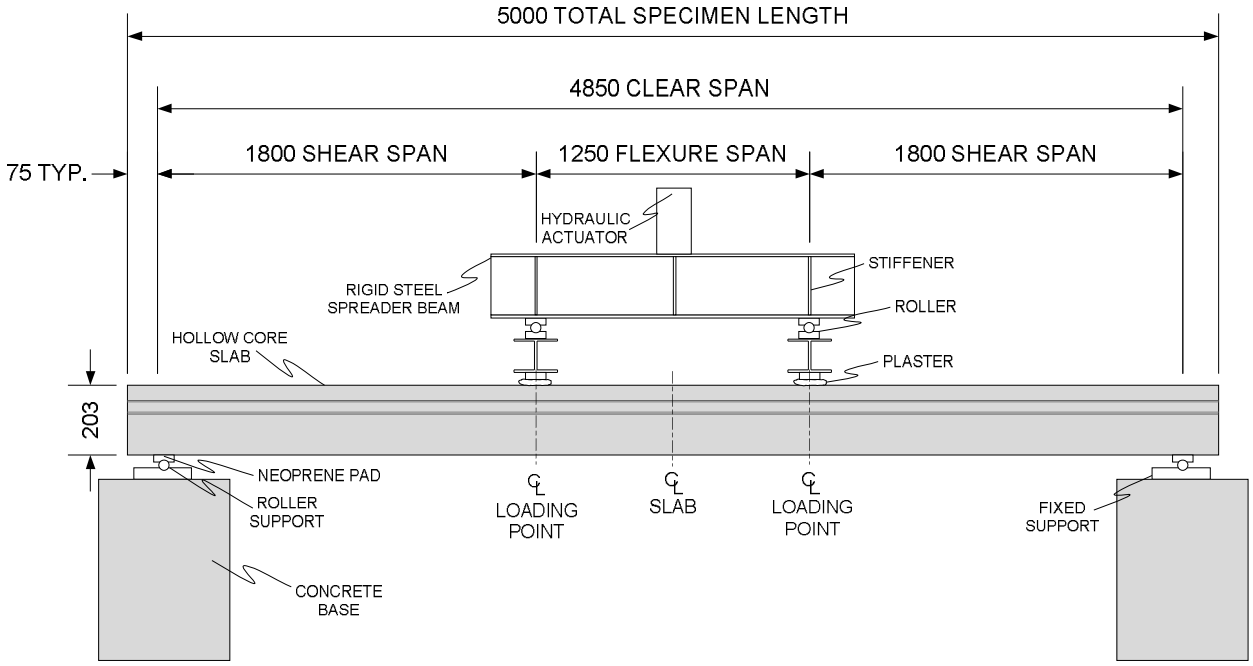

Figure 3.9 - Test Setup Schematic

Figure 3.10 illustrates a slab specimen resting on the simple supports. The plaster is allowed to harden prior to loading.

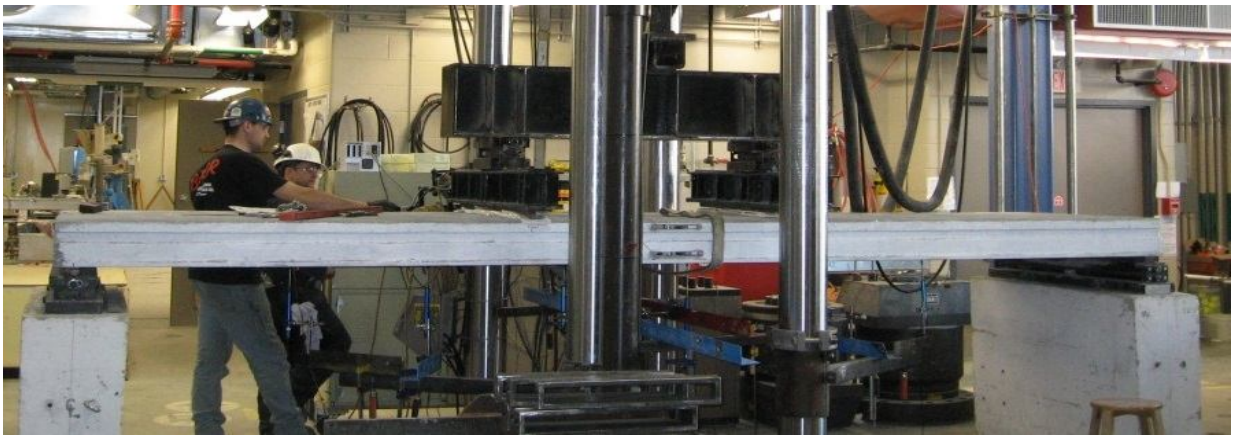

Figure 3.10 - Test Specimen Prior to Testing

AutoCAD drawings in ***Appendix C*** provide detailed plan and elevation views of each specimen as well as the loading configuration. Resting on the supports, the specimens have a clear span of 4,800 mm, divided into a pure bending middle span and two outside shear spans. The pure bending span is 1,250 mm, sufficiently long to allow for a conservative distance between the loading point and the nearest edge of the opening in the flexural zone. The distance between the edge of the opening and the loading point is 325 mm, 1.7 times the effective depth of the slab, and 60% greater than that recommended by research published in similar fields of study. The outer shear spans are 1800 mm long, to increase the shear capacity, and ensure that the flexural capacity is the limiting mode of failure.

3.5 Loading Procedure

The test procedure for all slab specimens was identical. Loading was applied monotonically at a stroke controlled rate of 1.0 mm/min until first cracking. After cracking the rate was increased to 2.0 mm/min until ultimate failure. Loading was interrupted intermittently approximately every 20 kN to delineate cracks with black marker and take photographs. Once 80% of the theoretical failure load was reached, loading was not stopped for the safety of those working around the specimens.

3.6 Instrumentation

The data collected is similar for each of the three series included in this experimental program. The instrumentation collected the following data: the deflection due to the externally applied load, the strain distribution along the internal steel tendons and NSM-CFRP strips, the

compressive strain near the top of each specimen, the cracking pattern, and the ultimate strength and mechanism of failure.

Deflection was monitored using linear variable differential transducers (LVDTs). The sensors were placed along the longitudinal profile of the slab specimens as shown in Figure 3.13. This layout is typical between all test series. The locations of the LVDTs were chosen to monitor the flexural behaviour near the edges of the openings. An LVDT was placed at the edge of each flexural and shear opening, and were symmetrical about the mid-span to ensure a deflection profile could be established along the slabs longitudinal axis. Figure 3.14 illustrates a typical LVDT setup prior to testing.

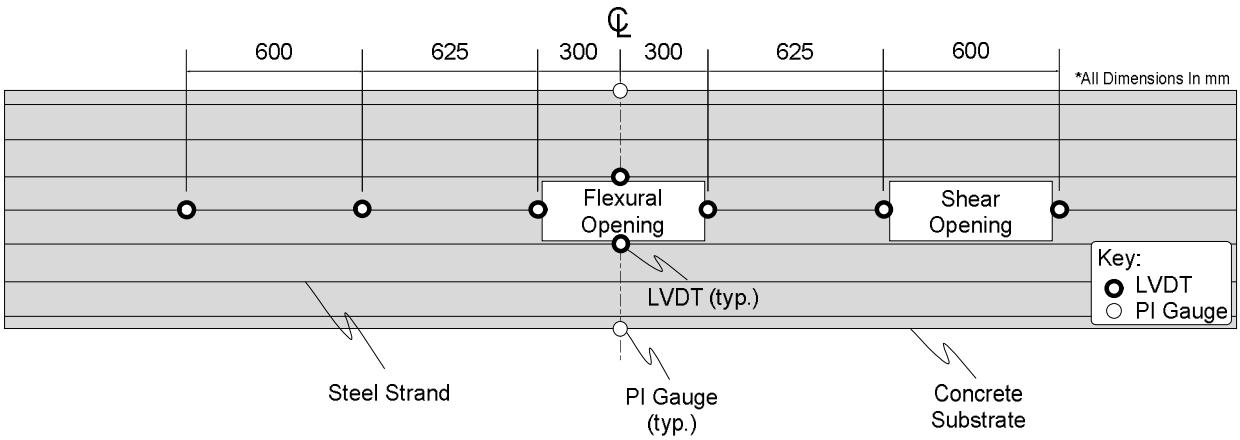

Figure 3.13: Instrumentation - LVDT Layout

Figure 3.14 - Instrumentation - LVDT Layout Image

Eight, 2-mm strain gauges were installed along the internal steel reinforcement to record the induced tensile strains. The sensors were placed at critical stress locations to monitor the flexural response of stress transfer between the internal steel tendons and the NSM-CFRP laminates. Sensors were strategically placed at the corners of the openings, in line with the likely crack pathway – 45 degrees from the corners of the openings. To install the steel strain gauges, the concrete cover over the tendon was carefully removed using a hammer drill and hand chisel. Care was taken to avoid contacting or damaging the prestressed tendons. The strain gauges were bonded directly onto the bottom surface of one wire of the 7-wire strand. Figure 3.15 illustrates the strain gauge layout along the internal steel tendons.

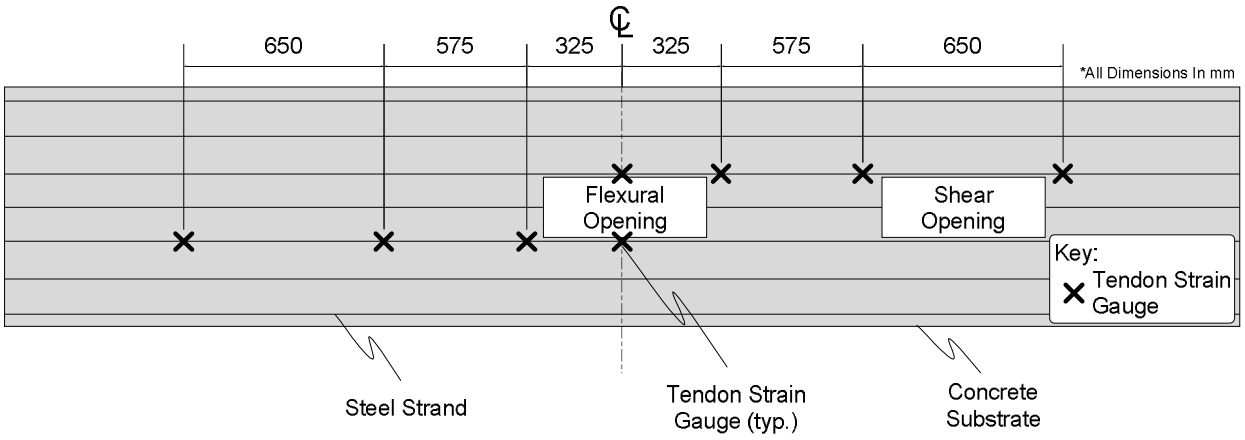

Figure 3.15: Instrumentation – Steel Strain Gauge Layout

Eight 6 mm strain gauges were installed along the NSM-CFRP reinforcement to record the induced tensile strains. Strain gauges were placed at all critical locations. The sensor layout along the CFRP laminates was identical to those along the steel tendons. Figure 3.16 illustrates the strain gauge layout along the longitudinal NSM-CFRP laminates for Series I and III

specimens. Figure 3.17 illustrates the strain gauges layout along the transverse NSM-CFRP laminates for Series III specimens.

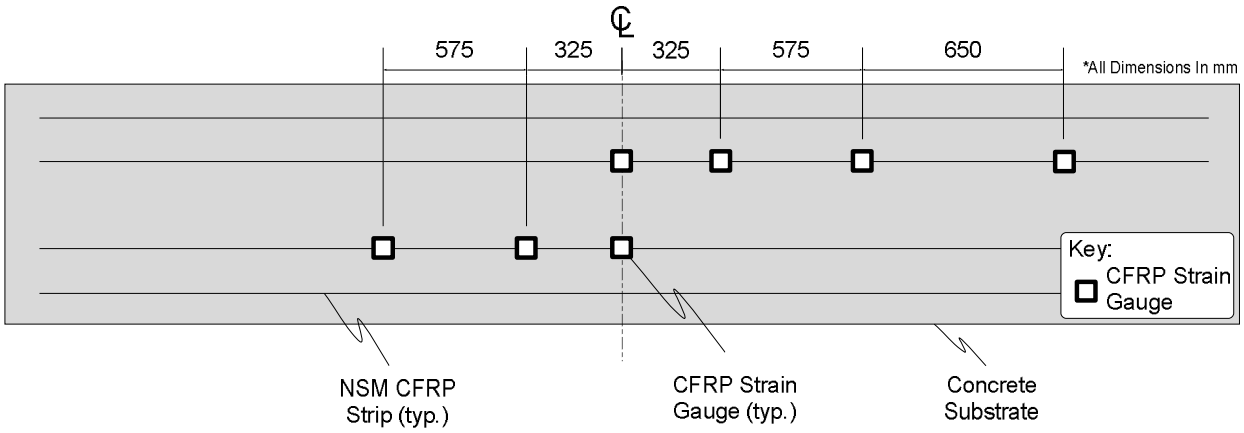

Figure 3.16: Instrumentation – Series I, III – Longitudinal CFRP Strain Gauge Layout

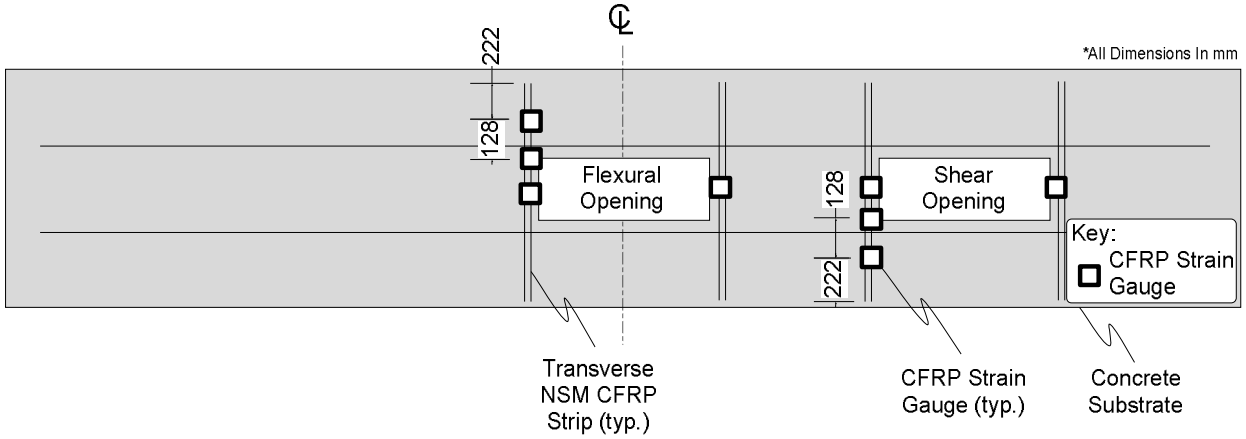

Figure 3.17: Instrumentation – Series III – Transverse CFRP Strain Gauge Layout

A single concrete strain gauge was installed within the compression zone along the side of each specimen, and centered at mid-span. The placement of the concrete strain gauge was dictated by the surface of the HC slab specimen. Since the side profile is irregular, the compression sensor was installed 10 mm from the top of each specimen. Figure 3.18 illustrates the type, orientation and location of the concrete strain gauge.

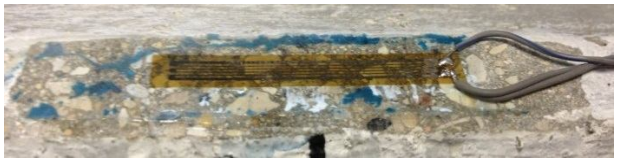

Figure 3.18: Instrumentation – Concrete Compressive Strain Gauge

A single PI gauge was installed within the tensile zone along the side of each specimen at midspan. The sensor was placed at the average depth of the internal reinforcement, typically 45 mm from the slab soffit. When no concrete strain gauges were available, a PI gauge would be employed to measure the compressive strains at the top of the specimen. Figure 3.19 illustrates the approximate location of the PI gauges at mid-span.

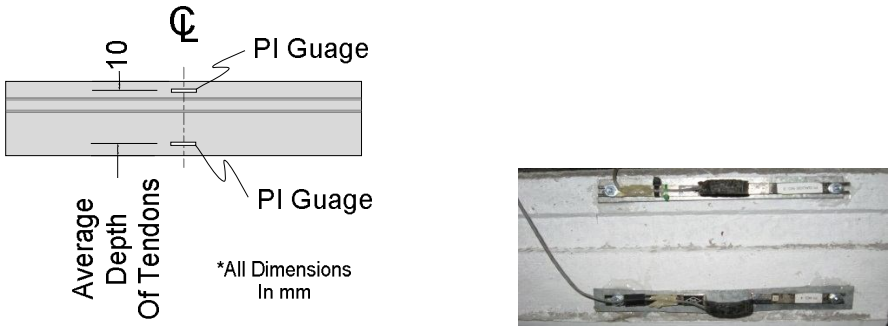

Figure 3.19 - Instrumentation – PI Gauge Layout Schematic

The data collected from all sensors includes the applied load, deflection, crack widths, and compressive and tensile strains. These readings were electronically recorded during the test using a data acquisition system.

3.7 Material Properties

3.7.1 Concrete

All specimens were cast using normal weight, ready-mix concrete with a target compressive strength of 28 MPa at 18 hours and 45 MPa at 28 days. The concrete was cast as part of a larger supply order for a local project in Winnipeg, Manitoba. At the time, approximately 150 m of each slab type was cast at once. The slabs were cast using zero-slump concrete, and were covered with an insulated tarp and steam-cured for 18 hours, until the concrete could effectively support the applied prestressing force. After steam curing, the slabs are cut to length and allowed to sit to reach the 28-day strength before testing. The compressive strength of the concrete is determined by cylinder tests performed on the day of the slab testing. The aggregates used for the test specimens were crushed limestone, with a nominal aggregate size of 20 mm. A summary of the mechanical properties for each specimen can be found in Table 3.4, including the initial and as-tested concrete compressive strengths. The initial concrete strengths were taken at the time of release, approximately 15 – 19 hours after casting, depending on the specimen. The cracking moment was determined from the following equation (CSA A23.2-04):

$$M_{cr} = \left[\frac{P_e}{A_g} + \frac{(P_e)(e)(y_b)}{I_g} + 0.6\lambda\sqrt{f'_c}\right]\frac{I_g}{y_b} \qquad \textbf{Equation 3.1}$$

Where P_e is the effective prestressing force after applicable losses, A_g is the gross area of the concrete section (including reinforcement), e is eccentricity from the neutral axis to the internal reinforcement, y_b is the distance from the neutral axis to the bottom fiber in tension, I_g is the gross moment of inertia, λ is the density factor of concrete, f'_c is the specified concrete strength.

Table 3.4: Specimen Mechanical Properties

	Specimen	Average Initial Compressive Strength (MPa)	Average As-Tested Compressive Strength (MPa)
Series I	I-1-S0-NO	32.8	64.1
	I-1-S2-NO	29.8	56.5
	I-1-S4-NO	32.8	64.1
	I-1-S8-NO	32.8	64.1
	I-2-S0-NO	28.4	56.5
	I-2-S2-NO	28.4	56.5
	I-2-S4-NO	28.4	56.5
Series II	I-1-S0-NO	32.8	64.1
	II-1-S0-FO	32.8	64.1
	II-1-S0-SO	29.8	56.5
Series III	I-1-S0-NO	32.8	64.1
	II-1-S0-FO	32.8	64.1
	III-1-S2-FO	29.8	56.5
	II-1-S0-SO	29.8	56.5
	III-1-S2-SO	29.8	56.5

3.7.2 Internal reinforcement – pretensioned steel tendons

The internal reinforcement used to prestress each hollow core slab were 7-wire low-relaxation high-strength steel strands. The applied prestress force was varied by changing the reinforcement ratio using different diameter strands. The strands were of grade 1860 and conform to CSA-G279. The tendons were anchored from one end of the 80 m precast bed and stressed from the other end. The anchor and tendon setup is illustrated in Figure 3.20.

Figure 3.20: Anchor and Prestressing Tendon Setup

Each 7-wire strand was tensioned individually, beginning with the center tendons and moving symmetrically outwards. The tendons were stressed to $0.75f_{pu}$. The stress in the steel is approximated from the Ramberg-Osgood function as provided by the 4th Edition of the CPCI Design Manual (CPCI 2007):

$$f_{ps} = 200\times10^{3}\varepsilon_{pf}\left\{0.025+\frac{0.975}{\left[1+\left(118\varepsilon_{pf}\right)^{10}\right]^{0.10}}\right\}\leq 1860MPa \qquad \textbf{Equation 3.2}$$

The effective level of prestressing was determined in accordance with CSA A23.4-04. The initial sources of loss considered were the elastic shortening of concrete (*ES*) and the immediate relaxation of the tendon stress (REL_1). The long-term losses include the effects of creep (*CR*), concrete shrinkage (*SH*), and the relaxation of the steel (REL_2).Where *t* is the cure time in days, f_{sj} is the jacking stress, f_{py} is the yield stress of the tendons, E_p is the elastic modulus for

prestressed steel, E_{ci} is the elastic modulus of concrete at transfer, and f_{cir} is the stress in the structural element, M_{sw} is the moment due to the self-weight of the section, and S is the first moment of area.

$$REL_1 = \frac{\log(24t)}{45}\left[\frac{f_{sj}}{f_{py}} - 0.55\right] f_{sj} \qquad \textbf{Equation 3.3}$$

$$ES = \frac{E_p}{E_{ci}} \cdot f_{cir} \qquad \textbf{Equation 3.4}$$

$$f_{cir} = -\frac{P}{A} \pm \frac{P_e}{S} \pm \frac{M_{sw}}{S} \qquad \textbf{Equation 3.5}$$

$$CR = \left[1.37 - 0.77\left(\frac{RH}{100}\right)^2\right] K_{cr}\left(\frac{E_p}{E_c}\right)(f_{cir} - f_{cds}) \qquad \textbf{Equation 3.6}$$

$$SH = (117 - 1.05RH) \qquad \textbf{Equation 3.7}$$

$$REL_2 = \left[\frac{f_{st}}{f_{pu}} - 0.55\right]\left[0.34 - \frac{CR + SH}{1.25 f_{pu}}\right]\frac{f_{pu}}{3} \geq 0.002 f_{pu} \qquad \textbf{Equation 3.8}$$

The jacking, effective prestressing force and prestress losses for each specimen category are summarized in Table 3.5. Prestress loss calculations can be found in ***Appendix E***.

Table 3.5: Steel Reinforcement Properties

Specimen Category	Area of Steel Tendons (mm^2)	Jacking Stress (MPa)	Initial Prestress Loss (MPa)	Long-Term Prestress Loss (MPa)	Total Prestress Loss (MPa)	Effective Prestressing Force (kN)
I-1	383.6	1395	54.3	130.6	184.9 (13.3%)	464.2
I-2	515.3	1395	61.6	142.6	204.2 (14.6%)	613.6

3.7.3 NSM reinforcement - carbon fiber reinforced polymer (CFRP)

Strengthened specimens were outfitted using commercially available carbon fiber reinforced polymer (CFRP) strips. According to the fabricator's product data sheet, the FRP reinforcement is a composite material which is suitable for increasing the flexural capacity of beams, strengthening beams for shear, strengthening slabs in flexure, and is applicable to concrete, masonry, and timber structures (Hughes Brothers 2002).

The CFRP strips employed in this study had dimensions of 2 mm in thickness, and 16 mm wide for a nominal area of 32 mm^2 – similar to a 6 mm diameter carbon rod. The specified physical properties according to the material data sheet are listed in Table 3.6. The stress-strain curve for the FRP material is linear elastic until failure.

Table 3.6: FRP Reinforcement Properties

	Dimensions (mm)	Cross Sectional Area, A_{FRP} (mm^2)	Tensile Strength, f_r (MPa)	Young's Modulus, E_{FRP} (MPa)	Ultimate Strain, ε_u
Aslan 500	2 × 16	32.0	2068.0	131000	0.017

3.7.4 Adhesive matrix – Kemko 038

The structural adhesive used to secure the NSM-CFRP laminates to the concrete substrate was Kemko 038. The adhesive is a two-component epoxy resin. It is primarily used for the structural repair of cracks and delaminations in concrete, masonry, or timber; for bonding steel or FRP to concrete; and for anchoring bolts, dowels, and rebar into concrete, masonry, or stone. The specified physical properties according to the material data sheet are listed in Table 3.7.

Table 3.7: Epoxy Adhesive Material Properties

	Tensile Strength (MPa)	Ultimate Tensile Strain (%)	Compressive Modulus (MPa)	Flexural Strength (MPa)	Flexural Modulus (MPa)	Bond Strength (MPa)
Kemko 038	62	2.0	2757	82	3792	19

3.8 Strengthening Procedure

The HC slab specimens were required to be strengthened along the positive moment side of the slabs, the same side as the prestressing tendons. To facilitate the installation process, each slab was delicately flipped using a 10-ton (100 kN) crane in the laboratory. Care was taken not to create any dynamic motion while the slabs were inverted as this additional stress combined with the pre-camber may induce unintentional cracking. Figure 3.21 highlights the key steps to strengthening each specimen.

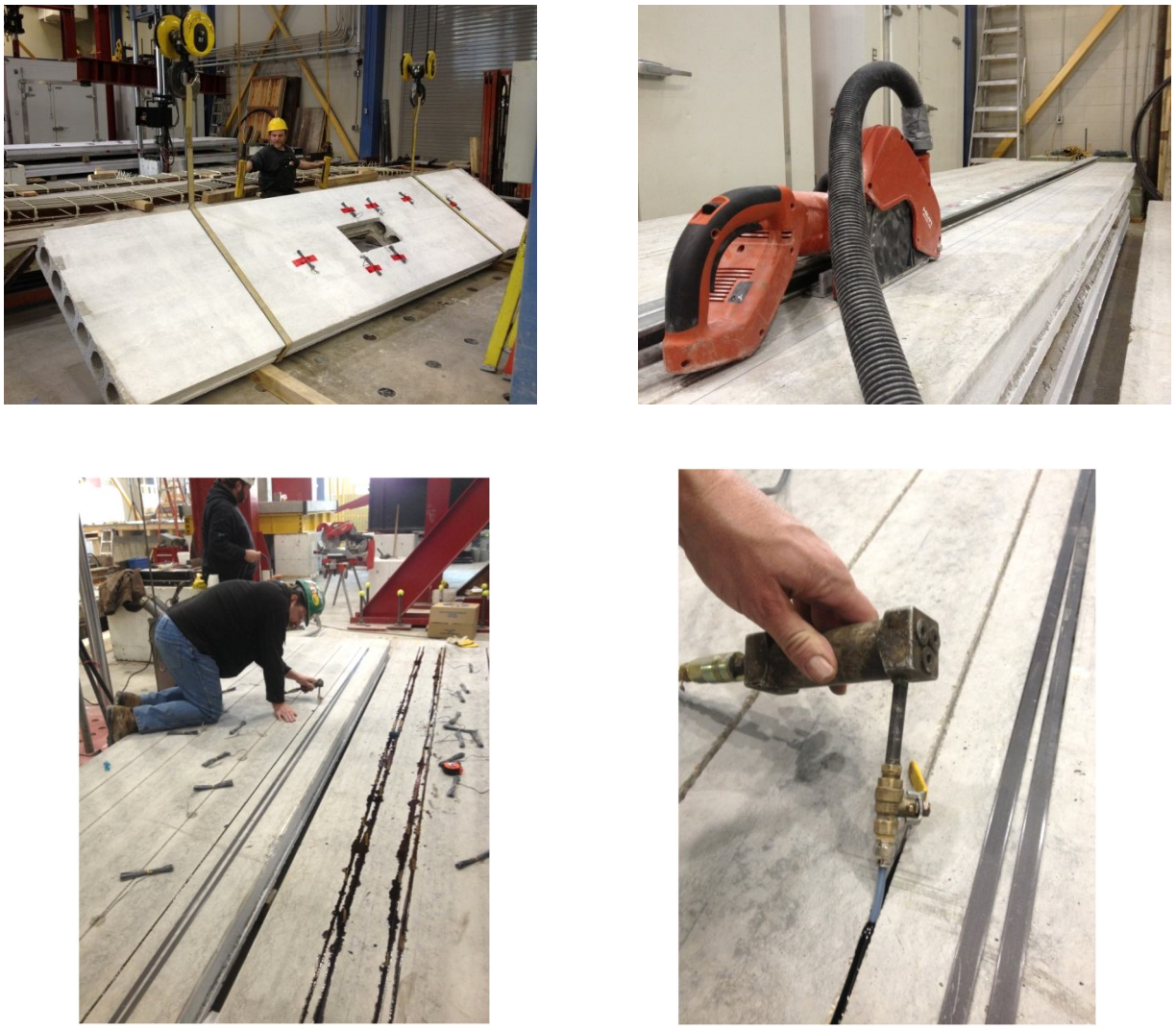

Figure 3.21: Strengthening Procedure

The locations of the grooves were centered beneath the interior webs, beneath the pretensioned steel strands. A concrete hand saw was used to cut longitudinal grooves along the inverted soffit of the specimens, resulting in a smooth groove surface texture. The height of the blade within the saw was adjusted and locked in place to achieve a specified and consistent cutting depth of approximately 22 mm. Two diamond blades were placed side-by-side to achieve an average groove thickness between 6 and 8 mm. The grooves were then thoroughly cleaned with compressed air. The structural adhesive was injected along the groove using specialized mixing

and dispensing equipment supplied by a local concrete restoration company. The equipment and epoxy product were procured from licenced applicators. Epoxy was applied until the groove was ¾ full, leaving sufficient space for the FRP laminate. The adhesive had a fluid enough viscosity to fill the small voids and surface fins along the groove walls. The CFRP strips were pushed into each groove, in a vertical orientation with the larger dimension perpendicular to the concrete surface. It was difficult to hold the laminates in place as the CFRP strips had a tendency to curl, and were found to float in the adhesive. Wooden toothpicks were used as shims along the length of the CFRP strips to maintain a centered position within the groove, effectively achieving the specified vertical and horizontal adhesive cover. Before the adhesive fully coagulated the toothpicks were removed. Epoxy paste was added or stricken-off to achieve a profile consistent with the concrete surface. All strengthening procedures were monitored and inspected in accordance with industry quality control standards.

CHAPTER 4 – ANALYSIS AND DISCUSSION OF TEST RESULTS

4.1 General

Data from the experimental program is collected and analyzed to determine the effectiveness of the parameter under consideration. Each specimen was analysed and compared to its respective control specimen against the following strength and durability behaviour: ultimate capacity and mode of failure, strain in steel and FRP reinforcement, load-deflection behaviour, and crack patterns. Each section is dedicated to analysing these characteristics individually, and is separated into three series of specimens.

4.2 Series I

This section summarizes test results of seven full-scale specimens strengthened with NSM-CFRP. Three levels of CFRP strengthening are near-surface mounted to slabs with two different ratios of prestressing reinforcement. The prestressed slab specimens under this series contain no openings.

4.2.1 Capacity and mode of failure

Series I test specimens were subjected to four-point bending under simply-supported conditions. Each specimen was tested until flexural failure was achieved. Observations were recorded and discussed in the following sections. Table 4.1 provides a brief summary of the sequence of failure for each test specimen. A summary and comparison of the general modes of failure experienced for this series are explained below. For a more detailed analysis and discussion for each individual specimen see ***Appendix G***.

Table 4.1: Series I – Mode of Failure Summary

	Specimen	Sequence and Mode of Failure
Series I	I-1-S0-NO	Steel yielding → concrete crushing → individual steel wire rupture
	I-1-S2-NO	Steel yielding → concrete crushing → CFRP splitting
	I-1-S4-NO	Steel yielding → minor concrete crushing → tendon/CFRP slip → individual steel wire rupture / CFRP splitting
	I-1-S8-NO	Type II FRP debonding → flexural-shear sudden collapse
	I-2-S0-NO	Steel yielding → flexural-shear
	I-2-S2-NO	Steel yielding → flexural-shear sudden collapse
	I-2-S4-NO	Steel yielding → flexural-shear sudden collapse

ACI 440.2R-08 (2008) recommends that strengthened specimens exhibit a ductile flexural response at the ultimate state, namely crushing of the concrete in compression. All specimens of Series I experienced steel yielding as the first stage of failure. This phenomenon is typical for high-strength concrete specimens, such as those tested in this study (56.5 – 64.1 MPa). Strengthened specimens with a lower prestressing ratio, such as I-1-S2-NO and I-1-S4-NO, experience concrete crushing at ultimate. As the internal reinforcement ratio was increased from 0.00274 to 0.00336 the sequence of failure after yielding changed from the more ductile concrete crushing behaviour, to the sudden and violent flexural-shear mode of failure. Two groups experienced this type of failure; specimen I-1-S8-NO with a lower prestressing ratio (0.00274) and a higher strengthening ratio (0.00183); and specimens I-2-S0-NO, I-2-S2-NO, and I-2-S4-NO, all with a higher prestressing ratio (0.00336). It is clear that increasing the prestressing and strengthening reinforcement ratios can change the mode of failure from a ductile response to a more brittle response. Therefore, there exists limiting reinforcement ratios, beyond which will not generate the desirable ductile failure behaviour. For specimens with low prestressing ratios that experienced concrete crushing when unstrengthened, the strengthening limit whereby the ultimate behaviour was changed to an undesirable mode of failure was 0.00183. Also, there exists an internal prestressing reinforcement ratio that exhibits a flexural-shear mode of failure, and that when strengthened, will not exhibit the desirable concrete crushing mode of failure. In this case, that limiting prestressing ratio is 0.00336. Figures G.5, G.6 and G.7 illustrate this brittle type of failure in detail. For specimens with larger prestressing and strengthening reinforcement ratios, shear behaviour became noticeable as the applied load approached the shear capacity. From observations, the flexural-shear mode of failure occurred at the loading points, and was initiated by cracking of the concrete substrate surrounding the NSM-FRP strips

(Type II FRP debonding failure – see Figure 2.7). It is possible that FRP debonding resulted from high shear stress concentrations generated around the loading points, and ultimately led to a brittle flexural-shear failure behaviour.

Table 4.2 lists the predicted shear capacity and summarizes the experimental cracking and ultimate moments, as well as the relative change in capacity compared to the unstrengthened control specimens. Predicted capacities can be found in Table 3.3 for reference.

Table 4.2: Series I - Experimental Results

			Experimental Results			
	Specimen	Calculated Shear Capacity, M_v (kNm)	Cracking Load, M_{cr} (kNm)	Ultimate Load, M_u (kNm)	Δ_{Mcr} (%)	Δ_{Mu} (%)
Series I	I-1-S0-NO*	193	73	97	-	-
	I-1-S2-NO	192	79	127	8	31
	I-1-S4-NO	193	76	155	4	60
	I-1-S8-NO	193	77	171	5	76
	I-2-S0-NO*	214	94	136	-	-
	I-2-S2-NO	214	103	165	9	21
	I-2-S4-NO	214	101	172	8	27

M_{cr}: Experimental cracking load (kNm)
M_u: Experimental ultimate flexural capacity (kNm)
ΔM_{cr}: Change in cracking load between strengthened specimen and unstrengthened control specimen ($M_{cr(i)}/M_{cr(Control)}$ *100)
ΔM_u: Change in ultimate capacity between strengthened specimen and unstrengthened control specimen ($M_{u(i)}/M_{u(Control)}$*100)
*: Unstrengthened control specimens with low and high prestressing reinforcement ratios

The addition of NSM-CFRP strips successfully increased the ultimate capacity compared to unstrengthened counterparts, for both low and high internal reinforcement ratios. The internal reinforcement ratio played an obvious role in the level of capacity enhancement. Specimens with different levels of internal reinforcement, strengthened with two CFRP strips, such as I-1-S2-NO

and I-2-S2-NO exhibited an increased strength of 31% and 21%, respectively. While specimens strengthened with four CFRP strips, such as I-1-S4-NO and I-2-S4-NO exhibited an increased strength of 60% and 27%, respectively. Clearly, specimens with strand code 2 experienced a smaller capacity enhancement than those specimens with strand code 1, having identical strengthening reinforcement ratios. For specimens with identical CFRP reinforcement ratios, an increased prestressing reinforcement ratio from 0.00274 to 0.00336 produced a diminished enhancement to the ultimate capacity. Similar to the conclusions reached by Yost et al. (2007) for non-prestressed concrete beams, that the expected increase in strength from NSM-CFRP reinforcement must consider the existing internal reinforcement ratio in the unstrengthened condition. Similar to the phenomenon exhibited by increasing the prestressing reinforcement ratio, it is evident that increasing the strengthening reinforcement ratio also produces a diminishing enhancement to the ultimate capacity. Doubling the number of laminates from 2 → 4 → 8 does not effectively double the level of capacity enhancement. Also, those specimens that exhibited a flexural-shear mode of failure did not fully reach the predicted shear limit, but instead only reached between 77 – 87% of the shear capacity. It is possible that the CSA and ACI code predictions overestimate the shear limit. Otherwise the high shear stresses generated around the loading points may expedite premature debonding failure of the NSM laminates. The transfer of tensile stresses from the inactive laminates to the internal reinforcement and surrounding concrete may be too sudden to be distributed effectively, resulting in pseudo-dynamic load behaviour.

4.2.2 Load-strain relationships

This section presents a summary of the strains in each of the constituent materials. The tensile strains were measured using electrical strain gauges affixed directly on the surface of the reinforcement. Figures 4.8 and 4.9 illustrate the load-tendon strain relationship for the specimen groups with low and high reinforcement ratios, respectively.

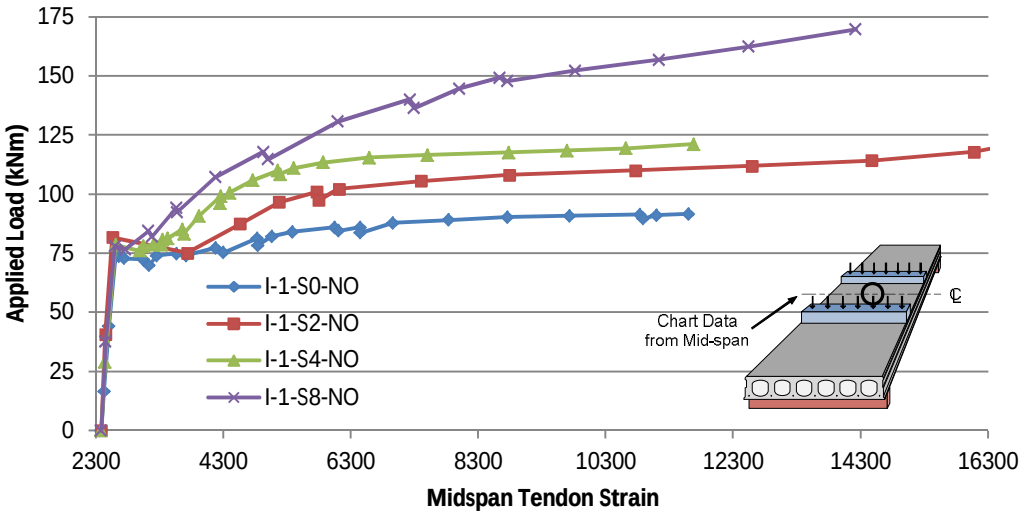

Figure 4.8: Series I – Low Reinforcement Ratio – Load vs. Mid-span Tendon Strain

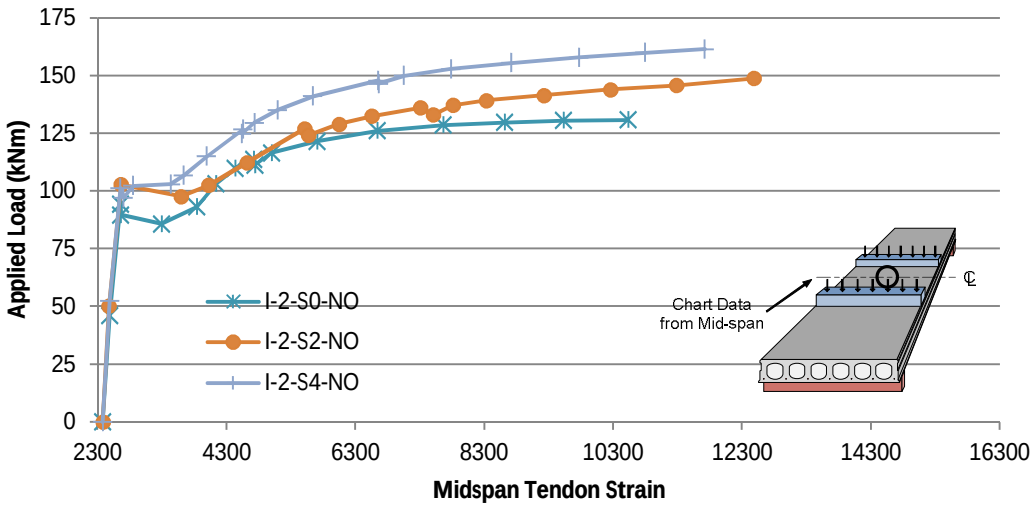

Figure 4.9: Series I – High Reinforcement Ratio - Load vs. Mid-span Tendon Strain

For control specimens I-1-S0-NO and I-2-S0-NO, the load-tendon strain behaviour is characteristic of a section subject to flexural loading. The initial pre-cracking stage suggests the concrete substrate tensile capacity and the initial prestress force within the concrete provides the majority of the load-carrying resistance, resulting in little increase in tendon strain. Similar to the load-deflection behaviour, the load-tensile strain is linear up to cracking due to the near-identical modulus of the concrete and internal reinforcement. This holds true for strengthened specimens as well. After the internal prestressing force and the tensile capacity of the concrete is achieved the section cracks and the load is more rapidly transferred to the internal steel tendons, as indicated by the sudden and dramatic increase in tensile strain. The positive increase in slope indicates the stiffening effect of the tendons is providing additional load-carrying capacity to the section. Once the load reaches the yielding stage, the slope of the tendon-strain curve reaches a plateau, indicating increased deformation with no corresponding increase in load-carrying capacity. However, those specimens strengthened with NSM-CFRP strips exhibit an increase in tensile strains after the control specimen has reached the yielding point. This indicates that the

internal steel tendons and the NSM-CFRP strips share the load-carrying duties, and result in a reserve capacity within the steel, effectively delaying the yielding stage.

Table 4.3 summarizes the tensile strains and associated moments in each specimen at various stages during loading, namely cracking, service, yielding, and at ultimate. The serviceability strain was determined from the maximum allowable stress in the prestressed steel in order to avoid inelastic deformations, according to ACI 440.2R-08 (2008). This strain was then used to determine the applied moment at this stage from experimental data. For prestressed steel tendons, yielding loads are determined when the stress in the tendons reach approximately 90% of the ultimate rupture stress. All strain calculations take into account the existing jacking stress of $75\% \cdot f_{pu}$ as well as the initial and long-term prestress losses. For the complete procedures for all strain calculations see ***Appendix H***.

Table 4.3: Series I - Strain Values

		@ Cracking	@ Service		@ Yielding		@ Ultimate
	Specimen	M_{cr} (kNm)	$\varepsilon_{ps,s}$ (10^6)	M_s (kNm)	$\varepsilon_{ps,y}$ (10^6)	M_y (kNm)	M_u (kNm)
Series I	I-1-S0-NO	73	7040	74	8590	80	97
	I-1-S2-NO	79		80		84	127
	I-1-S4-NO	76		79		105	155
	I-1-S8-NO	77		84		115	171
	I-2-S0-NO	94		86		114	136
	I-2-S2-NO	103		99		116	165
	I-2-S4-NO	101		103		132	172

M_{cr}: Experimental mid-span cracking moment (kNm)
$\varepsilon_{ps,s}$: Maximum allowable strain in prestressing steel at the serviceability state, according to ACI 440.2R-08
M_s: Experimental mid-span moment at the corresponding maximum serviceability strain (kNm)
$\varepsilon_{ps,y}$: Mid-span strain in prestressed tendon at yielding ($0.9 \cdot f_{pu}$)
M_y: Experimental mid-span moment at the corresponding yield stage (kNm)
M_u: Maximum ultimate moment during testing (kNm)
$\varepsilon_{cr\text{-}s}$: Experimental mid-span strain in prestressed tendon at estimated cracking stage

4.2.2.1 Serviceability limit state

ACI 440.2R-08 suggests limiting the service load to avoid inelastic deformations. The committee suggests limiting the stress in the steel to 82% of the yield stress, or to limit the compressive stress in the concrete to 45% of the compressive strength. The table above lists the applied moment (M_s) required to develop 82% of the yield stress in the prestressing tendons. The majority of Series I specimens have a suggested service load greater than the experimental cracking load, thus allowing inelastic deformations. The largest difference between service and cracking loads was found to be 8%. The ACI guideline also suggests limiting the stress in concrete to 45% of the compressive strength, which provides a more conservative limit to avoid inelastic deformations. The addition of eight CFRP strips provided an increase in service load of 13%, as is the case when comparing specimens I-1-S0-NO and I-1-S8-NO. Increasing the strengthening reinforcement ratio does not provide a significant improvement to the capacity at the serviceability state.

4.2.2.2 Yield point

The yield point is characterized by an increase in deflection of the member, or strain within the material, with no corresponding increase in load-carrying capacity. Steel yielding is typically followed by a load plateau of the load-tensile strain curve, where the moment capacity of the section remains approximately constant. As can be noted from Figures 4.8 and 4.9, the control specimens exhibit a distinct load plateau, albeit at different yield loads. The difference in yield load is attributed to the difference in section modulus as shown by a noticeable change in cracking load. Specimens with a lower internal reinforcement ratio exhibit a corresponding reduction in the concrete's tensile capacity; therefore the load is transferred to the tendons at an

earlier stage and a lower applied load. Increasing the internal reinforcement ratio results in a near identical yield behaviour compared with a slab having less prestressed reinforcement, albeit transposed by the difference in cracking load. As mentioned in the previous section, strengthened specimens exhibit a load-sharing behaviour between the internal steel reinforcement and the external FRP strips. As the strengthening reinforcement ratio increases, as is the case between I-1-S2-NO → I-1-S4-NO → I-1-S8-NO, the reserve stiffness of the internal steel reinforcement increases (slope of load-tensile strain curve), effectively delaying the yielding point.

For specimens strengthened with NSM-CFRP strips, the yield point, or the change from cracked-elastic to inelastic behaviour is less noticeable. The addition of eight CFRP strips for specimen I-1-S8-NO generates an approximate yield moment, M_y, of 115 kNm, which is approximately 44% greater than the yield moment experienced by the control specimen, I-1-S0-NO. At the ultimate stage, the same strengthened specimen experiences an increased moment capacity, M_u, of approximately 76% compared to the control specimen. The moment enhancement is much greater at the ultimate stage than the yielding stage. This trend is apparent with all test specimens, regardless of level of steel reinforcement ratio. This behaviour illustrates that for prestressed concrete, the NSM technique is much more effective at enhancing the ultimate limit state than the serviceability limit state.

4.2.2.3 Tensile strains in steel tendons

Specimens strengthened with two, four and eight strips experienced a noticeable enhancement in post-cracking stiffness, and correspondingly a noticeable enhancement in their respective yield loads. Compared to the control specimen, I-1-S0-NO, the approximate yield loads for slabs I-1-

S2-NO, I-1-S4-NO and I-1-S8-NO increased by 5, 31, and 44%, respectively. This phenomenon suggests that the increase in yield load diminishes with increasing strengthening reinforcement ratio, ρ_{frp}. This behaviour is similar to the trend discovered for the ultimate capacity in the previous section. Increasing the strengthening reinforcement ratio resulted in a diminishing increase in capacity at the yield stage. In other words, there exists a strengthening limit, where any additional strengthening will not provide a significant improvement in yield load.

The control specimen, I-1-S0-NO, experienced a 21% difference between the yield load, M_y, and the ultimate load, M_u, indicating that for unstrengthened prestressed concrete the yield point is relatively near the ultimate load stage. For strengthened specimens I-1-S2-NO, I-1-S4-NO and I-1-S8-NO, the ultimate loads were 51, 48, and 49% greater than the yield loads. This increase represents the reserve tensile energy provided by the CFRP strips after the yield stage, and is not available for unstrengthened specimens with no NSM-FRP reinforcement. This trend is similar for both steel reinforcement ratios.

4.2.2.4 Tensile strains in NSM-CFRP

Tensile strains in the NSM-CFRP strips were measured using 6 mm electronic strain gauges. Unfortunately these gauges are fragile and highly susceptible to damage during the loading procedure, particularly when tensile cracks form in the vicinity of the gauges. Once the gauge is damaged, the recoded data becomes unusable, as is the case for many specimens near the failure stage. In these cases, the strain at ultimate is approximated from interpolation using a linear curve of best fit. Figure 4.10 illustrates the load-mid-span CFRP strain for all strengthened specimens tested for Series I.

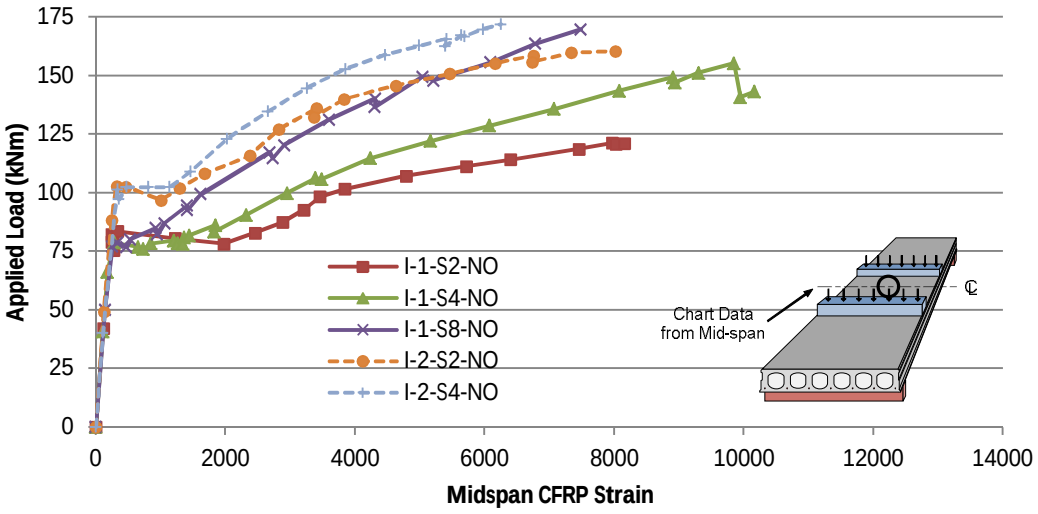

Figure 4.10: Series I - Load vs. Mid-span CFRP Strain

From the figure above, it is clear that changing the internal steel reinforcement ratio while maintaining a constant strengthening reinforcement ratio will yield very similar load-CFRP strain curves. Specimens I-1-S2-NO and I-2-S2-NO; and I-1-S4-NO and I-2-S4-NO illustrate this phenomenon. The biggest difference is the strain profile, which is governed by the internal steel reinforcement. A change in the steel reinforcement ratio changes the stiffness of the section, therefore creating a shift of the load-strain curve up or down corresponding to an increase or decrease of steel reinforcement, respectively.

Since relatively no FRP slip was observed at the ends of the strip reinforcement during experimental testing, an ideal bond is assumed between the CFRP strips and the adhesive matrix. However, there were sections along the strip reinforcement which had cleanly sheared away from the surrounding epoxy, leaving a perfectly rectangular void. This suggests that having a bonded length much greater than required allows for localized slip failures without resulting in an ultimate slip failure of the whole FRP strip. Bond failure was predominantly encountered in

the surrounding adhesive or the surrounding concrete substrate, as a tensile/shearing failure. Table 4.4 summarizes the ultimate CFRP tensile strains at mid-span, the maximum allowable strain as specified by the CSA and ACI codes, and the ratio of maximum strain to the design rupture strain of the CFRP. Recall that the CSA code specifies a limit of 7000 micro strain, independent of the tensile capacity of the FRP reinforcement. The ACI code recommends a debonding strain at 70% of the tensile capacity of the FRP reinforcement. All strain values are reported in micro strain.

Table 4.4: Tensile CFRP Strain at Ultimate Loading Stage

	Specimen	CFRP Mid-span Strain @ Ultimate	Recommended Strain by CSA	Recommended Strain by ACI	% of Ultimate Rupture Strain
Series I	I-1-S2-NO	9100	7000	11900	54
	I-1-S4-NO	9850			58
	I-1-S8-NO	7700			45
	I-2-S2-NO	8200			48
	I-2-S4-NO	6300			37

It is clear the CSA recommends a conservative estimate for maximum allowable strains when the specimen exhibits a purely flexural behaviour. The CSA recommendation is no longer accurate when the governing behaviour of flexural-shear leads to a premature failure. In all cases, the ACI overestimates the allowable strain regardless of the level of strengthening and mode of failure. The strain in the NSM-CFRP reinforcement does not reach more than 58% of its tensile capacity. However, in some cases, the internal longitudinal shear forces caused the strip to shear in half.

4.2.3 Load-deflection relationships

The following section highlights the load-deflection behaviour for all Series I specimens. It is divided into several subsections, organized to follow the behaviour of the flexural loading process. The first subsection is intended to provide a general overview of the test results; followed by an explanation of the pre-cracking behaviour and cracking load of strengthened specimens; then I t will discuss trends in the post-cracking behaviour, specifically the change in stiffness; and finally it will summarize the deflection response and ductility. Table 4.5 summarizes the predicted and experimental flexural and shear capacities for all Series I specimens.

Table 4.5: Series I – Theoretical vs. Experimental Results

		Theoretical Results			Experimental Results	
	Specimen	Cracking Moment (kNm)	Ultimate Flexural Capacity (kNm)	Ultimate Shear Capacity (kNm)	Cracking Moment (kNm)	Ultimate Flexural Capacity (kNm)
Series I	I-1-S0-NO	82.9	106.8	193.2	73	97
	I-1-S2-NO	81.5	125.2	191.5	79	127
	I-1-S4-NO	84.1	143.1	193.2	76	155
	I-1-S8-NO	84.7	179.5	193.2	77	171
	I-2-S0-NO	104.8	139.2	214.1	94	136
	I-2-S2-NO	105.7	156.6	214.1	103	165
	I-2-S4-NO	106.3	174.3	214.1	101	172

The load-mid-span deflection behaviour for all specimens with strand code ‘1’ and ‘2’ are plotted in Figures 4.11 and 4.12, respectively. Load-deflection curves illustrate the relationship between the total applied load, *M*, and the measured deflection at the midpoint of the clear span

for each simply supported test specimen. The load-deflection behaviour is an indicator of the effect that changing the internal and external reinforcement ratios has on the stiffness for each test specimen.

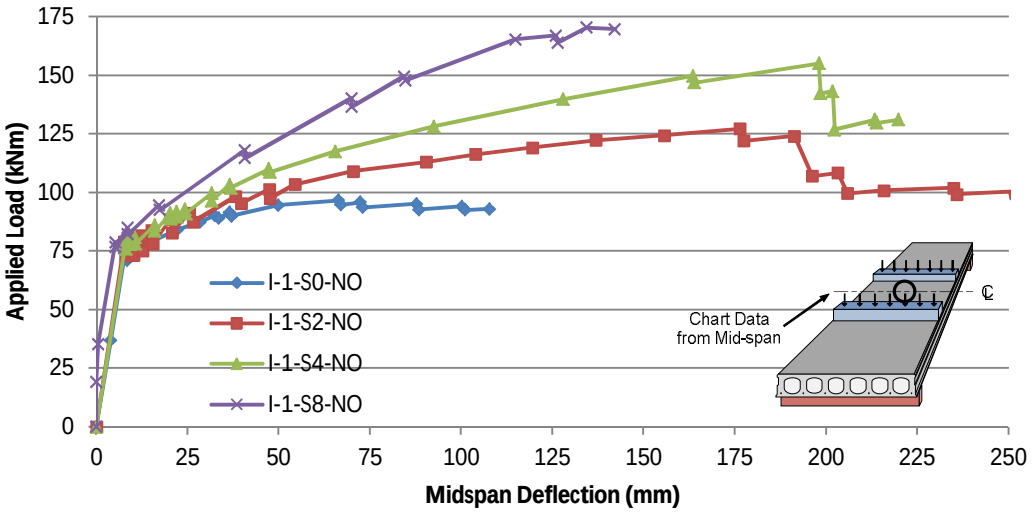

Figure 4.11: Series I – Low Reinforcement Ratio – Load vs. Mid-span Deflection

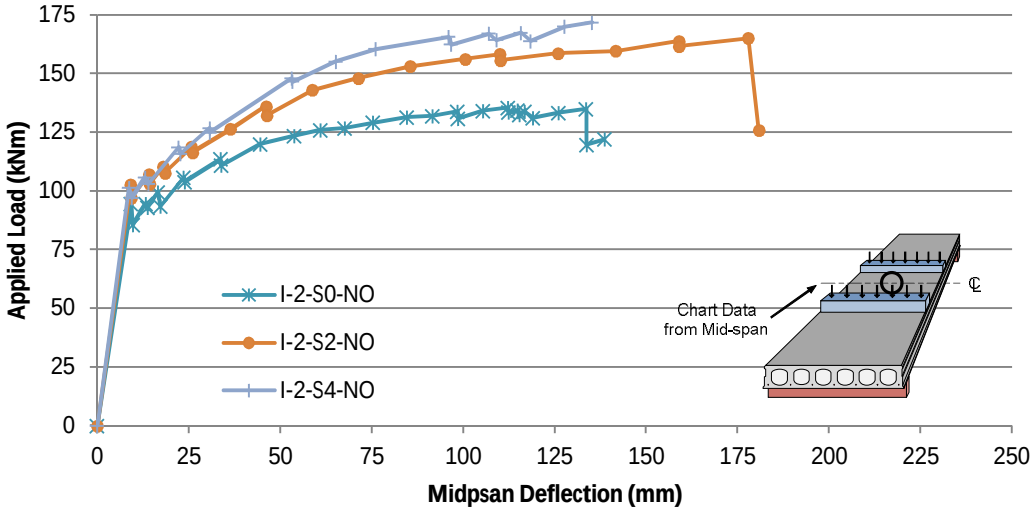

Figure 4.12: Series I – High Reinforcement Ratio – Load vs. Mid-span Deflection

Referring to the load-deflection behaviour of the control specimens I-1-S0-NO and I-2-S0-NO in the aforementioned figures, the flexural response for prestressed members is apparent. Initially, the reinforced section is uncracked and gross section properties are applicable and exhibit a perfectly elastic behaviour. At the cracking load (M_{cr}) the behaviour changes from uncracked to cracked-elastic, as indicated by the change in slope of the plotted curve. As the two-point applied load is increased, the section responds elastically until the yield strength of the pre-tensioned steel (f_y) is reached. At the corresponding yield load (M_y) the sections response changes to inelastic behaviour. The yield load is made evident as the load-deflection curve flattens, and the moment capacity of the section remains approximately constant. The load plateau is evident in the response of the control specimens as compared to those specimens strengthened with CFRP strips. This approximately constant moment behaviour continued until failure occurred by concrete crushing for under-reinforced sections. A notable objective for prestressed concrete compared to non-prestressed concrete is to increase the cracking load so that the section remains uncracked under service load conditions. Yielding of the high-strength steel was encountered soon after cracking, therefore reaching its ultimate capacity soon thereafter. Without any reserve stiffness, an unstrengthened section is not able to sustain any further increase in load. The following sections explain the flexural behaviour of strengthened test specimens as compared to their unstrengthened counterpart control specimens.

4.2.3.1 Pre-cracking behaviour and cracking load

The pre-cracking stiffness is determined as the slope of the load-deflection curve between at-rest conditions (0,0) and the cracking stage (P_{cr},δ_{cr}). Table 4.6 outlines the experimentally applied load at the approximate cracking stage, along with the recorded mid-span deflection associated

with this load. The transformed moment of inertia for each specimen is listed in the following table to provide an understanding of how much the internal steel reinforcement and externally bonded FRP reinforcement affects the properties of the cross section. These transformed moments of inertia were used to calculate the theoretical cracking loads.

Table 4.6: Series I – Pre-Cracking Characteristics

	Specimen	Transformed Moment of Inertia, I_g (mm^4)	Applied Load @ Cracking, M_{cr} (kNm)	Deflection @ Cracking, δ_{cr} (mm)	Pre-Cracking Stiffness (GPa)
Series I	I-1-S0-NO	6.9476×10^8	73	7.5	10.8
	I-1-S2-NO	7.0171×10^8	79	7.7	11.4
	I-1-S4-NO	7.0935×10^8	76	7.6	11.3
	I-1-S8-NO	7.1699×10^8	77	4.6	18.6
	I-2-S0-NO	7.3089×10^8	94	9.1	11.5
	I-2-S2-NO	7.3966×10^8	103	9.0	12.7
	I-2-S4-NO	7.4624×10^8	101	8.6	13.1

Prior to cracking the load-deflection relationship for control specimens and strengthened specimens exhibit near-identical behaviour. The addition of NSM-CFRP strips provides only a slight increase in the section moment of inertia, and a corresponding increase in the cracking load, albeit the increase is not proportional. Inserting two, four, and eight strips increases the cracking load by 8%, 4%, and 6%, respectively. And for strand code 02, two and four strips increase the cracking load by 10% and 7%, respectively. Although a slight increase is expected, the fact the increases do not increase proportionally with increasing reinforcement ratio suggests the results may be subject to experimental error. Previous studies have indicated that the provision of NSM strengthening reinforcement provides no noticeable enhancement to the cracking load or pre-cracking stiffness. Clearly the addition of externally bonded reinforcement

increases the section moment of inertia, indicating that theoretically there should be a slight increase in the cracking load and pre-cracking stiffness. Unfortunately, the increase in inertia is relatively small compared to the resistance provided by the concrete cross section, and any noticeable change in cracking load may be attributed to experimental error. This slight increase is negligible and should be considered negligible when designing NSM-FRP systems.

The changes in pre-cracking stiffnesses for strand codes 1 and 2 are within 5% and 14%, respectively. As the cracking load increases slightly, while the deflection at cracking remains relatively constant, within a variation of 6%, the stiffness is also expected to increase slightly. Specimen I-1-S8-NO experienced a decrease in deflection at cracking of 63%, while the cracking load remained unchanged. This behaviour is significantly different than all other specimens, and can be considered an outlier. A possible explanation for this behaviour is that instead of experiencing a single major crack, cracking began with much smaller micro cracks whose stress were quickly redistributed by the FRP reinforcement. This stress transfer effectively activated the FRP laminates at an early stage which may explain the significant increase in pre-cracking stiffness and composite action.

4.2.3.2 Post-cracking stiffness

After cracking, the tensile reinforcement begins to play a more significant role in the flexural resistance of the section. The flexural resistance of a concrete substrate experiences localized decreases in stiffness at locations of concrete cracking, as no tensile stresses are carried by the concrete across the crack. As flexural cracks develop, the tensile stresses are transferred from the concrete substrate to the internal – and if present, external – reinforcement. Any tensile

reinforcement within this section plays a significant role in contributing to the post-cracking moment of inertia. Figure 4.13 illustrates a plot of only the unstrengthened control specimens, I-1-S0-NO and I-2-S0-NO. This more clearly outlines the difference in flexural behaviour associated with increasing the internal reinforcement ratio.

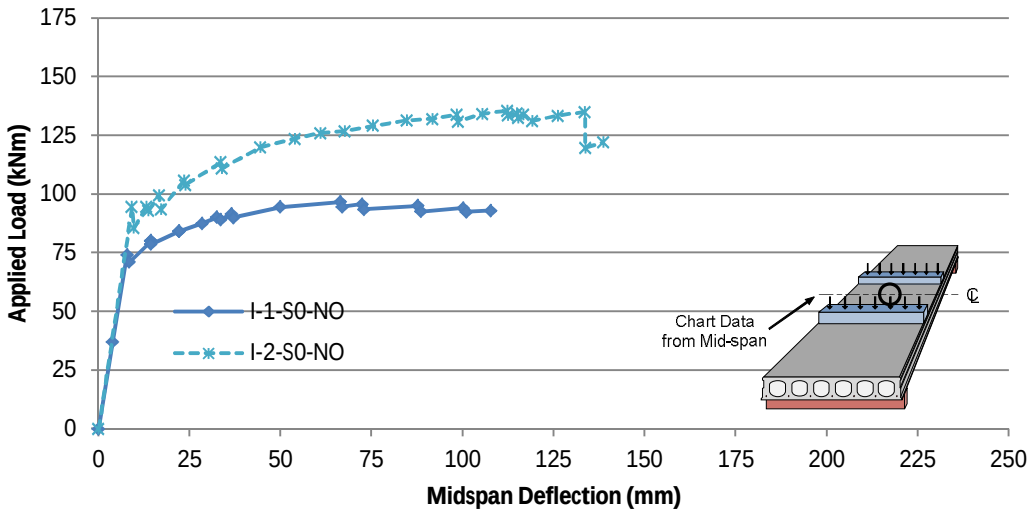

Figure 4.13: Series I – Load vs. Mid-span Deflection Curve for Control Specimens

The unstrengthened control specimens I-1-S0-NO and I-2-S0-NO experienced a slight increase in load-carrying capacity after cracking, as shown by the positive slope of the load-deflection curve following the localized minimum after the initial cracking load. This gain in strength continued until the yield state was achieved, after which the member continued to deform without significant increase in load-carrying capacity. Again referring back to Figure 4.11, strengthened specimens experienced a greater increase in stiffness until ultimate failure. In fact, after yielding of the steel tendons, the CFRP reinforcement constrained the widening of the cracks and subsequently reduced the mid-span deflection compared to the unstrengthened control specimen. The slope of the load-deflection curve remained positive until the ultimate load was

reached. This trend indicates that any additional load applied to the system after yielding was effectively transferred to- and resisted by the NSM reinforcement. The FRP reinforcement continued to provide the required stiffness to the system so that it could sustain the increasing load, effectively delaying ultimate failure. This increase in post-cracking stiffness is dependent on the FRP reinforcement ratio, as evidenced by the post-cracking response of specimens I-1-S2-NO, I-1-S4-NO and I-1-S8-NO. All three test specimens have identical design parameters, except for the FRP reinforcement ratios, which increases as the number of laminates increases from two to eight. The FRP reinforcement ratios for the aforementioned slab specimens are 0.046%, 0.091% and 0.183%, respectively. Approximating the slab stiffness with the slope of the line-of-best-fit taken from the localized minimum after the cracking load was reached, until the maximum load of the load-deflection curve, the post-cracking stiffness between the two strengthened slabs can be compared. Test results conclude that an increase in FRP reinforcement ratio of 100% results in an increase of 56% in the post-cracking stiffness. The improvement in stiffness in the inelastic region is not directly proportional to the increase in FRP reinforcement ratio.

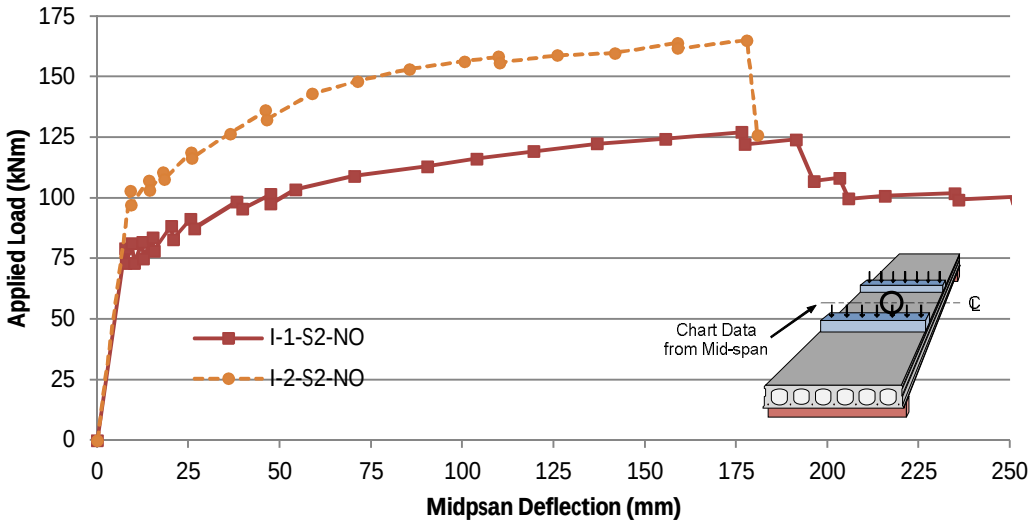

Figure 4.14: Series I – Load vs. Mid-span Deflection – Two CFRP Strips

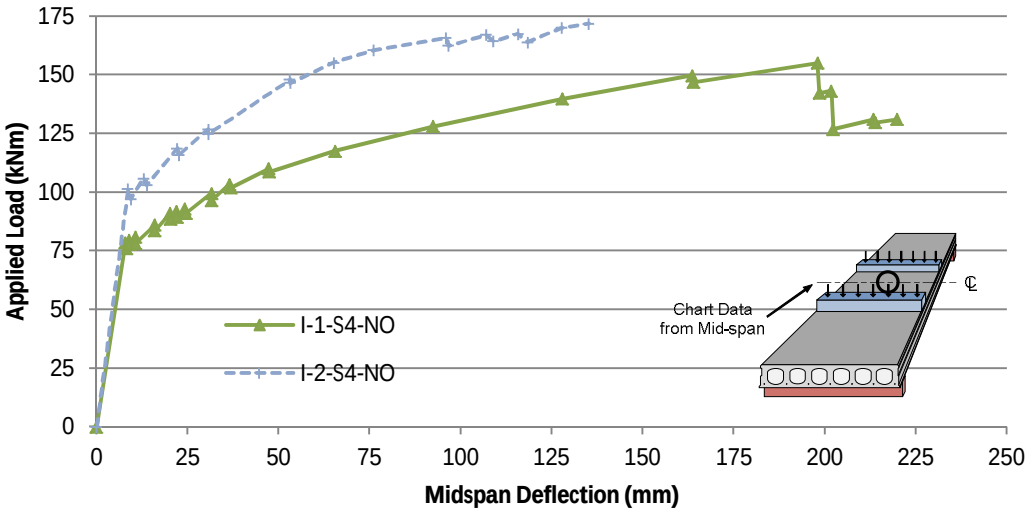

Figure 4.15: Series I – Load vs. Mid-span Deflection – Four CFRP Strips

4.2.3.3 Deflection response and ductility

The ductility of the specimens is analyzed in terms of the dimensionless ratio of the mid-span deflection corresponding to the ultimate load, and the mid-span deflection corresponding to the yielding load. The yield limit is not an instantaneous condition that occurs at a clearly defined load, deflection, or strain, however, in this case the yield load is considered to be the load corresponding to an induced stress of $0.9f_{py}$ in the steel tendon. Table 4.7 provides a summary of the ductility results in terms of deflections at the yield and ultimate states for Series I specimens.

Table 4.7: Series I – Deflection and Ductility Results

	Specimen	δ_{cr} (mm)	δ_y (mm)	δ_u (mm)	μ_d	$\mu_d/\mu_{d\text{-Control}}$
Series I	I-1-S0-NO	7.5	15.9	68.5	4.31*	(1.00)
	I-1-S2-NO	7.7	17.4	176.6	10.15	2.35
	I-1-S4-NO	7.5	40.8	197.9	4.85	1.13
	I-1-S8-NO	4.6	37.8	142.2	3.76	0.87
	I-2-S0-NO	9.1	35.5	112.0	3.15*	(1.00)
	I-2-S2-NO	9.0	22.5	176.7	7.85	2.49
	I-2-S4-NO	8.6	35.3	135.0	3.82	1.21

δ_{cr}: Mid-span deflection at the estimated cracking stage
δ_y: Mid-span deflection at $0.9f_{py}$
δ_u: Mid-span deflection corresponding to the ultimate load
μ_d: Deflection ductility (δ_u / δ_y)
* $\mu_{d\text{-Control}}$: Deflection ductility of control specimens I-1-S0-NO and I-2-S0-NO used as a reference points

Yost et al. (2007) and Bencardino et al. (2002) found that flexural strengthening with external laminates reduces the flexural ductility of a member compared to the unstrengthened control specimen. These studies were conducted for members reinforced with conventional steel reinforcing bars, and strengthened with NSM-CFRP strips. The ductility results from this study suggest a different conclusion for prestressed concrete strengthened with similar FRP

reinforcement. Results suggest that adding two NSM-CFRP strips increases the ductility by 135 and 149% for strand codes '1' and '2', respectively. The addition of four NSM-CFRP strips increases the ductility by 13 and 21% for strand codes '1' and '2', respectively. And the addition of eight NSM-CFRP strips leads to a decrease in ductility of 13% for reinforcement code '1'. Conventionally reinforced concrete strengthened with NSM laminates typically experienced minor changes in the deflection at the yielding and ultimate stages, but resulted in a relatively slight decrease in deflection ductility of approximately 10%. For prestressed concrete, the deflection encountered at yielding remained relatively unchanged compared to the significant changes at the ultimate stage. All strengthened specimens experienced a substantial increase in deflection at ultimate failure compared to the unstrengthened counterpart. This increase in deflection diminishes as the strengthening reinforcement ratio increases. The reason for this is that as the amount of strengthening increases, the strengthened member is more likely to reach the shear capacity and experience a premature flexural-shear mode of failure. The data suggests that if the shear capacity is sufficiently high, the deflection at ultimate and thus the deflection ductility should continue to increase. The results of this study suggest that for prestressed concrete, the addition of NSM laminates increases the deflection ductility for lower strengthening ratios, and may decrease the deflection ductility for higher strengthening ratios as the flexural response approaches the shear capacity.

4.2.4 Cracking behaviour

Crack formation in concrete is a natural behaviour. When an induced load generates a tensile stress greater than the tensile strength of the section the concrete cracks. No tensile stresses can be transferred across a crack, which effectively decreases the section stiffness in that region. The

load under which this occurs is termed the cracking load. Increasing the applied load beyond this initial cracking stage forces the tensile stresses to undergo a localized redistribution to the internal reinforcement and to areas of the section which remain uncracked. Continued redistribution of the load leads to the development of additional cracks, as well as the propagation and widening of existing cracks. As cracks form and the stiffness of the concrete in tension decreases, the induced stresses in the tensile reinforcement increase.

Flexural cracks are the result of an applied moment causing excessive tensile stresses normal to the cross section of an element. As the tensile stress exceeds the cracking strength of concrete a vertical flexural cracks is formed. As the applied load increases the tensile stresses increase, moving away from the outer-most fibre in tension, extending the crack towards the interface of the tension-compression zone, known as the neutral axis. Shear cracks often develop as a result of support reactions and high concentrated load regions. Near the supports the load is transferred to the support in an arching effect, effectively curving the neutral axis downward. The induced load in the beam creates a tensile stress which acts normal to a place inclined at an angle which changes with distance from the support. A range typical of this plane is between 30 and 60 degrees. Shear cracks develop when the induced tensile stress in the concrete exceeds the tensile strength, and propagates at an angle toward the inclined neutral axis.

The following schematics illustrate the progression of cracking for Series I specimens during the flexural loading test. Three stages are illustrated: the initial cracking stage, cracking propagation at 70% of the ultimate load (approximately corresponding to the yielding stage of the unstrengthened control specimen), and the ultimate stage at failure.

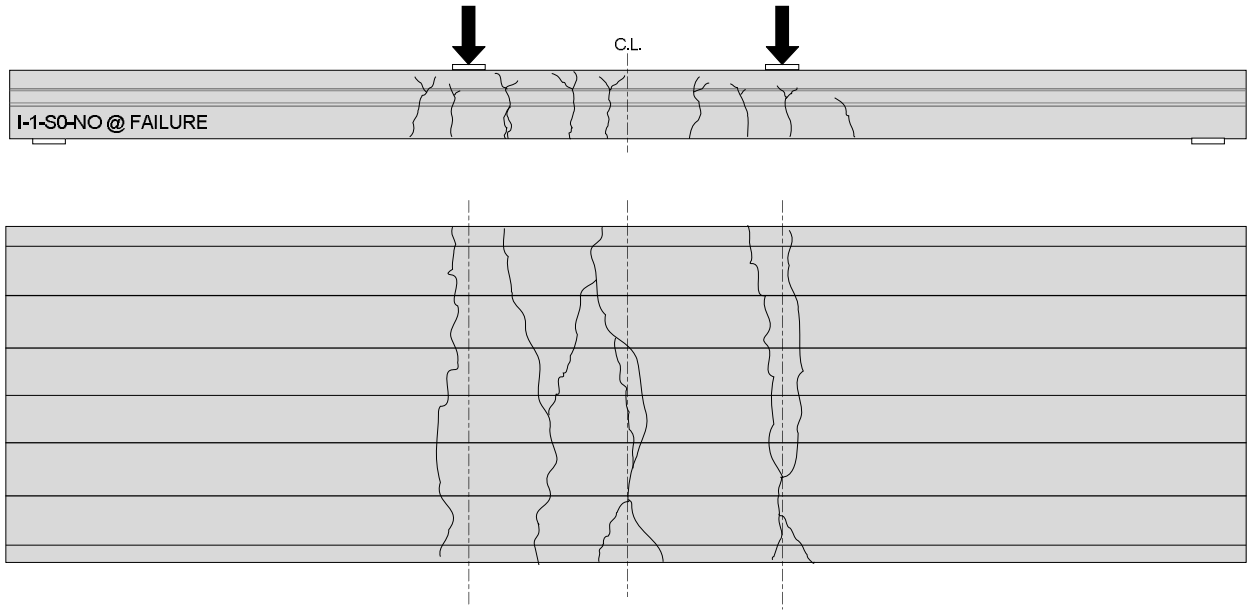

Figure 4.16: I-1-S0-NO Crack Pattern at Failure

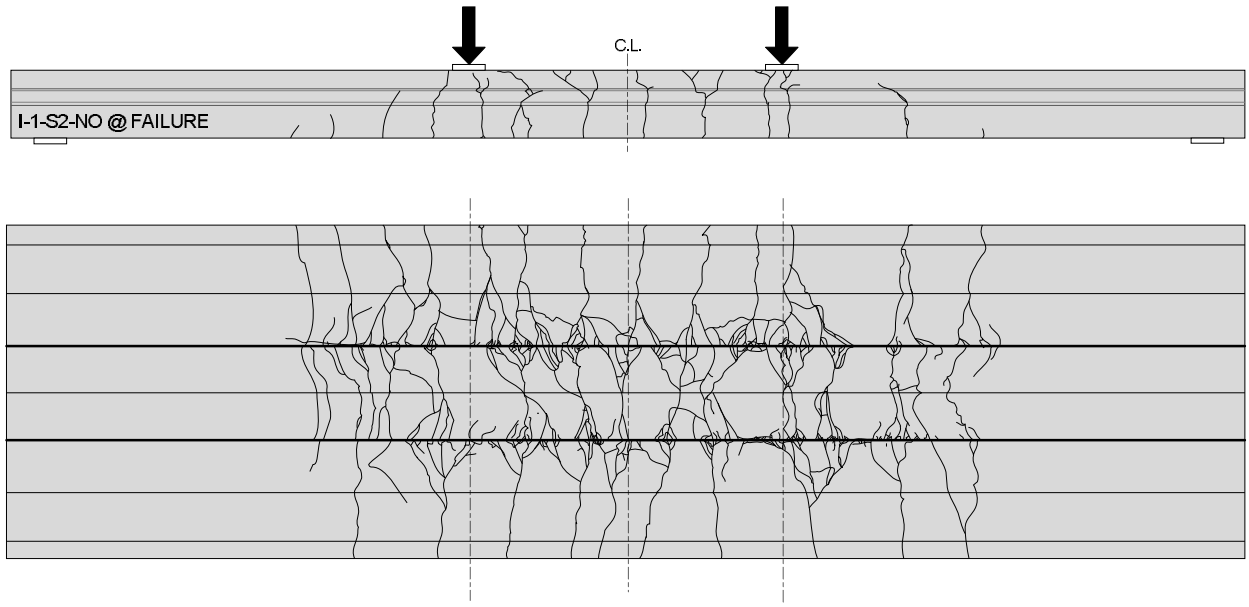

Figure 4.17: I-1-S2-NO Crack Pattern at Failure

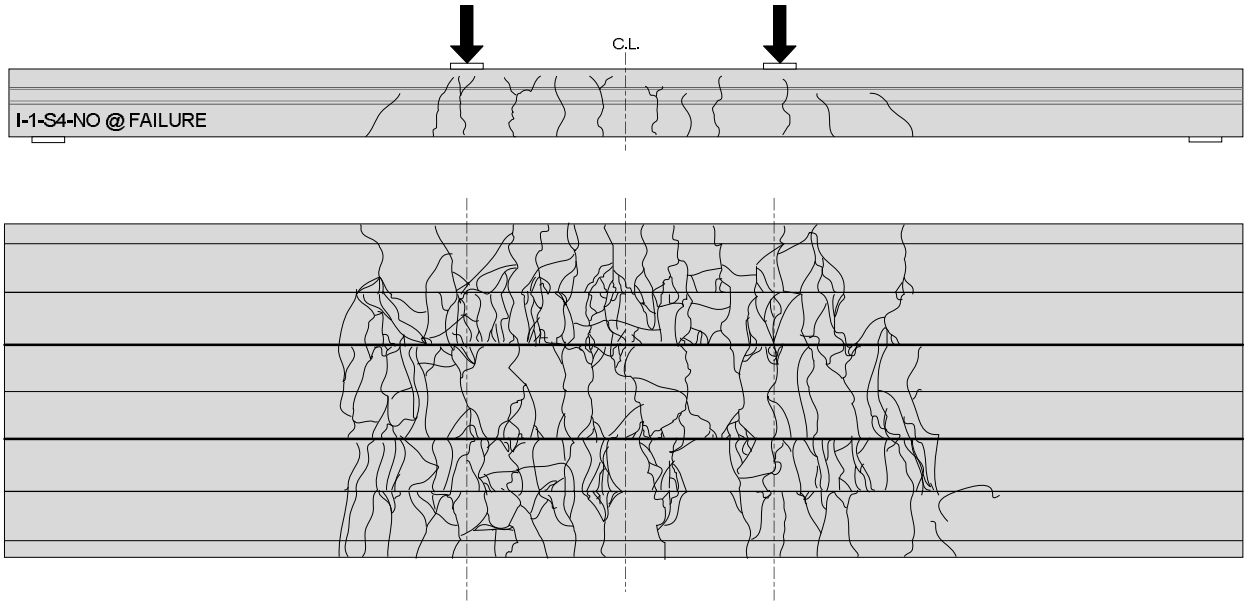

Figure 4.18: I-1-S4-NO Crack Pattern at Failure

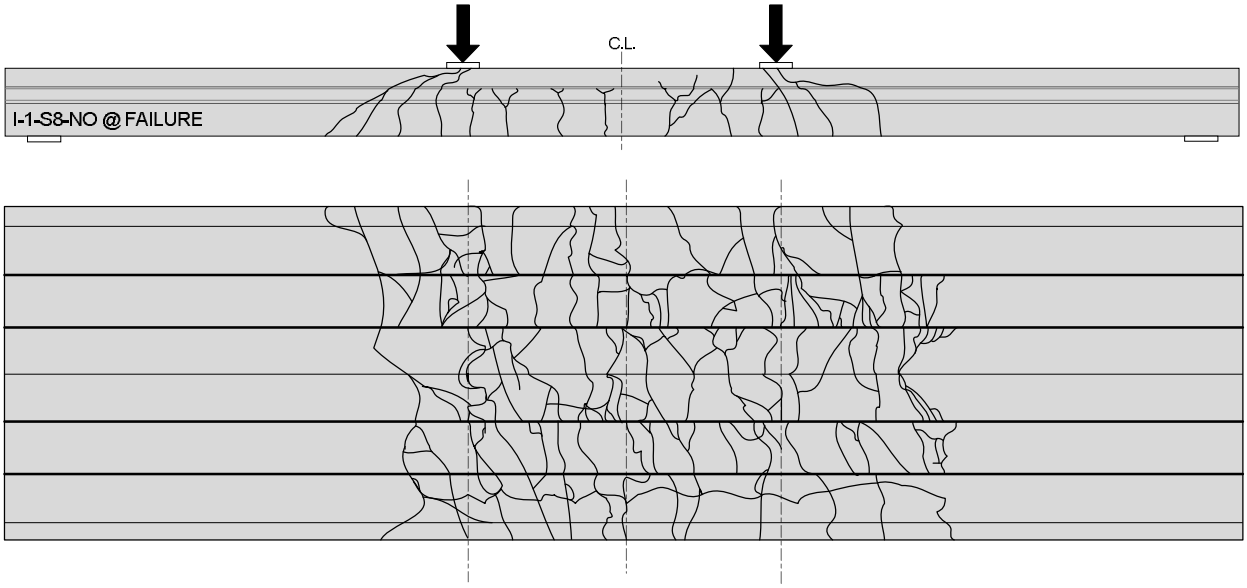

Figure 4.19: I-1-S8-NO Crack Pattern at Failure

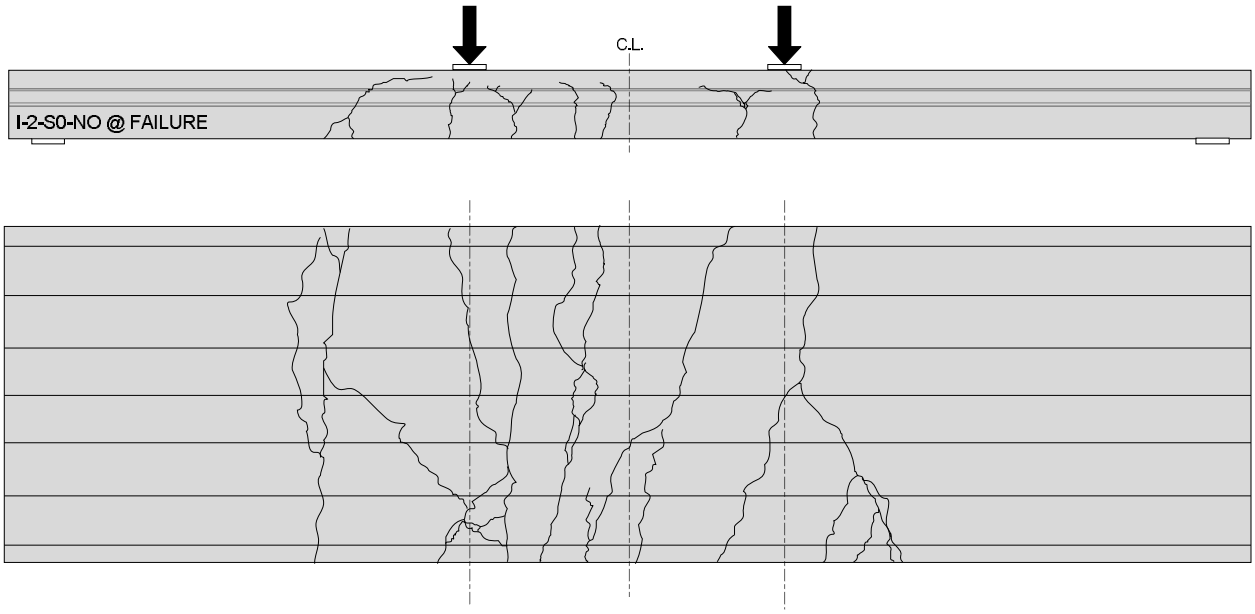

Figure 4.20: I-2-S0-NO Crack Pattern at Failure

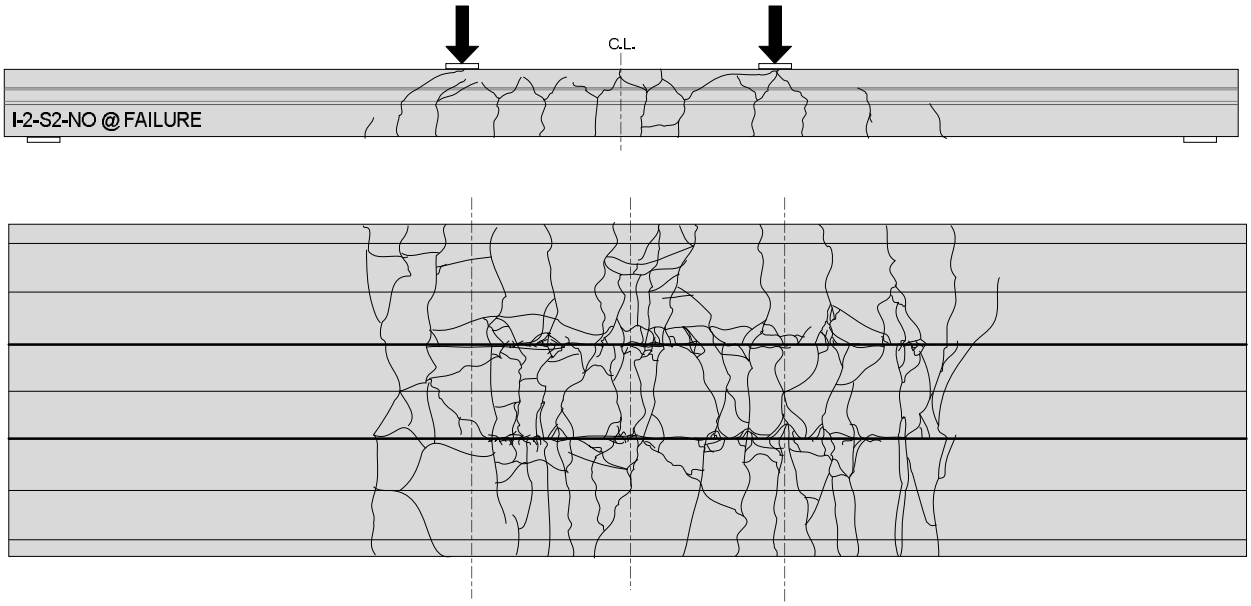

Figure 4.21: I-2-S2-NO Crack Pattern at Failure

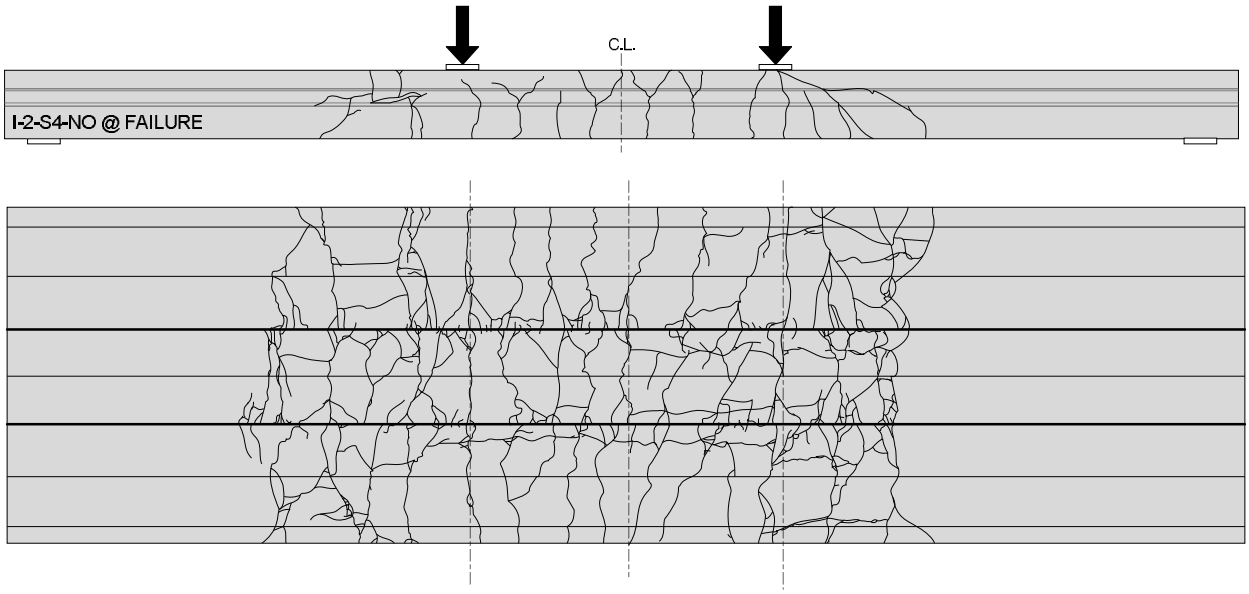

Figure 4.22: I-2-S4-NO Crack Pattern at Failure

Control specimens I-1-S0-NO and I-2-S0-NO exhibited typical flexural cracking behaviour. Cracking initiated with a single vertical flexural crack from the tension face of the member, close to the mid-span of the constant moment region. This initial crack corresponded to a dramatic decrease in applied load. As is common for prestressed concrete, the yield load was reached shortly after concrete cracking. As the internal tendons reached the yield stage, new cracks formed at a constant rate with an approximately even spacing. As the applied load approached the ultimate stage, new crack formation diminished, while existing cracks continued to widen, and propagate vertically towards the neutral axis. As the compressive stresses along the top of the slab neared the concrete strength in compression, the cracks began to deviate from a vertical orientation, propagating in an unorthodox manner. The cracks continued to increase in width and depth until the member ultimately failed in compression after steel yielding.

Initially the formation of cracks for all strengthened specimens followed a typical crack pattern for a member subject to four-point bending. The first cracks originated at the soffit of the slab,

between the loading points, near mid-span. Additional flexural cracks formed at a constant rate until the yielding load. The load-deflection curves for the strengthened specimens indicate sharp drops in load-carrying capacity for each major crack formation. After yielding of the steel tendons, the rate of development of side profile cracks decreased dramatically, while the formation of micro cracks along the soffit increased significantly.

NSM-CFRP strips acted as confinement, effectively reducing the width of the cracks by redistributing the tensile stresses. Compared to the control specimens, a greater number of cracks were experienced for the slabs strengthened with CFRP. The larger cracks were near evenly distributed along the constant moment region, regardless of the internal steel reinforcement ratio. The major cracks were clearly visible along the side profile of each specimen, however, the crack width decreased while the number of cracks increased as they approached a CFRP laminate along the slab soffit. As a crack nears an NSM laminate it splits into multiple micro cracks of hairline width. As a result of this phenomenon, the above schematics clearly illustrate the number of cracks increase with additional NSM laminates. This is true for specimen groups I-1-S2-NO and I-1-S4-NO; and I-2-S2-NO and I-2-S4-NO. It is not the case for specimen I-1-S8-NO because it failed prematurely in a flexural-shear type manner. The typical crack pattern on the soffit is illustrated in Figure 4.23.

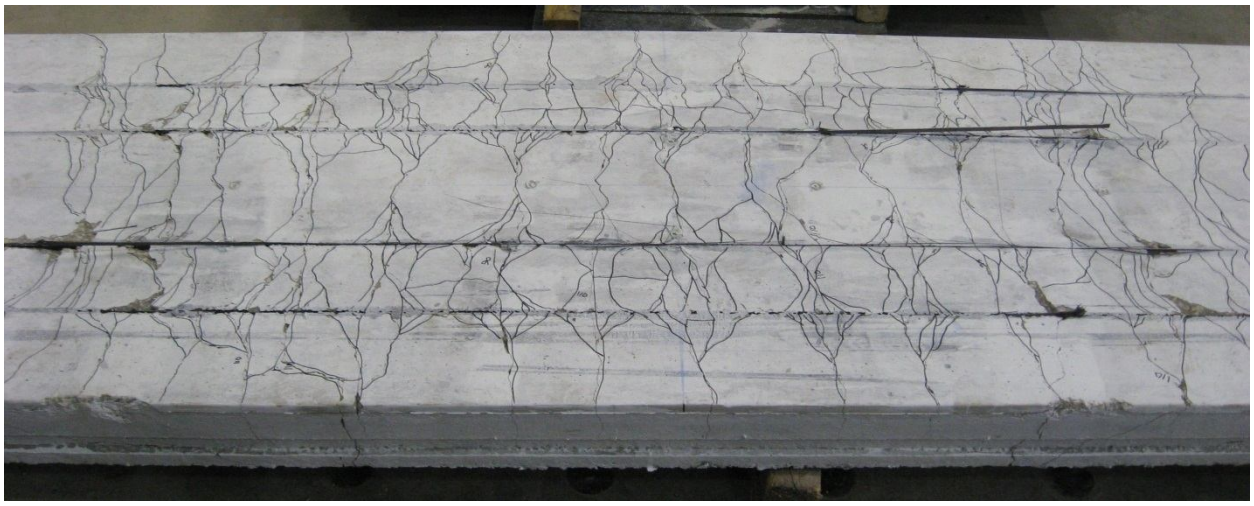

Figure 4.23: Typical Soffit Crack Pattern

The soffit micro cracks were confined between the NSM strips and did not develop outside of the outermost FRP strips. These micro cracks developed in a wave-like pattern, 'pointing' towards the mid-span. During this stage a noticeable crackling sound could be heard as the cracks developed. These cracks were concentrated along the flexural span to approximately two slab depths past the loading points. It was noted the average micro crack spacing at ultimate failure was approximately 20 mm.

For all strengthened specimens, cracking also developed along the shear span. The cracks were typically within a distance of two slab depths from the loading points. Cracking along the shear span behaved like flexural cracks, propagating vertically, until approximately 70 – 80% of the shear capacity was reached. Beyond this point the vertical cracks began propagating at an orientation towards the loading point. When this mode of failure governed, the rate of formation of micro cracks along the soffit decreased, while the width of the cracks along the shear spans continued to increase until the specimen sheared near the loading point. This behaviour is clear

for specimen I-1-S8-NO, where the eight NSM strips effectively redistributed the stresses to the shear span where the shear capacity was the limiting factor.

4.2.5 Series I summary of key findings

Capacity and Mode of Failure

- Increasing the prestressing and strengthening reinforcement ratios can change the mode of failure from a ductile response to an undesirable brittle response.
- For unstrengthened control specimens with a concrete compressive strength greater than 56.5 MPa, an internal prestressing reinforcement ratio of 0.00336 changed the ultimate behaviour from concrete crushing to a flexural-shear mode of failure. Therefore, any strengthening applied to high-strength concrete with this reinforcement ratio did not exhibit the favorable concrete crushing mode of failure as suggested by CSA S806-12 (2012) and ACI 440.2R-08 (2008).
- For specimens that initially experienced concrete crushing, the strengthening ratio 0.00183 changed the ultimate behaviour to a sudden and unfavourable NSM debonding failure mode.
- FRP debonding likely resulted from high shear stress concentrations generated by the loading points, and ultimately led to a brittle flexural-shear mode of failure.
- Three different debonding mechanisms were observed, specifically, splitting of the top epoxy cover, shear failure within the adhesive matrix, and cracking of the surrounding concrete substrate. In some cases combined failure modes were observed.
- The NSM-CFRP strengthening technique effectively enhanced the capacity of prestressed hollow core slabs by as much as 76%. The improvement in ultimate capacity

diminished with increasing internal reinforcement ratio. Therefore, when designing an NSM-FRP system, the expected increase in strength must consider the existing internal reinforcement ratio from the unstrengthened condition.

- Increasing the strengthening reinforcement ratio produced a diminishing enhancement to the ultimate capacity, for both prestressing reinforcement ratios. For specimens whose failure mode was not governed by bond failure of the NSM-CFRP strips, premature flexural-shear behaviour resulted in a maximum capacity between 77 – 87% of the shear capacity.
- Although not all minimum recommendations by ACI 440.2R-08 could be achieved for HC slabs (such as spacing between laminates of twice the depth of the NSM groove, or clear edge distance of four times the depth of the NSM groove), no significant influence on the capacity or mode of failure was observed.

Load-Strain Relationships

- The NSM technique allowed the load-carrying duties to be shared between the internal steel reinforcement and the NSM-FRP reinforcement, and effectively increased the yield load.
- Following the limit suggested by ACI for the maximum stress in the prestressed steel at the service state resulted in loads within 8% of the experimental cracking loads. Alternatively, limiting the compressive stress in concrete produced a conservative limit below the cracking loads, and effectively avoided inelastic deformations.

- Increasing the strengthening reinforcement ratio resulted in a diminishing increase in capacity at the yield stage. There exists a strengthening limit where any additional strengthening will not provide a proportionate improvement in yield load.
- For strengthened specimens, the enhancement of the ultimate moment was more prominent than at the yielding stage, indicating that the NSM technique was more effective at enhancing the ultimate limit state than the serviceability range.

Load-Deflection Relationships

- The presence of NSM reinforcement produced a slight increase on the gross moment of inertia of the section before cracking, as indicated by the increase in member stiffness.
- NSM reinforcement produced a negligible effect on the cracking load.
- The improvement in post-cracking stiffness for strengthened slabs is significant. This improvement diminishes with an increasing FRP strengthening ratio.
- Unlike conventionally reinforced concrete, this study suggests that for prestressed concrete, the addition of NSM laminates increases the deflection ductility for lower strengthening ratios, and may decrease the deflection ductility for higher strengthening ratios as the flexural response approach the shear capacity.

Cracking Behaviour

- Strengthened specimens experienced a larger number of cracks with an even distribution and smaller width.

- After steel yielding, transverse micro cracks developed at a rapid rate between the longitudinal CFRP reinforcement, and were concentrated along the flexural span, and extended two member depths past the loading points.
- NSM-FRP strips effectively redistribute stresses along the length of the member, as made evident by the stabilization of flexural cracks and the increasing width of flexural-shear cracks along the shear span.

4.3 Series II

This section summarizes the test results of three full-scale unstrengthened specimens with openings, measuring 600 × 308 mm along the longitudinal and transverse axes, respectively. The two opening layouts investigated in this study are centered at the midpoint along the flexural span, as well as two slab depths from the loading point along the shear span.

It should be noted the following Series II discussion and analysis section uses a similar approach to that of the Series I specimens. For that reason much of the preamble and background discussion will not be restated, but instead limited to only new observations particular to this specimen grouping. For further explanation and detail refer to the Series I discussion section or the appendices.

4.3.1 Capacity and mode of failure

Series II test specimens were subjected to four-point bending under simply-supported conditions. Each specimen was tested until flexural failure was achieved. Observations were recorded and are discussed in the following sections. Table 4.8 provides a brief summary of the sequence of failure for each test specimen.

Table 4.8: Series II – Mode of Failure Summary

	Specimen	Sequence and Mode of Failure
Series II	I-1-S0-NO	Steel yielding → concrete crushing → individual steel wire rupture
	II-1-S0-FO	Steel yielding → individual steel wire rupture → concrete crushing
	II-1-S0-SO	Steel yielding → flexural-shear failure in concrete → tendon shear/rupture → concrete crushing

Each specimen with an added opening experienced steel yielding as the first stage of failure. This was to be expected as the provision of an opening, along with the high-strength concrete maintains an under reinforced section. Also, each section experienced concrete crushing, albeit at different points during loading. Specimens I-1-S0-NO and II-1-S0-FO were flexure-critical, and ultimately failed by concrete crushing. The addition of an opening along the shear span, as is the case for specimen II-1-S0-SO, exhibited more of a flexural-shear failure mechanism prior to ultimate concrete crushing. It is possible this additional failure stage was caused by the superimposition of high stress concentrations generated by the loading point and the opening.

Table 4.9 summarizes the experimental results and the relative change in capacity compared to the unstrengthened control specimens. Detailed analysis and discussion is provided for each individual specimen in ***Appendix G***.

Table 4.9: Series II – Experimental Results

			Experimental Results			
	Specimen	Theoretical Shear Capacity, M_v (kNm)	Cracking Load, M_{cr} (kNm)	Ultimate Load, M_u (kNm)	Δ_{Mcr} (%)	Δ_{Mu} (%)
Series II	I-1-S0-NO	193	73	97	-	-
	II-1-S0-FO	193	62	83	-18	-17
	II-1-S0-SO	153	66	93	-11	-4

The addition of an opening decreased the ultimate capacity when compared to the control specimen, for both flexural and shear span locations. The location of an opening has a significant effect on the flexural and shear capacities of a pressed slab. For this flexural bending test setup, an opening along the flexural span decreased the ultimate capacity by 17%; compared to an opening along the shear span which produced a negligible decrease in capacity of 4%. Ultimate loads were reached well below the theoretical shear capacity, indicating that flexural behaviour was the dominant behaviour experienced by all specimens.

4.3.2 Load-strain relationships

This section presents a summary of the strains in the steel tendons for the unstrengthened specimens containing openings. Strain values are presented for critical locations along the longitudinal profile of the test specimens. See Chapter 3 for exact strain gauge locations. The following analysis and layout is similar to Series I. Figure 4.26 illustrates the load-tendon strain relationship for the specimens with an opening along the flexural and shear spans.

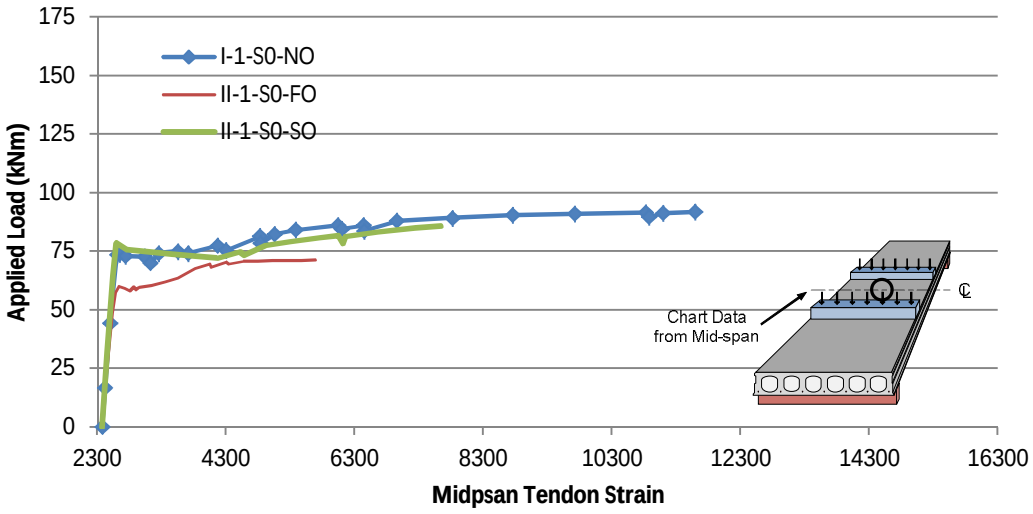

Figure 4.26: Series II – Load vs. Mid-span Tendon Strain

Each specimen exhibits a clear yield state, followed by a constant moment trend until failure. Table 4.10 summarizes the tensile strains and associated moments in each specimen at various stages during loading, namely cracking, service, yielding, and at ultimate. The service load was found from experimental data using the maximum allowable service stress in the prestressed steel, recommended by ACI 440.2R-08.

Table 4.10: Series II - Strain Values

		@ Cracking	@ Service		@ Yielding		@ Ultimate
	Specimen	M_{cr} (kNm)	$\varepsilon_{ps,s}$ (10^6)	M_s (kNm)	$\varepsilon_{ps,y}$ (10^6)	M_y (kNm)	M_u (kNm)
Series II	I-1-S0-NO	73	7040	74	8590	80	97
	II-1-S0-FO	62		60		71	83
	II-1-S0-SO	66		72		76	93

4.3.2.1 Serviceability limit state

Similar to the observations made for Series I, limiting the stress in the prestressing steel produces a service load comparable to the cracking load. For specimens I-1-S0-NO and II-1-S0-SO the service load is 1 and 9% greater than the cracking load. Only specimen I-1-S0-FO has a service load 3% less than the cracking load. Defining the serviceability limit state should be in relation to the cracking load, and incorporate the transformed moment of inertia to account for the NSM laminates.

4.3.2.2 Yield point

The presence of an opening along the flexural span effectively decreases the internal reinforcement ratio at mid-span, resulting in a corresponding decrease in yield and ultimate loads. Adding an in-situ opening to specimen II-1-S0-FO decreases the concrete cross-section and removes a steel tendon, resulting in a net increase in the internal reinforcement ratio by approximately 9%. This change results in a decreased yield load of 13%. Whereas increasing the internal reinforcement ratio between specimens I-1-S0-NO and I-2-S0-NO by 23% yields an increase in yield load by 44%. Although the presence of an opening increased the reinforcement ratio, the net stiffness of the section is significantly decreased, causing a lower cracking load, and thus allowing the specimen to reach the yielding stage at an earlier load. Adding an opening along the shear span resulted in a decrease in yield load of 5%. If the opening is sufficiently far enough from the maximum moment zone so as not to significantly influence the flexural stiffness, the yield load will remain relatively unchanged.

4.3.2.3 Tensile strains in steel tendons

As explained in Chapter 2, previous studies suggest that stress concentrations develop at the corners of openings. Figures 4.26 and 4.27 illustrate the load-tensile stain curves at the corners of the flexural and shear openings, respectively. The curves indicate the approximate load at which cracking originated at the corner of the opening.

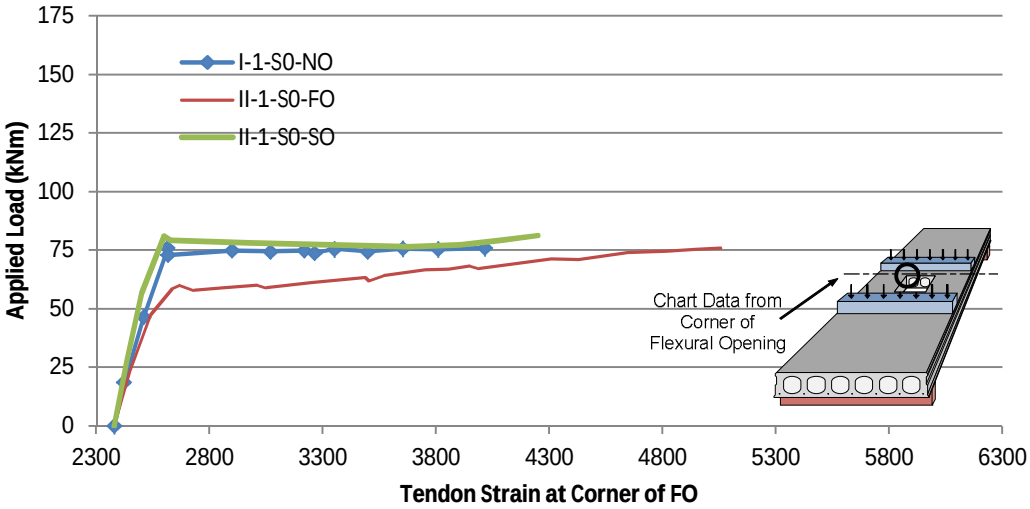

Figure 4.26: Series II - Load vs. Tendon Strain at corner of FO

The opening at midspan for specimen I-1-S0-FO initiates cracking at a much earlier stage, as indicated by the sudden increase of tensile strain at the corner of the opening. Considering specimen II-1-S0-NO, with an opening several member-depths from the location of the strain gauge, it is clear that the stress concentrations created by an opening extend only to a certain length.

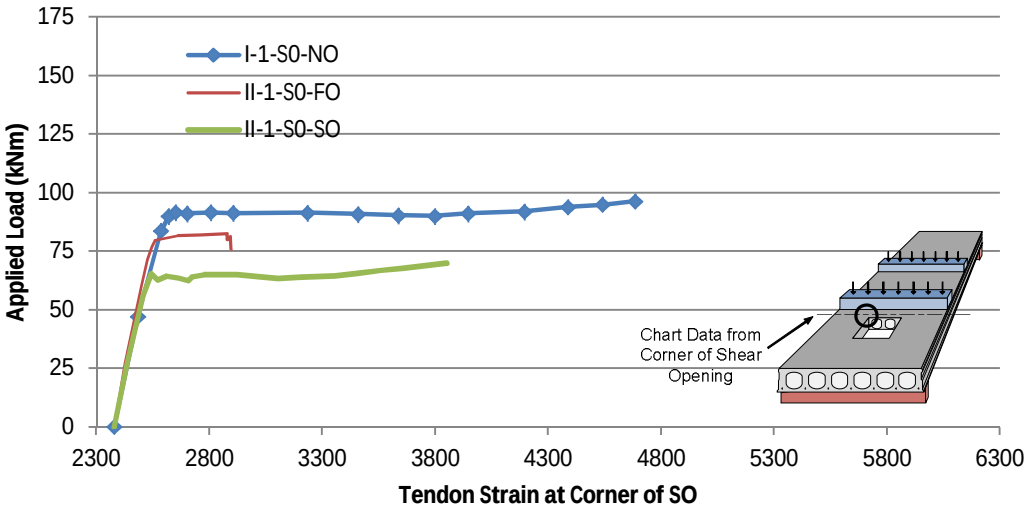

Figure 4.27: Series II - Load vs. Tendon Strain at corner of SO

A similar conclusion can be drawn from the curve of strains at the corner of an opening along the shear span. Specimen I-1-S0-SO experienced cracking at the corner of the opening at a much lower load than the other specimens. Cracking for all three Series II specimens occurred at lower loads when the opening is within the maximum moment region, and is delayed when the opening is along the shear span. This is expected since the two-point load test setup creates a critical region between the loading points, and any reduction in cross section or reinforcement will have a significant effect on the cracking behaviour.

4.3.3 Load-deflection relationships

The following section highlights the load-deflection relationship for all Series II specimens. Table 4.11 summarizes the predicted and experimental flexural and shear capacities for all Series II specimens. All values are expressed in moment capacities with units of *kNm*.

Table 4.11: Series II – Theoretical vs. Experimental Results

		Theoretical Results			Experimental Results	
	Specimen	Cracking Moment (kNm)	Ultimate Flexural Capacity (kNm)	Ultimate Shear Capacity (kNm)	Cracking Moment (kNm)	Ultimate Flexural Capacity (kNm)
Series II	II-1-S0-NO	82.9	106.8	193.2	73	97
	II-1-S0-FO	70.5	92.3	193.2	62	83
	II-1-S0-SO	68.8	92.3	152.5	66	93

The theoretical flexural capacities are derived using the strain compatibility method as recommended by the CSA and ACI design codes. The predicted values summarized above are from the ACI code as they more accurately represent the actual values as observed through experimentation. From the above table it becomes clear that adding a 308 × 600 opening along the flexural span effectively reduces the sections inertia, and is reflected as a decrease in ultimate capacity. Adding an opening along the flexural span reduces the ultimate capacity by 17%. Whereas adding a 308 × 600 opening along the shear span reduces the ultimate capacity by 4%. Since none of the ultimate failure loads are close to the predicted shear capacity, it can be assumed that flexural behaviour is the predominant behaviour and resulting mode of failure. Clearly, adding an opening two member depths from the concentrated loading point has a negligible effect on the ultimate failure load when a flexural failure is the governing mode of failure.

The load-mid-span deflection behaviour for Series II specimens is plotted in Figure 4.28. The trend lines indicate the effect that changing the location of an opening has on the flexural response for each test specimen.

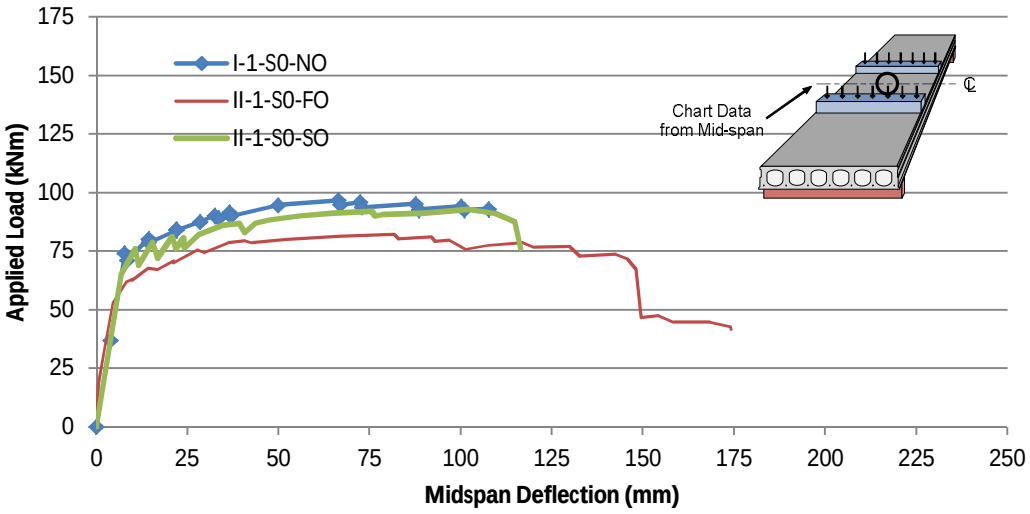

Figure 4.28: Series II - Load vs. Mid-span Deflection

The following sections explain the flexural behaviour of the unstrengthened specimens as the opening location varies from mid span to the shear span.

4.3.3.1 Pre-cracking behaviour and cracking load

Specimens I-1-S0-NO, II-1-S0-FO and II-1-S0-SO experienced different cracking loads and deflections, as indicated by the slope of their respective load-deflection relationships. Table 4.12 summarizes the deformability characteristics for all Series II specimens. The pre-cracking stiffness is expressed by the slope of the load-deflection curve from the onset of loading to the initial cracking stage. As expected, the control specimen, II-1-S0-NO, exhibited the largest pre-cracking stiffness. The addition of an opening along the flexural span decreased the flexural stiffness by 29%, resulting in a reduced cracking load of 18% and an increased deflection of 9%. The addition of an opening along the shear span, two slab depths from the loading point, resulted in a decrease in cracking load of 11%, and a decrease in deflection at cracking of 10%, resulting in an insignificant difference in the section's stiffness at mid-span compared to the control

specimen. This phenomenon confirms that an opening along the shear span which is sufficiently far enough from the critical moment region does not have a significant impact on the sections moment of inertia, as indicated by the near-identical stiffness compared to the control specimen. In the case of specimen II-1-S0-SO, the flexural response follows an identical linear path; however, due to the presence of an opening, the resulting stress concentrations are the corners initiate cracking at a lower load, but at a lower deflection as well. When an opening is added in the constant moment region, not only is cracking initiated at a lower applied load, but the inertia is decreased as well, allowing more deflection for a given load, resulting in a decrease in stiffness.

Table 4.12: Series II – Pre-Cracking Characteristics

	Specimen	Transformed Moment of Inertia, I_g (mm^4)	Applied Load @ Cracking, M_{cr} (kNm)	Deflection @ Cracking, δ_{cr} (mm)	Pre-Cracking Stiffness (GPa)
Series II	I-1-S0-NO	6.9476×10^8	73	7.5	10.8
	II-1-S0-FO	5.4500×10^8	62	8.2	8.4
	II-1-S0-SO	5.4500×10^8	66	6.8	10.8

The reduction in pre-cracking stiffness from 10.8 to 8.4 GPa, or 29%, caused by an opening along the flexural span yields a decrease in cracking load of 18%. The reduction in pre-cracking stiffness of only 1% caused by an opening along the shear span yields a decrease in the cracking load of 11%. The reduction in inertia at the shear opening location has only a slight overlap with the bending moment diagram. In other words, the reduction in inertia at the opening location along the shear span has little influence on the cracking behaviour which typically originates along the flexural span under a four-point bending test setup. In this case cracking originated

along the shear span at the corner of the opening closest to the flexural span. It is possible then that the reduction in cracking load for those specimens with openings is not governed by the decrease in inertia, but instead is more-so influenced by the presence of high stress concentrations at the corners of the openings. Therefore, if the opening is sufficiently large and close enough to the flexural span to influence the bending moment curve then cracking will originate around the opening and may decrease the effective cracking load of the structural element, essentially reducing the serviceability of the member.

4.3.3.2 Post-cracking stiffness

After cracking a non-linear behaviour was observed until failure. Unstrengthened specimens II-1-S0-NO, II-1-S0-FO, and II-1-S0-SO experienced a slight increase in load-carrying capacity after cracking, as shown by the positive slope of the load-deflection curve following the localized minimum after the initial cracking load. This gain in strength continued until the yield state was achieved, after which the member continued to deform without any increase in load-carrying capacity. The post-cracking stiffness for Series II specimens is nearly identical, except the presence of the opening shifts the trend line down in accordance with the decreased cracking load. This is to be expected as the strength of concrete is similar between specimens, and the prestressing reinforcement ratio differs by only 8%.

4.3.3.3 Deflection response and ductility

The ductility of the specimens is analyzed in terms of the dimensionless ratio of the mid-span deflection corresponding to the ultimate load, and the mid-span deflection corresponding to the yielding load. The yield limit is not an instantaneous condition that occurs at a clearly defined

load, deflection, or strain, however, in this case the yield load is considered to be the load corresponding to an induced stress of $0.9f_{pr}$ in the steel tendon. Table 4.13 provides a summary of the ductility results in terms of deflections at the yield and ultimate states for Series I specimens.

Table 4.13: Series II – Deflection and Ductility Results

	Specimen	δ_{cr} (mm)	δ_y (mm)	δ_u (mm)	μ_d	$\mu_d/\mu_{d\text{-Control}}$
Series II	II-1-S0-NO	7.5	15.9	68.5	4.31*	(1.00)
	II-1-S0-FO	8.2	19.1	85.4	4.47	1.04
	II-1-S0-SO	6.8	17.8	108.6	6.1	1.42

4.3.4 Cracking behaviour

The following schematics illustrate the final crack pattern for Series II specimens after the flexural loading test.

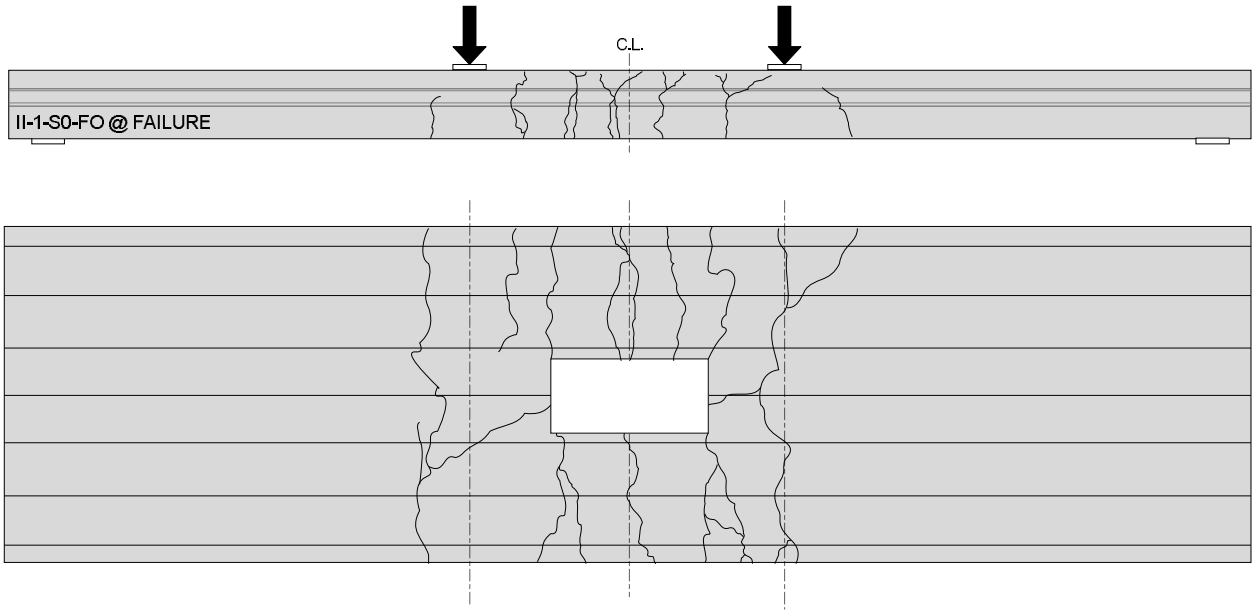

Figure 4.29: II-1-S0-FO Crack Pattern at Failure

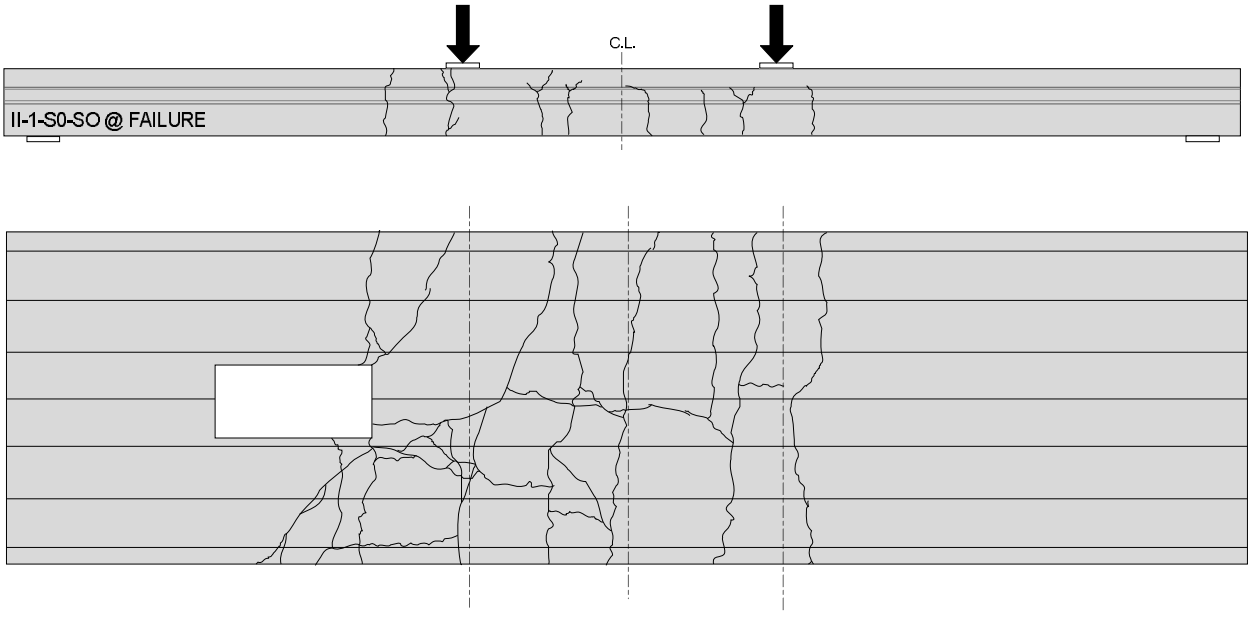

Figure 4.30: II-1-S0-SO Crack Pattern at Failure

For the specimen with an opening along the flexural span, II-1-S0-FO, cracking originated at a corner of the opening. The corner which experienced the first crack was the corner closest to the

drilled hole required to install the electrical steel strain gauge. This drilled hole was enough to facilitate crack formation. This behaviour was similar for the specimen with an opening along the shear span, II-1-S0-SO, who's crack originated at a corner of the opening closest to the strain gauge. After initial cracks developed at opening corners, the crack distribution developed similarly to the control specimen with no opening. Cracking was evenly distributed for the specimen with its opening centered at mid-span, and extended no further than one slab depth outside of the loading points. When the opening was located along the shear span, cracking was limited to the side of the opening closest to the maximum moment region. In this case cracks also only extended one slab depth away from the loading points.

The majority of cracks initiating from the corners of the openings traveled in a transverse orientation, directly towards the side of the slab. Contrary to some studies on openings in reinforced concrete which suggest that initial cracking propagates at 45 degrees from an opening corner, this research suggests that for openings in prestressed HC slabs, cracks travels directly to the side of the slab specimen.

4.3.5 Series II summary of key findings

Capacity and Mode of Failure

- When sufficient reinforcement and concrete area was present along the sides of an opening within the flexural span, the slabs mode of failure was similar to that of a slab without an opening.

- The presence of an opening along the shear span, two member depths from a concentrated loading point produced a negligible 4% decrease of the flexural capacity; and experienced different stages in its mode of failure as a result of increased shear stress concentrations.
- The location of an opening along the flexural and shear spans had a significant effect on the flexural and shear capacities, respectively.

Load-Strain Relationships

- An opening led to a net decrease in member stiffness, allowing the specimen to reach the serviceability stage at a lower applied load.
- The presence of an opening yielded higher tensile stress concentrations at the corners, as indicated by an earlier initiation of cracking when compared to the same location for a specimen with no opening, or an opening at a different location.

Load-Deflection Relationships

- An opening which is not located within the critical moment region does not have a significant impact on the sections moment of inertia, as indicated by the near-identical stiffness of the control specimen.

Cracking Behaviour

- An opening located within the maximum moment region effectively reduced the sections inertia, and initiated cracking at a lower applied load.

- Cracks originated at the corners of openings, most often in an orientation perpendicular to the slabs longitudinal axis.

4.4 Series III

This section summarizes the test results of five full-scale strengthened and unstrengthened specimens with and without openings. Those specimens with openings possess openings measuring 600 × 308 mm along the longitudinal and transverse axes, respectively. The two opening layouts investigated in this study are centered at the midpoint along the flexural span; as well as two slab depths from the loading point along the shear span. Each opening layout has an identical strengthened specimen constituting of two longitudinal NSM-CFRP strips, and four transvers NSM-CFRP strips.

It should be noted the following Series III discussion and analysis section uses a similar approach to that of the Series I specimens. For that reason much of the preamble and background discussion will not be restated, but instead limited to only new observations particular to this specimen grouping. For further explanation and detail refer to the Series I discussion section.

4.4.1 Capacity and mode of failure

Series III test specimens were subjected to four-point bending under simply-supported conditions. Each specimen was tested until flexural failure was achieved. A brief summary of the general modes of failure experienced for this series are explained below. For a more detailed analysis and discussion for each individual specimen see ***Appendix G***. Table 4.14 provides a brief summary of the sequence of failure for each test specimen.

Table 4.14: Series III Mode of Failure

	Specimen	Sequence and Mode of Failure
Series III	III-1-S0-NO	Steel yielding → concrete crushing → individual steel wire rupture
	III-1-S0-FO	Steel yielding → individual steel wire rupture → concrete crushing
	III-1-S2-FO	Steel yielding → partial CFRP rupture → localized CFRP delamination → concrete crushing
	III-1-S0-SO	Steel yielding → flexural-shear failure in concrete → tendon shear/rupture → concrete crushing
	III-1-S2-SO	Steel yielding → sudden flexural-shear failure & concrete crushing

Generally, all Series III specimens experienced steel yielding as the first stage of failure. As explained in the Series II analysis section, the unstrengthened specimens with openings, II-1-S0-FO and II-1-S0-SO, exhibited pure flexural behaviour; therefore there exists the possibility that when strengthened they will achieve the desirable concrete crushing failure mechanism, as suggested by ACI 440.2R-08 (2008). Strengthened specimen III-1-S2-FO experienced partial CFRP rupture and localized debonding. This suggests a strong bond between the FRP laminates and the concrete substrate, which ultimately led to concrete crushing. The strengthened opening along the shear span experienced premature laminate debonding which led to a sudden and violent flexural-shear failure mechanism with simultaneous concrete crushing.

Table 4.15: Series III – Experimental Results

			Experimental Results			
	Specimen	Theoretical Shear Capacity, M_v (kNm)	Cracking Load, M_{cr} (kNm)	Ultimate Load, M_u (kNm)	Δ_{Mcr} (%)	Δ_{Mu} (%)
Series III	I-1-S0-NO	193	73	97	-	-
	II-1-S0-FO	193	62	83	-18	-17
	III-1-S2-FO	192	63	116	2	40
	II-1-S0-SO	153	66	93	-11	-4
	III-1-S2-SO	153	79	121	20	30

Strengthening openings with two strips of NSM-CFRP effectively restored the flexural strength deficit incurred as a result of cutting the openings. Specimens with an opening along the flexural and shear spans incurred a decrease in strength of 17% and 4%, respectively. The addition of strengthening reinforcement to a flexural opening and a shear opening resulted in a significant capacity enhancement of 40% and 30%; which translates into a net increase of 23% and 26%, respectively. Recall from the Series I analysis that the capacity enhancement diminishes with a larger prestressing reinforcement ratio. Therefore, as expected, the capacity enhancement for specimen III-1-S2-FO is greater than specimen III-1-S2-SO, because the mid-span prestressing ratio is decreased with the removal of an internal steel tendon. Clearly, this phenomenon applies to the removal of internal reinforcement with the introduction of in-service openings. Also, specimen III-1-S2-SO which experienced a flexural-shear mode of failure only reached 80% of the predicted shear limit, similar to the behaviour experienced for strengthened specimens of Series I with no openings.

4.4.2 Load-strain relationships

This section presents a summary of the strains in the steel and CFRP for the specimens with strengthened openings. Strain values are presented for critical locations along the longitudinal profile of the test specimens. See Chapter 3 for exact strain gauge locations. The following analysis and layout is similar to Series I and II. Figures 4.33 and 4.34 illustrate the load-tendon strain for specimens with an opening along the flexural and shear spans, respectively.

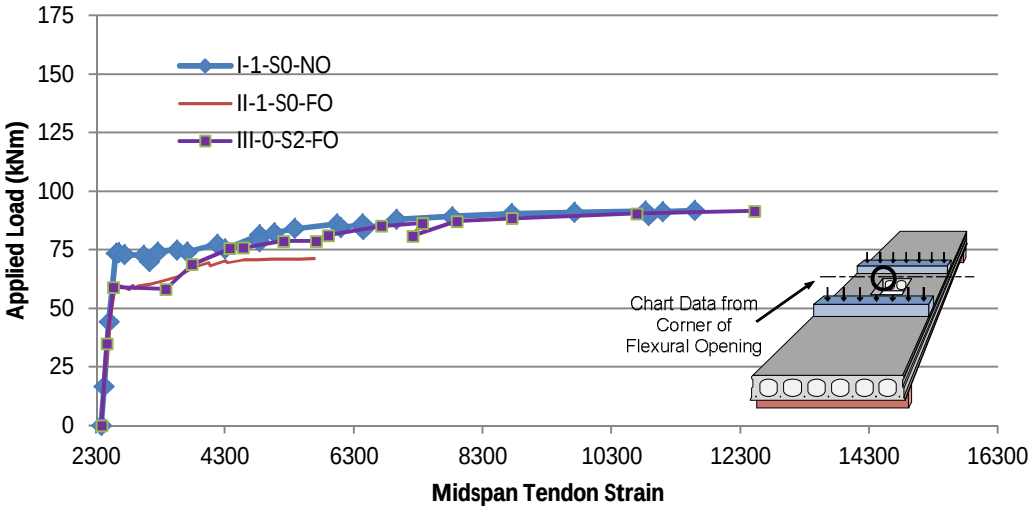

Figure 4.33: Series III – Load vs. Mid-span Tendon Strain (FO)

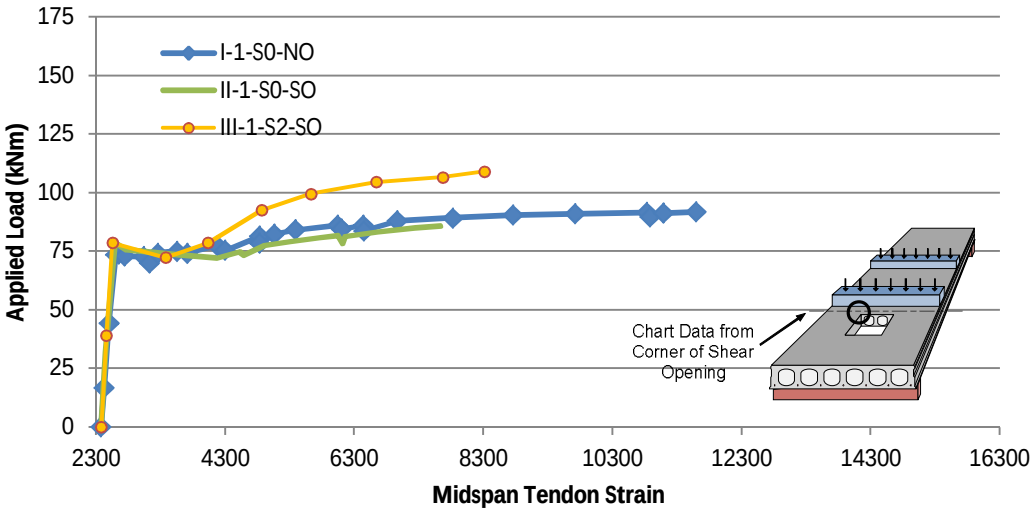

Figure 4.34: Series III – Load vs. Mid-span Tendon Strain (SO)

From the figures above it is clear that strengthened specimens III-1-S2-FO and III-1-S2-SO exhibit an improved post-cracking stiffness, as indicated by the increase in load-carrying capacity near the yield state. The strengthened opening along the shear span (III-1-S2-SO) exhibits a much more prominent stiffening effect compared with the strengthened opening along the flexural span (III-1-S2-FO), as indicated by the greater slope of the post-cracking load-strain curve. Table 4.16 summarizes the tensile strains and associated moments in each specimen at various stages during loading, namely cracking, service, yielding, and at ultimate. The service load was found from experimental data using the maximum allowable service stress in the prestressed steel, recommended by ACI 440.2R-08.

Table 4.16: Series III - Strain Values

		@ Cracking	@ Service		@ Yielding		@ Ultimate
	Specimen	M_{cr} (kNm)	$\varepsilon_{ps,s}$ (10^6)	M_s (kNm)	$\varepsilon_{ps,y}$ (10^6)	M_y (kNm)	M_u (kNm)
Series III	I-1-S0-NO	73	7040	74	8590	80	97
	II-1-S0-FO	62		60		71	83
	III-1-S2-FO	63		59		77	116
	II-1-S0-SO	66		72		76	93
	III-1-S2-SO	79		72		91	121

4.4.2.1 Serviceability limit state

Strengthening openings with NSM-CFRP did not produce any significant change to the service load compared to the unstrengthened specimens. The difference between the unstrengthened specimen II-1-S0-FO and its strengthened counterpart III-1-S2-FO is 2%. Similarly there is no difference between the unstrengthened specimen II-1-S0-SO and its strengthened counterpart III-1-S2-SO. This agrees with previous observations that NSM-CFRP strengthening has relatively little impact on the flexural behaviour before cracking and up to the yielding stage.

4.4.2.2 Yield point

Strengthening an opening within the maximum moment region increased the yield load from 71 kNm for specimen II-1-S0-FO to 77 kNm for specimen III-1-S2-FO; an increase of 9%. Strengthening an opening along the shear span increased the yield load from 76 kNm to 91 kNm for specimens II-1-S0-SO and III-1-S2-S0, respectively; an increase of 20%. Therefore, NSM reinforcement does not have as much of an improvement at the yield stage for an opening within the maximum moment region compared to an opening along the shear span.

4.4.2.3 Tensile strains in steel tendons

Figures 4.35, 4.36, and 4.37 illustrate the tensile strains in the steel tendons at the corners of the openings.

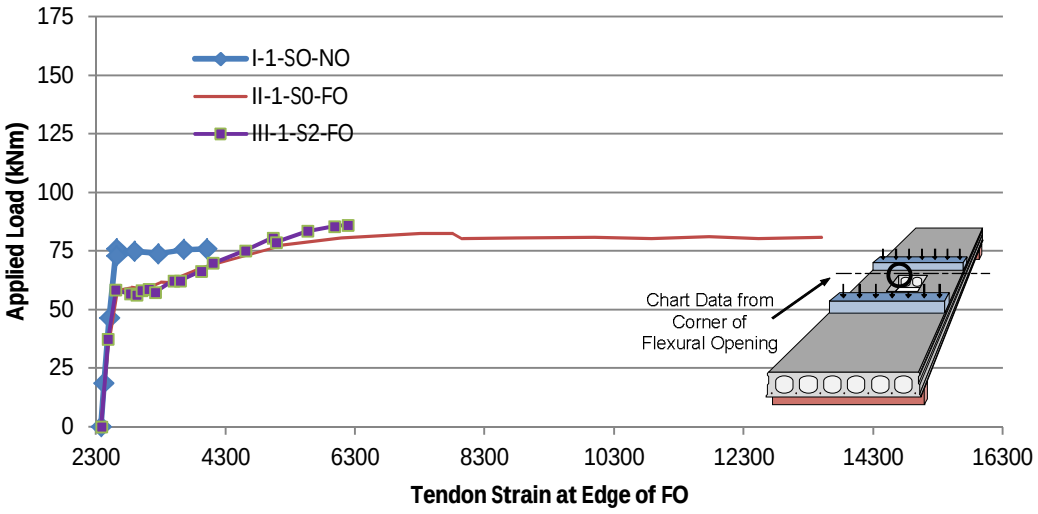

Figure 4.35: Series III – Load vs. Tendon Strain at Corner of FO

The presence of NSM-CFRP strips does not delay the initiation of cracking at the corners of the opening, as can be seen between the unstrengthened specimen II-1-S0-FO and III-1-S2-FO. This behaviour is similar to that discovered in Series I, whereby the presence of CFRP strengthening provides negligible enhancement to the sections moment of inertia and thus has little influence on the pre-cracking stiffness.

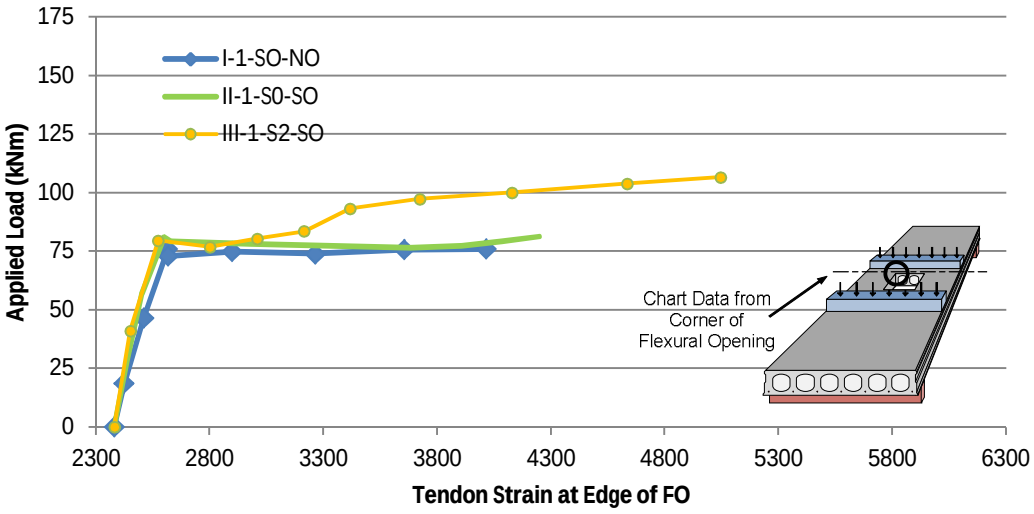

Figure 4.36: Series III – Load vs. Tendon Strain at Corner of FO

Figure 4.36 illustrates the strains in the tendon approximately three member-depths from the opening along the shear span. The cracking load at this location for all three specimens is nearly identical, suggesting that the increased stress distributions generated at the corners of the opening have a negligible effect on the strain and subsequent cracking behaviour three member-depths from the opening.

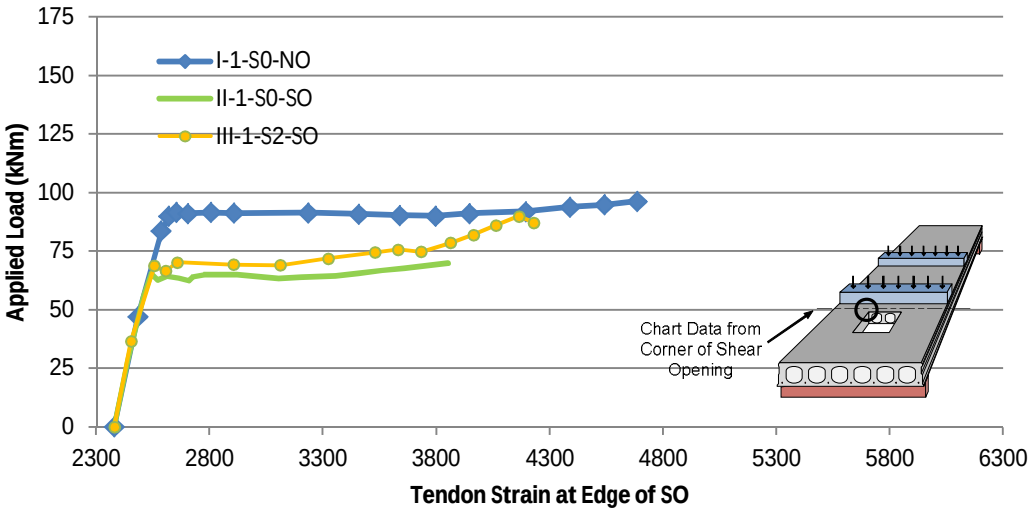

Figure 4.37: Series III – Load vs. Tendon Strain at Corner of SO

Similar strain behaviour is observed at the corner of openings along the shear span and the flexural span. Increased stress concentrations lead to increased strain, which induces cracking at a lower applied load.

4.4.2.4 Tensile strains in NSM-CFRP

Figure 4.38 presents the load-mid-span CFRP strain for all Series III specimens. Additional strain curves can be found in the ***Appendix I*** for the transverse NSM-CFRP strips.

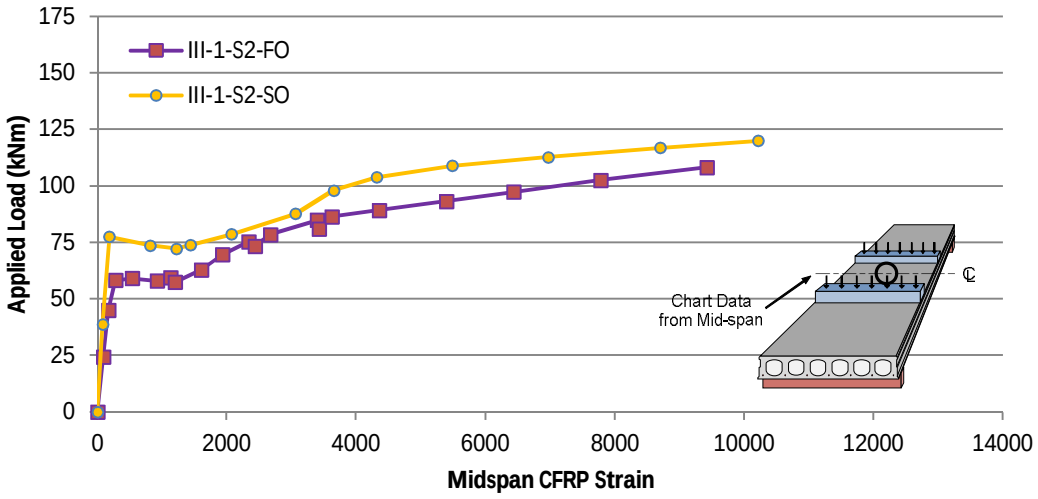

Figure 4.38: Series III – Load-CFRP Strain Curve for Specimens with Openings

4.4.3 Load-deflection relationships

The following section highlights the load-deflection behaviour for all Series III specimens. Similar to previous load-deflection analyses, it is divided into several subsections, organized to follow the steps of the flexural loading response. Table 4.17 summarizes the predicted and experimental flexural and shear capacities for all Series III specimens.

Table 4.17: Series III – Theoretical vs. Experimental Results

		Theoretical Results			Experimental Results	
	Specimen	Cracking Moment (kNm)	Ultimate Flexural Capacity (kNm)	Ultimate Shear Capacity (kNm)	Cracking Moment (kNm)	Ultimate Flexural Capacity (kNm)
Series III	I-1-S0-NO	82.9	106.8	193.2	73	97
	II-1-S0-FO	70.5	92.3	193.2	62	83
	III-1-S2-FO	69.4	109.3	191.5	63	116
	II-1-S0-SO	68.8	92.3	152.5	66	93
	III-1-S2-SO	69.4	109.3	152.5	79	121

As highlighted in the analysis of Series II, the addition of an opening effectively reduces the sections inertia, by decreasing the concrete surface area in tensile and compression zones, leading to a net increase in prestressing reinforcement ratio of 9%. From the table above it is clear the provision of an opening within the maximum moment region can reduce the ultimate capacity by 17%. Whereas adding an opening along the shear span, two member-depths from the constant moment region reduced the ultimate capacity slightly by 4%, but led to a flexural-shear mode of failure. Reinforcing the flexural opening with NSM-CFRP strips (III-1-S2-FO) increased the capacity by 40%. When compared to the original control specimen (I-1-S0-NO) the net increase in ultimate capacity is 20%. Reinforcing the shear opening with NSM-CFRP strips (III-1-S2-SO) increases the capacity by 30%. When compared to the original control specimen with no opening (I-1-S0-NO) the net increase in ultimate capacity is 25%. This data suggests that NSM technique has the ability to recover the decrease in ultimate capacity from the provision of an opening. In addition, it enhances the capacity beyond the original design strength to sustain additional superimposed loading; in this case by 20% for an opening at mid-span, and by 25% for an opening along the shear span. The load-mid-span deflection for Series III specimens are plotted in the following figures. Figure 4.39 illustrates the relationship between the unstrengthened specimens, to compare the effect of adding an opening with the original control specimen, namely I-1-S0-NO, II-1-S0-FO, and II-1-S0-SO. Figure 4.40 illustrates the relationship between the control specimen, and the strengthened and unstrengthened specimens with an opening along the flexural span, namely I-1-S0-NO, II-1-S0-FO, and III-1-S2-FO. Figure 4.41 illustrates the relationship between the control specimen, and the strengthened and unstrengthened specimens with an opening along the shear span, specifically I-1-S0-NO, II-1-

S0-SO, and III-1-S2-SO. The deflection curves were generated from LVDTs situated along the midpoint of the 4800 mm clear span.

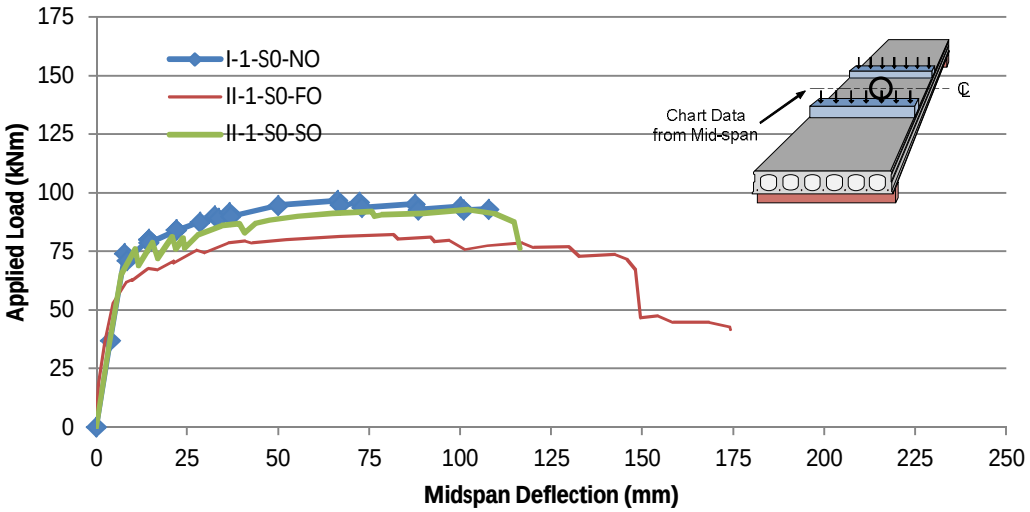

Figure 4.39: Series III – Load-Mid-span Deflection Curve for Unstrengthened Specimens

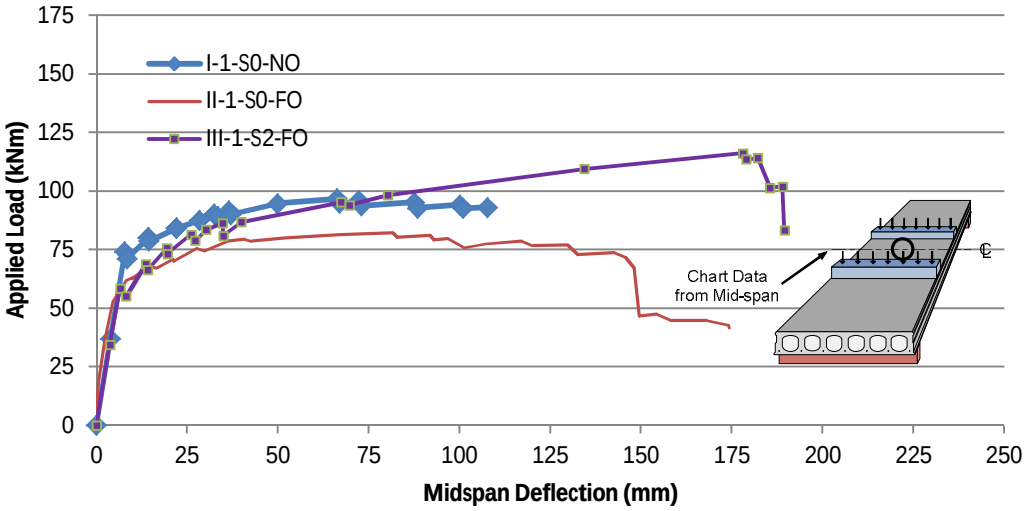

Figure 4.40: Series III – Load-Mid-span Deflection Curve for Specimens with FO

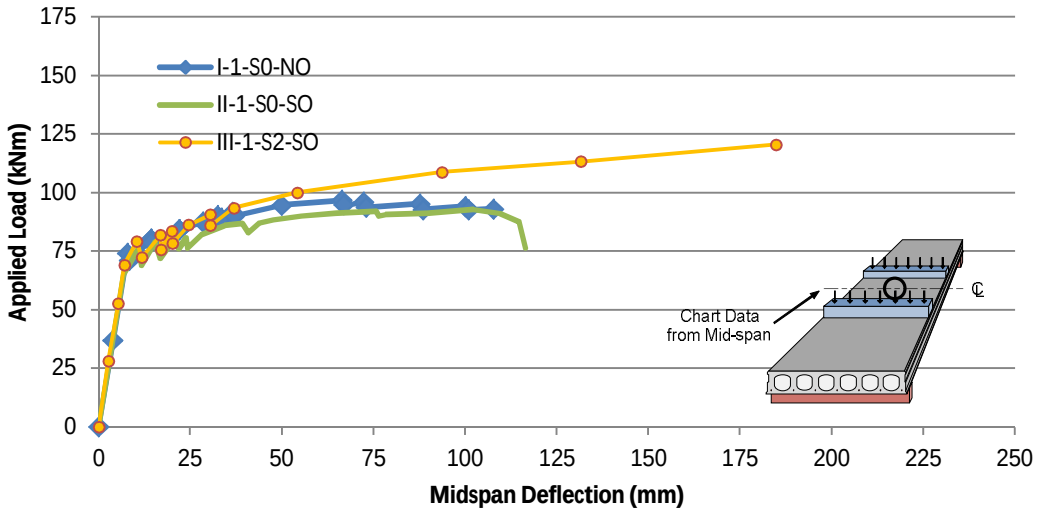

Figure 4.41: Series III – Load-Mid-span Deflection Curve for Specimens with SO

4.4.3.1 Pre-cracking behaviour and cracking load

The addition of openings and NSM strengthening had an effect on the precracking stiffness, as summarized in Table 4.18. The precracking stiffness is expressed by the slope of the load-mid-span deflection curve from the onset of loading to the initial cracking stage. The loads in the following table are expressed in kNm, and should be converted to an equivalent load in kN to determine the stiffness. For example, control specimen I-1-S0-NO has an applied cracking moment, M_{cr}, of approximately 73 kNm, which can be multiplied by the number of loading points (2), and divided by the length of the shear span (1.8 m), for an equivalent cracking load of approximately 81 kN. The load in units of kN can then be divided by the amount of deflection experienced at cracking, δ_{cr}, expressed in units of mm to determine the slope of the curve, thus arriving at the pre-cracking stiffness, expressed in units of giga pascals.

Table 4.18: Series III – Pre-Cracking Characteristics

	Specimen	Transformed Moment of Inertia, I_g (mm^4)	Applied Load @ Cracking, M_{cr} (kNm)	Deflection @ Cracking, δ_{cr} (mm)	Pre-Cracking Stiffness (GPa)
Series III	I-1-S0-NO	6.9476×10^8	73	7.5	10.8
	II-1-S0-FO	5.4500×10^8	62	8.2	8.4
	III-1-S2-FO	5.5154×10^8	63	10.1	6.9
	II-1-S0-SO	5.4500×10^8	66	6.8	10.8
	III-1-S2-SO	5.5154×10^8	79	10.4	8.5

The effect of the presence of an opening is discussed in Section 4.3, so only the effect of adding NSM-CFRP reinforcement will be discussed here. Adding two longitudinal CFRP strips to specimen III-1-S2-FO did not have an effect on the cracking load; however it did enhance the ductility of the member at cracking from 8.2 mm to 10.1 mm, and increase of 23%. The addition of NSM reinforcement yielded a decrease in stiffness of 22%. A similar trend is observed for the strengthened specimen with the shear opening, III-1-S2-SO. Both the cracking load and the ductility were increased, yielding a lower stiffness by 27%. It seems the addition of NSM reinforcement enhances the distribution of internal tensile stresses around the weaker areas within the concrete substrate, effectively postponing cracking, allowing the specimen to undergo increases in deflection with not increase in load until eventual cracking occurs. It should be noted that the concrete used for these specimens was from a different batch, where the unstrengthened specimen, II-1-S0-FO, had a compressive strength of 64.1 MPa, and the strengthened specimen III-1-S2-FO, had a lower compressive strength of 56.5 MPa. The lower concrete strength may have partially contributed to the increased ductility for the strengthened specimen III-1-S2-FO.

4.4.3.2 Post-cracking stiffness

It is clear from the load-deflection curves that unstrengthened specimens with openings encounter an obvious yield plateau, as indicated by an increase in deflection with minimal increase in load-carrying capacity. This trend is evident for specimens with openings at mid-span as well as along the shear span. Strengthening the openings with CFRP improves the post-cracking stiffness, as indicated by the increasing slope of the curve until ultimate failure. This phenomenon is encountered for strengthened specimens with or without any openings.

4.4.3.3 Deflection response and ductility

As we have seen, strengthening prestressed concrete is mainly to enhance the ultimate limit state, and does very little to improve or alter the serviceability limit state. However, it is noteworthy to explore the effect that strengthening has on the ductility of a member as it is loaded between the serviceability and ultimate limit states. If the ductility is reduced or held constant, this system may have an effective application; but if the deflections are too severe, this system may not be suitable for most rehabilitation projects. Table 4.19 summarizes the ductility results for openings strengthened with NSM-CFRP. Ductility is analyzed in terms of the dimensionless ratio of the mid-span deflection at the yield and ultimate load stages. All displacements are expressed in units of millimetres.

Table 4.19: Series III – Deflection and Ductility Results

	Specimen	δ_{cr} (mm)	δ_y (mm)	δ_u (mm)	μ_d	$\mu_d/\mu_{d\text{-Control}}$
Series III	III-1-S0-NO	7.5	15.9	68.5	4.31*	(1.00)
	III-1-S0-FO	8.2	19.1	85.4	4.47**	1.04
	III-1-S2-FO	10.1	21.6	178.0	8.24	1.84
	III-1-S0-SO	6.8	17.8	108.6	6.10**	4.42
	III-1-S2-SO	10.4	30.5	184.6	6.05	0.99

4.4.4 Cracking behaviour

The following schematics illustrate the progression of cracking for Series III specimens during loading. Three stages are illustrated for each specimen: the initial cracking stage, crack propagation at approximately 70% of the ultimate load, and the ultimate stage at failure.

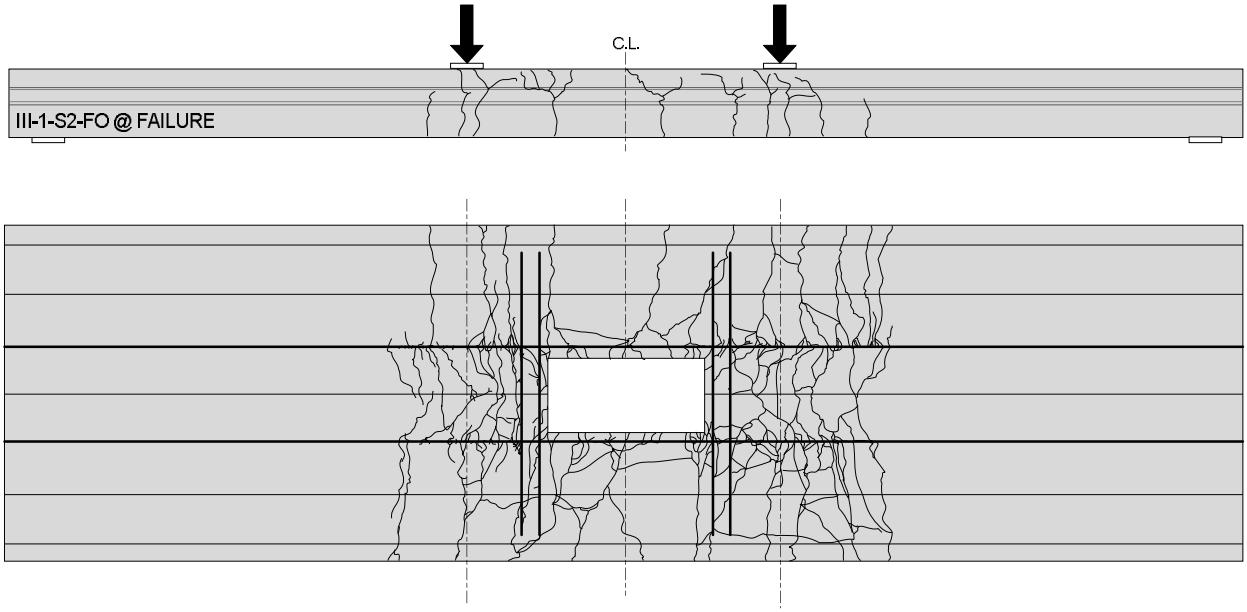

Figure 4.42: III-1-S2-FO Crack Pattern at Failure

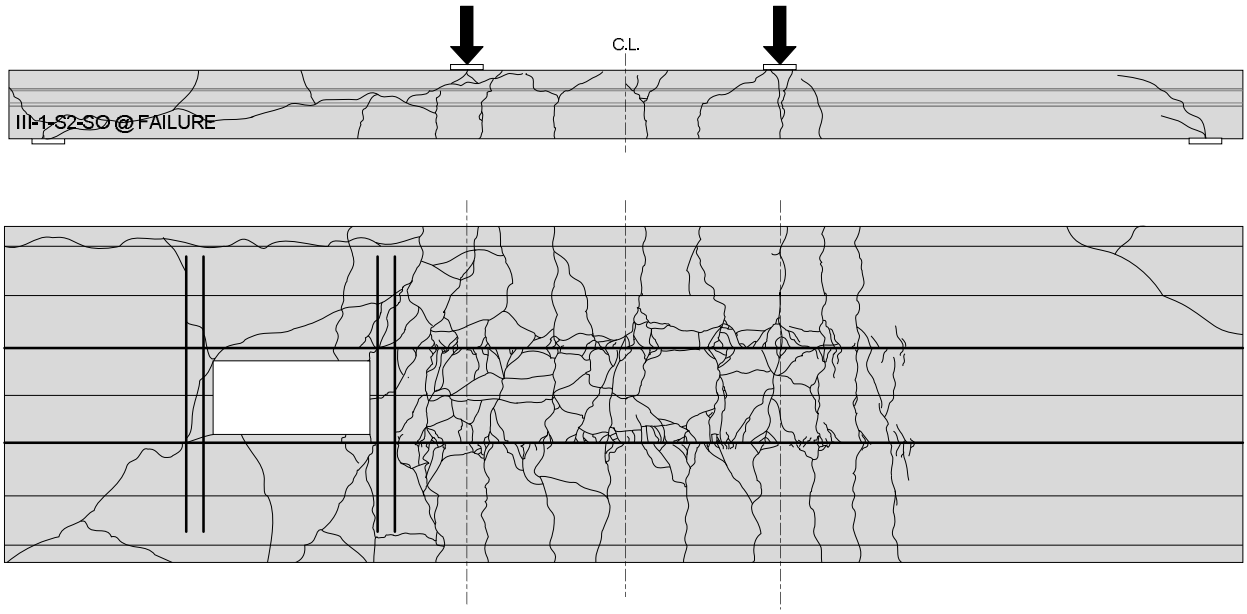

Figure 4.43: III-1-S2-SO Crack Pattern at Failure

Unstrengthened specimens with openings, such as II-1-S0-FO and II-1-S0-SO, experienced preliminary cracking at the corners of the openings. In accordance with existing studies as explained in Chapter 2, higher stress concentrations at each corner initiate cracking. Adding longitudinal and transverse NSM-CFRP strips initiate cracking at the corners, but also from the sides of the openings. Transverse cracks emanating from the sides of the openings occurred much sooner for specimens III-1-S2-FO and III-1-S2-SO than for their unstrengthened counterparts. It is possible the presence of CFRP strips distribute the stresses more evenly, maintaining the critical cracking location to the mid-span, where the bottom tensile fibres experience the largest tensile stress. Adding NSM-CFRP strips to specimen III-1-S2-FO initiated near-simultaneous cracking at the opening corners, as well as at mid-span, indicated that the tensile stress concentrations created at the corners of the opening were similar to those at mid-span.

After initial cracking, cracks developed at a constant rate up to steel yielding, which is approximately 70 – 80% of the ultimate load. Initial cracks originated around the corners of the openings, but then began developing between the loading points along the constant moment region. Strengthened specimen I-1-S2-NO experienced a greater number of cracks with a reduced spacing compared to the unstrengthened control specimen, I-1-S0-NO; whereas specimen III-1-S2-FO, with an opening at mid-span, experienced a similar number and spacing of cracks when compared to the unstrengthened specimen II-1-S0-FO. This trend is similar for the strengthened opening along the shear span when compared to its unstrengthened counterpart. It seems the presence of an opening creates an increased number of cracks with a tighter spacing regardless of the presence of NSM strengthening.

4.4.5 Series III summary of key findings

Capacity and Mode of Failure

- Strengthening openings with two strips of NSM-CFRP effectively restored the flexural strength deficit incurred as a result of cutting the openings, and provided a net increase in flexural capacity.
- Strengthening an opening along the flexural span resulted in a desirable concrete crushing failure mechanism, whereas strengthening an opening along the shear span yielded a premature debonding failure mechanism.
- The strengthened opening along the flexural span achieved substantial bond strength as indicated by the partial CFRP rupture; whereas the stress concentrations generated by the shear opening caused premature debonding failure.

- Eliminating the epoxy cover from the NSM laminate decreased the confinement pressure, and increases the chances the FRP strip will split and fray.
- The strength enhancement provided by NSM laminates diminished with an increased prestressing reinforcement ratio, as indicated by the removal of an internal steel tendon.
- Those specimens with openings that exhibited a flexural-shear mode of failure reached an ultimate capacity that was 80% of the predicted shear limit.
- No observable change to the mode of failure was generated by the addition of transverse NSM laminates around the openings, regardless of the opening location.

Load-Strain Relationships

- Strengthening an opening along the shear span produced a larger improvement to the yield load versus strengthening an opening along the flexural span.
- The presence of NSM-CFRP strips did not delay the initiation of cracking at the corners of the opening.
- The stress concentrations generated at the corners of openings had a negligible effect on the strain and subsequent cracking behaviour three member-depths from the opening.

Load-Deflection Relationships

- Adding NSM-CFRP strips effectively distributed the tensile stresses around the weakest areas within the concrete substrate, and delayed cracking as the member continued to deform.
- For specimens with an opening, the addition of NSM-CFRP caused a decrease in member stiffness between 22 – 27%.

Cracking Behaviour

- For specimens with NSM strengthening, cracking simultaneously originated at the corners of the openings and at the mid-span, indicating the NSM reinforcement effectively resists the stresses developed at the opening and redistributes them along the reinforcement profile.
- Crack number and spacing was not affected by the presence of NSM reinforcement if the slab had an opening.

4.5 CSA Standard and ACI Guideline Review

4.5.1 Capacity comparison

It is important to determine the accuracy of the code provisions for ultimate capacity, as provided by the Canadian Standards Association (CSA S806-12) and the American Concrete Institute (ACI 440.2R-08). As explained in Chapter 2 of this thesis, the CSA specifies a maximum permissible strain in the NSM reinforcement to be 0.007; while the ACI specifies the maximum permissible strain as a fraction of the ultimate tensile strain of the FRP reinforcement, as 70% of the ultimate tensile capacity. Table 4.20 summarizes the capacities as determined using the code provisions, and proceeds to illustrate the differences between the predicted results and the experimental results. Flexural limits are listed and compared as moment capacities with units of kNm.

Table 4.20: CSA and ACI Ultimate Capacity Comparison

		Exp. Result	ACI		CSA	
	Specimen	Flexural Capacity, M_u (kNm)	Flexural Capacity, M_{u-p} (kNm)	ACI vs. Exp. (%)	Flexural Capacity, M_{u-p} (kNm)	CSA vs. Exp. (%)
Series I, II, III	I-1-S0-NO	97	106.8	10.1	102.7	5.4
	I-1-S2-NO	127	125.2	-1.4	105.5	-20.7
	I-1-S4-NO	155	143.1	-8.3	117.4	-32.3
	I-1-S8-NO	171	179.5	5.0	139.3	-23.0
	I-2-S0-NO	136	139.2	2.4	133.4	-1.8
	I-2-S2-NO	165	156.6	-5.4	138.5	-19.3
	I-2-S4-NO	172	174.3	1.3	146.8	-17.1
	II-1-S0-FO	83	92.3	11.2	86.4	4.1
	II-1-S0-SO	93	92.3	-0.7	86.4	-9.3
	III-1-S2-FO	116	109.3	-6.1	92.5	-25.4
	III-1-S2-SO	121	109.3	-10.7	92.5	-30.8

M_{u-p}: Theoretical ultimate flexural capacity
M_u: Experimental ultimate flexural capacity

It is clear that the strain compatibility method as suggested for both CSA and ACI guidelines generally yield a conservative estimate of the flexural capacity of prestressed concrete strengthened with NSM-CFRP strip reinforcement. For unstrengthened prestressed concrete, the CSA and ACI guidelines overestimate the capacity by 5.4 and 10.1%, respectively. Considering only strengthened specimens, the ACI guide yields an average discrepancy of -3.7%; while the CSA guide yields an average discrepancy of -22.5%. The maximum strain as a factor of the ultimate tensile strength of the FRP, as suggested by the ACI guideline, yields a more accurate prediction for strengthened flexural capacities. As a result, the ACI code predictions were referenced throughout this thesis.

An argument can be made that as the CFRP strengthening ratio increases so too does the conservative difference between predicted and actual results, indicating that with greater capacity enhancement the guidelines increase the factor of safety. The strain compatibility approach becomes increasingly conservative for strengthened prestressed concrete. This trend remains valid until the mode of failure shifts from a ductile concrete compression failure to a sudden and violent flexural-shear type failure. Once the strengthened specimens reach a premature flexural-shear limit the codes predications become more accurate. The guidelines will forever suggest an increase in capacity as more strengthening reinforcement is added. The strain compatibility method is unable to account for this premature flexural-shear mode of failure. However, there exists a limit once the localized shear capacity is reached; any increase in strengthening provides no increase in flexural capacity. The strain compatibility method must have a limit below the shear capacity to account for this premature mode of failure for strengthened prestressed concrete. The premature mode of failure was found to occur between 77% and 87% of the shear capacity.

In terms of openings, since the flexural opening interrupts the middle tendon, the flexural capacity was calculated assuming the tendon does not exist, and that any strength developed after the opening is negligible. The section moment of inertia was also reduced to account for the addition of an opening at mid-span. For the specimen with an opening along the flexural span, the ACI guideline overestimates the capacity by a considerable 10.1%. However, for a slab with an opening along the shear span, sufficiently far enough away from the loading point so as not to decrease the bending moment capacity, the guideline is reasonably accurate with the flexural capacity.

CHAPTER 5 – SUMMARY & CONCLUSIONS

5.1 General

The understanding of strengthening techniques has shown significant progress; however there are some critical areas which still require in-depth investigation. One such area is the flexural strengthening of precast prestressed hollow core slabs using NSM-CFRP reinforcement. The research focuses on several significant and relevant design concepts, such as prestressed concrete, precast hollow core slabs, the complex behaviour of disturbed regions in reinforced concrete, fiber reinforced polymer composite materials, and the near-surface mounted strengthening technique. To understand the flexural performance and relationship of these design concepts, an experimental program was conducted. Eleven full-scale slab specimens were constructed and tested to failure under a four-point bending configuration. The program was separated into three key focus areas to investigate the following parameters: prestressing reinforcement ratio, CFRP strengthening ratio, and in-service opening location. The information presented in this thesis is applicable to civil infrastructure such as bridges, parking garages, marine structures, and commercial and industrial buildings.

5.2 Influence of NSM-FRP Reinforcement

The following conclusions summarize the key findings that the strengthening ratio and the internal prestressing ratio had on the capacity and mode of failure, the strain relationships, the deflection behaviour, and the crack patterns of PC slabs.

5.2.1 Capacity and Mode of Failure

- Increasing the prestressing and strengthening reinforcement ratios can change the mode of failure from a ductile response to an undesirable brittle response.
- For unstrengthened control specimens with a concrete compressive strength greater than 57 MPa, an internal prestressing reinforcement ratio of 0.00336 changed the ultimate behaviour from concrete crushing to a flexural-shear mode of failure. Therefore, any strengthening applied to high-strength concrete with this reinforcement ratio did not exhibit the favorable concrete crushing mode of failure as suggested by CSA S806-12 (2012) and ACI 440.2R-08 (2008).
- For specimens that initially experienced concrete crushing, the strengthening ratio of 0.00183 changed the ultimate behaviour to a sudden and unfavourable NSM debonding failure mode.
- FRP debonding likely resulted from high shear stress concentrations generated by the loading points, and ultimately led to a brittle flexural-shear mode of failure.
- Three different debonding mechanisms were observed, specifically, splitting of the top epoxy cover, shear failure within the adhesive matrix, and cracking of the surrounding concrete substrate. In some cases combined failure modes were observed.

- The NSM-CFRP strengthening technique effectively enhanced the capacity of prestressed hollow core slabs by as much as 76%. The improvement in ultimate capacity diminished with increasing internal reinforcement ratio. Therefore, when designing an NSM-FRP system, the expected increase in strength must consider the existing internal reinforcement ratio from the unstrengthened condition.
- Increasing the strengthening reinforcement ratio produced a diminishing enhancement to the ultimate capacity, for both prestressing reinforcement ratios. For specimens whose failure mode was not governed by bond failure of the NSM-CFRP strips, premature flexural-shear behaviour resulted in a maximum capacity between 77 – 87% of the shear capacity.
- Although not all minimum recommendations by ACI 440.2R-08 could be achieved for HC slabs (such as spacing between laminates of twice the depth of the NSM groove, or clear edge distance of four times the depth of the NSM groove), no significant influence on the capacity or mode of failure was observed.

5.2.2 Load-Strain Relationships

- The NSM technique allowed the load-carrying duties to be shared between the internal steel reinforcement and the NSM-FRP reinforcement, and effectively increased the yield load.
- Following the limit suggested by ACI for the maximum stress in the prestressed steel at the service state resulted in loads within 8% of the experimental cracking loads. Alternatively, limiting the compressive stress in concrete produced a conservative limit below the cracking loads, and effectively avoided inelastic deformations.

- Increasing the strengthening reinforcement ratio resulted in a diminishing increase in capacity at the yield stage. There exists a strengthening limit where any additional strengthening will not provide a proportionate improvement in yield load.
- For strengthened specimens, the enhancement of the ultimate moment was more prominent than at the yielding stage, indicating that the NSM technique was more effective at enhancing the ultimate limit state than the serviceability range.

5.2.3 Load-Deflection Relationships

- The presence of NSM reinforcement produced a slight increase on the gross moment of inertia of the section before cracking, as indicated by the increase in member stiffness.
- NSM reinforcement produced a negligible effect on the cracking load.
- The improvement in post-cracking stiffness for strengthened slabs is significant. This improvement diminishes with an increasing FRP strengthening ratio.
- Unlike conventionally reinforced concrete, this study suggests that for prestressed concrete, the addition of NSM laminates increases the deflection ductility for lower strengthening ratios, and may decrease the deflection ductility for higher strengthening ratios as the flexural response approach the shear capacity.

5.2.4 Cracking Behaviour

- Strengthened specimens experienced a larger number of cracks with an even distribution and smaller width.
- After steel yielding, transverse micro cracks developed at a rapid rate between the longitudinal CFRP reinforcement, and were concentrated along the flexural span, and extended two member depths past the loading points.

- NSM-FRP strips effectively redistribute stresses along the length of the member, as made evident by the stabilization of flexural cracks and the increasing width of flexural-shear cracks along the shear span.

5.3 Strength and Serviceability Effects of Openings in PC

The following conclusions summarize the key findings that the presence of in-service openings had on the capacity and mode of failure, the strain relationships, the deflection behaviour, and the crack patterns of PC slabs.

5.3.1 Capacity and Mode of Failure

- When sufficient reinforcement and concrete area was present along the sides of an opening within the flexural span, the slabs mode of failure was similar to that of a slab without an opening.
- The presence of an opening along the shear span, two member depths from a concentrated loading point produced a negligible 4% decrease of the flexural capacity; and experienced different stages in its mode of failure as a result of increased shear stress concentrations.
- The location of an opening along the flexural and shear spans had a significant effect on the flexural and shear capacities, respectively.

5.3.2 Load-Strain Relationships

- An opening led to a net decrease in member stiffness, allowing the specimen to reach the serviceability stage at a lower applied load.

- The presence of an opening yielded higher tensile stress concentrations at the corners, as indicated by an earlier initiation of cracking when compared to the same location for a specimen with no opening, or an opening at a different location.

5.3.3 Load-Deflection Relationships

- An opening which is not located within the critical moment region does not have a significant impact on the sections moment of inertia, as indicated by the near-identical stiffness of the control specimen.

5.3.4 Cracking Behaviour

- An opening located within the maximum moment region effectively reduced the sections inertia, and initiated cracking at a lower applied load.
- Cracks originated at the corners of openings, most often in an orientation perpendicular to the slabs longitudinal axis.

5.4 NSM-FRP Technique on Strength Restoration

The following conclusions summarize the key findings that NSM strengthening had on the capacity and mode of failure, the strain relationships, the deflection behaviour, and the crack patterns of specimens with in-service openings.

5.4.1 Capacity and Mode of Failure

- Strengthening openings with two strips of NSM-CFRP effectively restored the flexural strength deficit incurred as a result of cutting the openings, and provided a net increase in flexural capacity.
- Strengthening an opening along the flexural span resulted in a desirable concrete crushing failure mechanism, whereas strengthening an opening along the shear span yielded a premature debonding failure mechanism.
- The strengthened opening along the flexural span achieved substantial bond strength as indicated by the partial CFRP rupture; whereas the stress concentrations generated by the shear opening caused premature debonding failure.
- Eliminating the epoxy cover from the NSM laminate decreased the confinement pressure, and increases the chances the FRP strip will split and fray.
- The strength enhancement provided by NSM laminates diminished with an increased prestressing reinforcement ratio, as indicated by the removal of an internal steel tendon.
- Those specimens with openings that exhibited a flexural-shear mode of failure reached an ultimate capacity that was 80% of the predicted shear limit.
- No observable change to the mode of failure was generated by the addition of transverse NSM laminates around the openings, regardless of the opening location.

5.4.2 Load-Strain Relationships

- Strengthening an opening along the shear span produced a larger improvement to the yield load versus strengthening an opening along the flexural span.

- The presence of NSM-CFRP strips did not delay the initiation of cracking at the corners of the opening.
- The stress concentrations generated at the corners of openings had a negligible effect on the strain and subsequent cracking behaviour three member-depths from the opening.

5.4.3 Load-Deflection Relationships

- Adding NSM-CFRP strips effectively distributed the tensile stresses around the weakest areas within the concrete substrate, and delayed cracking as the member continued to deform.
- For specimens with an opening, the addition of NSM-CFRP caused a decrease in member stiffness between 22 – 27%.

5.4.4 Cracking Behaviour

- For specimens with NSM strengthening, cracking simultaneously originated at the corners of the openings and at the mid-span, indicating the NSM reinforcement effectively resists the stresses developed at the opening and redistributes them along the reinforcement profile.
- Crack number and spacing was not affected by the presence of NSM reinforcement if the slab had an opening.

5.5 CSA and ACI Guideline Comparison

The following conclusions highlight the major differences between the CSA S806-12 (2012) and the ACI 440.2R-08 (2008) guidelines for the design and construction of concrete structures with externally bonded FRP systems.

- The approach suggested by the ACI guidelines to determine the flexural capacity of strengthened prestressed concrete was more accurate than the approach suggested by the CSA guidelines.
- The strain compatibility approach as suggested by CSA and ACI guidelines yielded conservative flexural capacity predictions for lower levels of strengthening.
- Ultimate capacity predictions were within approximately 10% of the experimental capacities. This indicates that the applied design assumptions and the strain compatibility method yielded reasonable values for the flexural capacity of prestressed concrete with openings along the flexural and shear spans.
- As the strengthening reinforcement ratio increases, so does the difference between predicted and experimental results. Increasing the number of laminates yielded a more conservative theoretical capacity. This trend is valid up to 87% of the predicted shear capacity.

5.6 Recommendations for Future Research Areas

Although the objectives of this thesis were achieved, there are areas that require further study to fully understand the behaviour of precast prestressed hollow core slabs strengthened in flexure with NSM-CFRP reinforcement.

- Investigate the behaviour of strengthened prestressed concrete reinforced with unbonded tendons, in which strain compatibility is not applicable.
- Develop a parametric study to determine the effects that different parameters and load configurations have on the flexural behaviour of strengthened prestressed concrete.

- Since several test specimens experienced a premature flexural-shear mode of failure that did not coincide with the predicted shear capacity, a detailed analysis on the shear behaviour and capacity for prestressed hollow core slabs is recommended.
- The NSM-FRP technique has proven to significantly enhance the flexural capacity, effectively shifting the limit to the shear capacity. It is then necessary to develop a method for strengthening HC slabs to enhance the shear capacity.
- Additional analysis is required on the effect of varying the number of laminates centered at a single web for HC slabs. More specifically, to determine the effect that the distance from the NSM grooves to the HC void has on the bond stresses and the mode of failure. This parameter is specific to HC slabs.

REFERENCES

Abdalla, H. and Kennedy, J.B. (1995). *Design of Prestressed Concrete Beams with Openings*. ASCE, Journal of Structural Engineering, Vol. 121, No. 5, pp. 890-898.

Abdalla, H.A., Torkey, A.M., Haggag, H.A. and Abu-Amira, A.F. (2003). *Design Against Cracking at Openings in Reinforced Concrete Beams Strengthened with Composite Sheets*. ElSevier, Composite Structures, Vol. 60, No. 2, pp. 197-204.

ACI Committee 318. (2004). *Building Code Requirements for Structural Concrete and Commentary* (ACI 318M-05). American Concrete Institute (ACI), Detroit, MI. pp. 430.

ACI Committee 440. (2006). *Guide for the Design and Construction of Structural Concrete Reinforced with FRP Bars* (ACI 440.1R-06). American Concrete Institute (ACI), Detroit, MI. pp. 44.

ACI Committee 440. (2008). *Guide for the Design and Construction of Externally Bonded FRP Systems for Strengthening Concrete Structures* (ACI 440.2R-08). American Concrete Institute (ACI), Detroit, MI. pp. 76.

ASTM Committee C09. (2002). *Standard Test Method for Flexural Strength of Concrete (Using Simple Beam With Third-Point Loading)* (C 78 - 02). American Society for Testing Materials International, West Conshohocken, PA. pp.1-9.

Agbossou, A., Michel, L., Lagache, M., and Hamelin, P. (2008). *Strengthening Slab using Externally-Bonded Strip Composites: Analysis of Concrete Covers on the Strengthening*. ElSevier, Composites: Part B, Vol. 39, No. 7-8, pp. 1125-1135.

Al-Mahmoud, F., Castel, A., Francois, R., and Tourneur, C. (2009). *Strengthening of RC members with near-surface mounted CFRP rods*. ElSevier, Composite Structures, Vol. 91, No. 2, pp. 138-147.

Al-Rousan, R., Issa, M., and Shabila, H. (2011). *Performance of Reinforced Concrete Slabs Strengthened with Different Types and Configurations of CFRP*. ElSevier, Composites: Part B, Vol. 43, No. 2, pp. 510-521.

Aprile, A. and Benedetti, A. (2004). *Coupled Flexural-Shear Design of R/C Beams Strengthened with FRP*. ElSevier, Composites: Part B, Vol. 35, No. 1, pp. 1-25.

Badawi, M. and Soudki, K. (2009). *Flexural Strengthening of RC Beams with Prestressed NSM CFRP Rods - Experimental and Analytical Investigation*. ElSevier, Construction and Building Materials, Vol. 23, No. 10, pp. 3292-3300.

Bakis, C.E., Bank, L.C., Brown, V.L., Cosenza, E., Davalos, J.F., Lesko, J.J., Machida, A., Rizkalla, S.H., and Triantafillou, T.C. (2002). *Fiber-Reinforced Polymer Composites for Construction - State-of-the-Art Review*. ASCE, Journal of Composites for Construction, Vol. 6, No. 2, pp. 73-87.

Bonaldo, E.,de Barros, J.A.O., and Lourenco, P.B. (2008). *Efficient Strengthening Technique to Increase the Flexural Resistance of Existing RC Slabs*, ASCE, Journal of Composites for Construction, Vol. 12, No. 2, 149-159.

Canadian Precast/Prestressed Concrete Institute. (2007). *Design Manual - Precast and Prestressed Concrete*. Canadian Precast/Prestressed Concrete Institute (CPCI), Ottawa, ON.

Canadian Standards Association. (2002). *Design and Construction of Building Components with Fiber-Reinforced Polymers* (CAN/CSA-S806-02). Canadian Standards Association, Toronto, ON, pp. 177.

Canadian Standards Association. (2012). *Design and Construction of Building Components with Fiber-Reinforced Polymers* (CAN/CSA-S806-12). Canadian Standards Association, Toronto, ON, pp. 187.

Canadian Standards Association. (2006). *Canadian Highway Bridge Design Code* (CAN/CSA-S6-06). Canadian Standards Association, Toronto, ON, pp. 733.

Capozucca, R. (2009). *Static and Dynamic Response of Damaged RC Beams Strengthened with NSM CFRP Rods*. ElSevier, Composite Structures, Vol. 91, No. 3, pp. 237-248.

Chaallal, O., Nollet, M.J., and Perraton, D. (1998). *Strengthening of Reinforced Concrete Beams with Externally Bonded Fiber-Reinforced-Plastic Plates: Design Guidelines for Shear and Flexure*. Canadian Journal for Civil Engineering, Vol. 25, No. 4, pp. 692-704.

Darby, J. J. and Hollaway, L. C.(1999). *Strengthening of Reinforced Concrete Structures - Using Externally-Bonded FRP Composites in Structural and Civil Engineering*. 2000 Corporate Blvd, NW, Boca Raton FL 33431, USA, Woodhead Publishing Ltd. and CRC Press LLC.

De Lorenzis, L. (2004). *Anchorage Length of Near-Surface Mounted Fiber-Reinforced Polymer Rods for Concrete Strengthening - Analytical Modeling*. American Concrete Institute (ACI) Structural Journal, Vol. 101, No. 3, pp. 375-386.

De Lorenzis, L., Lundgren, K., and Rizzo, A. (2004). *Anchorage Length of Near-Surface Mounted Fiber-Reinforced Polymer Bars for Concrete Strengthening - Experimental Investigation and Numerical Modeling*. American Concrete Institute (ACI) Structural Journal, Vol. 101, No. 2, pp. 269-278.

De Lorenzis, L. and Nanni, A. (2001). *Characterization of FRP Rods as Near-Surface Mounted Reinforcement*. ASCE, Journal of Composites for Construction, Vol. 5, No. 2, pp. 114-121.

De Lorenzis, L. and Nanni, A. (2002). *Bond Between Near-Surface Mounted Fiber-Reinforced Polymer Rods and Concrete in Structural Strengthening*. American Concrete Institute (ACI) Structural Journal, Vol. 99, No. 2, pp. 123-132.

De Lorenzis, L. and Teng, J. G. (2006). *Near-Surface Mounted FRP Reinforcement: An Emerging Technique for Strengthening Structures*. ElSevier, Composites Part B: Engineering, Vol. 38, No. 2, pp. 119-143.

Elgabbas, F., El-Ghandour, A. A., Abdelrahman, A.A., and El-Dieb, A.S. (2009). *Different CFRP Strengthening Techniques for Prestressed Hollow Core Concrete Slabs; Experimental Study and Analytical Investigation*. ElSevier, Composite Structures, Vol. 92, No. 2, pp. 401-411.

El-Hacha, R. and Rizkalla, S. H. (2004). *Near-Surface-Mounted Fiber-Reinforced Polymer Reinforcements for Flexural Strengthening of Concrete Structures*. American Concrete Institute (ACI) Structural Journal, Vol. 101, No. 5, pp. 717-726.

El-Mogy, M. (2010). *Behaviour of Continuous Concrete Beams Reinforced with FRP*. Ph.D. Thesis, University of Manitoba, Winnipeg, Manitoba, Canada, pp. 198.

El-Salakawy, E. (2010). *Prestressed Concrete Course Notes* (CIVL 7100). University of Manitoba, Winnipeg, Manitoba, Canada.

El-Salakawy, E. (2010). Use *of FRP in Structural Design Course Notes* (CIVL 4030). University of Manitoba, Winnipeg, Manitoba, Canada.

Enochsson, O., Lundqvist, J., Taljsten, B., Rusinowski, P., and Olofsson, T. (2007). *CFRP Strengthened Openings in Two-Way Concrete Slabs – An Experimental and Numerical Study*. ElSevier, Construction and Building Materials, Vol. 21, No. 4, pp. 810-826.

Foret, G. and Limam, O. (2006). *Experimental and Numerical Analysis of RC Two-way Slabs Strengthened with NSM CFRP Rods*. ElSevier, Construction and Building Materials, Vol. 22, No. 10, pp. 2025-2030.

Galati, D. and De Lorenzis, L. (2009). *Effect of Construction Details on the Bond Performance of NSM FRP Bars in Concrete*. Advances in Structural Engineering, Vol. 12, No. 5, pp. 683-700.

GangaRao, H. V. S., Taly, N., and Vijay, P.V. (2007). *Reinforced Concrete Design with FRP Composites*. Taylor & Francis Group, LLC, FL. pp. 260.

Gentile, C. J. (2000). *Flexural Strengthening of Timber Bridge Beams Using FRP*. M.Sc. Thesis, University of Manitoba, Winnipeg, Manitoba, pp. 134.

Hassan, T. K. (2002). *Flexural Performance and Bond Characteristics of FRP Strengthening Techniques for Concrete Structures*. Ph.D. Thesis, University of Manitoba, Winnipeg, Manitoba, pp. 304.

Hassan, T. K. and Rizkalla, S. H. (2003). *Investigation of Bond in Concrete Structures Strengthened with Near Surface Mounted Carbon Fiber Reinforced Polymer Strips*. ASCE, Journal of Composites for Construction, Vol. 7, No. 3, pp. 248-257.

Hassan, T. K. and Rizkalla, S. H. (2004). *Bond Mechanism of Near-Surface-Mounted Fiber-Reinforced Polymer Bars for Flexural Strengthening of Concrete Structures*. American Concrete Institute (ACI) Structural Journal, Vol. 101, No. 6, pp. 830-839.

Hollaway, L. C. and Leeming, M. B. (1999). *Strengthening of Reinforced Concrete Structures Using Externally-Bonded FRP Composites in Structural and Civil Engineering*. Boca Raton, Woodhead Publishing Ltd. and CRC Press LLC.

Hosny, A., Sayed-Ahmed, E. Y., Abdelrahman, A.A., and Alhlaby, N.A. (2006). *Strengthening Precast-Prestressed Hollow Core Slabs to Resist Negative Moments Using Carbon Fiber Reinforced Polymer Strips: An Experimental Investigation and a Critical Review of Canadian Standards Association S806-02*. Canadian Journal of Civil Engineering (CJCE), Vol. 33, No. 8, pp. 955-967.

ISIS Canada. (2002*). Strengthening Reinforced Concrete Structures with Externally-Bonded Fiber Reinforced Polymers*. (Manual No. 4) ISIS Canada Research Network, University of Manitoba, Winnipeg, Manitoba.

ISIS Canada. (2008*). FRP Rehabilitation of Reinforced Concrete Structures*. (Manual No. 4, Version 2), ISIS Canada Research Network, University of Manitoba, Winnipeg, Manitoba.

Kodur, V.K.R., Bisby, L.A., (2005). *Thermal Behaviour of Fire-Exposed Concrete Slabs Reinforced with Fiber-Reinforced Polymer Bars*. American Concrete Institute (ACI), Structural Journal, Vol. 102, No. 6, pp. 799-807.

Larson, K.H., Peterman, R.J., and Rasheed, H.A. (2005). *Strength-Fatigue Behaviour of Fiber Reinforced Polymer Strengthened Prestressed Concrete T-Beams*. ASCE, Journal of Composites for Construction, Vol. 9, No.4, pp. 313-326.

Li, L. J., Guo, Y. C., Liu, F., and Bungey, J. H. (2006). *An Experimental and Numerical Study of the Effect of Thickness and Length of CFRP on Performance of Repaired Reinforced Concrete Beams*. ElSevier, Construction and Building Materials, Vol. 20, No. 10, pp. 901-909.

Nordin, H. and Taljsten, B. (2006). *Concrete Beams Strengthened with Prestressed Near Surface Mounted CFRP*. ASCE, Journal of Composites for Construction, Vol. 10, No. 1, pp. 60-68.

Novidis, D.G. and Pantazopoulou, S.J. (2008). *Bond Tests of Short NSM-FRP and Steel Bar Anchorages*. ASCE, Journal of Composites for Construction, Vol. 12, No. 3, pp.323-333.

Novidis, D., Pantazopoulou, S.J., and Tentolouris, E. (2006). *Experimental Study of Bond of NSM-FRP Reinforcement*. ElSevier, Construction and Building Materials, Vol. 21, No. 8, pp. 1760-1770.

Padmarajaiah, S.K., and Ramaswamy, A. (2002). *A finite Element Assessment of Flexural Strength of Prestressed Concrete Beams with Fiber Reinforcement*. ElSevier, Cement & Concrete Composites, Vol. 24, No. 2, pp. 229-241.

Raafat, E.-H. and Sami, H. R. (2004). *Near-Surface-Mounted Fiber-Reinforced Polymer Reinforcements for Flexural Strengthening of Concrete Structures*. American Concrete Institute (ACI), Structural Journal, Vol. 101, No. 5, pp. 717-726.

Rosenboom, O., Hassan T. K., and Rizkalla, S. (2007). *Flexural Behaviour of Aged Prestressed Concrete Girders Strengthened with Various FRP Systems*. ElSevier, Construction and Building Materials, Vol. 21, No. 4, pp. 764-776.

Smith, S. T. and Kim, S. J. (2009). *Strengthening of One-Way Spanning RC Slabs with Cutouts using FRP Composites*. ElSevier, Construction and Building Materials, Vol. 23, No. 4, pp. 1578-1590.

Tan, K. H. and Zhao, H. (2004). *Strengthening of Openings in One-Way Reinforced-Concrete Slabs using Carbon Fiber-Reinforced Polymer Systems*. ASCE, Journal of Composites for Construction, Vol. 8, No 5, pp. 393-402.

Teng, J. G., De Lorenzis, L., Wang, B., Li, R., Wong, T. N., and Lam, L. (2006*). Debonding Failures of RC Beams Strengthened with Near Surface Mounted CFRP Strips*. ASCE, Journal of Composites for Construction, Vol. 10, No. 2, pp. 92-105.

Yost, J. R., Gross, S. P., Dinehart, D. W., and Mildenberg, J. J. (2007). *Flexural Behaviour of Concrete Beams Strengthened with Near-Surface-Mounted CFRP Strips*. American Concrete Institute (ACI), Structural Journal, Vol. 104, No. 4, pp. 430-437.

Zia, P. and Mostafa, T. (1977). *Development Length of Prestressing Strand*. Precast Concrete Institute, Vol. 22, No. 5, Sept-Oct., pp. 54-65.

APPENDIX A – REINFORCEMENT CHARACTERISTICS

The following sections provide a synopsis of the mechanical characteristics for the reinforcement materials employed in this research program, namely high-strength steel and FRP.

A.1 Mild and High-Strength Steel

Nilson (1978) confirmed that the stress-strain characteristics of prestressing steel and reinforcing bars are different. Prestressing steel does not exhibit a definite yield plateau, but instead yielding develops gradually throughout the inelastic range until failure. The yield load is much greater for high-strength steel, making it better suited for higher service load applications. The difference between the nominal yield strength and the ultimate tensile strength of high strength steel is significantly smaller than for corresponding values of regular reinforcing bars. Figure A.1 illustrates the yielding behaviour for mild and high-strength steel.

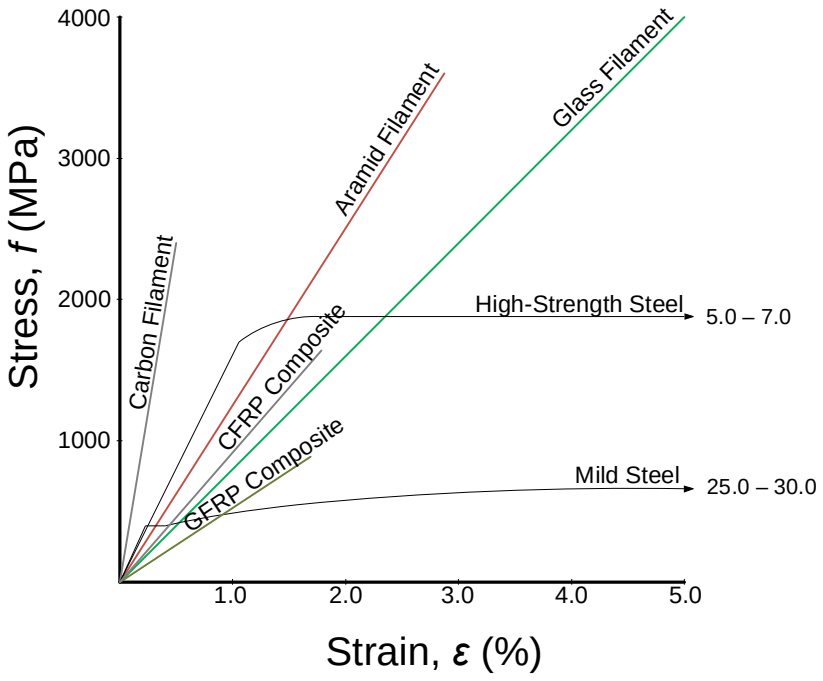

Figure A.1: Stress-Strain Relationship for Reinforcement Materials

A.2 Fiber Reinforced Polymers (FRP)

Fiber reinforced polymers (FRP) are anisotropic composite materials comprised of high strength and high modulus fibers embedded in a resin matrix. The constituent materials act together to achieve properties that cannot be achieved by the components acting alone. The fibers contribute the majority of the strength, while the resin acts as a binder holding the fibers in a desired layout (GangaRao et al., 2007). The nature and layout of the components make FRP reinforcement strongest in the axial direction, and weaker in the transverse and radial direction. Unlike the standardized physical and mechanical properties of steel and concrete, those of FRP depend on the manufacturer's fabrication techniques. The manufacturing method typically used for FRP composite structural shapes is the pultrusion process. This continuous process is highly automated, and consists of 'pulling' resin impregnated filament bundles and fabrics through a

heated curing die into a desired shape (Bakis et. al., 2002). As this process varies between manufacturers, the quantity and properties of FRP components will also differ. FRP composites are manufactured with unique fiber-resin combinations, resulting in different elastic moduli, tensile strength, cross-sectional area and shape, and fiber configurations. Common fibers used in structural applications include glass, carbon and aramid. Resins commonly used as binders include thermoplastic and thermosetting polymers. The characteristics of fibers and resins are discussed in the following sections.

A.2.1 Fiber types

For an FRP composite material, the type of fiber determines its strength properties. Fibers are most effective when subject to a pure tensile stress along the axial direction. Fibers by themselves are susceptible to degradation, which makes a resin coating necessary to preserve the structural integrity and maintain the mechanical properties of the composite. The fiber content is the amount of filaments present in a composite, and is expressed as a percentage of volume of the composite. The most common fibers used in structural applications are glass, carbon and aramid. Figure A.1 illustrates the stress-strain behaviour of typical filaments and common FRP composites used as reinforcement. The mechanical properties of the fiber-resin composite are provided in Table A.1, along with those of mild steel and high-strength steel.

Table A.1: Properties of FRP Composites and Reinforcing Steel

Reinforcement Type	Tensile Strength (MPa)	Modulus of Elasticity (GPa)	Elongation at Failure (%)
Glass	800-1200	45-65	1.5-2.2
Carbon	1500-2400	120-160	1.2-1.4
Mild Carbon Steel	600	200	20
High-Strength Steel	1860	195	6 – 7

Source: ISIS Canada (2007) – Design Manual No. 3

A.2.1.1 Glass filaments

Glass filaments and molten glass resin are the main components of glass-fiber reinforced polymer (GFRP) reinforcement. Glass fibers have a high tensile strength combined with superior mechanical properties. The fibers provide high chemical resistance and excellent insulating properties. Relative to other fibers, glass fibers have a low tensile modulus, high specific gravity, are sensitive to abrasion when handling, and have a lower resistance to fatigue. The types of glass fibers vary in alkali content and stiffness. Those most commonly found in structural applications are E-glass and S-glass, representing general purpose and high-strength characteristics, respectively.

A.2.1.2 Carbon filaments

Carbon filaments containing at least 90% carbon by weight are the main strength component for carbon-fiber reinforced polymer (CFRP) reinforcement. Carbon fibers offer a high tensile strength to weight ratio, high elastic modulus, and high fatigue strength. The main advantages of carbon fibers are their excellent durability and low relaxation under sustained load. The disadvantages include high brittleness and therefore low impact resistance, and electrical

conductivity. As a result of the superior strength characteristics, carbon fibers have a higher cost and are typically used only for special applications, such as prestressing or as strengthening reinforcement. This type of high-strength filament is most suitably applied to strengthen prestressed concrete.

A.2.1.3 Aramid filaments

Aramid fibers have a low thermal conductivity, low flammability, and no melting point. Most notably they have excellent strength-to-weight properties, and also exhibit a high degree of yielding under compression, making it a suitable material to resist impact and dynamic loading (GangaRao 2007). Some disadvantages of aramid fibers are the high ability to absorb moisture, they exhibit a loss of strength and modulus at elevated temperatures, and they are difficult to cut and machine. Aramid fibers are found to be sensitive to UV light, such that any exposure will cause the mechanical properties to deteriorate.

A.2.2 Resins

Resins are composite materials made up of polymers, filler material, catalysts, and hardeners. These components work in concert to achieve properties that make the resin compatible with a given type of fiber. Resins act as a matrix, holding the fibers in place, and as a protective cover to preserve the mechanical properties of the fibers. Resins typically exhibit a much lower elastic modulus and tensile strength relative to the final FRP composite. The amount of resin is expressed as a percentage of total volume of the composite material. Resins are often classified

by their behavior when exposed to heat and pressure, as thermoplastic and thermosetting polymers.

APPENDIX B – NSM DESIGN PARAMETERS

The following sections provide a brief summary of the investigation into each of NSM design variables. Each section will highlight the nature of the study, its proposed objectives and parameters, the type of specimens, and any relevant conclusions.

B.1 Concrete Strength

Al-Mahmoud et al. (2009) conducted an experimental investigation using steel reinforced concrete beams strengthened with CFRP rods. The studied parameter was the concrete compressive strength. The objective of the study was to determine the amount of influence the compressive strength of the concrete had on the flexural response of the strengthened sections. Increasing the concrete strength effectively decreased the number of flexural cracks, and increased the crack spacing. This is attributed to the higher tensile strength of concrete. As expected, any increase in the cylinder compressive strength produced a corresponding increase in the cracking load and the stiffness of the section. The increase in stiffness however was relatively negligible compared to the increase in stiffness attributed to the strengthening material. As confirmed by Hassan and Rizkalla (2003), an increase in concrete tensile strengths improves the bond strength of the NSM system. However, beams whose failure mode was governed by the bond strength at the FRP-epoxy interface saw no influence by the compressive concrete strength on the ultimate load.

B.2 Laminate Surface Characteristics

De Lorenzis and Nanni (2002) performed a series of experimental tests using unreinforced concrete T-beams specimens, strengthened with NSM-FRP bars. Test parameters included bond length, size of reinforcement, type of FRP material, size of groove, and surface configuration of the reinforcement, namely deformed ribs and a sandblasted coating. The objective of the study was to compare the bond strengths between the two aforementioned surface configurations, by varying other parameters and analyzing the shear stress concentrations and the modes of failure. Results show that deformed bars generally lead to progressive cracking in the surrounding epoxy and concrete, exhibiting a ductile behaviour until reaching the typical epoxy splitting failure. Sandblasted rods however did not have enough surface deformation to provide as much mechanical interlock, thus bond was primarily governed by chemical adhesion, as well as friction after sufficient slip had occurred between the reinforcement and the surrounding epoxy. As a result, a pull-out failure was typical for salted bars. Varying the groove dimensions and bond lengths, the deformed bars achieved an average of 47% greater increase in ultimate strength compared to sand-coated bars. The authors concluded that deformed bars generally provide greater bond strength than sandblasted bars, regardless of any variation of other design parameters.

B.3 Anchorage Length

Hassan and Rizkalla (2004) examined the behaviour of simply supported T-beam consisting of internal tensile, compression, and shear reinforcement, and designed to avoid concrete crushing and premature failure due to shear. The beam specimens were each strengthened with a single

NSM CFRP bar, with anchorage lengths of $15d_b$, $55d_b$, $80d_b$, and $120d_b$. The rationale behind the study was to develop a general methodology to evaluate the development length of NSM FRP bars of different configurations. Experimental results generally indicated that increasing the embedment length increases the bond strength of the NSM laminate. Short embedment lengths of 15 bar diameters ($15d_b$) were shown to provide insignificant increase in stiffness or strength due to early debonding failure, when compared to the control specimen. Increasing the anchorage length by 50% yielded an increase in tensile stress in the CFRP bars of less than 7.5%. Despite this increasing trend, embedment length is not directly proportional to bond strength; there exists an effective range of bonded length which develops the maximum tensile stress in the FRP, and beyond which will provide no improvement in flexural capacity. Embedment lengths, greater than $80d_b$, did not provide any significant increase in bond strength.

B.4 Groove Spacing

Hassan and Rizkalla (2004) studied the flexural response of simply supported reinforced concrete beams, strengthened with CFRP bars. The objective of the analysis was to determine if tensile stresses around two adjacent NSM FRP bars can overlap and noticeably increase the tensile stress experienced by the surrounding concrete. The clear spacing between grooves was varied from $0.25d_b$ to $2.0d_b$. The analysis suggests that increasing the clear groove-spacing-to-bar-diameter ratio reduces the tensile stresses in the surrounding concrete. For a closely spaced arrangement of NSM bars the tensile stresses were magnified in the surrounding concrete, and expedited a concrete splitting failure. This trend was valid up to a groove spacing of $2.0d_b$; while increasing the groove spacing beyond this limit yielded no noticeable effect on the induced tensile stresses in the concrete. The results conclude that the minimum clear spacing between

NSM bars should be twice the diameter of the bars; a lesser ratio will result in overlapping of the tensile stresses, and accelerate debonding failure.

B.5 Edge Distance

Using a finite element model, Hassan and Rizkalla (2004) conducted an analytical study to determine the susceptibility of the concrete cover along the side of the NSM groove to spalling due to tensile stresses transmitted from the NSM reinforcement. The generalized distribution of tensile stresses emanating from the FRP laminates is illustrated in Figure B.1. The objective of the analysis was to determine if the distribution of tensile stresses surrounding the groove were large enough to prematurely fracture the edge of the concrete. Applying a unit radial pressure at the centroid of the NSM FRP reinforcement, the edge distance was varied from $2.0d_b$ to $6.0d_b$. Analytical results suggest that increasing the concrete edge cover reduced the tensile stresses up to a distance of four times the bar diameter; beyond which no edge failures of the concrete were reported. A minimum edge distance of $4.0d_b$ is required to minimize the chance of a premature side concrete cover failure.

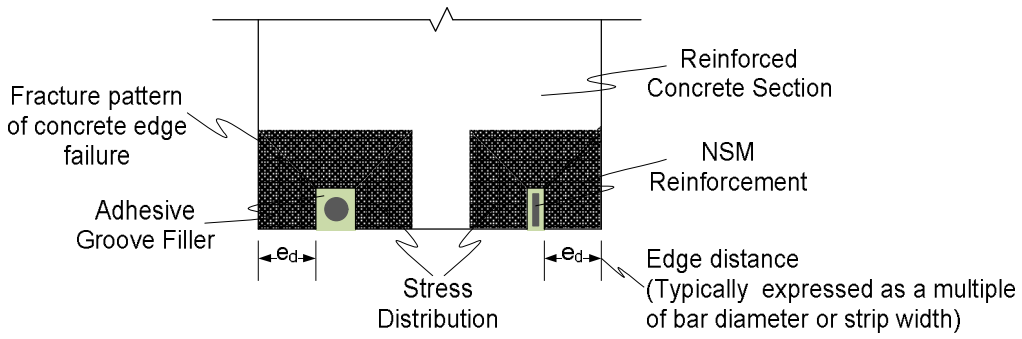

Figure B.1: Stress Distribution Surrounding NSM Reinforcement

Galati and De Lorenzis (2009) however conducted an experimental pull-out investigation which concluded that an edge distance of twice the groove width was sufficient concrete cover to avoid a premature spalling failure.

B.6 External Laminate Restraints

Galati and De Lorenzis (2009) carried out a series of experimental pull-out tests on single deformed FRP bars embedded into reinforced concrete blocks. At one end, a tensile force was applied to the FRP coupon, the mid-section of the bar was embedded into a rectangular groove over a length of 180 mm, and the other end was free to easily measure any slip during loading. The NSM reinforcing bar was covered with a single ply of externally bonded FRP sheet. The objective of this study was to determine the effectiveness of confining the NSM joint by analyzing the resulting bond-slip behaviour. The study concluded that external confinement could increase the bond strength of the NSM bar-groove system by 25%. The presence of an external sheet increases the transverse stiffness of the cover over the NSM bar, improving the allowable normal pressure which can be applied to the epoxy cover. Clearly, this technique is only effective when bond failure is governed by the tensile strength of the epoxy. The extra confinement increases the capacity of the system to resist splitting action along the surface of the epoxy, and was noted to shift the mode of failure to splitting of the concrete surrounding the groove.

B.7 Groove Filler

De Lorenzis et al. (2004) conducted an experimental and analytical study using a modified pull-out test of 34 specimens. The purpose of the research is to investigate the influence of the adhesive matrix on the bond performance of NSM-FRP bars. The two groove-filling materials under consideration are epoxy paste, and cement-based expansive paste. Results indicate that specimens with epoxy-filled grooves experience internal microcracking in the epoxy at a load level close to 50% of the ultimate load. Soon after, longitudinal cracking formed in the epoxy, which then crossed the adhesive-concrete boundary and propagated into the concrete specimen. Ultimate failure occurred by cracking of the concrete surrounding the groove. For specimens with cement-filled grooves, cracking began along the bar cover at much lower loads than that of epoxy-filled grooves. The cement adhesive experienced gradual crack propagation, occasionally crossing the adhesive-concrete interface. Specimens with cement-filled grooves had, in all cases, lower bond failure load than specimens with epoxy-filled grooves. This phenomenon is attributed to the higher tensile strength of epoxy, which delays the formation of splitting cracks in the cover and allows greater shear stresses to develop along the bar and surrounding material. Cement-based filler typically led to a pull-out based mode of failure, which is to be expected due to its lower shear strength.

Galati and De Lorenzis (2009) carried out a series of experimental pull-out tests on single deformed FRP bars embedded into reinforced concrete blocks. The parameter under consideration is the type of groove-filling epoxy. Two commercially available epoxies were selected with significantly different values of tensile strength and modulus of elasticity – 23% and 210%, respectively. The high modulus epoxy yielded a bond strength increase of

approximately 75%. This gain in strength was accompanied by a 400% reduction of ductility, resulting in a very sudden and brittle failure. Compared with the control specimen, the failure mode shifted from cracking in the epoxy, to splitting within the concrete surrounding the groove. High-modulus epoxies will increase the bond strength of the NSM system until the limiting variable becomes the tensile strength of the concrete substrate. However, Hassan and Rizkalla (2004) found that if the bond-failure method is governed by the tensile strength of the surrounding concrete, a higher epoxy strength provides no significant improvement of the ultimate capacity of the strengthened section.

APPENDIX C – DESIGN DRAWINGS

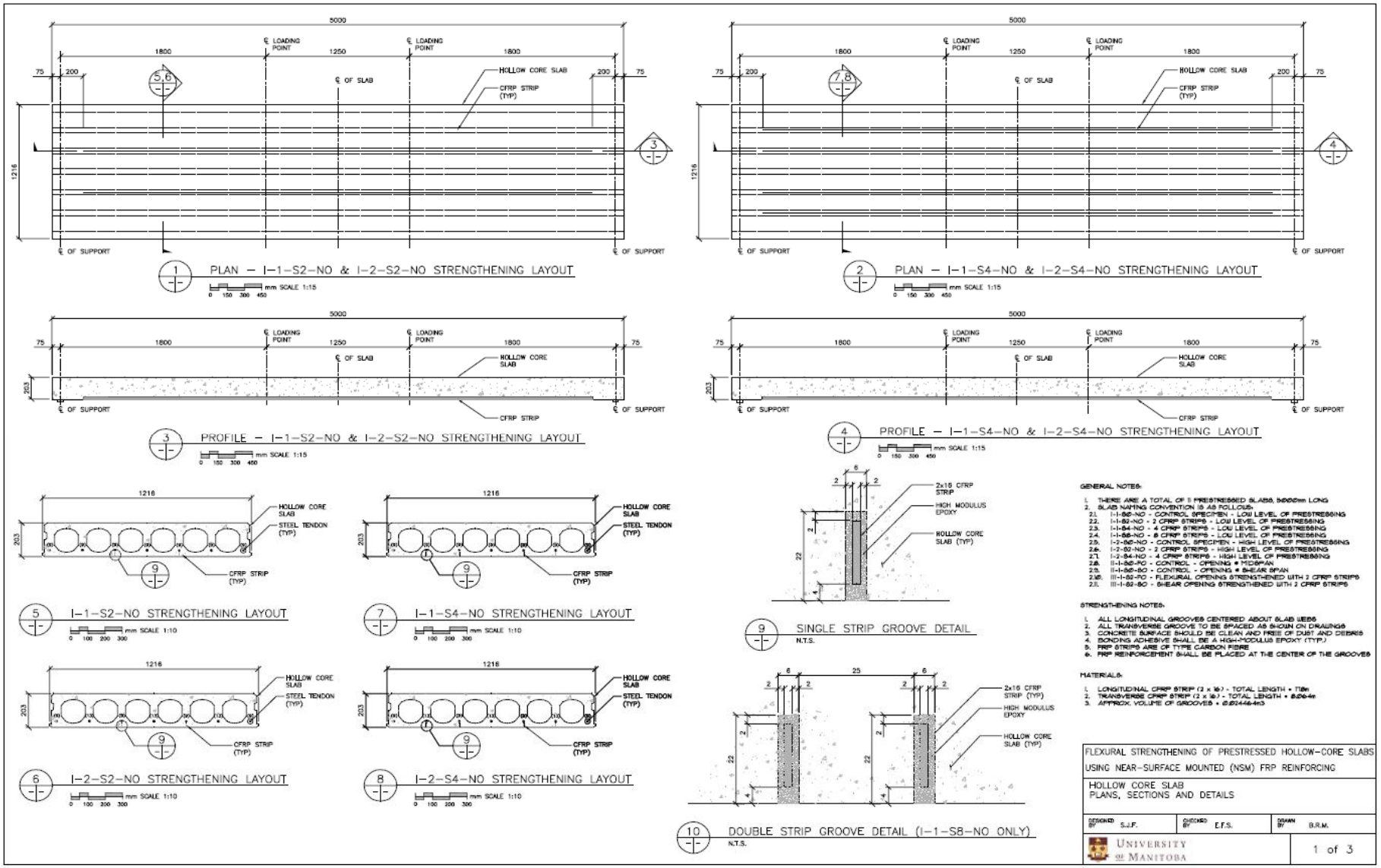

Figure C.1: Design Drawing 1 of 3

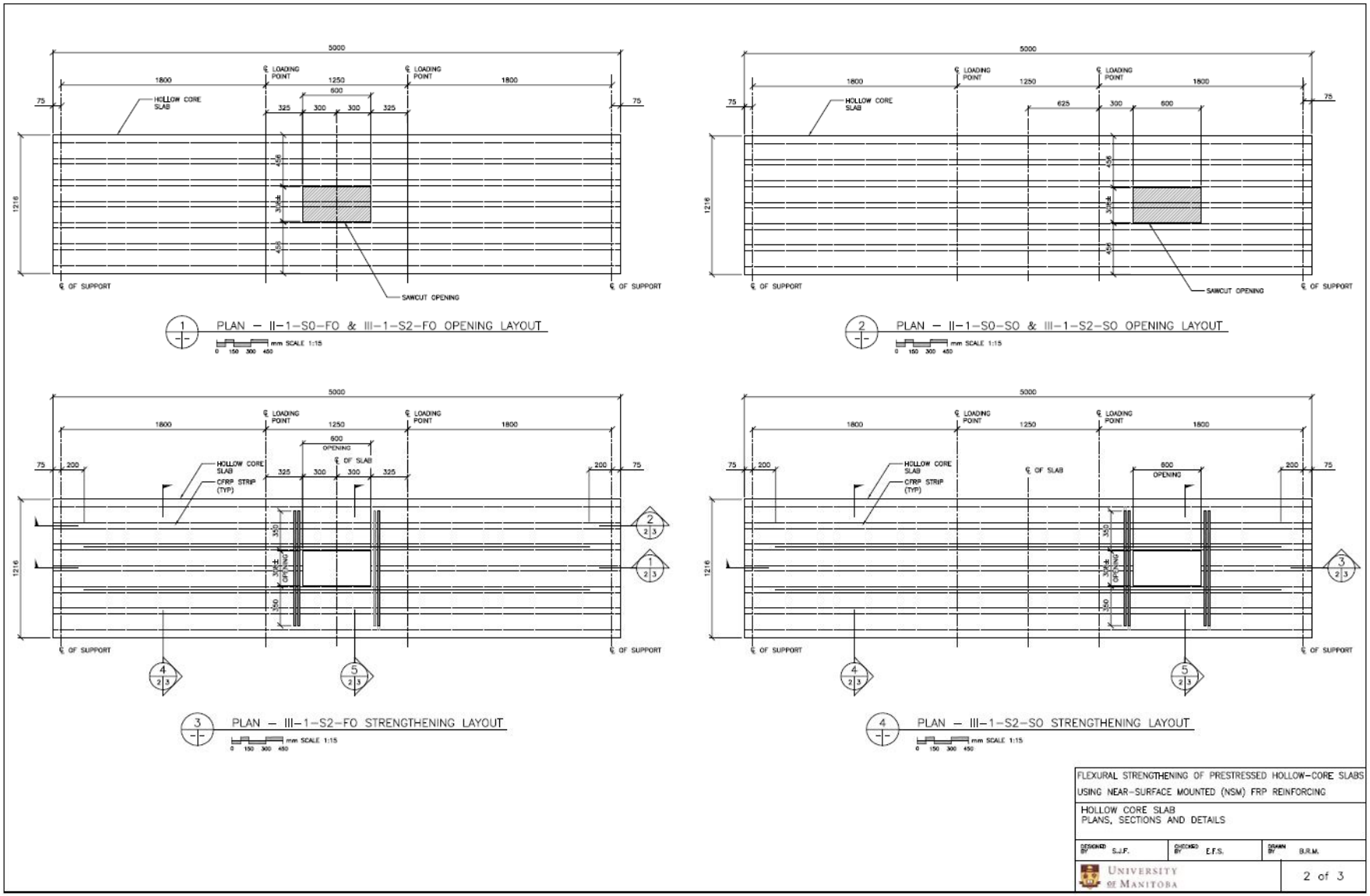

Figure C.2: Design Drawing 2 of 3

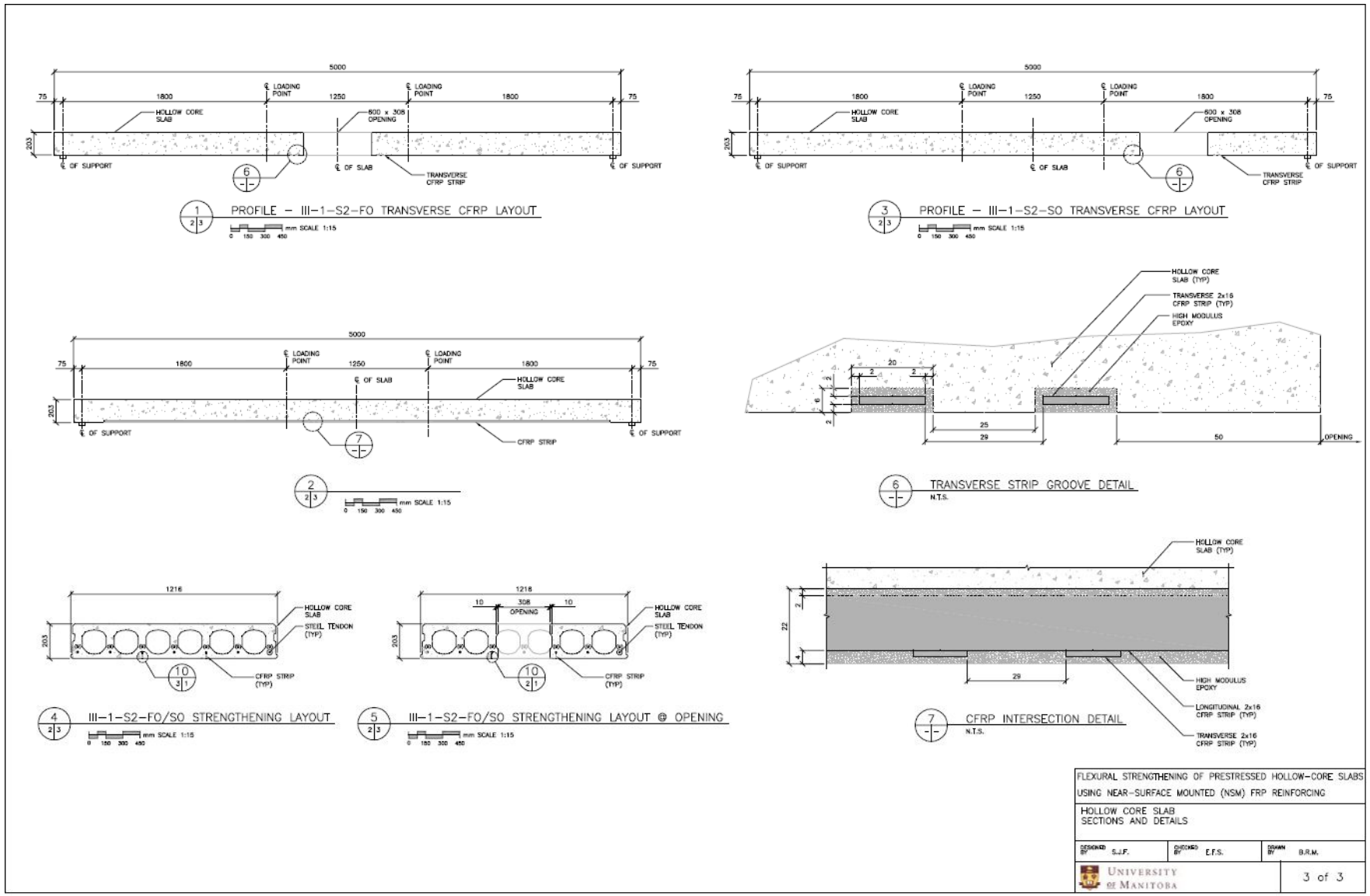

Figure C.3: Design Drawing 3 of 3

APPENDIX D – SPECIMEN DESIGN DETAILS

The following table summarizes the design properties for all test specimens.

Table D.1: Specimen Design Details

<table>
<tr><th>Specimen</th><th>Effective Width (mm)</th><th>Effective Thickness (mm)</th><th>Initial Concrete Strength (MPa)</th><th>Concrete Strength @ 28 Days (MPa)</th><th>Area of Prestressing Steel (mm^2)</th><th>Tensile Strength of Steel Tendons (MPa)</th></tr>
<tr><td>I-1-S0-NO</td><td rowspan="8">1200</td><td rowspan="11">203</td><td>32.8</td><td>64.1</td><td rowspan="4">383.6</td><td rowspan="11">1860</td></tr>
<tr><td>I-1-S2-NO</td><td>33.0</td><td>56.5</td></tr>
<tr><td>I-1-S4-NO</td><td rowspan="2">32.8</td><td rowspan="2">64.1</td></tr>
<tr><td>I-1-S8-NO</td></tr>
<tr><td>I-2-S0-NO</td><td rowspan="3">28.4</td><td rowspan="3">56.5</td><td rowspan="3">515.3</td></tr>
<tr><td>I-2-S2-NO</td></tr>
<tr><td>I-2-S4-NO</td></tr>
<tr><td>II-1-S0-FO</td><td rowspan="4">862 (opening)</td><td>32.8</td><td>64.1</td><td rowspan="4">328.8</td></tr>
<tr><td>II-1-S0-SO</td><td rowspan="3">33.0</td><td rowspan="3">56.5</td></tr>
<tr><td>III-1-S2-FO</td></tr>
<tr><td>III-1-S2-SO</td></tr>
</table>

Specimen	Average Depth to Steel (mm)	Gross Area of Concrete Section (mm^2)	Gross Moment of Inertia @ Midspan (mm^4)	Transformed Moment of Inertia (mm^4)	Total Length (mm)	Clear Span (mm)
I-1-S0-NO	158	140194	6.9476×10^8	6.9476×10^8	5000	4800
I-1-S2-NO				7.0171×10^8		
I-1-S4-NO				7.0935×10^8		
I-1-S8-NO				7.1699×10^8		
I-2-S0-NO				7.3089×10^8		
I-2-S2-NO				7.3966×10^8		
I-2-S4-NO				7.4624×10^8		
II-1-S0-FO		109968.2	5.4500×10^8	5.4500×10^8		
II-1-S0-SO			6.9476×10^8	5.4500×10^8		
III-1-S2-FO			5.4500×10^8	5.5154×10^8		
III-1-S2-SO			6.9476×10^8	5.5154×10^8		

APPENDIX E – PRESTRESS LOSS CALCULATIONS

Prestress loss calculations are separated between the two strand codes, namely '1' and '2', which designate low and high prestressing reinforcement ratios, respectively. Losses are determined using the Canadian Highway Bridge Design Code CAN/CSA-S6-06 (2006).

E.1 Initial Prestress Losses [Strand Code 1]

The following prestress loss calculations apply to all specimens with strand code designation '1':

I-**1**-S0-NO
I-**1**-S2-NO
I-**1**-S4-NO
I-**1**-S8-NO
II-**1**-S0-FO
II-**1**-S0-SO
III-**1**-S2-FO
III-**1**-S2-SO

$$\Delta_{FS1} = REL_1 + ES$$

$$REL_1 = \frac{\log(24t)}{45}\left[\frac{f_{sj}}{f_{py}} - 0.55\right] f_{sj} \qquad \text{(CHBDC 8.7.4.2.4)}$$

$$f_{sj} = 0.75 f_{pu} = 0.75(1860) = 1395\, MPa$$

$$f_{py} = 0.9f_{pu} = 0.9(1860) = 1674\ MPa$$

$$REL_1 = \frac{\log(24 \cdot 3)}{45}\left[\frac{1395}{1674} - 0.55\right]1395 = 16.3\ MPa$$

$$ES = nf_{cir} \qquad \text{(CHBDC 8.7.4.2.5)}$$

$$n = \frac{E_p}{E_{ci}} = \frac{195000}{4500\sqrt{35}} = 7.3$$

$$f_{cir} = \frac{P_j}{A_g} - \frac{P_j e^2}{I_g} + \frac{M_{sw} e}{I_g}$$

$$P_j = 0.75A_p f_{pu} = 0.75(383.6)(1860) = 535.1\ kN$$

$$M_{sw} = \frac{w\ell^2}{8}$$

$$w = \Upsilon_{pc} A_g = 24.5(140194) = 3.43\ kN/m$$

$$M_{sw} = \frac{3.43(5)^2}{8} = 10.7\ kNm$$

$$e = d - (h - y_b) = 158 - (203 - 100) = 54\ mm$$

$$f_{cir} = \frac{-535.1 \times 10^3}{140194} - \frac{(535.1 \times 10^3)(54^2)}{6.9476 \times 10^8} + \frac{(10.7 \times 10^6)(54)}{6.9476 \times 10^8}$$

$$= -3.8 - 2.2 + 0.8 = -5.2\ MPa$$

$$ES = (7.3)|-5.2| = 38.0\ MPa$$

$\Delta_{FS1} = 16.3 + 38.0 = \mathbf{54.3\ MPa}$

Force in steel tendons: $P_e = (f_{sj} - \Delta_{FS1})A_p = (1395 - 54.3)(383.6) = 514.3\ kN$

E.2 Long-Term Prestress Losses (60 – 90 days) [Strand Code 1]

$\frac{A_s}{A_{ps}} \leq 1.0\ then\ \Delta_{fs2} = CR + SH + REL_2$ (*CHBDC* 8.7.4.3.1)

$\frac{0}{383.6} = 0 < 1.0\ therefore\ \Delta_{fs2} = CR + SH + REL_2$

$$CR = \left[1.37 - 0.77\left(\frac{RH}{100}\right)^2\right] K_{cr}\left(\frac{E_p}{E_c}\right)(f_{cir} - f_{cds})$$ (*CHBDC* 8.7.4.3.2)

$$f_{cds} = \frac{M_{ds}e}{I} = 0$$

$$K_{cr} = \begin{cases} 2.0\ for\ pretensioned\ components \\ 1.6\ for\ posttensioned\ components \end{cases}$$

$$E_c = 4500\sqrt{f'_c} = 4500\sqrt{60} = 34856.85\ MPa$$

$$CR = \left[1.37 - 0.77\left(\frac{70}{100}\right)^2\right] 2.0\left(\frac{195000}{34856.85}\right)(4.976 - 0) = 55.3\ MPa$$

$$SH = (117 - 1.05RH) = [117 - (1.05 \cdot 70)] = 43.5\ MPa \quad (CHBDC\ 8.7.4.3.3)$$

$$REL_2 = \left[\frac{f_{st}}{f_{pu}} - 0.55\right]\left[0.34 - \frac{CR + SH}{1.25 f_{pu}}\right]\frac{f_{pu}}{3} \geq 0.002 f_{pu} \qquad (CHBDC\ 8.7.4.3.4)$$

$$f_{st} = f_{sj} - \Delta_{fs1} = 0.75(1860) - 52.7 = 1342.3\ MPa$$

$$REL_2 = \left[\frac{1342.3}{1860} - 0.55\right]\left[0.34 - \frac{55.3 + 43.5}{1.25 \cdot 1860}\right]\frac{1860}{3} \geq 0.002 \cdot 1860$$

$$REL_2 = [0.172][0.298]620 = 31.8 > 3.7$$

$\Delta_{fs2} = CR + SH + REL_2 = 55.3 + 43.5 + 31.8 = \mathbf{130.6\ MPa}$

$Losses\ at\ final = \Delta_{fs1} + \Delta_{fs2} = 52.7 + 130.6 = \mathbf{183.3\ MPa}$

$Effective\ prestress\ force, P_f = [0.75(1860) - 183.3]383.6 = 464.8\ kN$

E.3 Initial Prestress Losses [Strand Code 2]

The following prestress loss calculations apply to all specimens with strand code designation '2':

I-**2**-S0-NO
I-**2**-S2-NO
I-**2**-S4-NO

$\Delta_{FS1} = REL_1 + ES$

$$REL_1 = \frac{\log(24t)}{45}\left[\frac{f_{sj}}{f_{py}} - 0.55\right] f_{sj} \qquad \text{(CHBDC 8.7.4.2.4)}$$

$$f_{sj} = 0.75 f_{pu} = 0.75(1860) = 1395\ MPa$$

$$f_{py} = 0.9 f_{pu} = 0.9(1860) = 1674\ MPa$$

$$REL_1 = \frac{\log(24 \cdot 3)}{45}\left[\frac{1395}{1674} - 0.55\right] 1395 = 16.3\ MPa$$

$$ES = n f_{cir} \qquad \text{(CHBDC 8.7.4.2.5)}$$

$$n = \frac{E_p}{E_{ci}} = \frac{195000}{4500\sqrt{35}} = 7.3$$

$$f_{cir} = \frac{P_j}{A_g} - \frac{P_j e^2}{I_g} + \frac{M_{sw} e}{I_g}$$

$$P = 0.7 A_p f_{pu} = 0.7(515.3)(1860) = 670.9\ kN$$

$$M_{sw} = \frac{w\ell^2}{8}$$

$$w = \Upsilon_{pc} A_g = 24.5(140194) = 3.43\ kN/m$$

$$M_{sw} = \frac{3.43(5)^2}{8} = 10.7\ kNm$$

$$e = d - (h - y_b) = 158 - (203 - 100) = 54\ mm$$

$$f_{cir} = \frac{-670.9 \times 10^3}{140194} - \frac{(535.1 \times 10^3)(54^2)}{6.9476 \times 10^8} + \frac{(10.7 \times 10^6)(54)}{6.9476 \times 10^8}$$

$$= -4.8 - 2.2 + 0.8 = -6.2\ MPa$$

$$ES = (7.3)|-6.2| = 45.3\ MPa$$

$\Delta_{FS1} = 16.3 + 45.3 = \mathbf{61.6\ MPa}$

Force in steel tendons: $P_p = (f_{sj} - \Delta_{FS1})A_p = (1395 - 61.6)(515.3) = 687.1\ kN$

E.4 Long-Term Prestress Losses (60 – 90 days) [Strand Code 2]

$\frac{A_s}{A_{ps}} \leq 1.0\ then\ \Delta_{fs2} = CR + SH + REL_2$ ($CHBDC$ 8.7.4.3.1)

$\frac{0}{383.6} = 0 < 1.0\ therefore\ \Delta_{fs2} = CR + SH + REL_2$

$$CR = \left[1.37 - 0.77\left(\frac{RH}{100}\right)^2\right] K_{cr}\left(\frac{E_p}{E_c}\right)(f_{cir} - f_{cds}) \qquad (CHBDC\ 8.7.4.3.2)$$

$$f_{cds} = \frac{M_{ds}e}{I} = 0$$

$$K_{cr} = \begin{cases} 2.0\ for\ pretensioned\ components \\ 1.6\ for\ posttensioned\ components \end{cases}$$

$$E_c = 4500\sqrt{f'_c} = 4500\sqrt{60} = 34856.85 MPa$$

$$CR = \left[1.37 - 0.77\left(\frac{70}{100}\right)^2\right] 2.0\left(\frac{195000}{34856.85}\right)(6.2 - 0) = 68.9\ MPa$$

$$SH = (117 - 1.05RH) = [117 - (1.05 \cdot 70)] = 43.5\ MPa \quad (CHBDC\ 8.7.4.3.3)$$

$$REL_2 = \left[\frac{f_{st}}{f_{pu}} - 0.55\right]\left[0.34 - \frac{CR + SH}{1.25 f_{pu}}\right]\frac{f_{pu}}{3} \geq 0.002 f_{pu} \qquad (CHBDC\ 8.7.4.3.4)$$

$$f_{st} = f_{sj} - \Delta_{fs1} = 0.75(1860) - 61.6 = 1333.4\ MPa$$

$$REL_2 = \left[\frac{1333.4}{1860} - 0.55\right]\left[0.34 - \frac{68.9 + 43.5}{1.25 \cdot 1860}\right]\frac{1860}{3} \geq 0.002 \cdot 1860$$

$$REL_2 = [0.167][0.292]620 = 30.2\ MPa > 3.7$$

$$\Delta_{fs2} = CR + SH + REL_2 = 68.9 + 43.5 + 30.2 = \mathbf{142.6\ MPa}$$

$Losses\ at\ final$ = Δ_{fs1} + Δ_{fs1} = 61.6 + 142.6 = $\mathbf{204.2\ MPa}$

$Effective\ prestress\ force, P_f$ = [0.75(1860) – 204.2]515.3 = 613.6 kN

APPENDIX F – SAMPLE MOMENT CAPACITY CALCULATIONS

The following section outlines the steps to calculate the theoretical moment capacity and cracking moment for the unstrengthened control specimen, a specimen outfitted with two NSM-CFRP strips, and a specimen with an opening centered at mid-span, or I-1-S0-NO, I-1-S2-NO, and II-1-S0-FO, respectively. Calculations include procedures recommended by both CSA S806-12 and ACI 440.2R-08.

F.1 Design Procedure for Control Specimen I-1-S0-NO

Note: Control specimens have no strengthening and no openings.

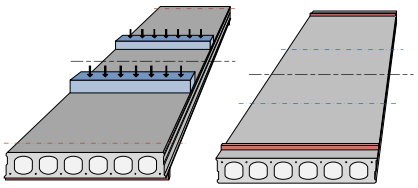

Figure F.1: I-1-S0-NO Schematic

F.1.1 Flexural Capacity – Strain Compatibility Method [CSA S806-12]

According to CSA A23.3-04 (Clause 10.1.7):

$$\alpha_1 = 0.85 - 0.0015 f'_c \geq 0.67$$

$$\alpha_1 = 0.85 - 0.0015(64.1) = 0.754$$

$$\beta_1 = 0.97 - 0.0025f'_c \geq 0.67$$

$$\beta_1 = 0.97 - 0.0025(64.1) = 0.810$$

$$a = \frac{A_p f_{pu}}{\alpha_1 f'_c b_f} \leq h_f \rightarrow \frac{(383.6)(1860)}{(0.754)(64.1)(1200)} = 12.3 < 35\,mm \;\therefore R - section\ behaviour$$

$$C_f = T_p$$

$$\alpha_1 f'_c \beta_1 c b_f = A_p f_{pr}$$

$$(0.754)(64.1)(0.810)(1200)c = 383.6 f_{pr}$$

$$c = 0.0082 f_{pr}$$

$$\varepsilon_{pr} = \varepsilon_{pe} + \varepsilon_{ce} + \varepsilon_{su}$$

$$\varepsilon_{pe} = \frac{f_{sj} - \Delta_{FS}}{E_p} = \frac{1395 - 183.3}{195000} = 0.0062$$

$$\varepsilon_{ce} = negligible$$

$$\frac{\varepsilon_{su}}{158 - c} = \frac{0.0035}{c}$$

$$\varepsilon_{su} = \frac{0.553}{c} - 0.0035$$

$$\varepsilon_{pr} = 0.0062 + \frac{0.553}{c} - 0.0035 = 0.0027 + \frac{0.553}{c} \quad (1)$$

$$f_{pr} = (190 \times 10^3)\varepsilon_{pr}\left\{0.025 + \frac{0.975}{\left[1 + \left(118\varepsilon_{pr}\right)^{10}\right]^{0.1}}\right\} \leq 1860\ MPa \quad (2)$$

$$c = 0.0082 f_{pr} \quad (3)$$

Iterations using equations (1), (2) and (3)…

Try: $\varepsilon_{pr} = 0.05 \rightarrow f_{pr} = 1807.4\ MPa \rightarrow c = 14.82\ mm \rightarrow \varepsilon_{pr} = 0.04$

Try: $\varepsilon_{pr} = 0.04 \rightarrow f_{pr} = 1755.2\ MPa \rightarrow c = 14.39\ mm \rightarrow \varepsilon_{pr} = 0.041$

Try: $\varepsilon_{pr} = 0.041 \rightarrow f_{pr} = 1765.1\ MPa \rightarrow c = 14.47\ mm \rightarrow \varepsilon_{pr} = 0.041 \quad Ok.$

$$a = \beta_1 c = 0.81(14.47) = 11.7\ mm$$

$$M_r = T\left(d - \frac{a}{2}\right) = A_p f_{pr}\left(d - \frac{a}{2}\right)$$

$$M_r = (383.6)(1765.1)\left[158 - \frac{11.7}{2}\right] = \mathbf{103.0\ kNm}$$

Maximum theoretical machine load:

$$P_{max} = 2\left(\frac{M_{max}}{\ell_{shear}}\right) = 2\left(\frac{103.0\ kNm}{1.8\ m}\right) = 114.4\ kN$$

F.1.2 Flexural Capacity – Strain Compatibility Method [ACI 440.2R-08]

According to ACI 318M-05 (2005) for high-strength concrete:

$$\beta_1 = 0.65$$

$$C = T_p$$

$$\alpha_1 f'_c \beta_1 c b_f = A_p f_{ps}$$

$$(0.65)(64.1)(0.65)(1200)c = 383.6 f_{pr}$$

$$c = (11.8 \times 10^{-3}) f_{pr}$$

$$\varepsilon_{ps} = \varepsilon_{pe} + \frac{P_e}{A_g E_c}\left(1 + \frac{e^2}{r^2}\right) + \varepsilon_{pnet} \leq 0.035$$

$$\varepsilon_{pe} = \frac{f_{sj} - \Delta_{FS}}{E_p} = \frac{1395 - 183.3}{196500} = 0.0062$$

$$\frac{P_e}{A_c E_c}\left(1 + \frac{e^2}{r^2}\right) = Negligible$$

$$\varepsilon_{pnet} = (0.003)\left(\frac{d_p - c}{c}\right) = (0.003)\left(\frac{158 - c}{c}\right) = \frac{0.474 - 0.003c}{c}$$

$$\varepsilon_{ps} = 0.0062 + \frac{0.474 - 0.003c}{c} \quad (1)$$

$$f_{ps} = \begin{cases} 196500\,\varepsilon_{ps} \; for \; \varepsilon_{ps} \geq 0.0086 \\ 1860 - \frac{0.276}{\varepsilon_{ps} - 0.007} \; for \; \varepsilon_{ps} > 0.0086 \end{cases} \quad (2)$$

$$c = (11.8 \times 10^{-3}) f_{pr} \quad (3)$$

Iterations using equations (1), (2) and (3)…

Try: $\varepsilon_{ps} = 0.012 \rightarrow f_{ps} = 1804.8\,MPa \rightarrow c = 21.3\,mm \rightarrow \varepsilon_{ps} = 0.025$

Try: $\varepsilon_{ps} = 0.025 \rightarrow f_{ps} = 1844.7\,MPa \rightarrow c = 21.8\,mm \rightarrow \varepsilon_{ps} = 0.0249 \quad Ok.$

$$a = \beta_1 c = 0.65(21.8) = 14.17\,mm$$

$$M_r = A_p f_{pr}\left(d - \frac{a}{2}\right) + \varepsilon_{FRP} E_{FRP} A_{FRP}\left(h - \frac{a}{2}\right)$$

$$M_r = (383.6)(1844.7)\left[158 - \frac{14.17}{2}\right]$$

$$M_r = \mathbf{106.8\ kNm}$$

Maximum theoretical machine load:

$$P_{max} = 2\left(\frac{M_{max}}{\ell_{shear}}\right) = 2\left(\frac{106.8\ kNm}{1.8\ m}\right) = 118.7\ kN$$

F.1.3 Cracking Moment

$$M_{cr} = \left[\frac{P}{A_g} + \frac{Pey_b}{I_g} + 0.6\lambda\sqrt{f'_c}\right]\frac{I_g}{y_b}$$

$$M_{cr} = \left[\frac{499.4 \times 10^3}{140194} + \frac{(499.4 \times 10^3)(54)(103.8)}{6.9476 \times 10^8} + 0.6(1)\sqrt{64.1}\right]\frac{6.9476 \times 10^8}{103.8}$$

$$= \mathbf{82.9\ kNm}$$

Cracking theoretical machine load:

$$P_{cr} = 2\left(\frac{M_{cr}}{\ell_{shear}}\right) = 2\left(\frac{82.9\ kNm}{1.8\ m}\right) = 92.1\ kN$$

F.2 Design Procedure for Specimen I-1-S2-NO

Note: Specimen strengthened with two CFRP strips.

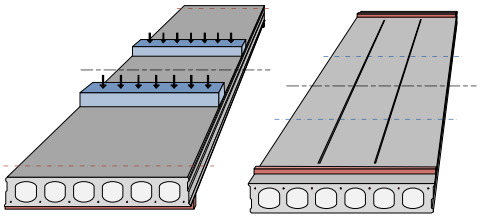

Figure F.2: I-1-S2-NO Schematic

F.2.1 Flexural Capacity – Strain Compatibility Method [CSA S806-12]

$$\alpha_1 = 0.85 - 0.0015 f'_c \geq 0.67$$

$$\alpha_1 = 0.85 - 0.0015(56.5) = 0.765$$

$$\beta_1 = 0.97 - 0.0025 f'_c \geq 0.67$$

$$\beta_1 = 0.97 - 0.0025(56.5) = 0.829$$

$$C = T_p + T_{FRP}$$

$$\alpha_1 f'_c \beta_1 c b_f = A_p f_{pr} + \varepsilon_{FRP} E_{FRP} A_{FRP}$$

The CSA committee recommends that a maximum allowable strain in the NSM-FRP be 0.007 (clause 11.3.1.3).

$$(0.765)(56.5)(0.829)(1200)c = 383.6 f_{pr} + (0.007)(131000)(2 \times 32)$$

$$c = 0.0089 f_{pr} + 1.37$$

$$\varepsilon_{pr} = \varepsilon_{pe} + \varepsilon_{ce} + \varepsilon_{su}$$

$$\varepsilon_{pe} = \frac{f_{sj} - \Delta_{FS1}}{E_p} = \frac{1395 - 183.3}{195000} = 0.0062$$

$$\varepsilon_{ce} = negligible$$

$$\frac{\varepsilon_{su}}{158 - c} = \frac{0.007}{203 - c}$$

$$\varepsilon_{su} = \frac{(158 - c)(0.007)}{203 - c} = \frac{1.106 - 0.007c}{203 - c}$$

$$\varepsilon_{pr} = 0.0062 + \frac{1.106 - 0.007c}{203 - c} \quad (1)$$

$$f_{pr} = (190 \times 10^3)\varepsilon_{pr}\left\{0.025 + \frac{0.975}{\left[1 + \left(118\varepsilon_{pr}\right)^{10}\right]^{0.1}}\right\} \leq 1860\ MPa \quad (2)$$

$$c = 0.0089 f_{pr} + 1.37 \quad (3)$$

Iterations using equations (1), (2) and (3)…

Try: $\varepsilon_{pr} = 0.012 \rightarrow f_{pr} = 1622.15\ MPa \rightarrow c = 15.81\ mm \rightarrow \varepsilon_{pr} = 0.0115$

Try: $\varepsilon_{pr} = 0.0115 \rightarrow f_{pr} = 1617.31\ MPa \rightarrow c = 15.76\ mm \rightarrow \varepsilon_{pr} = 0.0115 \quad Ok.$

Check:

$$\frac{\varepsilon_c}{c} = \frac{\varepsilon_{FRPu}}{h-c} \; where \; \varepsilon_c < \varepsilon_{cu} = 0.0035$$

$$\frac{\varepsilon_c}{15.76} = \frac{0.007}{203-15.76} \; where \; \varepsilon_c = 0.0006 < 0.0035 \quad Ok.$$

$$a = \beta_1 c = 0.829(15.76) = 13.1 \; mm$$

$$M_r = A_p f_{pr}\left(d - \frac{a}{2}\right) + \varepsilon_{FRP} E_{FRP} A_{FRP}\left(h - \frac{a}{2}\right)$$

$$M_r = (383.6)(1617.31)\left[158 - \frac{13.1}{2}\right] + (0.007)(131000)(2 \times 32)\left[203 - \frac{13.1}{2}\right]$$

$$M_r = 94.0 + 11.5 = \mathbf{105.5\ kNm}$$

Maximum theoretical machine load:

$$P_{max} = 2\left(\frac{M_{max}}{\ell_{shear}}\right) = 2\left(\frac{105.5\ kNm}{1.8\ m}\right) = 117.2\ kN$$

F.2.2 Flexural Capacity – Strain Compatibility Method [ACI 440.2R-08]

According to ACI 318M-05 (2005) for high-strength concrete:

$$\beta_1 = 0.65$$

$$C = T_p + T_{FRP}$$

$$\alpha_1 f'_c \beta_1 c b_f = A_p f_{ps} + \varepsilon_{FRP} E_{FRP} A_{FRP}$$

Based on existing studies (Hassan and Rizkalla 2003; De Lorenzis et al. 2004; Kotynia 2005) the ACI committee recommends that a maximum allowable strain in the NSM-FRP be 70% of the ultimate tensile capacity.

$$(0.65)(56.5)(0.829)(1200)c = 383.6 f_{pr} + (0.0119)(131000)(2 \times 32)$$

$$c = (10.5 \times 10^{-3}) f_{pr} + 2.73$$

$$\varepsilon_{ps} = \varepsilon_{pe} + \frac{P_e}{A_g E_c}\left(1 + \frac{e^2}{r^2}\right) + \varepsilon_{pnet} \leq 0.035$$

$$\varepsilon_{pe} = \frac{f_{sj} - \Delta_{FS}}{E_p} = \frac{1395 - 183.3}{195000} = 0.0062$$

$$\frac{P_e}{A_c E_c}\left(1 + \frac{e^2}{r^2}\right) = Negligible$$

$$\varepsilon_{pnet} = (\varepsilon_{fe} + \varepsilon_{bi})\left(\frac{d_p - c}{d_f - c}\right) = (0.0119 + \cancel{0.000019})\left(\frac{158 - c}{203 - c}\right) = \frac{1.8802 - 0.0119c}{203 - c}$$

$$\varepsilon_{ps} = 0.0062 + \frac{1.8802 - 0.0119c}{203 - c} \qquad (1)$$

$$f_{ps} = \begin{cases} 196500\,\varepsilon_{ps} \; for \; \varepsilon_{ps} \geq 0.0086 \\ 1860 - \frac{0.276}{\varepsilon_{ps} - 0.007} \; for \; \varepsilon_{ps} > 0.0086 \end{cases} \quad (2)$$

$$c = (10.5 \times 10^{-3}) f_{pr} + 2.73 \quad (3)$$

Iterations using equations (1), (2) and (3)…

Try: $\varepsilon_{ps} = 0.012 \rightarrow f_{ps} = 1804.8\,MPa \rightarrow c = 21.68\,mm \rightarrow \varepsilon_{ps} = 0.015$

Try: $\varepsilon_{ps} = 0.015 \rightarrow f_{ps} = 1825.5\,MPa \rightarrow c = 21.9\,mm \rightarrow \varepsilon_{ps} = 0.0151 \quad Ok.$

Check:

$$\frac{\varepsilon_c}{c} = \frac{\varepsilon_{FRPu}}{h - c} \; where \; \varepsilon_c < \varepsilon_{cu} = 0.003$$

$$\frac{\varepsilon_c}{21.9} = \frac{0.0119}{203 - 21.9} \; where \; \varepsilon_c = 0.0014 < 0.003 \quad Ok.$$

$$a = \beta_1 c = 0.65(21.9) = 14.2\,mm$$

$$M_r = A_p f_{pr} \left(d - \frac{a}{2}\right) + \varepsilon_{FRP} E_{FRP} A_{FRP} \left(h - \frac{a}{2}\right)$$

$$M_r = (383.6)(1825.5)\left[158 - \frac{14.2}{2}\right] + (0.0119)(131000)(2 \times 32)\left[203 - \frac{14.2}{2}\right]$$

M_r = 105.7 + 19.5 = $\mathbf{125.2\ kNm}$

Maximum theoretical machine load:

$$P_{max} = 2\left(\frac{M_{max}}{\ell_{shear}}\right) = 2\left(\frac{125.2\ kNm}{1.8\ m}\right) = 139.1\ kN$$

F.2.3 Cracking Moment

$$M_{cr} = \left[\frac{P}{A_g} + \frac{Pey_b}{I_t} + 0.6\lambda\sqrt{f'_c}\right]\frac{I_t}{y_b}$$

$$M_{cr} = \left[\frac{499.4 \times 10^3}{140194} + \frac{(499.4 \times 10^3)(54)(103.8)}{7.0171 \times 10^8} + 0.6(1)\sqrt{56.5}\right]\frac{7.0171 \times 10^8}{103.8}$$

$$= \mathbf{81.5\ kNm}$$

Cracking theoretical machine load:

$$P_{cr} = 2\left(\frac{M_{cr}}{\ell_{shear}}\right) = 2\left(\frac{81.5\ kNm}{1.8\ m}\right) = 90.6\ kN$$

F.3 Design Procedure for Specimen II-1-S0-FO

Notes: Contains no strengthening; opening centered at midspan resulting in a reduction in cross sectional area.

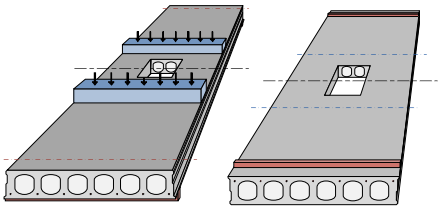

Figure F.3: II-1-S0-FO Schematic

F.3.1 Flexural Capacity – Strain Compatibility Method [CSA S806-12]

$$\alpha_1 = 0.85 - 0.0015 f'_c \geq 0.67$$

$$\alpha_1 = 0.85 - 0.0015(64.1) = 0.754$$

$$\beta_1 = 0.97 - 0.0025 f'_c \geq 0.67$$

$$\beta_1 = 0.97 - 0.0025(64.1) = 0.810$$

$$a = \frac{A_p f_{pu}}{\alpha_1 f'_c b_f} \leq h_f \rightarrow \frac{(328.8)(1860)}{(0.754)(64.1)(862)} = 14.7\ mm < 35\ mm \ \therefore R - section\ behaviour$$

$$C_f = T_p$$

$$\alpha_1 f'_c \beta_1 c b_f = A_p f_{pr}$$

$$(0.754)(64.1)(0.810)(862)c = 328.8 f_{pr}$$

$$c = 0.00974 f_{pr}$$

$$\varepsilon_{pr} = \varepsilon_{pe} + \varepsilon_{ce} + \varepsilon_{su}$$

$$\varepsilon_{pe} = \frac{f_{sj} - \Delta_{FS}}{E_p} = \frac{1395 - 183.3}{195000} = 0.0062$$

$$\varepsilon_{ce} = negligible$$

$$\frac{\varepsilon_{su}}{158 - c} = \frac{0.0035}{c}$$

$$\varepsilon_{su} = \frac{0.553}{c} - 0.0035$$

$$\varepsilon_{pr} = 0.0062 + \frac{0.553}{c} - 0.0035 = 0.0027 + \frac{0.553}{c} \quad (1)$$

$$f_{pr} = (190 \times 10^3)\varepsilon_{pr}\left\{0.025 + \frac{0.975}{\left[1 + \left(118\varepsilon_{pr}\right)^{10}\right]^{0.1}}\right\} \leq 1860\ MPa \quad (2)$$

$$c = 0.00974 f_{pr} \quad (3)$$

Iterations using equations (1), (2) and (3)…

Try: $\varepsilon_{pr} = 0.0405 \rightarrow f_{pr} = 1763.67\ MPa \rightarrow c = 17.18\ mm \rightarrow \varepsilon_{pr} = 0.0349$

Try: $\varepsilon_{pr} = 0.0349 \rightarrow f_{pr} = 1735.69\ MPa \rightarrow c = 16.90\ mm \rightarrow \varepsilon_{pr} = 0.0354$

Try: $\varepsilon_{pr} = 0.0354 \rightarrow f_{pr} = 1738.07\ MPa \rightarrow c = 16.93\ mm \rightarrow \varepsilon_{pr} = 0.0354 \quad Ok.$

$$a = \beta_1 c = 0.810(16.93) = 13.7mm$$

$$M_r = T\left(d - \frac{a}{2}\right) = A_p f_{pr}\left(d - \frac{a}{2}\right)$$

$$M_r = (328.8)(1738.07)\left[158 - \frac{13.7}{2}\right] = \mathbf{86.4\ kNm}$$

Maximum theoretical machine load:

$$P_{max} = 2\left(\frac{M_{max}}{\ell_{shear}}\right) = 2\left(\frac{86.4\ kNm}{1.8\ m}\right) = 96.0\ kN$$

F.3.2 Flexural Capacity – Strain Compatibility Method [ACI 440.2R-08]

According to ACI 318M-05 (2005) for high-strength concrete:

$$\beta_1 = 0.65$$

$$C = T_p$$

$$\alpha_1 f'_c \beta_1 c b_f = A_p f_{ps}$$

$$(0.65)(64.1)(0.65)(1200)c = 328.8 f_{pr}$$

$$c = (10.1 \times 10^{-3}) f_{pr}$$

$$\varepsilon_{ps} = \varepsilon_{pe} + \frac{P_e}{A_g E_c}\left(1 + \frac{e^2}{r^2}\right) + \varepsilon_{pnet} \leq 0.035$$

$$\varepsilon_{pe} = \frac{f_{sj} - \Delta_{FS}}{E_p} = \frac{1395 - 183.3}{196500} = 0.0062$$

$$\frac{P_e}{A_c E_c}\left(1 + \frac{e^2}{r^2}\right) = Negligible$$

$$\varepsilon_{pnet} = (0.003)\left(\frac{d_p - c}{c}\right) = (0.003)\left(\frac{158 - c}{c}\right) = \frac{0.474 - 0.003c}{c}$$

$$\varepsilon_{ps} = 0.0062 + \frac{0.474 - 0.003c}{c} \quad (1)$$

$$f_{ps} = \begin{cases} 196500\,\varepsilon_{ps} \; for \; \varepsilon_{ps} \geq 0.0086 \\ 1860 - \frac{0.276}{\varepsilon_{ps} - 0.007} \; for \; \varepsilon_{ps} > 0.0086 \end{cases} \quad (2)$$

$$c = (10.1 \times 10^{-3}) f_{pr} \quad (3)$$

Iterations using equations (1), (2) and (3)…

Try: $\varepsilon_{ps} = 0.012 \rightarrow f_{ps} = 1804.8\,MPa \rightarrow c = 18.2\,mm \rightarrow \varepsilon_{ps} = 0.029$

Try: $\varepsilon_{ps} = 0.029 \rightarrow f_{ps} = 1847.5\,MPa \rightarrow c = 18.7\,mm \rightarrow \varepsilon_{ps} = 0.0285 \quad Ok.$

$a = \beta_1 c = 0.65(18.7) = 12.16\,mm$

$$M_r = A_p f_{pr}\left(d - \frac{a}{2}\right)$$

$$M_r = (328.8)(1847.5)\left[158 - \frac{12.16}{2}\right]$$

$$M_r = \mathbf{106.8\ kNm}$$

Maximum theoretical machine load:

$$P_{max} = 2\left(\frac{M_{max}}{\ell_{shear}}\right) = 2\left(\frac{106.8\,kNm}{1.8\,m}\right) = 118.7\,kN$$

APPENDIX G – CAPACITY AND MODE OF FAILURE DETAILED ANALYSIS

The following sections present a detailed analysis of the ultimate capacity and mode of failure for each test specimen.

G.1 I-1-S0-NO (Control) Failure Mode

The unstrengthened control specimen, I-1-S0-NO, experienced a pure flexural-type failure. Failure was initiated by steel yielding, followed by concrete crushing. The relatively high-strength concrete with an as-tested strength of 64 MPa, allowed the concrete to undergo gradual crushing as the slab continued to deflect with no increase in load-carrying capacity. The load continued to drop in large increments with each new tensile crack and each significant burst of concrete in the compression zone at mid-span. Figure G.1 illustrates the test specimen at failure. Once the specimen was removed from the test setup the concrete was hammered away to expose the steel tendons. Two individual wires of the 7-wire strands were found to have ruptured during testing, as shown below. The ultimate flexural capacity was 97 kNm.

Figure G.1: I-1-S0-NO Mode of Failure

G.2 I-1-S2-NO Failure Mode – Strengthened Slab w/ 2 Strips

Specimen I-1-S4-NO was outfitted with two CFRP strips. This strengthened specimen experienced an ultimate load of 127 kNm, compared to 97 kNm for the unstrengthened control specimen, resulting in a 131% increase in ultimate capacity. Failure began with steel yielding, followed by concrete crushing under excessive deformation, as shown in Figure G.2. Tendon and CFRP slip was observed to be negligible. Epoxy split failure was observed close to the ultimate load. Once the epoxy cover had burst open, the confining pressure on the strips weakened, resulting in the bottom-most CFRP fibres splitting as deflection increased. This is a clear indication of an adequate transfer of stress between the concrete substrate, the epoxy matrix, and the CFRP strip. With no indication of slip, this system exhibits ideal behaviour, with the limiting factor being the compressive strength of the concrete substrate. The predicted capacity is found to be in agreement with the results determined from experimental testing, indicating the ACI predictions are acceptable for relatively lower prestressing forces.

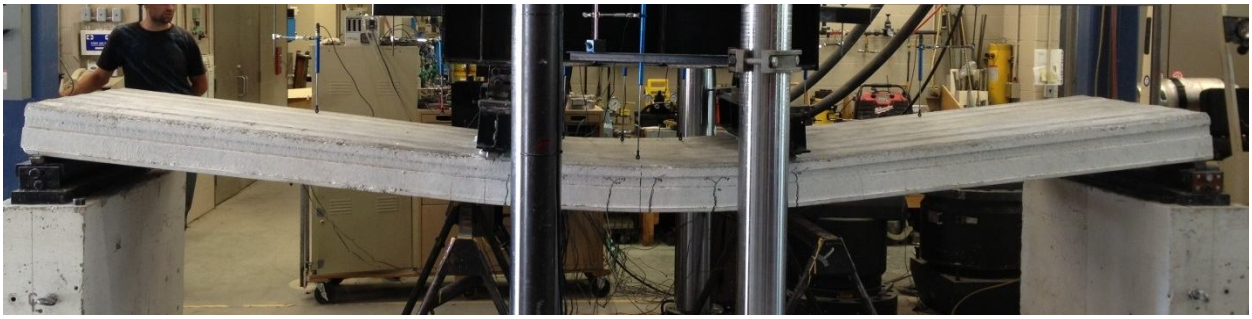

Figure G.2: I-1-S2-NO Mode of Failure

G.3 I-1-S4-NO Failure Mode – Strengthened Slab w/ 4 Strips

Specimen I-1-S4-NO was outfitted with four CFRP strips. The ultimate capacity was found to be 155 kNm, yielding an increase in capacity of 160% relative to the control specimen. This specimen exhibited a pure flexural mode of failure; beginning with steel yielding, followed by minor concrete crushing along the top of the slab, followed by intermittent tendon and CFRP slip; and finally individual steel wire rupture and CFRP partial rupture. Bond failure initiated at the laminate-adhesive interface. Once a large enough length of laminate had effectively debonded from the adhesive, the epoxy cover burst off, eliminating any confinement for the laminate causing the CFRP tape to split in half. Figure G.3 illustrates the specimen resting on the supports immediately prior to the ultimate failure point; as well as the split CFRP strip after the epoxy cover was eliminated.

Figure G.3: I-1-S4-NO Mode of Failure

G.4 I-1-S8-NO Failure Mode – Strengthened Slab w/ 8 Strips

The addition of eight CFRP laminates enhanced the ultimate capacity to 171 kNm, or by 76% compared to the control specimen. The flexural capacity was effectively improved, until the specimen failed in a flexural-shear type manner. Failure began first with steel yielding. Significant flexural-shear cracks developed along the shear span of the slab, propagating towards the loading points. The slab ultimately failed in a violent and sudden collapse. Figure G.4 illustrates the extent of the brittle failure. It should be noted that the failure load (171 kNm) is only 87% of the shear capacity (197 kNm), indicating that this setup produces a premature failure mode with increased levels of strengthening. The sudden failure of the strengthened specimen is attributed to a break-down of bond strength of the NSM reinforcement near the

loading points, followed closely by a shear-type failure of the section. Portions of the concrete substrate were noted to be still attached to the debonded CFRP strips, just as portions of the epoxy adhesive were observed to be still bonded to the concrete substrate. This suggests a combination of type II and type III mechanisms of failure, namely cracking of the surrounding concrete as well as cracking of the surrounding adhesive matrix. An even distribution of concrete was found on the debonded FRP strips and adhesive on the concrete substrate. This suggests that the bond strength at the adhesive-FRP and adhesive-concrete interfaces were approximately in equilibrium. Having used the maximum allowable bonded length (to avoid an early pull-out failure), and with the shear stresses in equilibrium along the two critical interfaces, this phenomenon suggests that if the shear capacity did not govern that FRP rupture may have been possible.

Figure G.4: I-1-S8-NO Mode of Failure

G.5 I-2-S0-NO (Control) Failure Mode

This unstrengthened control specimen experienced typical flexural-type behaviour. Steel yielding was the first sign of failure. At approximately 85% of its ultimate capacity the vertical flexural cracks began propagating horizontally towards mid-span and the loading points. Ultimate failure was encountered at the interface between the shear span and the flexural span, under the loading point. The flexural-shear crack propagated the complete depth of the slab and the concrete along the surface of the slab began to crush with a rapid decrease in load carrying capacity. The

ultimate capacity of the unstrengthened control specimen with additional internal prestressed steel was found to be 136 kNm; compared to 97 kNm for specimen I-1-S0-NO with a lower level prestressed reinforcement. Figure 4.5 illustrates the location of the failure cracks beneath the loading points.

Figure G.5: I-2-S0-NO Mode of Failure

G.6 I-2-S2-NO Failure Mode – Strengthened Slab w/ 2 Strips

Specimen I-2-S2-NO was strengthened with two strips and experienced a similar flexural behaviour to that of the unstrengthened control specimen, I-2-S0-NO. The addition of NSM-CFRP strips effectively increased the ultimate capacity of the slab by 21% to 165 kNm. The mode of failure remained unchanged from that of the control specimen. Vertical flexural cracks

began to propagate horizontally towards mid-span and the loading points. A flexural-shear mode of failure was experienced at the interface of the shear span and the flexural span, around the loading point as shown in Figure G.6. The failure was sudden and considerably more violent compared to that of the control specimen. The concrete in compression experienced a sudden burst around the loading point, eliminating any resistance to the applied load and the slab's self-weight; causing the slab to fall from its end supports. No bond failure was noted between the laminate, adhesive, and concrete substrate prior to failure. The failure load was approximately 77% of the shear capacity, indicating premature flexural-shear behaviour was the cause of failure.

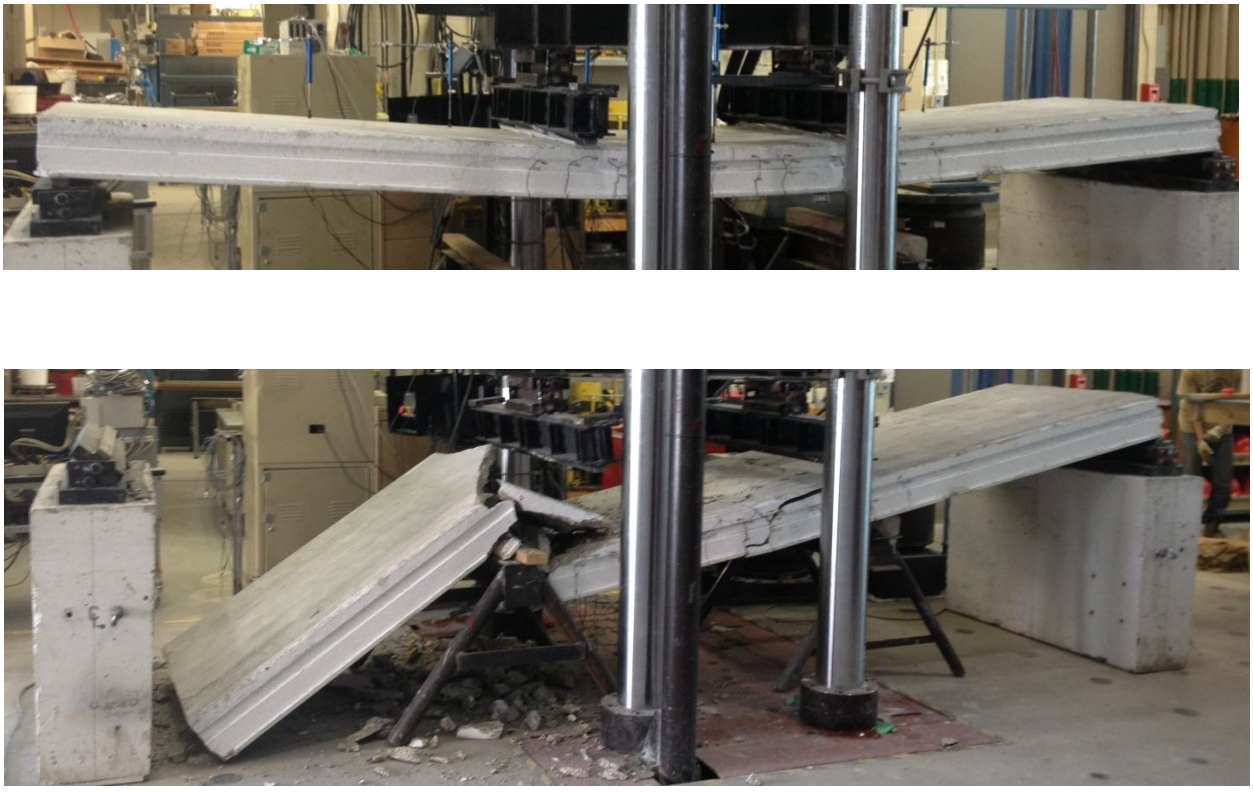

Figure G.6: I-2-S2-NO Mode of Failure

G.7 I-2-S4-NO Failure Mode – Strengthened Slab w/ 4 Strips

Specimen I-2-S4-NO was strengthened with four strips and experienced a similar mode of failure to that of other specimens reinforced with the higher level of internal prestressed reinforcement. The addition of four CFRP strips increased the ultimate capacity to 172 kNm, or by 27%. Cracking initiated at mid-span, propagating vertically. Once new crack formation stabilized, the flexural cracks began to widen, particularly along the shear span. The flexural cracks originating along the shear span began to propagate towards the loading points. No bond failure was observed prior to failure. The ultimate capacity was approximately 80% of the theoretical shear capacity, indicating that the flexural-shear behaviour once again resulted in the governing mode of failure.

Figure G.7: I-2-S2-NO Mode of Failure

G.8 II-1-S0-FO Failure Mode – 308 × 600 Opening Along Flexural Span

Cutting an opening along the flexural span of a simply supported HC slab decreased the ultimate capacity from 97 kNm, as experienced by control specimen I-1-S0-NO, to 83 kNm, a change of 17%. Both specimens encountered yielding, followed by the rupture of a single wire of the 7-wire pretensioned strand. Ultimately, concrete crushing in compression was the final stage of

failure, substantially reducing the capacity of the test specimen. The near-identical behaviour between the control specimen and this specimen with an opening, suggests that adding a 308 × 600 opening along the flexural span does not significantly change the behaviour of the specimen. The tensile stresses were successfully redirected around the opening, and did not produce any unorthodox behaviour. The theoretical flexural capacity as predicted by the strain compatibility method was determined to be 86.4 kNm, a difference of only 4.1% from the actual ultimate capacity. An opening that is 30% of the width of the slab still provides sufficient reinforcement and concrete area on either side of the opening that the specimen continues behave as if no opening were present.

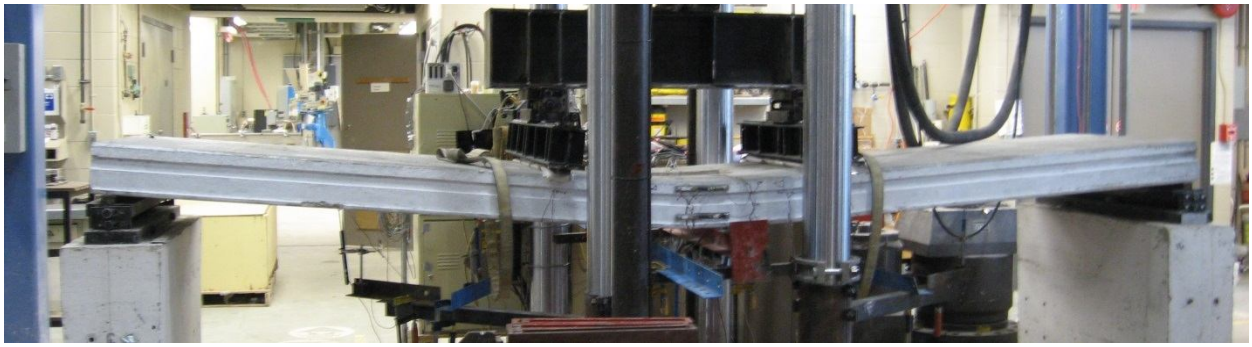

Figure G.8: II-1-S0-FO Specimen at Failure

G.9 II-1-S0-SO Failure Mode – 308 × 600 Opening Along Shear Span

The presence of an opening along the shear span of a simply supported HC slab decreased the ultimate capacity from 97 kNm to 93 kNm, a change of 4%. This indicates that if the opening is positioned far enough from the critical bending moment region, and has sufficient shear capacity, then the ultimate capacity will remain approximately similar to a specimen with no opening when flexural failure is the governing mode of failure. The initiation and final steps of failure were similar to the control specimen; both encountered steel yielding, and both experienced

concrete crushing at the final stage. The behaviour was different between these stages. At approximately 80% of the ultimately load, the concrete experience a sudden flexural-shear failure. This fracture occurred between the opening and the loading point, along the shear span. According to previous studies on disturbed regions, openings and loading points are areas which create non-linear stress concentrations in an area approximately one member-depth away. The opening and loading point are separated by two member depths, so theoretically there should be no superposition of the disturbances. However, in this case, the concrete section between the opening and loading point experienced enough shear stress to effectively crack the section in a flexural-shear manner almost the entire depth of the section. At this point a significant portion of the stresses were transferred to the internal steel tendons. Unlike the control specimen which experienced partial tendon rupture, specimen II-1-S0-SO experienced full tendon rupture in the form of shearing. This occurred at the nearest tendon running alongside the opening. The angle of the rupture plane is approximately 45 degrees, confirming a significant shear stress concentration between the opening and the loading point.

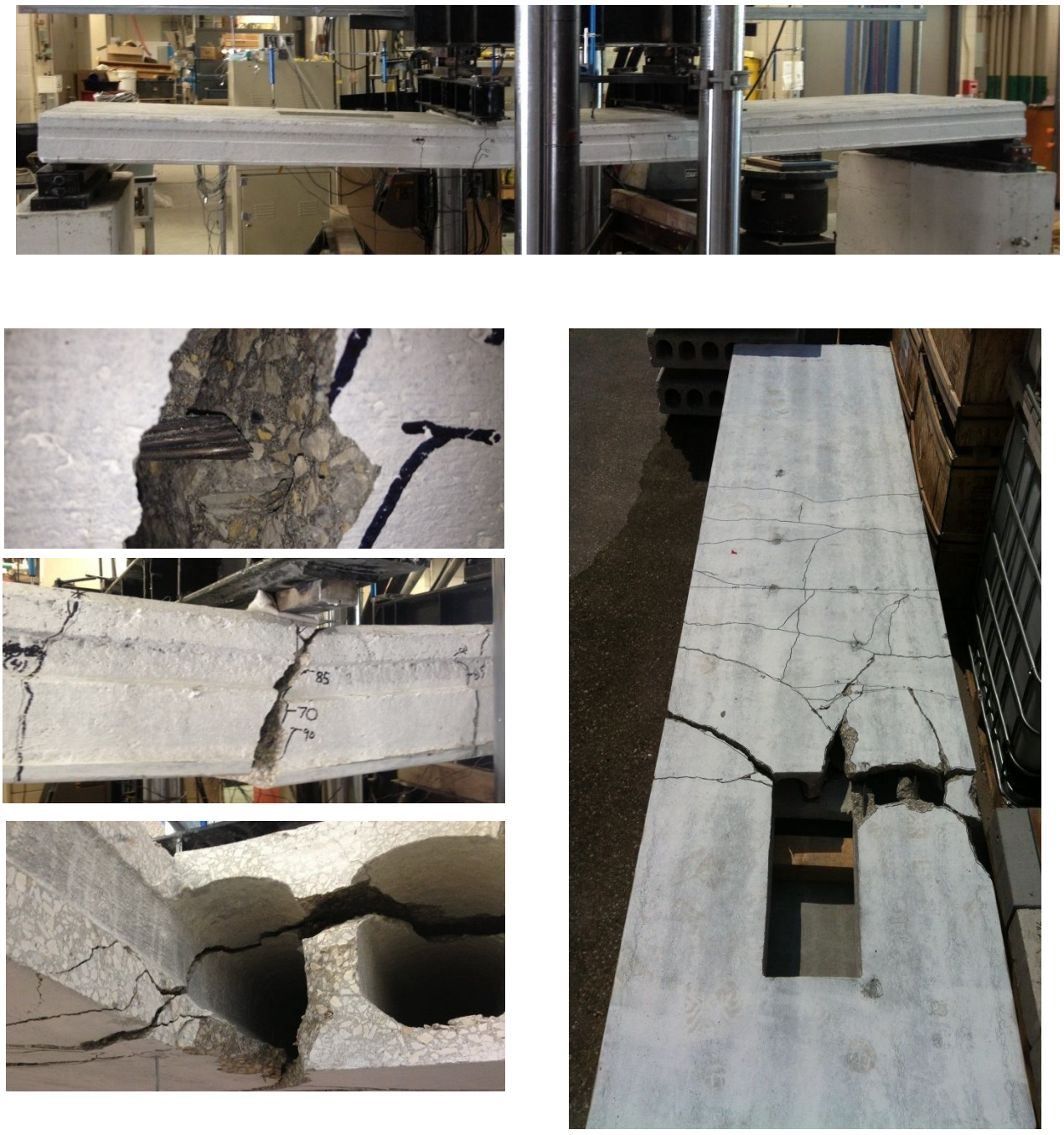

Figure G.9: II-1-S0-SO Specimen at Failure

G.10 III-1-S2-FO Failure Mode – 308 × 600 Flexural Opening – Strengthened w/ 2 Strips

This section will comment on the effect that adding two NSM-CFRP strips has on the mode of failure compared to the unstrengthened specimen with an opening, namely II-1-S0-FO. The presence of a longitudinal CFRP strip and two transverse CFRP strips on each side of the opening increases the ultimate capacity from 83 kNm to 116 kNm, a change of 40%. Compare this increase with the 31% enhancement experienced by specimen I-1-S2-NO compared to its unstrengthened counterpart, I-1-S0-NO. In the case of this study, the presence of an opening intercepts the middle steel tendon, and therefore decreases the effective internal prestressing reinforcement ratio. As concluded from the analysis in Series I, a greater increase in ultimate capacity can be expected for lower internal reinforcement ratios. In other words, as the internal reinforcement ratio increases, the capacity enhancement provided by an NSM system diminishes. This trend is also valid for specimens whose internal reinforcement is interrupted by openings. Furthermore, comparing this change in strength to the control specimen with no opening, and no strengthening, I-1-S0-NO, the capacity was increased from 97 kNm to 116 kNm, a change of 20%. This indicates that even after the capacity of the slab is reduced with the addition of an in-situ opening along the flexural span, the NSM technique can effectively increase the ultimate capacity to hold additional load if required.

The initial and final stages of failure are similar to that of the unstrengthened control specimen with an opening in the same location. Steel yielding is encountered first, and ultimately fails by concrete crushing. At a load near ultimate failure, a pair of transverse strips delaminated from the concrete substrate in a combination of type 2 and 3 delamination failure. Failure occurred in the surrounding concrete substrate as well as the surrounding adhesive matrix. Following the

delamination of the transverse strips, the longitudinal strips experienced a partial type-4 delamination failure. Several sections of the epoxy covering the longitudinal strips spalled off (adhesive cover spall), but did not fully debond from the substrate. This occurred within the maximum moment zone, and effectively reduced the confinement of the longitudinal NSM reinforcement. Further increase in the load lead to the outermost tensile fibres of the CFRP strips to fray, essentially breaking away from the reinforcements internal resin matrix. Figure G.10 illustrates the various stages of failure.

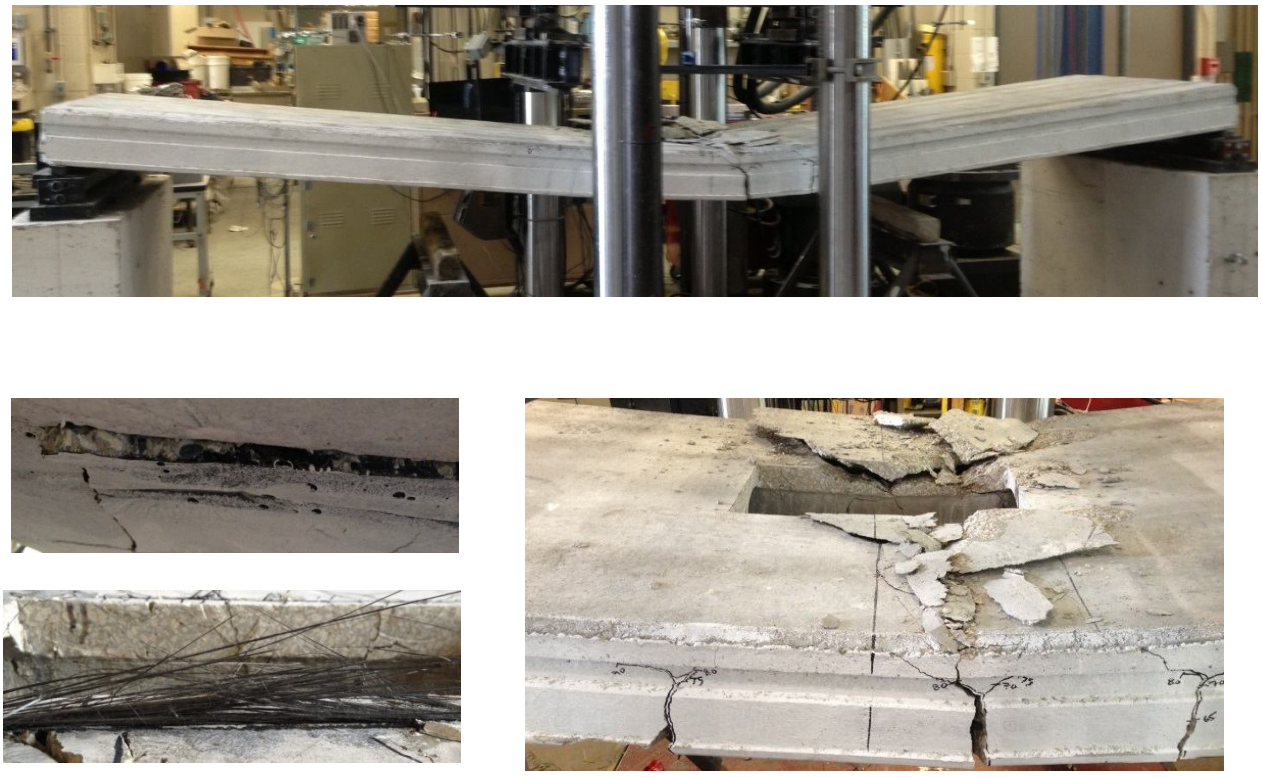

Figure G.10: III-1-S2-FO Specimen at Failure

G.11 III-1-S2-SO Failure Mode – 308 × 600 Shear Opening – Strengthened w/ 2 Strips

This section will comment on the effect that adding two NSM-CFRP strips has on the mode of failure compared to the unstrengthened specimen with an opening, namely II-1-S0-SO. The presence of a longitudinal CFRP strip and two transverse CFRP strips on each side of the opening increases the ultimate capacity from 93 kNm to 121 kNm, a change of 30%. Comparing this change in strength to the control specimen with no opening, and no strengthening, I-1-S0-NO, the capacity was increased from 97 kNm to 121 kNm, a change of 25%. This indicates that even after the capacity of the slab is reduced with the addition of an in-situ opening along the shear span, the NSM technique can effectively increase the ultimate capacity to hold additional load if required.

Ultimate failure was sudden and violent. Due to the unsafe nature of the strengthened specimen as it approached the ultimate load, it was impossible to get close enough to determine where delamination first originated. It is certain that upon delamination of the transverse and longitudinal strips around the vicinity of the opening, that the sudden transfer of the remaining stress to the internal reinforcement was too great and cause a violent flexural-shear type failure. Upon inspection of the NSM system after failure, it could be seen that the failure interface for the transverse strips was predominantly within the epoxy, and did not extend into the surrounding concrete substrate. In the case of this specimen, the reduction in surface area when placing the strips horizontally does not provide enough surface area to equally transfer the stresses between the concrete substrate, the epoxy matrix, and the CFRP laminate. Conversely, bond failure was noted equally within the epoxy matrix and the surround concrete substrate for the CFRP strips inserted in the vertical orientation. As previous research suggests, and as outlined in Chapter 2,

this increase in surface area clearly plays an important role in the failure mechanism for NSM-FRP reinforcement.

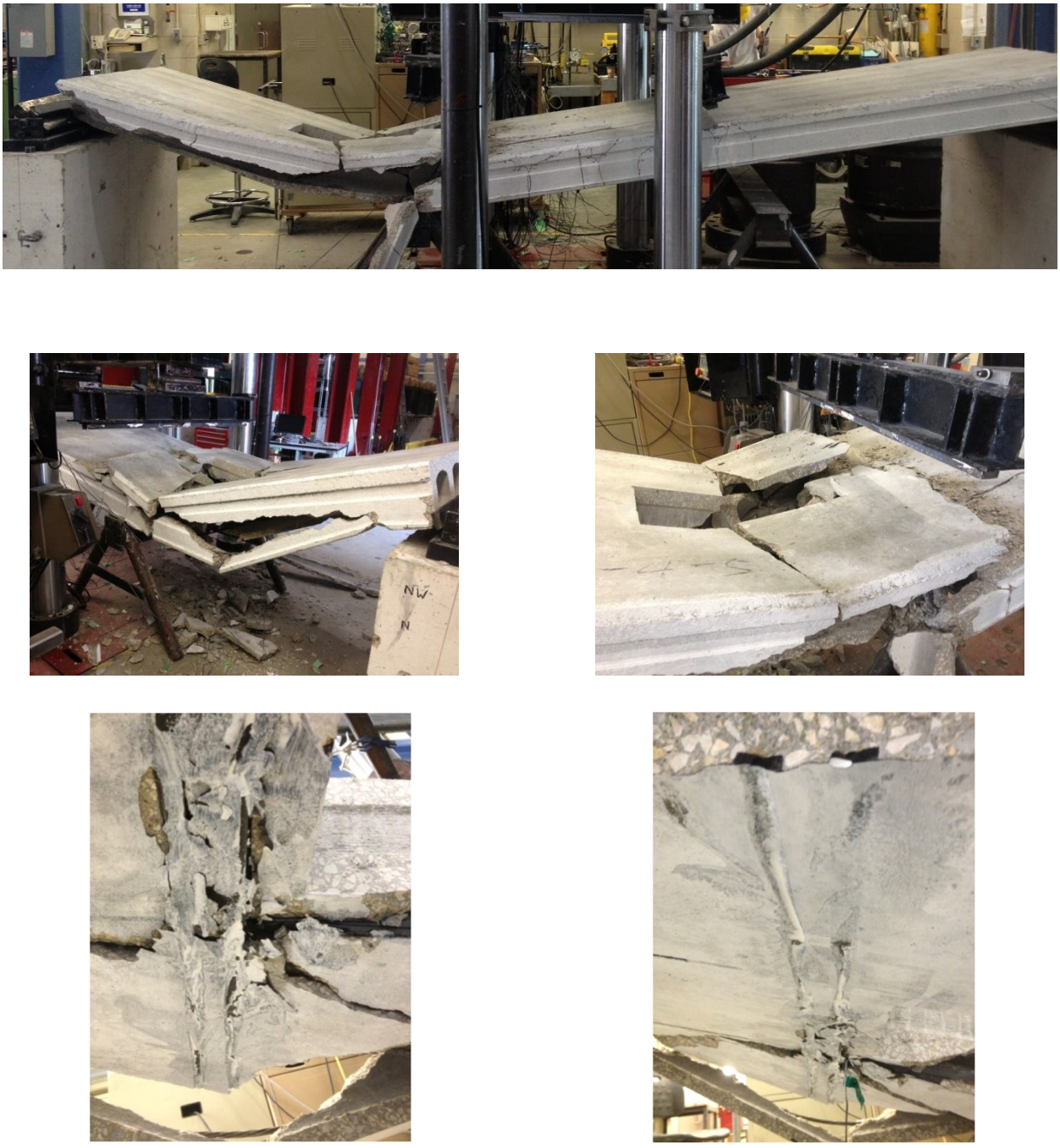

Figure G.11: III-1-S2-SO Specimen at Failure

APPENDIX H – STRAIN IN PRESTRESSED STEEL CALCULATIONS

According to CPCI yielding of high-strength steel occurs at 90% of the ultimate stress.

$$\sigma_y = 0.9(f_{pr}) = 0.9(1860) = 1674MPa$$

$$\sigma = E\epsilon \rightarrow \epsilon_y = \frac{\sigma_y}{E_s} = \frac{1674}{195000} = 0.00859$$

The yield strain for the high-strength steel tendons was determined to be 0.00859, or 8590 micro strain. The strain caused by applied loading required to reach the yield strain is determined by subtracting the initial jacking strain and the strain due to short and long term losses.

$$\epsilon_{Applied} = \epsilon_y - [\epsilon_j - (\epsilon_{\Delta 1} + \epsilon_{\Delta 2})]$$

H.1 Initial Strain in Code 1 Tendons After Prestress Losses

$$\sigma_\Delta = 0.75(f_{sj}) - (Short\ Term\ Losses + Long\ Term\ Losses)$$

$$\sigma_\Delta = 0.75(1860) - (52.7 + 130.6) = 1211.7MPa$$

$$\sigma_\Delta = E_s\epsilon_\Delta \rightarrow \epsilon_\Delta = \frac{\sigma_\Delta}{E_s}$$

$$\epsilon_\Delta = \frac{1211.7MPa}{195000MPa} = 0.00621$$

Therefore the allowable strain due to the applied load to reach the yield strain is:

$$\epsilon_j = \frac{0.75(1860)}{195000} = 0.00715$$

$$\epsilon_{Applied} = \epsilon_y - \left[\epsilon_j - (\epsilon_{\Delta 1} + \epsilon_{\Delta 2})\right]$$

$$\epsilon_{Applied} = 0.00859 - [0.00621] = \mathbf{0.00238}$$

H.2 Initial Strain in Code 2 Tendons After Prestress Losses

$$\sigma_\Delta = 0.75(f_{sj}) - (Short\ Term\ Losses + Long\ Term\ Losses)$$

$$\sigma_\Delta = 0.75(1860) - (61.6 + 142.6) = 1190.8MPa$$

$$\sigma_\Delta = E_s\epsilon_\Delta \rightarrow \epsilon_\Delta = \frac{\sigma_\Delta}{E_s}$$

$$\epsilon_\Delta = \frac{1190.8MPa}{195000MPa} = 0.00611$$

Therefore the allowable strain due to the applied load to reach the yield strain is:

$$\epsilon_{Applied} = \epsilon_y - \left[\epsilon_j - (\epsilon_{\Delta 1} + \epsilon_{\Delta 2})\right]$$

$$\epsilon_{Applied} = 0.00859 - [0.00611] = \mathbf{0.00248}$$

H.3 Serviceability Strain Limit for Internal Prestressed Reinforcement

According to ACI 440.2R-08, to avoid inelastic deformations of a member strengthened with NSM-FRP, the internal prestressed steel should not reach yielding under service load levels. Therefore the maximum allowable stress in the steel is determined as follows:

$$f_{ps,s} \leq 0.82 f_{py}$$

$$f_{py} = 0.9 f_{pu} = 0.9(1860MPa) = 1674MPa$$

$$f_{ps,s} = 0.82(1674) = 1372.7MPa$$

Therefore the maximum allowable strain at the serviceability state is determined as follows:

$$\varepsilon_{ps,s} = \frac{f_{ps,s}}{E_p} = \frac{1372.7}{195000} = 0.00704$$

The allowable strain due to the applied load to reach the serviceability state for strand code '1' is:

$$\varepsilon_{ps,s-applied} = Allowable\ strain\ at\ serviceability$$
$$- [(Initial\ strain\ at\ jacking) - (short\ and\ long\ term\ losses)]$$
$$= 0.00704 - [0.00621] = 0.00083 = 830x10^{6}$$

The allowable strain due to the applied load to reach the serviceability state for strand code '2' is:

$$\varepsilon_{ps,s-applied} = Allowable\ strain\ at\ serviceability$$
$$- [(Initial\ strain\ at\ jacking) - (short\ and\ long\ term\ losses)]$$
$$= 0.00704 - [0.00611] = 0.00093 = 930x10^{6}$$

APPENDIX I – ADDITIONAL STRAIN DATA

The following strain data was collected from CFRP strain gauges affixed to the transverse CFRP laminates bordering the flexural and shear openings. Figure I.1 illustrates the layout of four strain gauges surrounding the flexural opening of specimen III-1-S2-FO.

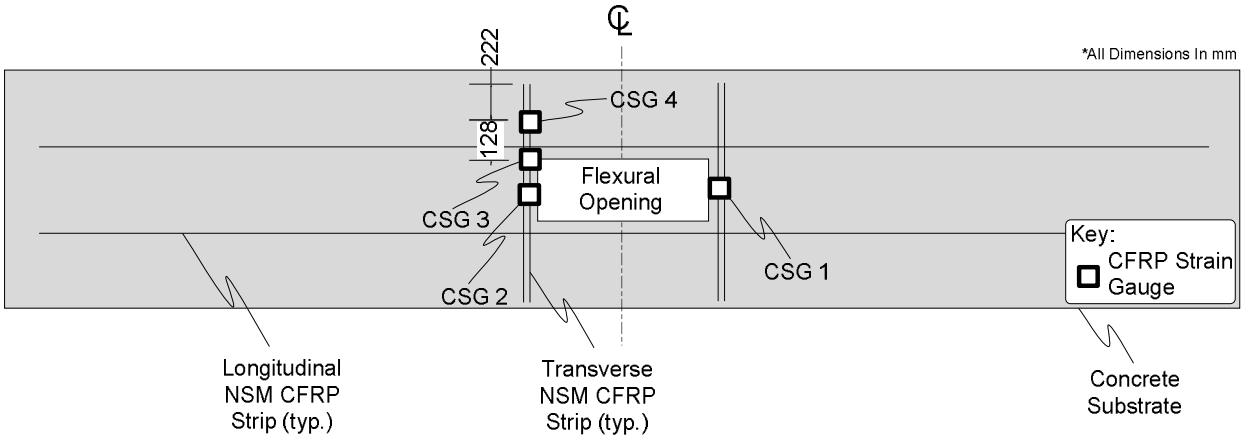

Figure I.1: Transverse Strain Gauge Layout for Specimen III-1-S2-FO

Using the above schematic for reference, the following curves illustrate the load - CFRP strain relationship recorded by each of the strain sensors along the transverse reinforcement for specimen III-1-S2-FO.

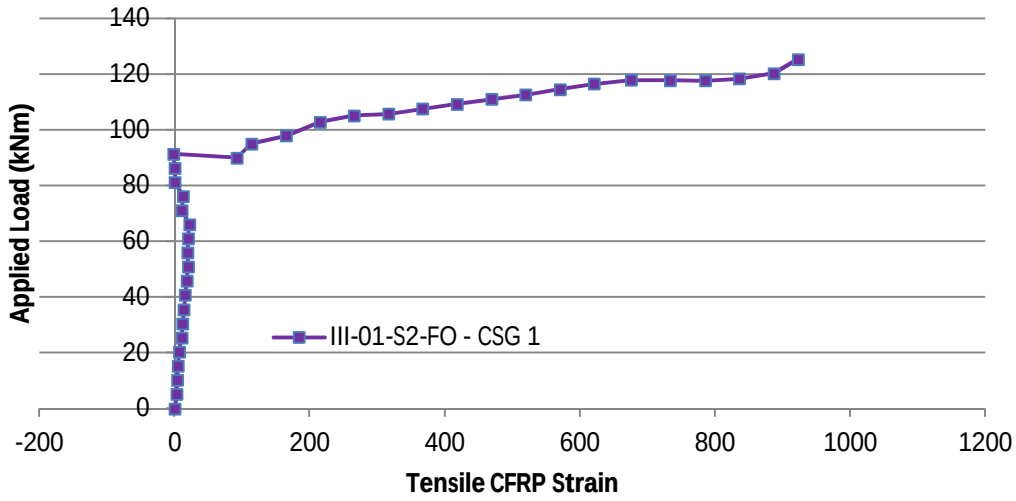

Figure I.2: Load –CFRP Strain for Specimen III-1-S2-FO – CSG 1

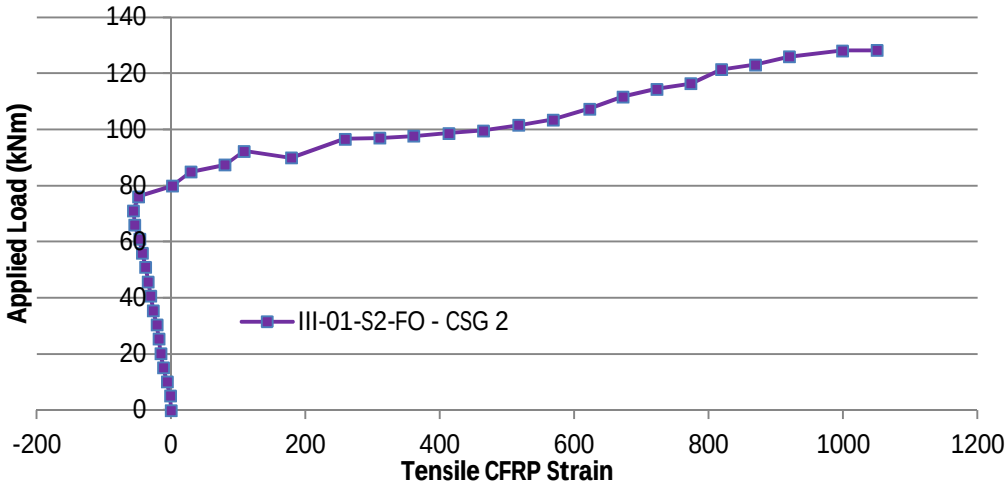

Figure I.3: Load – CFRP Strain for Specimen III-1-S2-FO – CSG 2

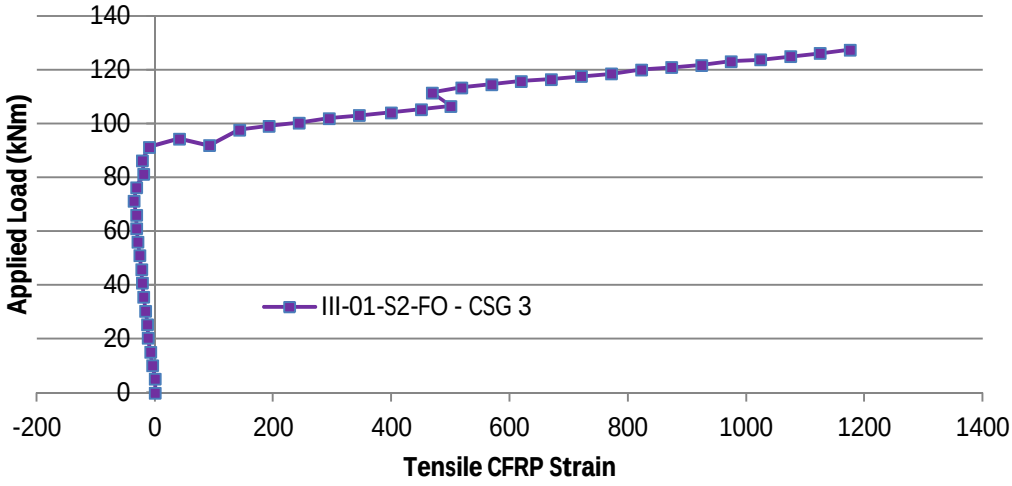

Figure I.4: Load – CFRP Strain for Specimen III-1-S2-FO – CSG 3

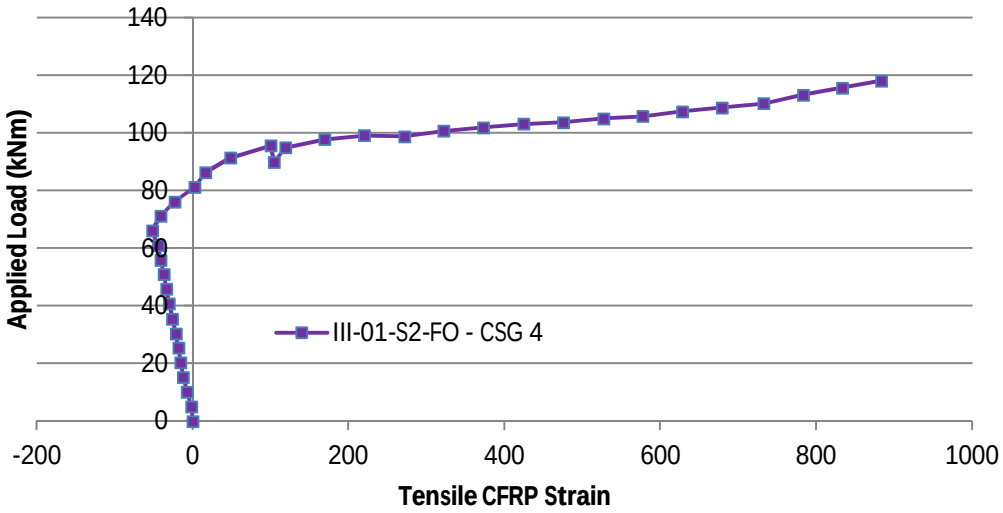

Figure I.5: Load – CFRP Strain for Specimen III-1-S2-FO – CSG 4

Figure I.6 illustrates the layout of four strain gauges surrounding the shear opening of specimen III-1-S2-SO.

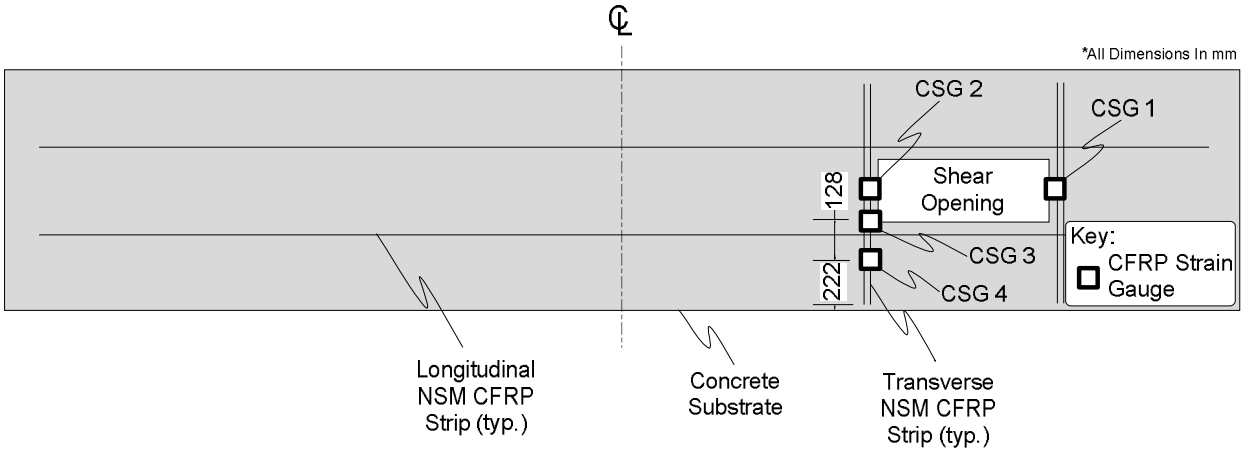

Figure I.6: Transverse Strain Gauge Layout for Specimen III-1-S2-SO

Using the above schematic for reference, the following curves illustrate the load - CFRP strain relationship recorded by each of the strain sensors along the transverse reinforcement for specimen III-1-S2-SO.

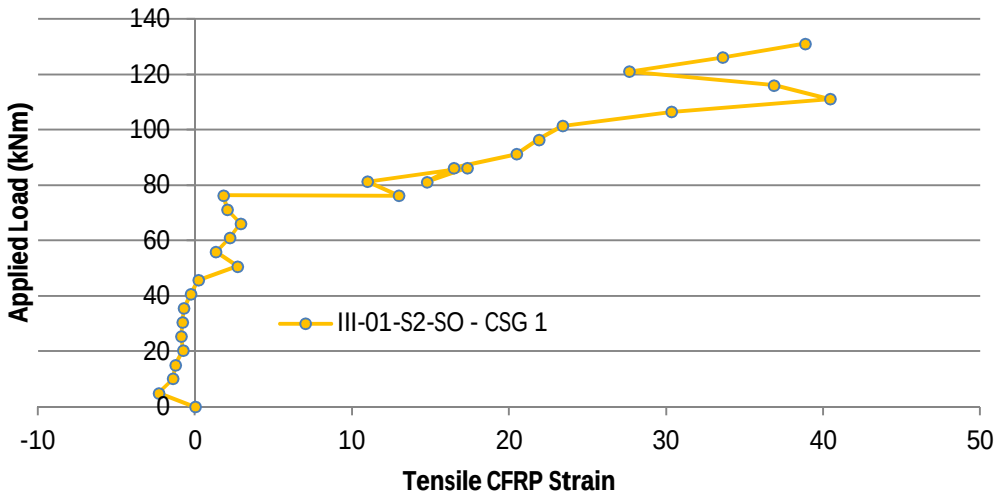

Figure I.7: Load – CFRP Strain for Specimen III-1-S2-SO – CSG 1

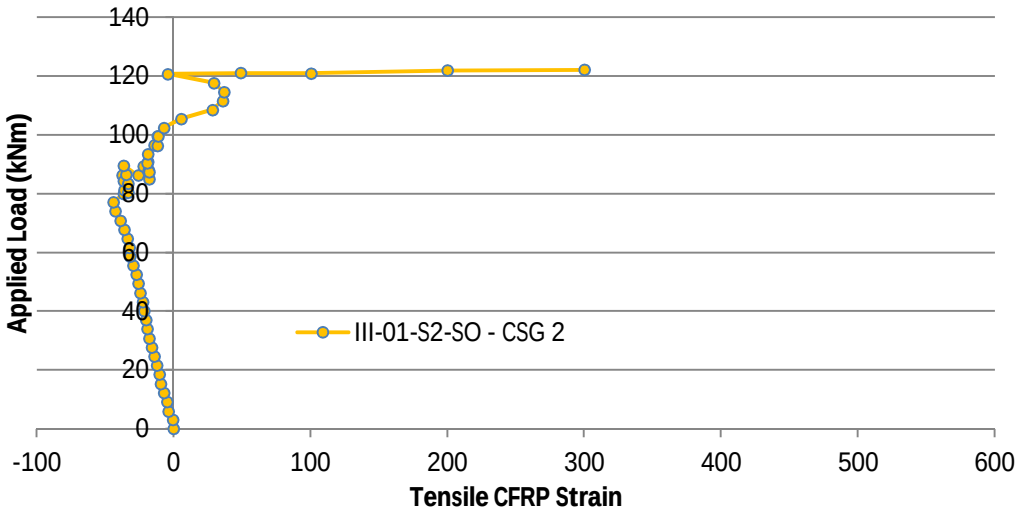

Figure I.8: Load – CFRP Strain for Specimen III-1-S2-SO – CSG 2

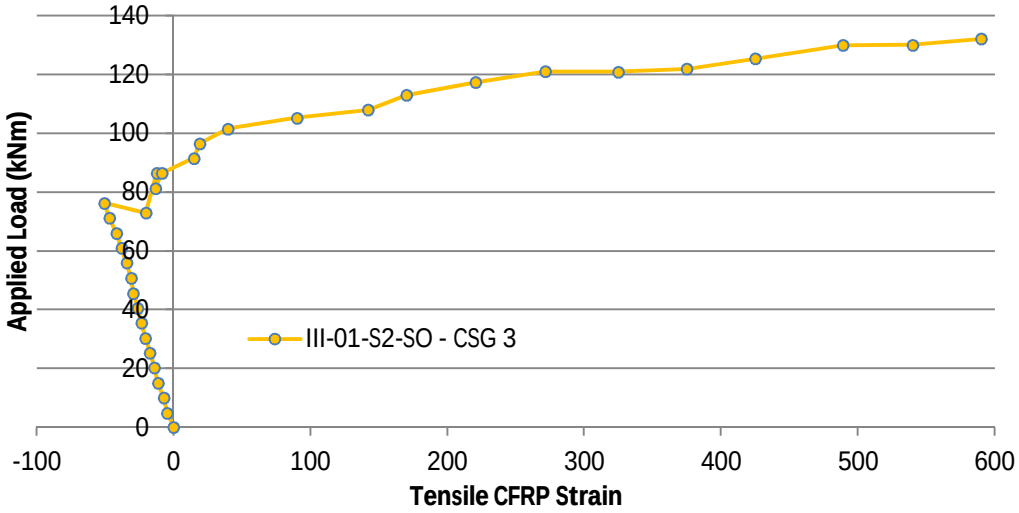

Figure I.9: Load – CFRP Strain for Specimen III-1-S2-SO – CSG 3

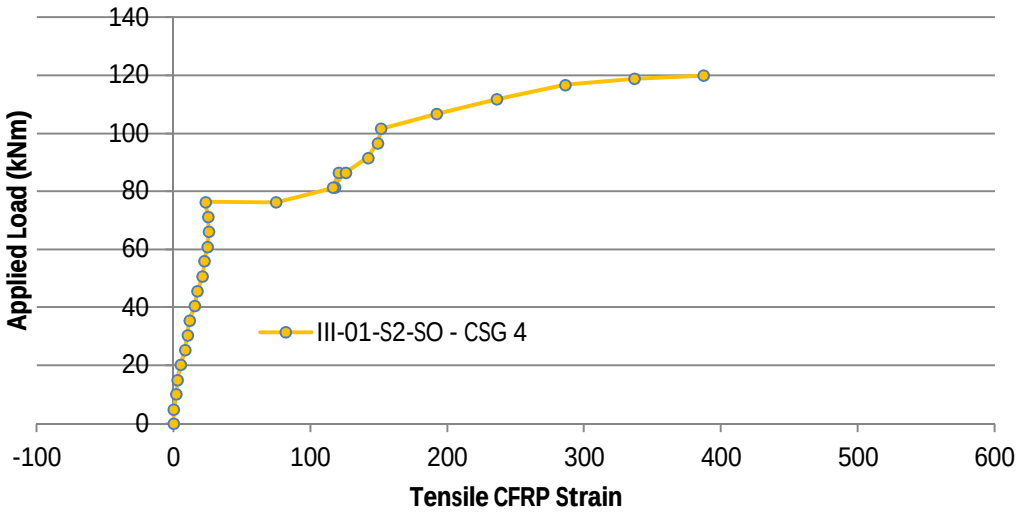

Figure I.10: Load – CFRP Strain for Specimen III-1-S2-SO – CSG 4

APPENDIX J – CRACK PATTERNS

The following schematics illustrate the crack patterns at three distinct stages during loading for each specimen. The three stages include initial cracking, approximately 70% of the ultimate capacity, and at ultimate failure.

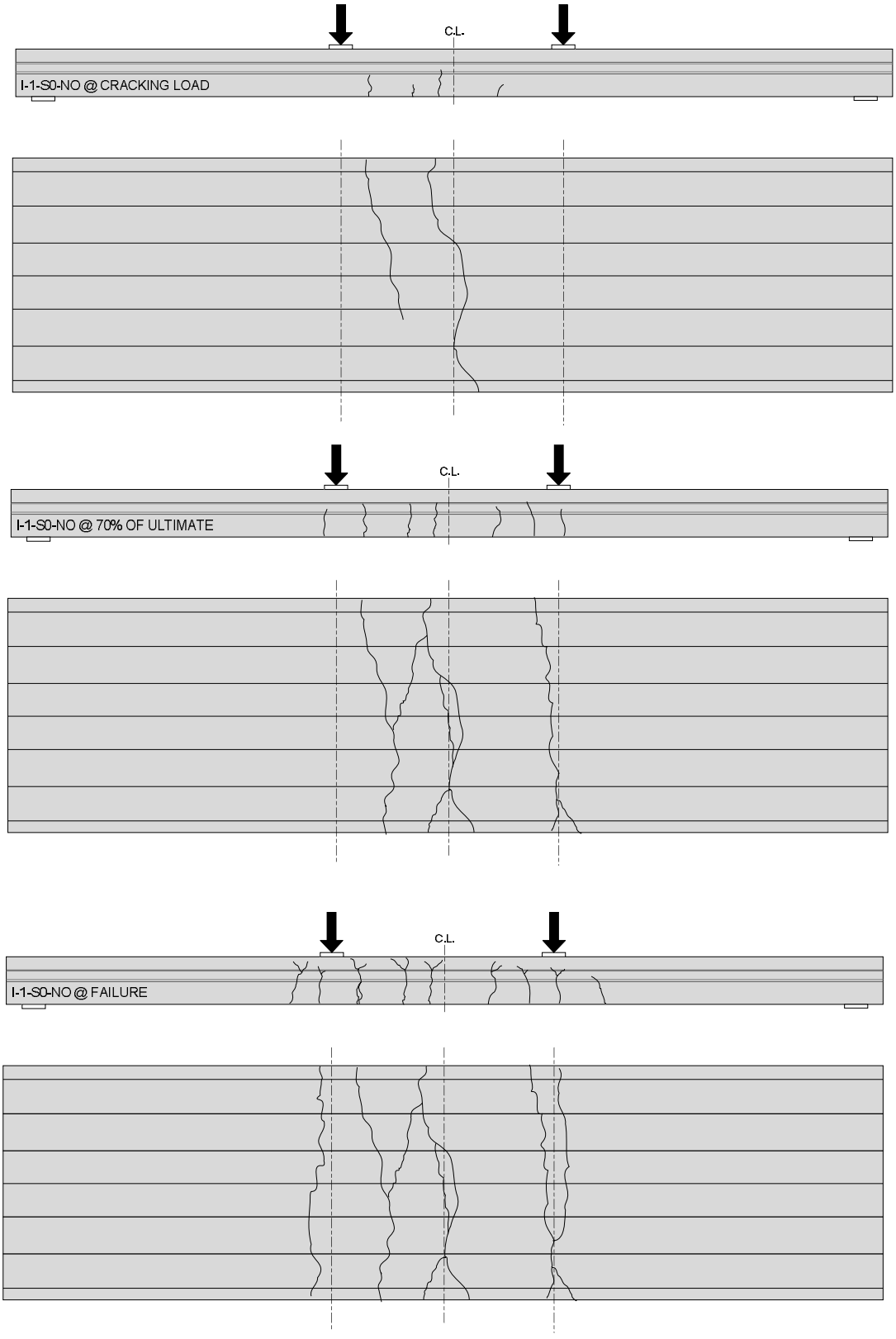

Figure J.1: I-1-S0-NO Crack Pattern

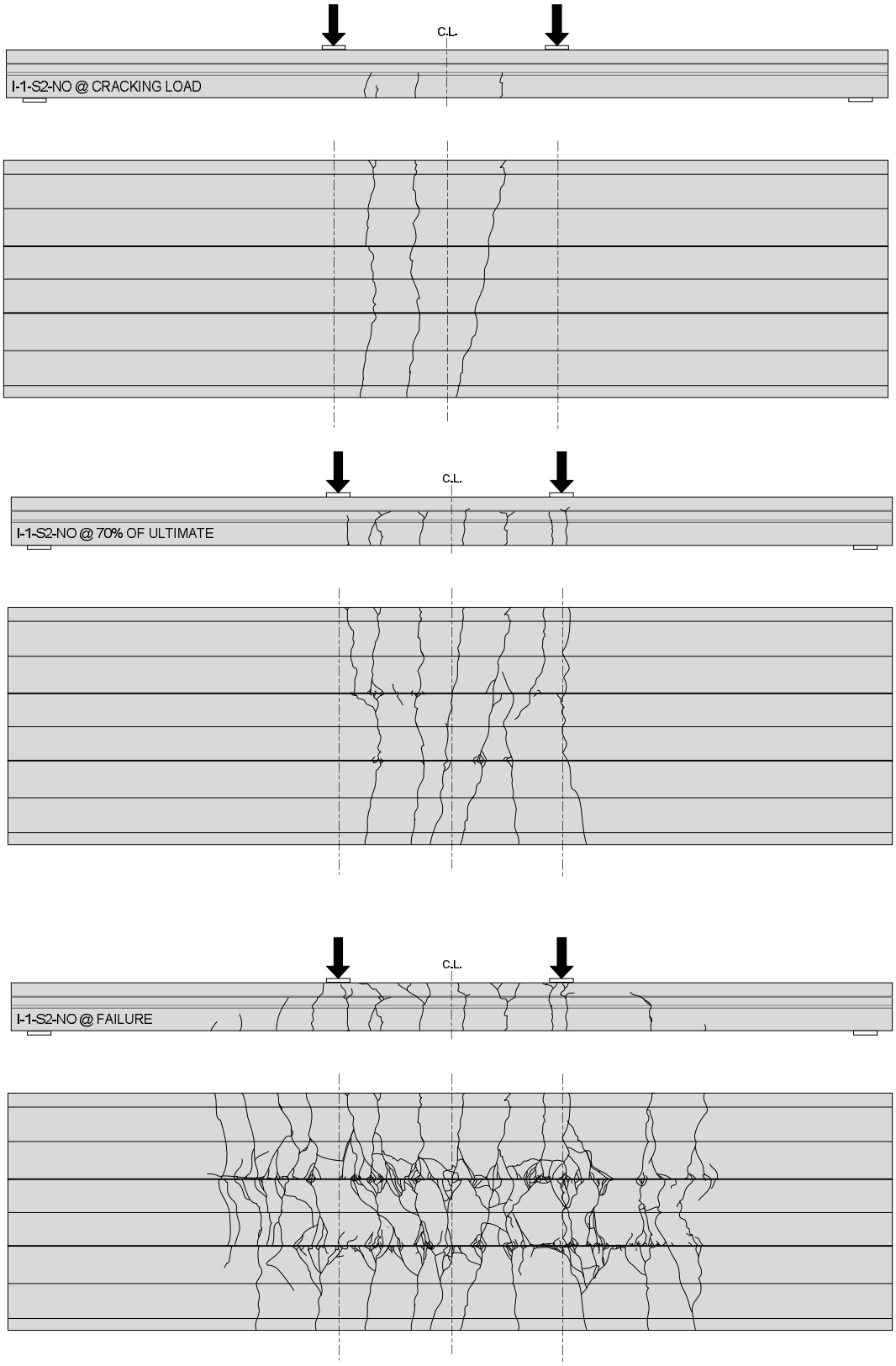

Figure J.2: I-1-S2-NO Crack Pattern

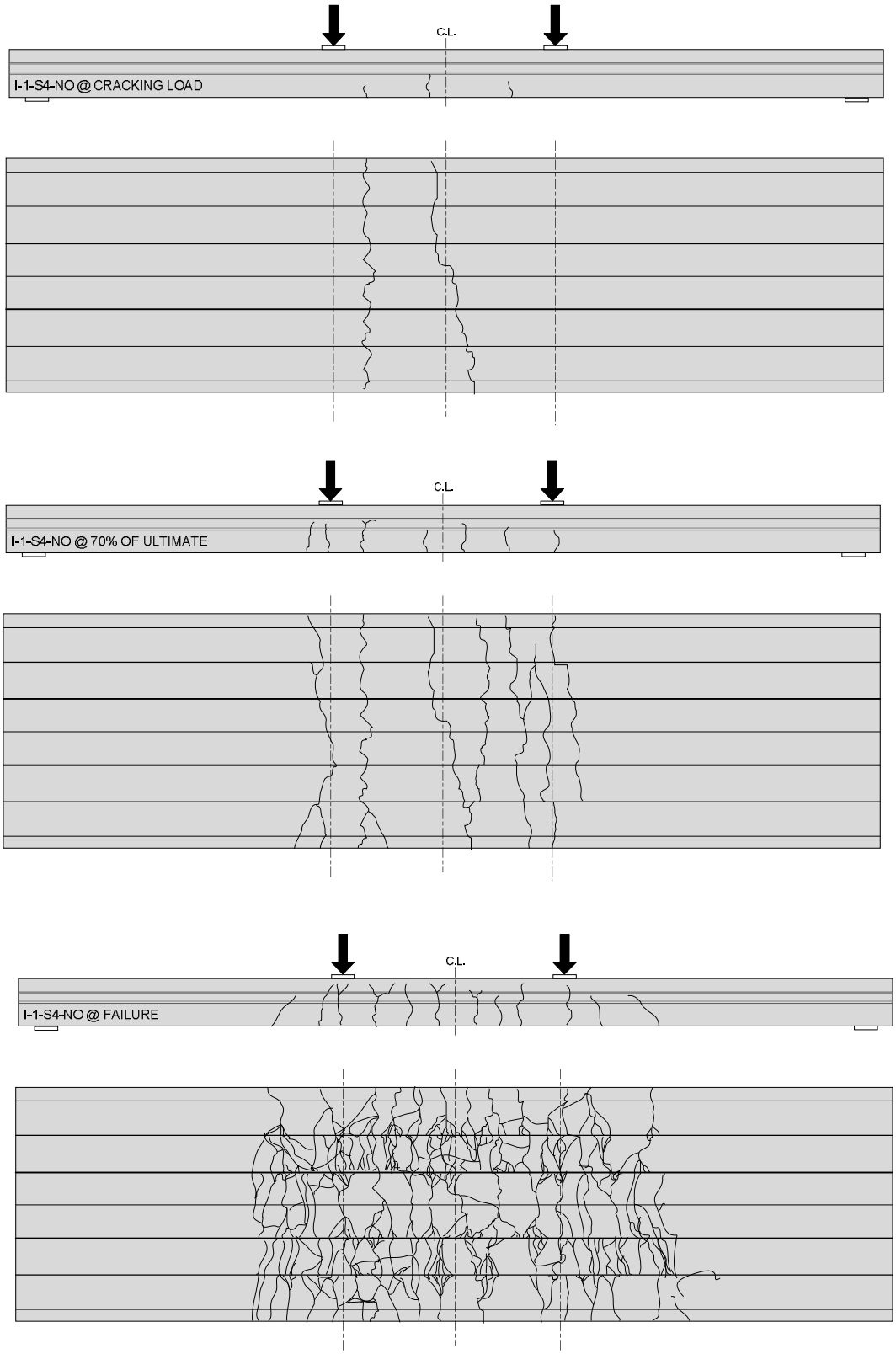

Figure J.3: I-1-S4-NO Crack Pattern

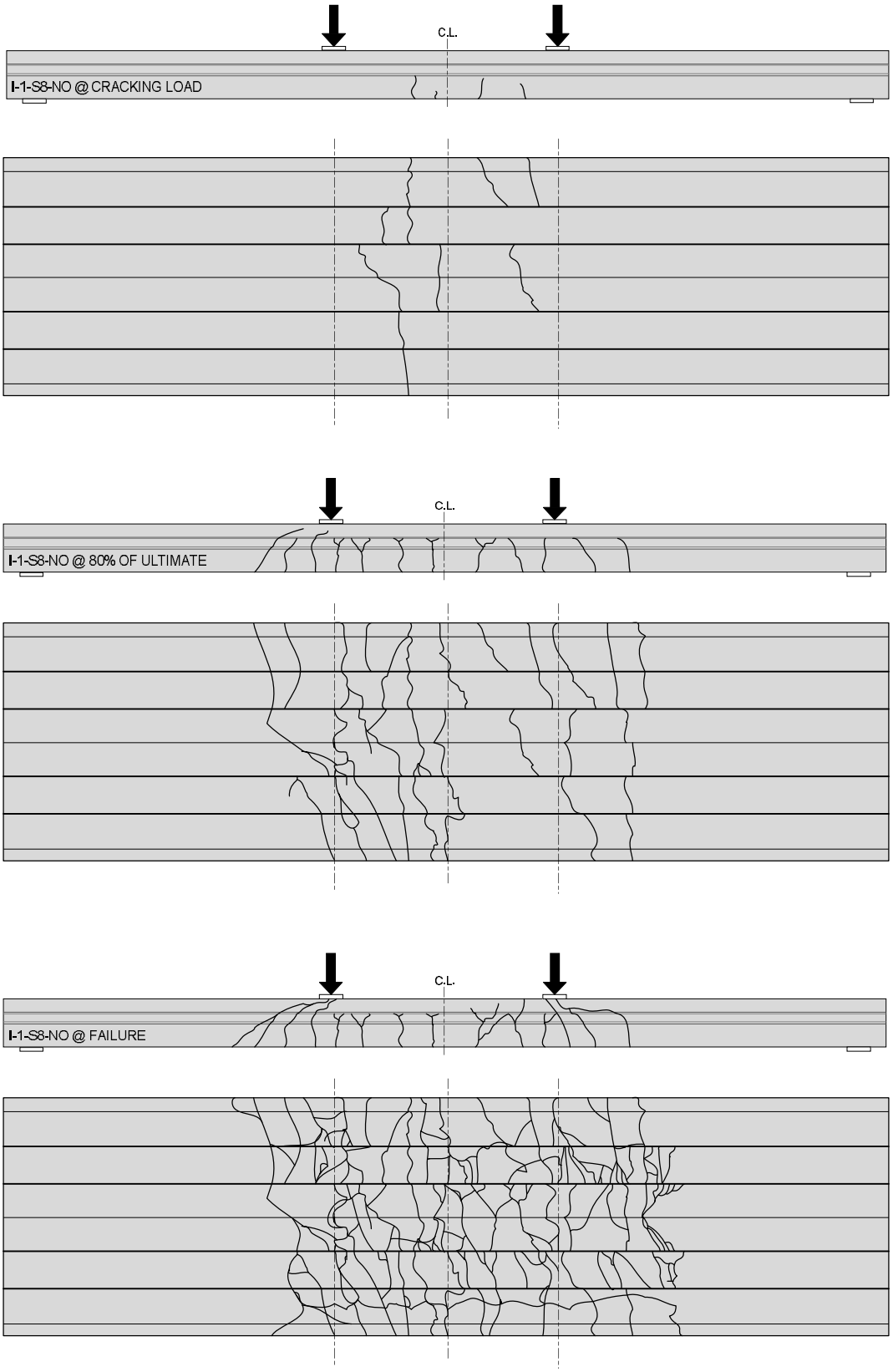

Figure J.4: I-1-S8-NO Crack Pattern

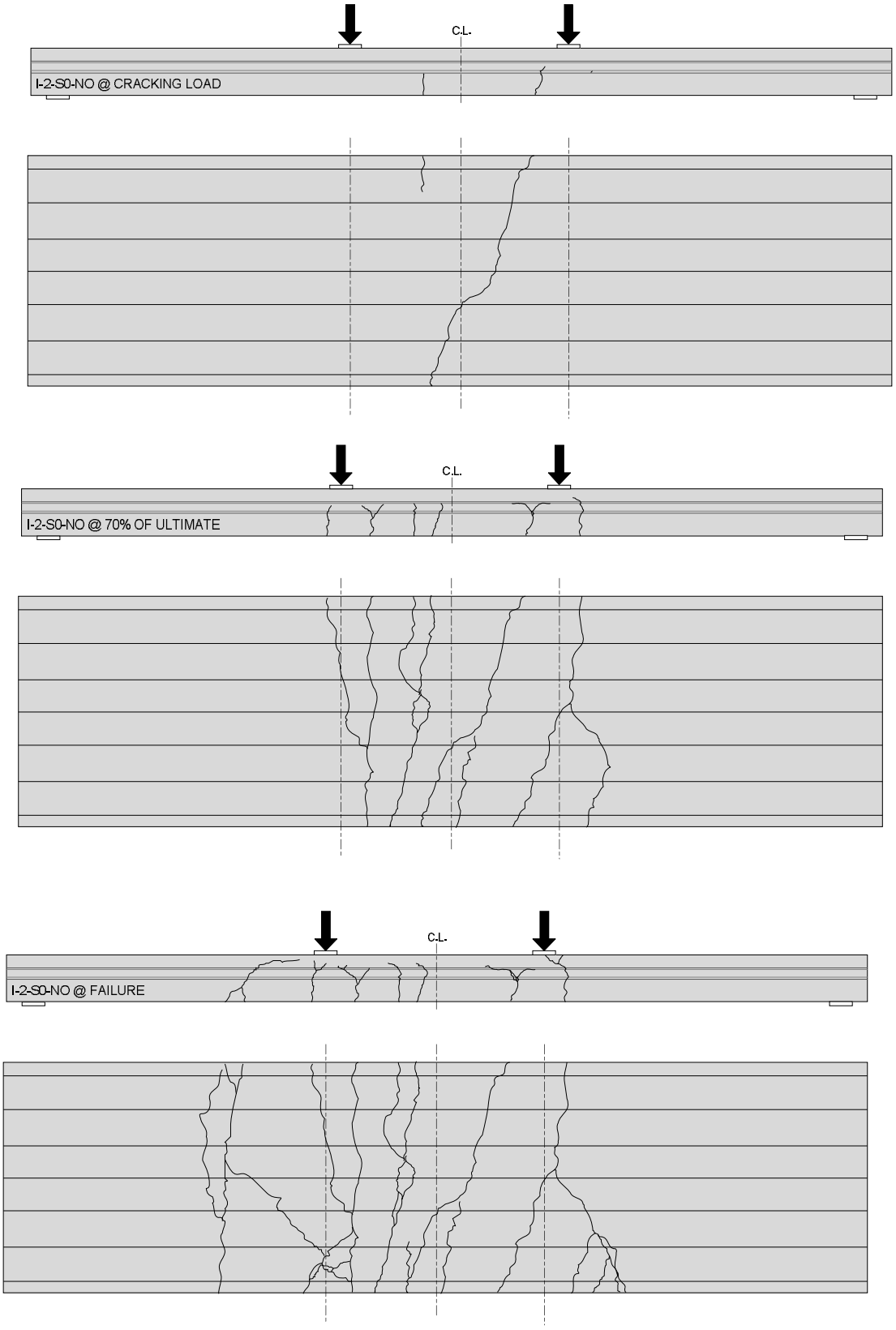

Figure J.5: I-2-S0-NO Crack Pattern

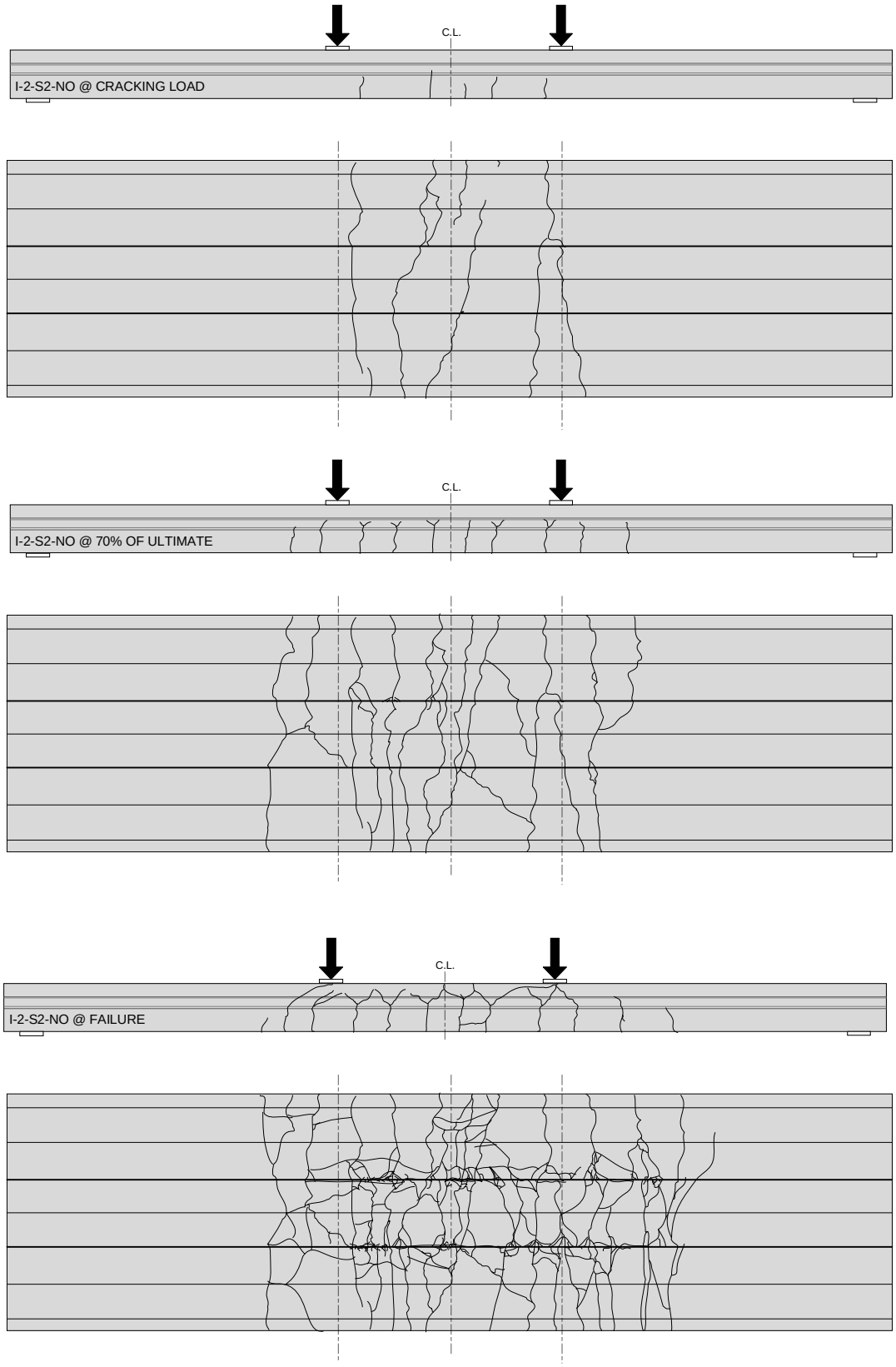

Figure J.6: I-2-S2-NO Crack Pattern

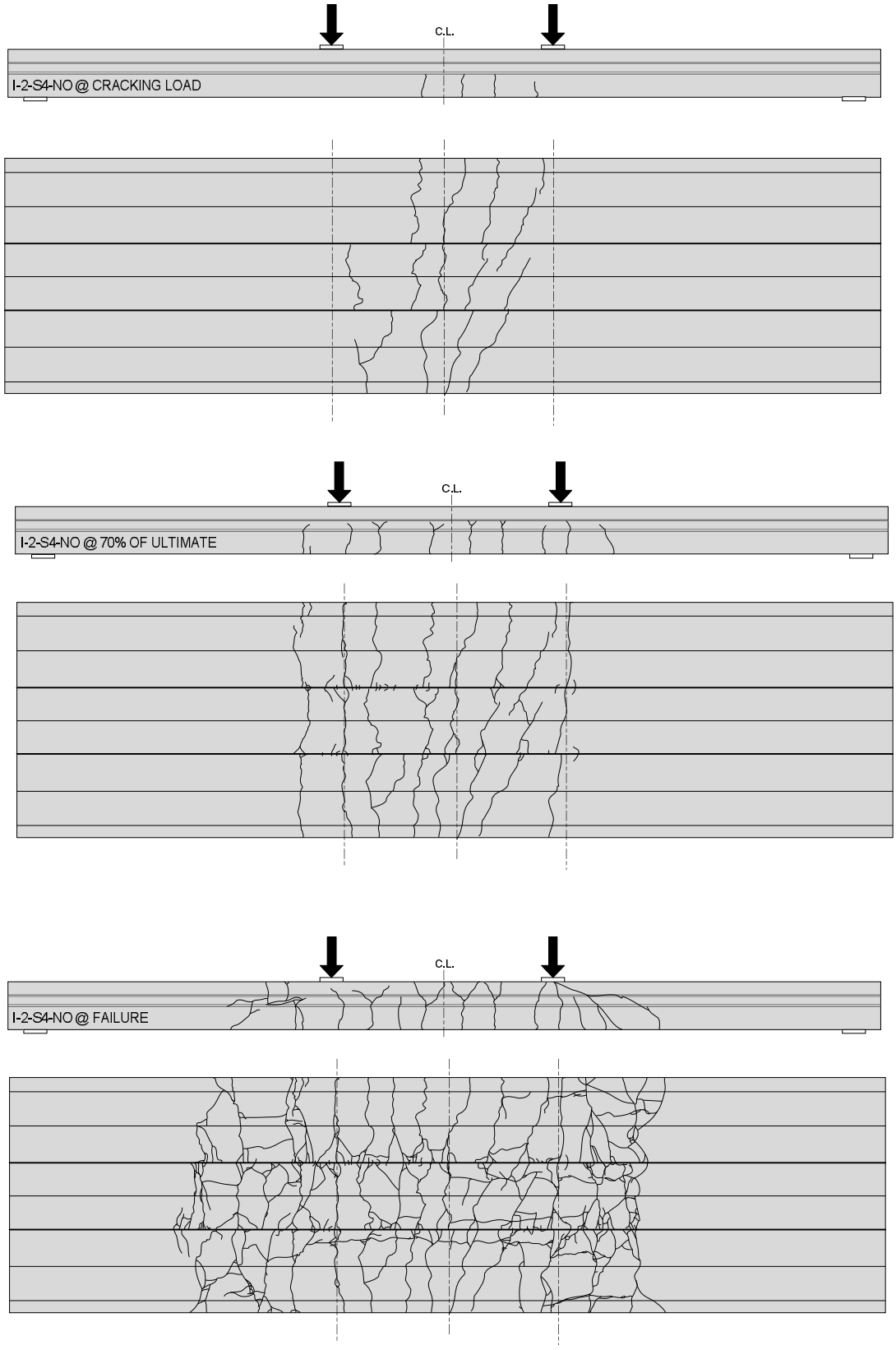

Figure J.7: I-2-S4-NO Crack Pattern

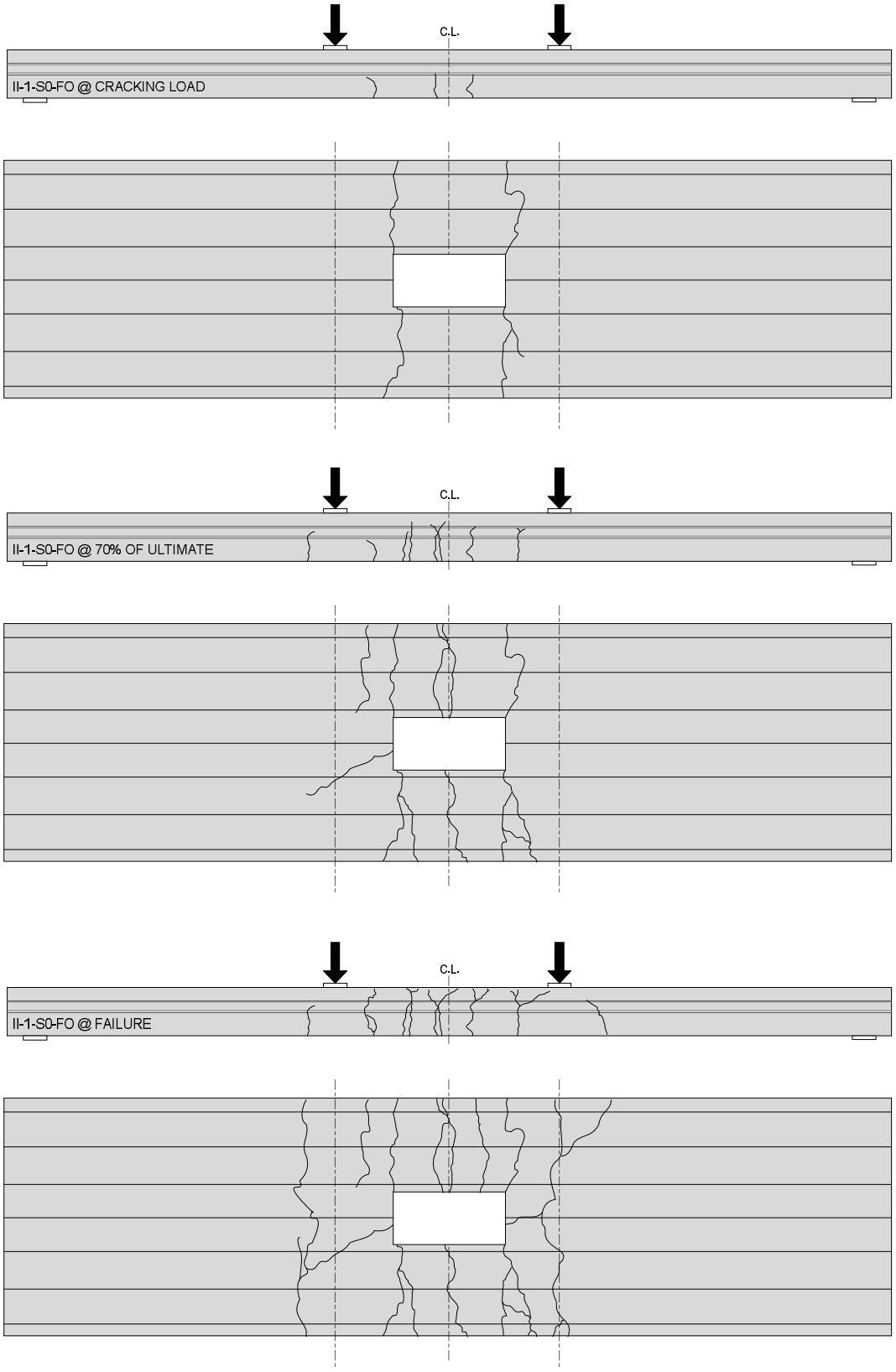

Figure J.8: II-1-S0-FO Crack Pattern

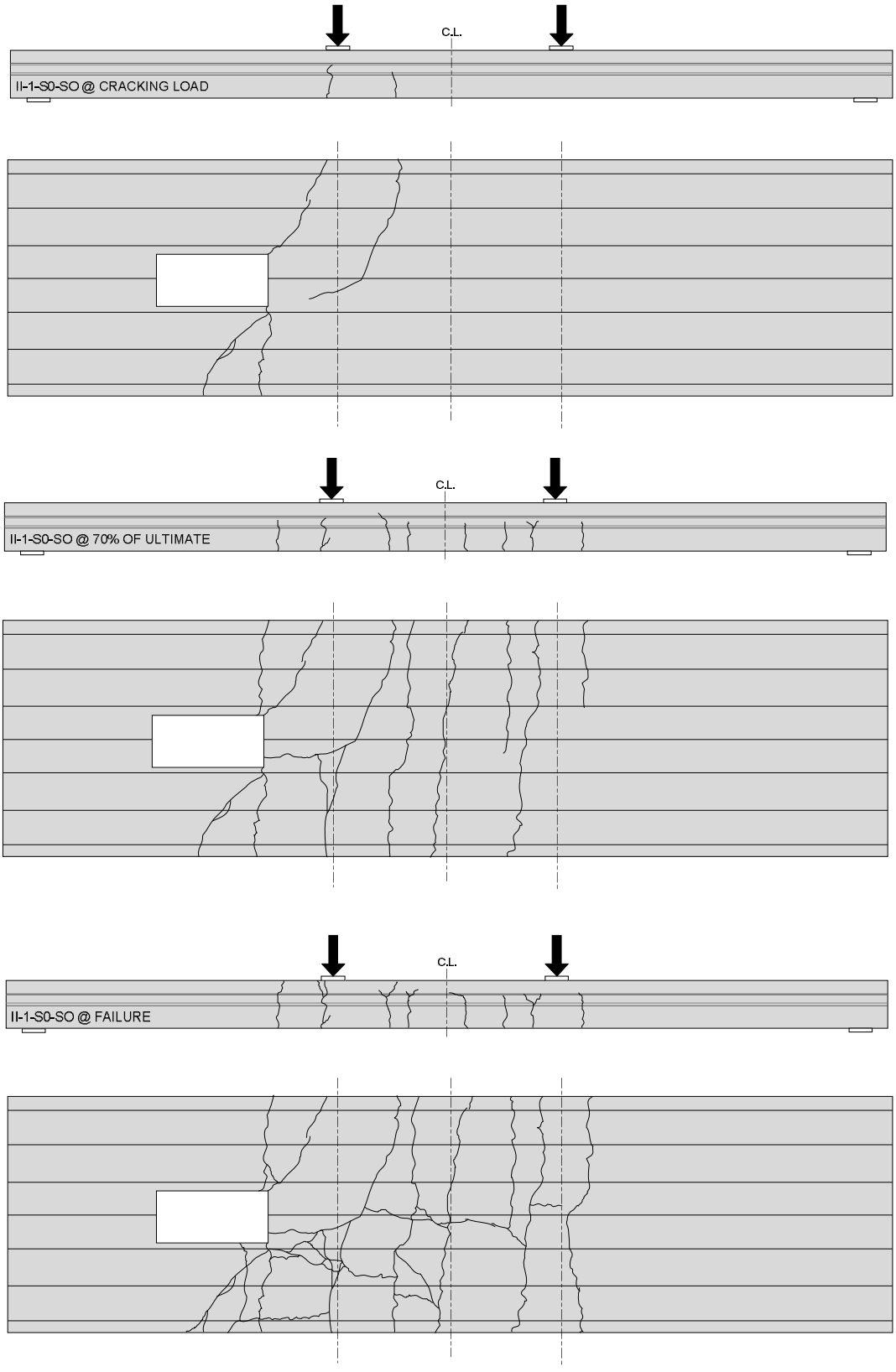

Figure J.9: II-1-S0-SO Crack Pattern

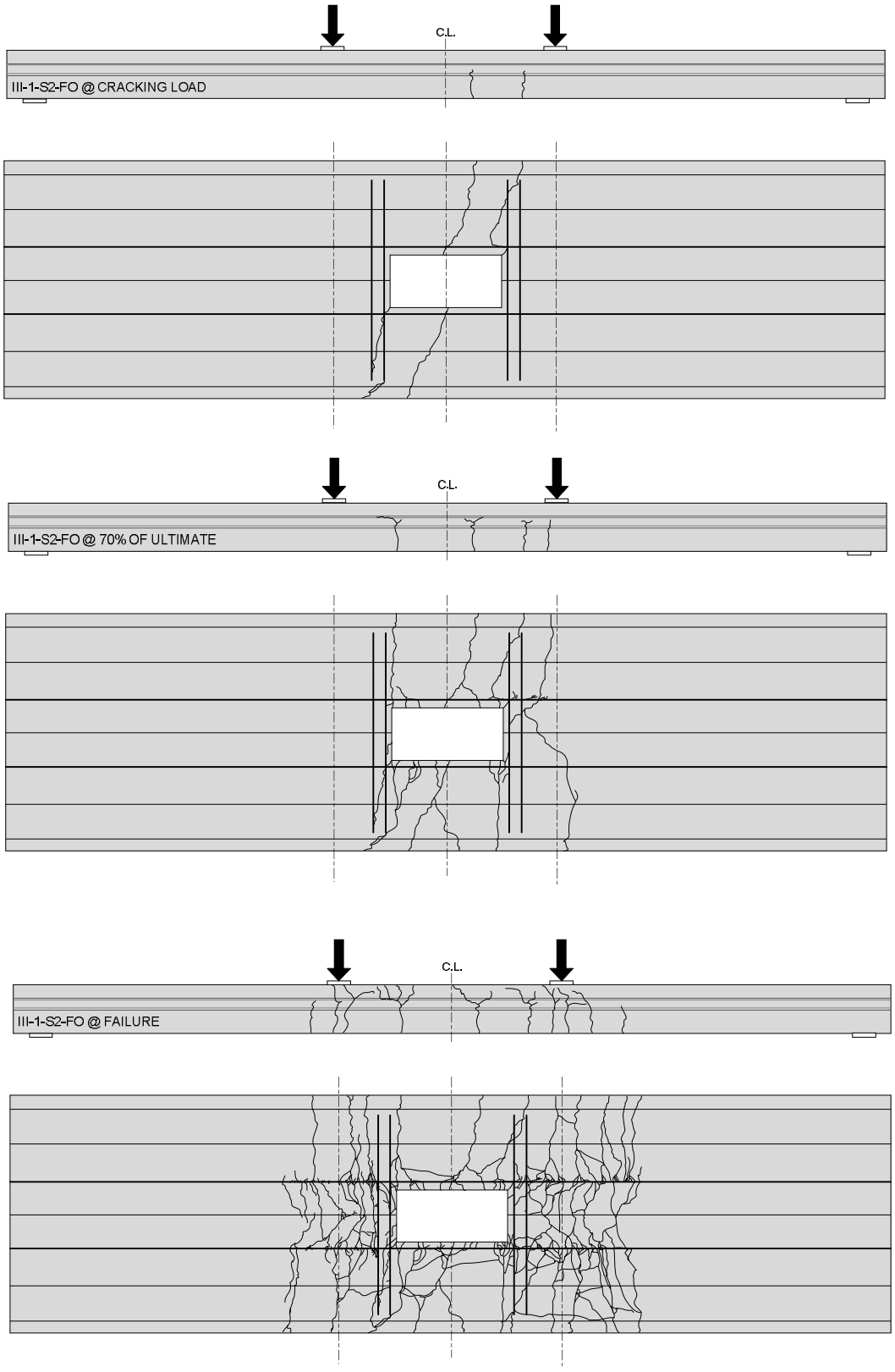

Figure J.10: III-1-S2-FO Crack Pattern

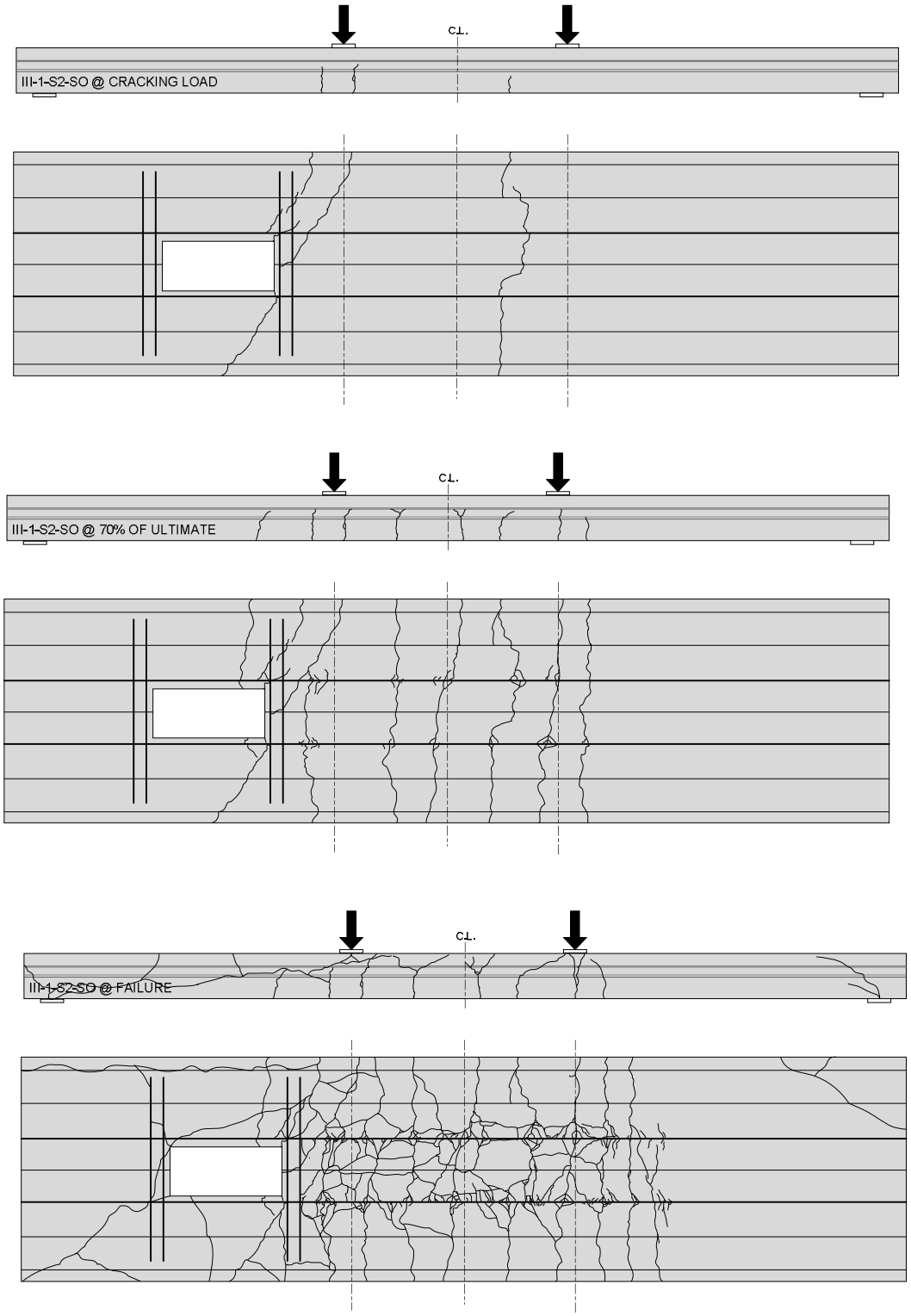

Figure J.11: III-1-S2-SO Crack Pattern

Congratulations, you made it to the end of a brilliant masterpiece. You are ⟷ much smarter.

"Although this might be the end for you, it's only a beginning for me."

The Foobs.